PWM TECHNIQUES FOR CONTROL OF DUAL-INVERTER SUPPLIED SIX-PHASE DRIVES

FAZLLI PATKAR

A thesis submitted in partial fulfilment of the requirements of Liverpool John Moores University for the degree of Doctor of Philosophy

November 2013

ABSTRACT

Among the different multiphase ac drive solutions, one of the most widely reported in the literature is the six-phase machine. The machines can be realised into two different configurations, symmetrical and asymmetrical. For the symmetrical configuration, the stator winding consists of two sets of three-phase windings that are spatially shifted by 60° where spatial displacement between any two consecutive phases is the same and equal to 60°. For the asymmetrical configuration, the two sets of three-phase windings are spatially shifted by 30°. As a result, the spatial shift between consecutive phases becomes non-equidistant.

In this thesis, modulation techniques for both symmetrical and asymmetrical six-phase machines are investigated. The machines are configured in open-end winding configuration where both ends of the stator winding are connected to separate isolated inverters in a topology known as dual-inverter supply. Compared to conventional single-sided supply topology where one end of the winding is connected to an inverter while the other side is star-connected, some additional benefits are offered by the dual-inverter supply topology. First, fault tolerance of the drive is improved, since the supply is realised with two independent inverters. In case one of the inverters is faulted, the other can continue to provide power to the machine. Second, the same phase voltages can be achieved with half the dc-link voltages on the two inverter inputs compared to the single-sided supply, which can be useful in applications such as electric and hybrid electric vehicles and medium sized ships, where the dc voltage levels are limited. Further, due to the nature of the topology, additional diodes and capacitors like in the Neutral Point Clamped (NPC) and Flying Capacitor (FC) VSIs are not required. The latter results in a further advantage - capacitor voltage balancing techniques are not required.

Two pulse width modulation (PWM) techniques for control of the dual-inverter supplied six-phase drives are proposed in this thesis. The first is a reference sharing algorithm where the inverters are modulated using reference voltage that is shared equally and unequally between the two modulators. For both symmetrical and asymmetrical six-phase drives, a better performance, in term of total harmonic distortion (THD) of phase voltage is obtained when the reference is shared unequally between the two modulators. The second technique is carrier-based modulation where the modulation of the two inverters is determined by the disposition of the carrier signals. Three variations of carrier signals disposition are investigated namely; the phase disposition (PD-PWM), alternate phase opposition disposition (APOD-PWM) and phase-shifted PWM (PS-PWM). For the symmetrical six-phase drive, the best phase voltage and current THDs are obtained using APOD-PWM while for asymmetrical six-phase drive, the APOD-PWM produces the worst current THD despite having the best voltage THD among the three methods.

All the developed modulation techniques are analysed using simulations and experiments undertaken using a laboratory prototypes. The waveforms and spectra of phase voltage and load current obtained from the simulation and experimental works are presented in this thesis together with the THD of both the voltage and current over entire linear modulation range.

ACKNOWLEDGEMENT

In the name of Allah, the Most Gracious and the Most Merciful

Alhamdulillah, all praises to Allah for the strengths and His blessing in completing this thesis.

First of all, I would like to acknowledge the Malaysian Government and Universiti Teknikal Malaysia Melaka for giving me the opportunity and financial support to pursue my PhD at Liverpool John Moores University, United Kingdom.

My deepest gratitude goes to my supervisors, Prof. Emil Levi and Dr. Martin Jones, for their invaluable guidance, advices and support throughout the duration of this study. Without their guidance and persistence help, this thesis would not have been possible.

My sincerest appreciation goes to my colleagues, in particular Dr. Wahyu Satiawan, Dr. Nando Bodo, Dr. Obrad Dordevic, Lim Chee Shen, and Chee Han Seng for their help, idea and support. Thanks for the friendship and memories and I consider it an honour to work with all of you.

My special appreciation goes to my beloved parents, Haji Patkar bin Haji Tamsir and Hajjah Siti Isyah binti Haji Wagiran, for their endless love, prayers and encouragement. I am also greatly indebted to my beloved wife, Cik Sapiah binti Che Khalib and also my children Nur Izzatun Nadhirah and Muhammad Zharith Fakhri for their love, prayers and support.

Last but not least, I wish to express my sincere thanks to all those who have one way or another helped me in making this study a success.

CONTENTS

LIST OF PRINCIPAL SYMBOLS

a	Number of phases for each machine sub-winding.
$a, b, c,\ldots,n$	Phases of the machine/machine or used in subscript to associate the principal symbol with a certain phase.
$A, B, C,\ldots, N$	Inverter legs in general or used in subscript to associate the principal symbol with a certain leg.
f	Frequency.
f_s	Switching frequency.
i	Current.
k	Number of machine sub-winding.
l	Number of levels of the inverter voltage output.
L	Inductance.
m	Number of cells for multicell inverter.
M	Modulation index; an added subscript identifies association with a particular inverter.
n	Number of phases of the machine (or the inverter).
N	Neutral points of the machine/machine or the negative rail of the dc bus; indices 1 and 2 refer to a particular inverter.
N_{sw}	Number of switching state combinations.
R	Resistance.
t	Time.
T	Times of application (or dwell times) of space vectors, where a subscript identifies association with a particular space vector.
T_s	Switching period.
v	Voltage.
V	Space vector, where a subscript identifies association with a particular space vector of switching state combination.
V_{dc}	dc bus voltage; an added sub-script identifies association with a particular inverter.
(α-β)	2-D plane with torque producing quantities.
(x-y)	2-D planes with none-torque producing quantities.
(0_+-0_-)	2-D planes with none-torque producing quantities.

v^*	Voltage reference; a subscript identifies association with a particular inverter or phase voltage.
$\underline{v}^*$	Reference vector.
$\underline{v}$	Space vector groups in (α-β) and (x-y) planes, where a subscript indicates particular amplitude of the space vector group. An added subscript denotes the numbering of space vectors in each group.
v_z	Space vectors groups in (0_+-0_-) axes or space vectors of 0_--components, where a subscript indicates particular magnitude of space vector group. A superscript defines association with a particular inverter.
α	Phase delay angle.
θ	Instantaneous reference space vector position.
ρ	Control variable.
ω	Angular velocity.

LIST OF USED ABBREVIATIONS

ac	Alternating current
APOD-PWM	Alternate phase opposition disposition PWM
COTS	Commercial-off-the-shelf
CSI	Current Source Inverter
CHB	Cascaded H-Bridge
dc	Direct current
DSP	Digital Signal Processor
ERS	Equal Reference Sharing
FC	Flying Capacitor
FFT	Fast Fourier Transformation
LS-PWM	Level-shifted PWM
MMF	Magneto-motive Force
MV	Medium voltage
NPC	Neutral Point Clamped
PWM	Pulse Width Modulation
rms	Root mean square
PD-PWM	Phase disposition PWM
POD-PWM	Phase opposition disposition PWM
PI	Proportional Integral
p.u.	Per-unit
PS-PWM	Phase-shifted PWM
SPWM	Sinusoidal Pulse Width Modulation
SVPWM	Space Vector Pulse Width Modulation
THD	Total Harmonic Distortion
URS	Unequal Reference Sharing
VSD	Vector Space Decomposition
VSI	Voltage Source Inverter
2D	Two-dimensional

Chapter 1

INTRODUCTION

1.1 Preliminary considerations

Higher power demands on converters and drives are continuously being imposed by industrial users. The reasons for this are the requirements to reach higher production rates, cost reduction (large-scale economy), improved efficiency, etc. Available mature drive topologies, which are mainly based on two-level inverters and three-phase machines, are currently unable to meet the high power demands due to the lack of availability of semiconductor devices that possess the required high current carrying and voltage blocking capability. Since the available semiconductor devices (which are currently up to 6 kV and 6 kA [Franquelo et al. (2010)]) can only be used for limited power applications, alternative solutions have to be devised for higher power industrial applications in the region of tens of megawatt.

High power demands are currently met by using two different approaches. The first approach is to continue to use the three-phase machine, but the per-phase power of the machine is distributed among a higher number of semiconductor devices than the number normally used in a two-level inverter. Such an inverter is known as multilevel inverter, and it produces output leg voltage with more than two levels. Multilevel inverters produce a better quality of output voltage waveform, but the implementation requires a higher number of semiconductor devices; hence request for more complex switching strategy. Nevertheless, various multilevel inverter topologies have been reported for various high power industrial applications such as traction, mining, automotive, renewable energy, adjustable speed drives and uninterruptible power supply [Franquelo et al. (2008)].

In the second approach, the high power demand is met by utilising a multiphase machine, which is a machine with stator winding consisting of more than three phases. The idea is to divide the total power across more phases, so that a reduced per-phase power rating can be achieved, hence allowing the usage of the currently available power semiconductor devices. As the number of phases increases, higher power demands can be

meet. For example, a six-phase winding has been used for a 25 MW synchronous motor drive [Zdenek (1986)] while a nine-phase winding has been utilised for a 36.5MW ship propulsion drive [Gritter et al. (2005)]. Another example is utilisation of a fifteen-phase 19MW induction motor drive for military ship application [Benamatmane and McCoy (1998)].

Certain aspects however, regarding the utilisation of multiphase drives for high power application, such as the required converter topology, converter control strategy, and the machine construction, ask for significant modifications of the methods and techniques that are conventionally applied to the three-phase drives. In terms of the construction of the multiphase machine, the phase number of a stator winding can be selected either as an odd number or as an even number. Different winding arrangements can be made, and in general the winding can be realised as a symmetrical or asymmetrical configuration [Levi et al. (2007)]. Machine with a prime number of phases (5, 7, 11, 13 and etc) can only be realised using a symmetrical configuration, and the stator windings are connected to a single neutral point. For this configuration, a spatial displacement between any two consecutive phases is always equal to $\alpha = 2\pi/n$, where n is the number of phases. Examples of such a machine are mainly reported for five-phase machines [Shuai and Corzine (2005), Ward and Härer (1969)] and seven-phase machines [Casadei et al. (2010), Grandi et al. (2006), Khan et al. (2009)].

As for a machine with an even phase number (4, 6, 8, 10 and etc) or with an odd composite phase number (9, 15, 21 and etc), the arrangement of the stator windings can be realised in at least four different ways. Consider a machine that has an $n = ak$ number of phases with $a = 3, 5, 7 \ldots$ and $k = 2, 3, 4 \ldots$ For symmetrical configuration, with $\alpha = 2\pi/n$, the complete winding can be configured to have k sub-winding with a phases each. Alternatively, the windings can also be constructed as asymmetrical configuration, where the first phases of the k sub-winding are spatially displaced by $\alpha = \pi/n$. For both symmetrical and asymmetrical configurations, the windings could either be connected to a single neutral point or to k isolated neutral points. Multiphase machine, having phase number equal to a multiple of three, are regularly considered for such configurations. For example, a symmetrical configuration with winding connected into a single neutral point is reported for six-phase machines [Dujic et al. (2007a), Kianinezhad et al. (2005)] and nine-phase machines [Dujic et al. (2007b), Grandi et al. (2007b)], while windings connected to multiple neutral points are reported for six-phase machine (with two neutral points) [Correa et al. (2003b)], nine-phase machine (with three neutral points) [Grandi et al.

(2007a)] and fifteen-phase machine (with five neutral points) [Youlong et al. (2007)]. For the asymmetrical configuration, multiphase machines with two isolated neutral points are the most common for six-phase machines [Bakhshai et al. (1998), Gopakumar et al. (1993), Hadiouche et al. (2006), Marouani et al. (2008), Prieto et al. (2010), Zhao and Lipo (1995)]. Also, an example of a machine with windings connected to multiple neutral points has been reported for nine-phase machine (with three neutral points) [Steiner et al. (2000)]. Next, multiphase machine can also be realised by using multiple sets of five-phase windings. Such a configuration, for example, is reported for fifteen-phase machine [Benamatmane and McCoy (1998)].

One particular even phase number, very frequently considered in the literature, is six. In this project, the scope of research is focused towards the development of PWM techniques for six-phase machines, where both asymmetrical and symmetrical winding configurations will be considered. The windings of the machine are excited by using inverter topologies that are able to produce multilevel voltage waveforms. The supply of the machines is obtained from two two-level inverters in so-called open-end winding configuration.

In what follows a brief review of various multiphase variable speed drive aspects is provided. The emphasis of the review is placed mainly on the current state-of-the-art in the area of six-phase drives and also multiphase drives that have a composite number of phases.

1.2 An overview of PWM control of multiphase drives

Multiphase drives, although known for many decades, have started to attract greater attention of researchers and industry worldwide only relatively recently. Multiphase drives are at present considered as serious contenders for specialised applications, where high reliability and high power ratings are required, such as electric ship propulsion [Gritter et al. (2005), Parsa and Toliyat (2005)], locomotive traction [Abolhassani (2005), Steiner et al. (2000)], industrial high power applications [McSharry et al. (1998)], electric and hybrid-electric vehicles [Bojoi et al. (2005), Parsa et al. (2005)] and more-electric aircraft [Atkinson et al. (2005)].

An upsurge in interest in multiphase drives has been driven by several benefits of multiphase machines, which include higher torque density, lower per-phase power handling requirement, improved reliability, increased fault tolerance, improved noise characteristics and greater efficiency [Levi et al. (2007), Parsa (2005)]. Different types of

multiphase machines have been developed, designed and studied. These include induction and synchronous machines having stator windings with different number of phases where five, six and seven are the most dominant ones. Thus an opportunity exists to explore different control strategies that are best suited for a given application [Levi (2008)]. Detailed mathematical models of multiphase machines have been derived and this, combined with the rapid development of digital signal processors and power electronic components, has enabled investigation and implementation of numerous control methods for multiphase machines [Levi et al. (2007)].

Utilisation of multiphase machines in industrial applications is possible due to the fact that an ac machine, when used in a variable speed drive system, is not connected directly to the utility supply. Instead, there is an interface between the utility supply and the machine, a power electronic converter. The converter can easily provide the required number of phase voltages (with the necessary phase difference) that matches the number of machine's stator winding phases. The converter is most frequently an inverter, and inverter that produces more than three-phase output is normally referred to as a multiphase inverter.

In the pre-PWM era and early days of multiphase machines, multiphase inverter was switched at a fundamental frequency. Six-step mode of operation of three-phase inverter inevitably produces low frequency torque ripple and at the time the utilisation of multiphase machines was considered as one approach to solve the problem. A six-phase induction machine, constructed based on asymmetrical stator winding configuration with two isolated neutrals, was extensively investigated in order to push the harmonics to higher frequencies. The six-phase supply of the machine was normally obtained by means of two three-phase voltage source inverters (VSI) [Abbas et al. (1984), Nelson and Krause (1974)] or by two three-phase current source inverters (CSI) [Gopakumar et al. (1984)].

When the era of PWM started, this advantage became less important since the harmonics can now be effectively controlled by using a PWM technique. However, for very high power applications, in order to maintain low switching losses, this advantage is still relevant due to the limitation of the switching frequency of currently available semiconductors. Research on PWM techniques for multiphase inverters has also gradually increased, particularly for low and medium power applications.

In the following sub-sections, PWM techniques, applicable to two-level and multilevel multiphase drives, are discussed.

1.2.1 Two-level inverter supplied multiphase drives

At present, multiphase variable speed drives are invariably supplied from two-level multiphase inverters, which are controlled using appropriate PWM techniques. Two main groups of PWM techniques are usually considered which are carrier-based PWM and space vector PWM (SVPWM).

For multiphase inverters, the simplest way to implement the carrier-based PWM technique is by comparing a set of sinusoidal reference voltages (with appropriate phase difference) with a triangular carrier waveform. The technique is normally known as sinusoidal PWM (SPWM) and the output from the comparison is used to generate switching signals for the semiconductor switches in each inverter leg. Further, the carrier-based PWM is usually implemented with an injection of appropriate harmonics into the reference signals. Similar to three-phase inverter with the third harmonic injection, it is also possible to improve the utilisation of the dc bus voltage of multiphase inverters (without moving into over-modulation range) by injecting the appropriate zero-sequence harmonics into the reference voltages. This technique can be easily extended to multiphase inverters with an odd number of phases and single neutral point. However, the effect of improvement that can be achieved regarding dc bus voltage utilisation is weakened as the number of phases increases [Iqbal et al. (2006)].

The principle of carrier-based PWM with zero-sequence harmonic injection can also be utilised for asymmetrical multiphase machines that have a number of phases that is a multiple of three. The machines are configured to have a number of three-phase sub-windings and each sub-winding needs to be connected to an isolated neutral point and supplied by a three-phase inverter. Such an implementation has been realised for an asymmetrical six-phase induction machine with two isolated neutral points, constructed by using two sets of three-phase windings. Zero-sequence harmonics are injected into the reference voltage of each set [Bojoi et al. (2002)], resulting in the same improvement of the dc bus voltage utilisation as in the three-phase inverter.

For SVPWM techniques, the set of sinusoidal reference voltages is represented as a reference voltage vector that needs to be generated by the inverter. Each switching state combination of inverter legs produces a different voltage vector. By using SVPWM, a certain number of space vectors will be used over one switching period, each with an appropriately calculated dwell time, in order to produce output voltage vector that has an average value equal to the reference.

Basically, compared to SVPWM, carrier-based PWM technique is simpler and more straightforward to implement, since the modulator just has to compare the carrier and the reference signals. This advantage becomes more and more pronounced as the number of phases increases [Dong et al. (2008a)]. Implementation of carrier-based PWM has been considered for a nine-phase inverter [Dong et al. (2008a)] and a fifteen-phase inverter (with three isolated neutral points) [Benamatmane and McCoy (1998)]. For SVPWM implementation, the number of switching state combinations for two-level multiphase inverter can be calculated as $N_{sw} = 2^n$. Therefore, compared to a three-phase inverter where the number of switching states is $2^3 = 8$, the process of selecting the appropriate space vectors and devising SVPWM from, for example, $2^{15} = 32768$ switching state combinations for fifteen-phase machine is obviously not an easy task.

For a machine with a single neutral point, the other advantage of the SVPWM technique, which relates to dc bus voltage utilisation, also becomes less significant for machines with high number of phases. While SVPWM can improve the dc bus voltage utilisation of a three-phase inverter by 15.47%, the improvement that can be achieved in a nine-phase inverter is 1.54% and in a fifteen-phase inverter is merely 0.55% [Dong et al. (2008a)]. The same improvements in the dc bus voltage utilisation can be obtained by means of carrier-based PWM methods if zero-sequence injection is used. However, it is important to notice that the dc bus utilisation in multiphase VSI supplied drives with a composite stator phase number varies depending on the winding configurations (symmetrical or asymmetrical) and also the number of neutral points [Dujic et al. (2010)]. For example, asymmetrical six-phase drive with stator winding of the machine connected to a single neural point has a maximum dc bus voltage utilisation of 103.53% while with stator winding connected to two isolated neutral points, the maximum dc bus voltage utilisation is 115.47%. For symmetrical six-phase drive with machine's stator winding connected to a single neutral point, no increase of dc bus voltage utilisation is obtained, i.e. the utilisation is 100%.

By and large, the existing research in connection with SVPWM control of two-level inverters is mainly related to multiphase machines with a lower number of phases such as five, six, seven, and nine. For these machines, the SVPWM approach is in general analysed more frequently than the carrier-based PWM because it offers a better insight into the properties of multiphase drives. SVPWM techniques for two-level multiphase inverters have been widely applied for six-phase VSIs, in both symmetrical configuration [Correa et al. (2003a), Dujic et al. (2007a), Kianinezhad et al. (2005)] and asymmetrical configuration

[Bakhshai et al. (1998), Gopakumar et al. (1993), Hadiouche et al. (2006), Marouani et al. (2008), Prieto et al. (2010), Zhao and Lipo (1995)], as well as for nine-phase VSIs [Dujic et al. (2007b), Grandi et al. (2007a), Grandi et al. (2007b), Kelly et al. (2003)]. SVPWM approach for fifteen-phase inverter is rarely investigated, and one example of such a study is reported in [Youlong et al. (2007)]. A comprehensive analysis of the relationship between carrier-based PWM and SVPWM techniques for multiphase inverters has been reported for a five-phase inverter [Iqbal and Moinuddin (2009)].

1.2.2 Multilevel inverter supplied multiphase drives

Multilevel inverters operate by synthesising a near-sinusoidal output voltage from several dc voltage levels, usually obtained from capacitors as voltage sources. As the number of levels increases, the synthesised output waveform has more and more steps. Hence a staircase waveform is produced that approaches the desired sinusoidal waveform. Multilevel inverters have some distinct advantages compared to two-level inverters. They lead to higher power capability, without requiring high voltage rating of semiconductor devices. Besides that, multilevel inverters also produce low harmonic distortion, reduced switching frequency, increased efficiency and good electromagnetic compatibility. However, as the number of levels increases, the complexity of the control circuit also increases.

Since the birth of the first multilevel three-phase inverter about 30 years ago [Nabae et al. (1981)], extensive research on multilevel inverters has been carried out worldwide. Today, multilevel inverters are considered as one of the most viable solutions for high-power and high-power quality demanding applications [Rodriguez et al. (2009)]. Over the years, a number of different types of multilevel inverter topologies have been developed. The most frequently considered and well established topologies are diode-clamped inverter (which is usually also called neutral point clamped inverter (NPC)), flying capacitor inverter (FC) and cascaded H-bridge inverter (CHB) [Wu (2006)].

Today, multilevel inverters have been commercialised by many manufactures, with variety of control methods in use, in order to cater for different markets [Franquelo et al. (2008)]. NPC VSIs have become a mature solution for high power ac motor drive applications such as conveyors, pumps, fans and mills, which offer solutions for various industries such as oil and gas, power generation and distribution, mining, water, metal and marine [Klug and Klaassen (2005)]. On the other hand, FC VSIs have found specific applications for high-power-bandwidth high-switching-frequency applications such as

medium-voltage traction drives [Meynard et al. (2002)]. As for CHB VSIs, they have been successfully commercialized for very high power and power quality demanding applications, due to their series expansion capability. Some examples of areas of application for CHB VSIs are reactive power compensation [Dixon et al. (2005)], electric vehicles [Zhong et al. (2006)] and photovoltaic power supplies [Naik and Udaya (2005)].

As has been explained at the beginning of this chapter, the demand for high power industrial applications is currently met either by using multilevel inverters or by using multiphase drives. Since both methods are able to produce a high output power (by using only medium power semiconductor devices), combination of multilevel inverters and multiphase drives is expected to be able to produce higher output power than any of the two can individually, while at the same time retaining the advantages offered by each of them. For this reason, an initial attempt to integrate the multilevel inverter and multiphase machine has been carried out and the advantages of combining both topologies have been described in [Lu and Corzine (2005)].

The benefits of combining multilevel inverters and multiphase drives have lead to interest in investigation of multilevel multiphase drives. Currently, there are two different arrangements for multilevel multiphase drives. The first arrangement is so-called a single-sided supply. One end of the machine's multiphase winding is connected to a multilevel inverter, while the other end is star-connected. The second arrangement is a dual-inverter supply. Here, both ends of the machine windings are connected to either two-level or multilevel inverters. This arrangement is also known as an open-end winding topology. The two inverters that are connected at both ends of the open-end windings can have an equal or different number of levels.

The number of switching state combinations for multilevel multiphase inverter supply depends on the number of inverter's phase legs n (i.e. machine's phases) and the number of inverter's output voltage levels l. For a single-sided topology, the number of switching states can be calculated as $N_{sw} = l^n$. For example, if the number of output voltage levels is three, a three-phase inverter has $3^3 = 27$ switching state combinations, while a five-phase inverter has $3^5 = 243$ switching state combinations and a six-phase inverter has $3^6 = 729$ switching state combinations. Therefore, with an increase in the number of voltage levels, the difference between the number of switching state combinations for three-phase and multiphase inverters becomes bigger and bigger.

For an open-end winding topology, both ends of the machine's winding are connected to two different inverters. Therefore, the total number of switching states is

multiplication of the number of switching states produced by each inverter, i.e. $N_{sw} = l_1^n \; l_2^n$, where indices 1 and 2 refer to the first and the second inverter. If the open-end winding is supplied by two three-level inverters, the number of switching states for an open-end winding three-phase drive is 3^3 x 3^3 = 729, for a five-phase drive 3^5 x 3^5 = 59,049, while for an open-end winding six-phase drives it is 3^6 x 3^6 = 531,441. This is much higher than the number of switching states for the single-sided supply topology. The abundance of switching states provides some advantages for drives with the open-end winding configuration. One of them is that a higher number of output voltage levels can be achieved, where for example utilisation of two two-level inverters produces the same output voltage as a three-level inverter in a single-sided topology [Shivakumar et al. (2001a), Stemmler and Guggenbach (1993)]. The selection of which switching states are to be used will also have an effect on the performance of the multilevel multiphase drive in terms of harmonic content, common mode voltage, dc bus voltage utilisation, etc.

Multilevel multiphase drives, in a single inverter or dual-inverter supply topology, always possess a higher number of switching states than the traditional two-level multiphase drives. However, some of the switching states lead to the same voltage vectors. Therefore, for both topologies, the total number of voltage vectors is always less than the number of switching states, meaning that there are redundant switching states (the difference between the total number of switching states and the number of different space vectors). These redundant switching states are very beneficial, especially for determining switching sequence that could minimise the switching losses of the inverters.

PWM techniques for multilevel multiphase drives, implemented by using single-sided and dual-inverter supply, are reviewed next.

1.2.2.1 Multilevel multiphase drives with single-sided supply

For a single-sided configuration, an initial attempt to integrate a multilevel inverter with a multiphase machine was carried out for a five-phase NPC VSI [Lu and Corzine (2005)]. The inverter is modulated by using a SVPWM strategy and it has been found that, compared to a two-level VSI supplied five-phase drive, torque ripple in three-level five-phase system can be reduced significantly, due to the abundance of space vectors. However, the basic rule which says that the number of applied vectors must equal the number of phases, was not respected. Instead, the nearest three vector concept was used, as

in three-phase drives, leading to uncontrollable harmonics in the stator current that belong to the second plane.

More research has followed, mainly based on the SVPWM approach. Investigations and new developments of SVPWM for three-level five-phase NPC VSI have been supported by simulation [Song et al. (2006)] and by experimental [Gao and Fletcher (2010)] results. Development of a general SVPWM scheme for multiphase multilevel VSIs, including implementation of SVPWM for five-level five-phase CHB VSI, has been reported in [Lopez et al. (2008)] and [Lopez et al. (2009)].

An attempt to develop a SVPWM scheme for asymmetrical six-phase induction machine, by means of two five-level three-phase NPC VSIs, is described in [Oudjebour et al. (2004)]. Further, a SVPWM scheme has also been developed for six-phase synchronous motor, supplied by two three-level three-phase NPC VSIs having the same dc bus capacitor [Yao et al. (2006)].

Research on multilevel multiphase drives that utilise carrier-based PWM has been carried out to a lesser extent. One example, related to asymmetrical six-phase induction machine, is carried out by using two five-level three-phase VSIs [Oudjebour and Berkouk (2005)]. The switches of each inverter's leg are controlled based on the signal generated by comparing the sinusoidal reference voltages with four triangular carrier signals.

Multilevel multiphase drives, based on single-sided supply, are at present already considered for a few industrial applications. One example is the supply of 36.5MW ship propulsion drive from four- or five-level nine-phase NPC VSI [Gritter et al. (2005)]. A nine-phase transformerless ac traction drive supplied by three three-level three-phase VSI bridges has been discussed in [Steiner et al. (2000)]. A rather unusual application of multilevel multiphase drives has also been reported, where the drive has been considered for micro-electromechanical systems (MEMS) [Neugebauer et al. (2004)].

1.2.2.2 Multilevel multiphase drives with dual-inverter supply

Multilevel multiphase drives with dual-inverter supply topology have several advantages, compared to the single-sided topology. One advantage is that the effect of a multilevel supply can be achieved by using two-level inverters. Besides that, if one of the inverters is inoperable, the system can be reconfigured to be driven by a single inverter [Grandi et al. (2011)].

Dual-inverter supply topology for machines with open-end windings was initially introduced for three-phase drives [Stemmler and Guggenbach (1993)]. Two two-level VSIs

have been used, with supply coming from isolated dc bus voltage sources. This arrangement effectively operates as a three-level VSI equivalent in single-sided supply topologies. A number of alternative solutions have been also investigated. These include use of three-level inverter in conjunction with a two-level inverter at two winding sides, with a suggestion that one of the sources can be a capacitor that supplies only reactive power [Kawabata et al. (1996)]. The dc supplies have a 2:1 ratio and the resulting feeding scheme can emulate four-level equivalent of single-sided supply inverter. By using asymmetrical dc voltage sources (i.e. voltage ratio different from unity), two two-level inverters can produce voltages which are identical to those generated by three-level and four-level inverters in single-sided supply mode [Corzine et al. (1999)].

Although numerous versions of dual-inverter supply for three-phase drive systems have been reported, implementation of this topology in the multiphase drives has started to gain momentum only recently. Such an attempt was initially carried out for asymmetrical six-phase machine fed by four two-level three-phase VSIs [Mohapatra et al. (2002)], [Mohapatra and Gopakumar (2006)]. However, the goal of the research was harmonic elimination, rather than multilevel operation. Hence the created output voltages are not those that would result with a multilevel supply.

In the last few years, several modulation strategies that are able to create multilevel output voltage, produced in an open-end winding multiphase configuration, have been reported. Two main types of drive topology have been considered. The first is to use two two-level inverters to supply the open-end winding machine with five [Bodo et al. (2011b), Bodo et al. (2012b), Jones et al. (2012), Levi et al. (2012), Satiawan (2012)], six [Jones et al. (2013), Patkar et al. (2012)], seven [Bodo et al. (2011a)] and nine [Bodo et al. (2013a)] phases. The second topology is to utilise four two-level inverters where asymmetrical machine with six phases is the main focus of the study [Grandi et al. (2010a), Grandi et al. (2010b)]. The current state-of -the-art regarding the control of multiphase open-end drive is summarised in [Levi et al. (2013)].

The control strategies and drive topologies for the multiphase drives which are discussed throughout Section 1.2 are developed based on strategies and topologies that have been explored before for the three-phase drives. The correlation between the developed drive topologies for the multiphase and three-phase drives and the advantages and disadvantages of each topology are depicted in Fig.1.1.

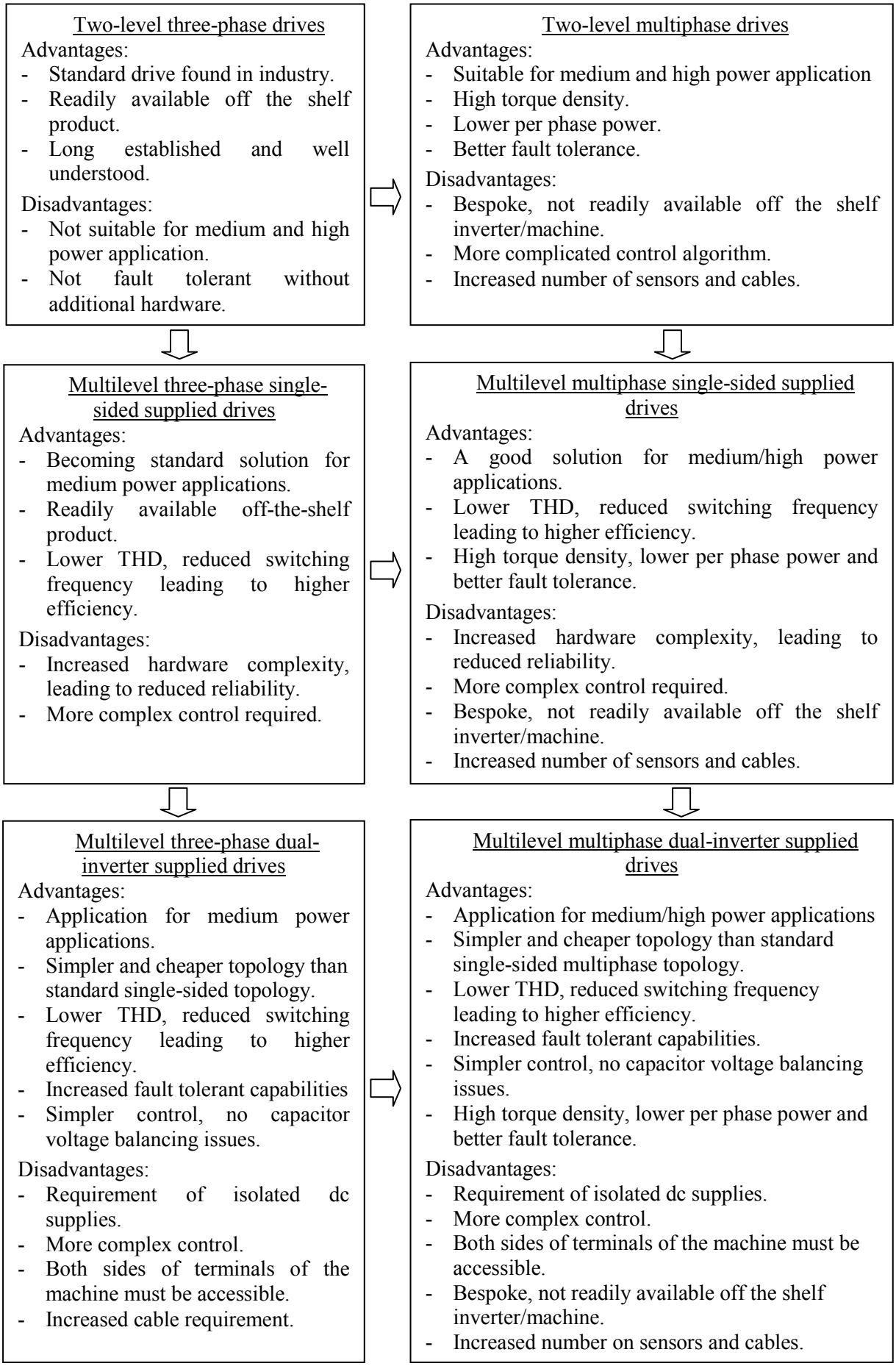

Fig. 1.1: Research development in the area of multiphase VSI supplied drives.

1.3 Research aim and objectives

The aim of the research is to develop PWM techniques for control of dual-inverter supplied six-phase machines with both symmetrical and asymmetrical winding configurations.

The goal of the research has been met by achieving a number of research objectives, which are the following:

1) Development of reference sharing algorithms for control of two six-phase two-level inverters based on open-end topology, using PWM techniques that initially developed for single-sided six-phase inverters.
2) Development of carrier-based PWM techniques for the control of six-phase machines, supplied by two two-level six-phase inverters.
3) Creation of computer simulation for the developed PWM techniques using MATLAB/Simulink software.
4) Implementation of the developed PWM techniques in the available laboratory rigs and experimental verification of theoretical findings.

1.4 Research contributions

This research constitutes a part of a wider research project, related to multilevel multiphase drive systems, which comprise four PhD theses. The work commenced with the first PhD [Satiawan (2012)] and continued with the subsequent two projects, [Bodo (2013)] and [Dordevic (2013)].

In principle, multilevel supply waveform can be realised using either a single-sided supply mode, with the multiphase machine having an isolated neutral point, or using dual-inverter supply in conjunction with an open-end winding topology. Further, a multiphase stator winding can be designed to have an odd prime number, an odd composite number or an even number of phases. The four projects are designed to cater for the two different supply options (single-sided mode and dual-inverter supply) and for different phase numbers.

In particular, [Satiawan (2012)] deals with an open-end winding topology of a five-phase machine and relies on utilisation of two two-level five-phase inverters. [Bodo (2013)] extends the work of [Satiawan (2012)] by looking at seven- and nine-phase drives in dual-inverter supply mode, using at each side two-level inverters, as well as the five-phase drives in various conditions not covered by [Satiawan (2012)]. Finally, [Dordevic

(2013)] is intended to cover again odd phase numbers (the emphasis is on five and seven, with a possible extension to nine), but this time using a single-sided supply mode with a three-level NPC multiphase inverter.

It follows from the description above that the three current PhD projects all deal with odd phase numbers in either single-sided or dual-inverter supply mode. This project is therefore designed to cover dual-inverter supply modes, but for machines with even phase numbers. The emphasis in the research is placed on six-phase machines, where multilevel supply for both symmetrical and asymmetrical winding topologies of six-phase machines is investigated.

The contribution of the research is backed by the publications listed in Appendix 2.

1.5 Organisation of the thesis

This thesis is organised in eight chapters and two appendices.

Chapter 1 gives a brief review of various aspects of multiphase variable speed drives. Different arrangements of stator winding for the multiphase drives are explained and various inverter topologies and PWM control strategies for the drives are described. The emphasis of the review is placed mainly on the current state-of-the-art in the area of six-phase drive. Finally, the aim, objectives and originality of the research have also been stated.

Chapter 2 presents a literature review in the area of PWM control for the six-phase drive. PWM techniques for two-level six-phase drive are discussed first, followed by the PWM techniques for multilevel multiphase drives, covering both single-sided and dual-inverter supply topologies. Reviews of PWM techniques for the dual-inverter supplying open-end windings of three-phase drives are included for the sake of completeness of the literature studies.

Chapter 3 discusses space vector model of a two-level six-phase VSI fed asymmetrical machine with both two isolated neutral and single neutral points configuration. Then, several PWM techniques for two-level asymmetrical six-phase VSI with machine windings connected to two isolated neutral points are described. Simulation study has been conducted to analyse the performance. The investigated PWM techniques are as follows:

i. Carrier-based SPWM,
ii. Carrier-based PWM with double zero-sequence injection [Bojoi et al. (2002)],
iii. Conventional SVPWM [Gopakumar et al. (1993)],

iv. Vector Space Decomposition SVPWM [Zhao and Lipo (1995)].

Besides that, PWM techniques for two-level six-phase VSI with machines connected to a single neutral point are also addressed. Two carrier based PWM techniques are investigated, which are:

i. Carrier-based SPWM,
ii. Carrier-based PWM with zero-sequence injection.

Finally, simulation and experimental studies of two carrier-based PWM techniques (carrier-based PWM with zero-sequence injection and carrier-based PWM with double zero-sequence injection) are carried out in order compare the performance between the two winding configurations (single and two isolated neutral) of an asymmetrical six-phase machine.

Chapter 4 elaborates a space vector model of a two-level symmetrical six-phase VSI. Only the case of machine with a single neutral point is addressed. Several SVPWM strategies proposed in [Correa et al. (2003b)] and [Dujic et al. (2007a)] are described and their performance is again analysed by a simulation study.

Chapter 5 introduces drive topology and space vector model for a dual-inverter supply (with equal dc bus voltage) of both symmetrical and asymmetrical six-phase drives. The mathematical expression of phase voltage space vectors is also derived.

Chapter 6 discuss two reference sharing algorithms proposed for the six-phase drive with dual-inverter supply. In essence, the algorithms are implemented based on equal and unequal partitioning of the total reference between the two inverters, a method that is first developed in [Satiawan (2012)]. In this thesis, the algorithms are extended to both symmetrical and asymmetrical winding configuration of open-end six-phase machine. Simulation and experimental studies for the proposed algorithms are conducted and their performance is compared based on the THD of phase voltage and current, and also their axes component for operation at linear range of modulation index.

Chapter 7 presents carrier based modulation techniques for the six-phase drive with dual-inverter supply. The modulation techniques are adopted from modulation strategies widely known for the three-phase drives, which are level-shifted and phase-shifted PWM. The algorithms are once more implemented for both symmetrical and asymmetrical winding configuration of six-phase machine. The performance is again analysed and compared using the same performance indicator used in the previous chapter.

Chapter 8 gives a conclusion of the work that has been done in this thesis. The findings are highlighted and some possible extension for the future research is suggested.

Chapter 9 lists the references used in this thesis.

The simulation and experimental setup used to examine and verify the considered modulation methods presented in this thesis are described in Appendix 1.

Appendix 2 lists papers that are published as the result of this thesis.

Chapter 2

LITERATURE REVIEW

2.1 Preliminary remarks

In this chapter, PWM techniques for two-level and multilevel multiphase drives are reviewed. Since this thesis is a part of project that encompass four PhD theses, the discussion of the two-level multiphase drives are mainly focused on the six-phase drives where the detailed discussion for the other multiphase drives have already been done in the other theses [Satiawan (2012)],[Bodo (2013)] and [Dordevic (2013)]. The discussions of the PWM techniques for multilevel multiphase inverters are covered for both single-sided and dual-inverter supply topologies. With regards to PWM techniques for the dual-inverter supply topologies, the majority of the available literature is related to three-phase drives, while only a small number of papers present PWM algorithms for multiphase drives. Therefore, PWM techniques for dual-inverter supply for open-end three-phase drives are also reviewed in the last sub-section, alongside the papers that elaborate PWM techniques for the open-end multiphase drives, so that wider aspects of PWM techniques for dual-inverter supply topologies are sufficiently covered.

It has to be mentioned that multiphase machines can be designed either to have a distributed or a concentrated stator winding. The distributed stator windings yield a sinusoidal (or at least near sinusoidal) magneto-motive force (MMF) distribution, while the concentrated stator windings produce a quasi-rectangular MMF distribution. In this chapter, the majority of the reviewed literature is related to the drives with a machine having a distributed stator windings. Therefore, unless stated otherwise, the literature discussed in this chapter considers multiphase machines with the distributed stator winding.

2.2 PWM control of two-level six-phase drives

Multiphase drives are typically supplied from two-level multiphase inverters, and are controlled by using either carrier-based PWM or SVPWM algorithms. Among all the

phase numbers higher than three, the six-phase ac machine is one of the machines that have been considered most frequently by researchers. This is so since six-phase machines can be realised in a rather simple way, by modifying only the stator winding of an existing three-phase machine. In other words, there is no need to design and manufacture new stator laminations, since the number of slots in three-phase machines is automatically suitable for six-phase machines as well, as long as there are at least two slots per phase per pole (i.e. suitable numbers of slots of a four-pole three-phase machine are 24, 48, etc.). This is so since six is divisible by three, in contrast to five or seven, for example (a five-phase four-pole machine asks for a minimum of 20 slots and is usually built using 40 slots; neither of the two is divisible by three and there are no three-phase machines with these slot numbers, so that realisation of a five-phase machine usually asks for new stator laminations).

There are two different topologies of six-phase machines, which can be realised. The most common one is an asymmetrical, while the other topology is a symmetrical. Stator windings of an asymmetrical six-phase machine consist of two sets of three-phase windings that are spatially shifted by 30°. This leads to non-equidistant spatial shift between consecutive phases. For a symmetrical six-phase machine, stator windings are configured by two sets of three-phase windings that are spatially shifted by 60°, so that spatial displacement between any two consecutive phases is the same and equal to 60°. For both topologies, the two sets of three-phase stator windings can either share a single neutral connection or may have two isolated neutral points.

Six-phase machines are a six-dimensional system, since there are six supply voltages. This system can be decomposed into three two-dimensional planes (or subsystems), known as (α-β), (x-y) and (0_+-0_-). The three planes are mutually perpendicular (orthogonal) in the six-dimensional space and the machine can then be described by three pairs of mutually decoupled equations [Zhao and Lipo (1995)]. The electromechanical energy conversion takes place only in the (α-β) plane as long as the machine is designed with sinusoidal flux (magneto-motive force) distribution. The other two planes only contribute to losses, so that current components in these subsystems should be ideally zero (i.e. the drive control needs to minimise them). The most frequently considered type of ac machine, associated with a six-phase stator winding, is an induction machine.

Stator winding of six-phase machines is nowadays typically supplied using a six-leg two-level VSI. In general, a two-level inverter with n legs produces at the output the number of voltage vectors according to 2^n law, so that 64 voltage vectors are obtained from

a six-leg VSI. These voltage vectors are in essence six-dimensional and they can be projected into (α-β), (x-y) and (0_+-0_-) planes. In the (α-β) and (x-y) planes, these space vectors lay at the vertices of four 12-sided polygons. Voltage vectors on the (0_+-0_-) plane are all zero if the two sets of three-phase stator windings have mutually isolated neutral points. However, if single neutral point is used, there are some nonzero voltage vectors in the (0_+-0_-) plane [Correa et al. (2003b), Dujic et al. (2007a), Zhao and Lipo (1995)].

It should, at this stage, be pointed out that, strictly speaking, 0_+ and 0_- components do not constitute a plane which can be regarded as a complex plane. In essence, both 0_+ and 0_- components are real quantities and different harmonics map into each of the two. This contrasts with all the other planes, which are the planes that can be regarded as complex planes. Nevertheless, since 0_+ and 0_- quantities are customarily shown in a plane with these two axes taken as the horizontal and the vertical axis, in what follows (0_+-0_-) will also be treated as a plane. However, the fact that the 0_+ and 0_- quantities are both real will be accounted for in the mathematical description.

2.2.1 Asymmetrical six-phase drives

Among the different multiphase drive solutions, one of the most widely reported in the literature is an asymmetrical six-phase machine. The machine has two sets of three-phase stator windings that are spatially shifted by 30°. The neutral points of the stator windings can be configured in two different ways. The first is to connect the stator three-phase winding sets to form two isolated neutral points while the second is to connect the windings together to form a single neutral point.

By and large, the existing research on asymmetrical six-phase drives has been mainly conducted for configuration with two isolated neutral points. In an early investigation of six-phase variable speed drives, two two-level three-phase VSIs were operated based on the six-step mode and were used to supply an asymmetrical six-phase machine [Abbas et al. (1984), Nelson and Krause (1974)]. This produced a lower torque ripple than in a three-phase machine and increased the ripple frequency to a higher value (this was, as noted, the main aim for investigation of higher phase order (HPO) machines [Klingshirn (1983a), Klingshirn (1983b)]). Another obvious gain of using a multiphase machine with two (or more) three-phase windings is that two (or more) three-phase VSIs can be easily configured to supply the machine.

The problem of low-frequency torque ripple was eliminated by the introduction of PWM control strategies. The PWM strategies are not only beneficial for three-phase machines, but also for multiphase machines. Numerous PWM strategies for multiphase machines have been developed and the most widely investigated are the carrier-based PWM and SVPWM.

For carrier-based PWM, the modulation strategies used for a three-phase machine can be easily extended to a six-phase machine, since it is only necessary to introduce an appropriate phase shift (30° for an asymmetrical machine) between the two sets of modulation (reference) signals for the two three-phase modulators. This consideration applies to both carrier-based SPWM and carrier-based PWM with zero-sequence injection (which is now termed double zero-sequence injection), which improves utilisation of the dc bus voltage without moving into the over-modulation region [Bojoi et al. (2002)].

In the SVPWM technique, a set of sinusoidal reference voltages is represented as a reference voltage vector and certain number of space vectors will be used over one switching period (each with appropriately calculated dwell time) in order to produce output voltage vector that has an average value that is equal to the reference. Since only voltages and currents in the (α-β) plane are related to electromechanical energy conversion, the goal of SVPWM is to synthesize the (α-β) voltage vector that satisfies the machine's torque and flux control requirements. Simultaneously, since references in other planes are zero, it also has to maintain the average volt-seconds in (x-y) and (0_+-0_-) planes equal to zero during every inverter switching period, since this eliminates low-order harmonics from the output voltage.

Several ways of selecting the most appropriate voltage vectors have been reported for the implementation of SVPWM for an asymmetrical six-phase machine with two isolated neutral points. One possibility is to use in essence conventional three-phase SVPWM approach. The desired reference voltage vector is synthesized by using only three voltage vectors (two active voltage vectors and one zero voltage vectors), similar to the SVPWM widely used for three-phase machines. These two active voltage vectors are selected from the outermost 12-sided polygon (i.e the largest magnitude space vector) of the (α-β) plane [Gopakumar et al. (1993)]. This selection implies low switching frequency and maximises dc bus voltage utilization of the inverter. However, since control is only exercised in the (α-β) plane, the voltages in (x-y) plane are not averaged to zero and current harmonics in this plane are left free to flow. As a result, large low-order harmonic currents (especially

the fifth and the seventh harmonics), that do not contribute to flux/torque production, flow in the motor phases, hence causing a significant power loss in the machine.

The low-order current harmonics can be greatly reduced by using Vector Space Decomposition (VSD) based technique [Zhao and Lipo (1995)]. Harmonic components of the order $6k \pm 1$ (k = 1, 3, 5...) can be eliminated in a drive with two isolated neutral points if the reference voltage vector is synthesized by using four neighbouring active voltage vectors of the largest magnitude (rather than just two), and one zero voltage vector. The aim of this technique is to achieve on average reference (α-β) components, but at the same time it also intends to minimise the average voltage in the (x-y) plane. Significant low-order harmonic reduction is achieved in this way, but unfortunately at the expense of heavier computational burden.

In order to reduce the computational burden, one paper has reported the derivation of mathematical equations to calculate the dwell time of applied voltage vectors. The equations are derived by introducing a fictitious mid voltage vector [Shan et al. (2005)]. Twelve mid voltage vectors are introduced and each vector is composed from three adjacent voltage vectors with the largest amplitude. The equations to calculate the dwell time are firstly derived based on utilisation of two mid voltage vectors and a zero space vector. The dwell times for the four active space vectors are then derived based on the relationship between the mid space vectors and three active space vectors that generate the mid space vector.

The computational burden can also be significantly reduced if the dwell time of the voltage vectors is calculated offline [Hadiouche et al. (2006)]. Two modulation strategies are then realised, continuous and discontinuous, which differ in the placement of the zero vectors during the sampling period. The modulation technique is continuous when on/off switching occurs within every sampling period, for all inverter legs and all sectors. The modulation technique is discontinuous when one (or more) inverter leg stop(s) switching, i.e the corresponding phase voltage is clamped to the positive or negative dc bus rail for at least one sector. Both modulation techniques lead to different harmonic distortion characteristics where the discontinuous modulation technique produces the best result.

The SVPWM techniques reported in [Hadiouche et al. (2006), Shan et al. (2005), Zhao and Lipo (1995)] are developed based on dividing the (α-β) and (x-y) planes into twelve 30° sectors. Some SVPWM strategies unfortunately cause asymmetrical switching sequence in some of the inverter's legs and normally more than two switch transitions (from high to low or from low to high) are encountered during a sampling period. In order

to simplify digital signal processor (DSP) implementation of the control strategy and to reduce switching losses due to the high number of on/off transitions of the switches, a SVPWM technique that is based on 24 sectors (15° each) is developed [Marouani et al. (2008)]. The 24-sector SVPWM scheme is executed by utilising three voltage vectors with the largest-magnitude, one voltage vector with the smallest magnitude and a zero space vector during a sampling period where once again different positioning of the zero space vector during the switching period leads to either continuous or discontinuous modulation. The dwell times were also computed offline for optimal DSP implementation and low algorithm execution time. Besides being easy to implement digitally, the proposed scheme also reduces unwanted stator current harmonics which appear due to the structure of the machine.

Numerous types of continuous and discontinuous SVPWM techniques can be implemented due to differences in selection of applied vectors, arrangement in switching sequence and also due to differences in placement and selection of the zero space vector states. Another variation of 12-sector based continuous SVPWM technique has been presented in [Prieto et al. (2010)]. The technique is a modification of the discontinuous SVPWM technique presented in [Hadiouche et al. (2006)] and its performance has been compared with the other 12-sector based techniques, discussed in [Hadiouche et al. (2006)]. Using the proposed modulation, slightly better stator current waveforms in the (α-β) plane can be achieved and better current harmonic content over the medium and low voltage range can be produced.

The appropriate voltage vector selection and the subsequent dwell time calculation are easier to implement if the six-phase inverter is considered as two independently switched three-phase inverters. Several SVPWM approaches based on this three-phase strategy have been explored, leading to the modulation of two three-phase VSIs. In one approach, the appropriate voltage vectors and dwell times of each three-phase VSI are determined by using vector classification technique [Bakhshai et al. (1998), Yazdani et al. (2007)]. Using the proposed approach, two reference voltage vectors (that have the same magnitude but are phase shifted by 30°) need to be synthesized. The appropriate voltage vectors and their dwell times are different for the two inverters, and are independently determined by the classification algorithm (which is based on the neural network theory). The implementation of vector classification technique has been conducted for six-phase induction machine [Bakhshai et al. (1998)] and also for six-phase permanent magnet synchronous machine [Yanhui et al. (2010)].

In another three-phase based approach, the reference voltage vectors for the two three-phase inverters are synthesized by using the well known three-phase SVPWM approach (two active and one zero space vectors per sampling period) [Grandi et al. (2008)]. The reference voltage vector for each three-phase system is determined based on the relationships between the multiple space vectors of the six-phase system and the two space vectors of three-phase sub-systems. Using the proposed method, the space vectors of the two three-phase VSIs can also be independently regulated.

A slightly different SVPWM approach has been suggested in [Fangbin et al. (2009)]. The reference voltage vector is practically synthesized by using two neighbouring large space vectors of the six-phase VSI. In order to generate a similar PWM waveform obtainable with these two large space vectors, two voltage vectors in different sectors of two identical three-phase VSIs are used with an objective to reduce switching losses and requirements of hardware implementation. However, since the control is practically exercised in the (α-β) plane only, the low-order harmonics are left free to flow in the (x-y) plane, hence contributing to the machine losses.

In addition to all the SVPWM techniques that have been discussed above, a SVPWM strategy that concentrated on achieving zero common mode voltage has also been reported. The common mode voltages create coupling currents that flow through the motor parasitic capacitances toward the rotor iron. These currents find their way via the motor bearings back to the grounded stator case and form the so-called bearing currents which cause bearing deterioration. The necessary condition to achieve zero common mode voltage is that the sum of all six leg voltages must be equal to zero instantaneously. This constraint forces the inverter to operate with three upper and three lower switches closed at all times [Oriti et al. (1997)]. As a consequence, only twenty voltage vectors out of 64 switching states can be utilised. The other 44 cannot be used; this restricts maximum achievable fundamental voltage to a lower value, compared to other methods, but has the benefit of eliminating the common mode voltage.

Two-level inverter supplying an asymmetrical six-phase machine with stator winding connected to a single neutral point is rarely used in practice. Due to utilisation of the single neutral point, the drive utilise a lower maximum dc bus voltage compared to drive with two-isolated neutral points. Besides that, flow of the zero-sequence current flow is also become possible with a single neutral point connection. This configuration however offers better post-fault operating characteristics since, after one phase becomes faulty, there are still four degrees of freedom left (in the two neutral points configuration only two degrees

of freedom for post-fault control remain). These extra degrees of freedom give more flexibility for designing post fault control strategies such as discussed in [Dong et al. (2008b), Jen-Ren and Lipo (1994), Zhao and Lipo (1996a), Zhao and Lipo (1996b)]. The superiority of performance produced by machine with a single neutral point over configuration with two isolated neutral points, in terms of the achievable torque and stator winding losses during post-fault operation is investigated [Che et al. (2013)]

2.2.2 Symmetrical six-phase drives

Compared to the asymmetrical six-phase drives, the operation of a six-leg inverter has been less investigated for symmetrical configuration of six-phase drives. It was shown in early days of multiphase drives that, even though the symmetrical six-phase drives with two isolated neutral points can also be easily supplied by two two-level three-phase VSIs operated based on the six-step mode, their pulsating components of torque occur at the same frequency as for the three-phase drives, hence becoming less advantageous than the asymmetrical configuration [Nelson and Krause (1974)]. A similar investigation has also been conducted recently for six-phase induction machines with an arbitrary angle of displacement between the two stator winding sets. It has been found that the performance of a six-phase machine with 30° displacement leads to smoother machine operation than the 60° displacement due to the reduction in torque ripple [Singh et al. (2003)].

An early attempt to implement SVPWM technique to control a six-phase VSI supplying symmetrical six-phase induction motors with two isolated neutral points is reported in [Correa et al. (2003a)]. With two isolated neutrals points, the voltage vectors in (0_+-0_-) plane are all equal to zero, therefore the main objective of the investigation is how to devise an appropriate space vector approach so that a reference vector in (x-y) plane is on average equal to zero. Three approaches were examined. In the first one, called six-phase mapping, the space vector region in the (α-β) plane is divided into twelve 30° sectors, while in the second approach, termed fragmented mapping, the (α-β) plane is split into six 60° sectors (each is then divided into four triangular areas). The third approach is double three-phase mapping where the six-phase machine is treated as two independent three-phase machines. In the first and the second approach, the reference vector is synthesised by using five active voltage vectors (although four are sufficient when neutrals are isolated),while in the last approach the apportioned reference vector is synthesised independently by each of three-phase inverter by utilising two active space vectors during

a sampling period. A performance comparison between the three approaches has been presented and it has been concluded that the fragmented sector mapping and double three-phase mapping yield better performance than the six-phase mapping in terms of total harmonic distortion (THD).

SVPWM techniques for symmetrical six-phase drives with a single neutral point have also been investigated. In principle, having a symmetrical six-phase machine with single neutral point means that the selection of space vectors becomes more involved, compared to the configuration with two isolated neutral points, since there are some nonzero voltage vectors in (0_+-0_-) plane. For this configuration, the position of 64 voltage vectors in (α-β) and (x-y) planes can be visualised as being composed of three different polygons formed by vectors of different amplitudes, known as the large vector set, medium vector set and small vector set. In order to minimise current harmonics, one SVPWM method has been suggested, which utilises two coincident voltage vectors from the medium vector set of (α-β) plane, for which in (x-y) and (0_+-0_-) planes corresponding voltage vectors are in the opposite direction or have a zero value [Kianinezhad et al. (2005)]. Two different switching sequences, asymmetric and symmetric, were analysed. However, since these two coincident voltage vectors are selected from the medium vector set, the utilisation of the dc bus voltage cannot be maximised.

A different SVPWM scheme, that systematically applies large, medium and small voltage vectors during one period, has managed to produce sinusoidal or near-sinusoidal output across the whole range of the achievable fundamental output voltage [Dujic et al. (2007a)]. Using the proposed SVPWM scheme, the undesirable low-order harmonics are kept at zero values up to the output fundamental equal to 86.6% of the maximum achievable. Beyond that, the low-order harmonics are gradually introduced and they only reach the maximum values when the reference reaches the maximum achievable fundamental output voltage.

There are also some papers that report a strategy to eliminate or reduce common mode voltage. In order to achieve instantaneous zero common mode voltage, a dual three-phase bridge inverter is used to generate balanced excitation for a dual-voltage three-phase induction motor [von Jauanne and Haoran (1999)]. The common mode voltage can also be eliminated by using SVPWM approach [Correa et al. (2003a)]. Twenty voltage vectors that can be used to produce zero common mode voltage are utilised in conjunction with sectors of either 30° or 60° span. Then, several approaches to the space vector selection have been investigated in order to eliminate either the mean value or the instantaneous value of the

instantaneous common mode voltage. Besides that, the SVPWM scheme reported in [Dujic et al. (2007a)] has also been able to produce a common mode voltage that is zero on average and does not contain any low-frequency components.

Besides that, it has to be mentioned that similar to asymmetrical six-phase system, some literatures have also report the post-fault strategies for two-level symmetrical six-phase drives. Among the literatures are [Jacobina et al. (2004), Kianinezhad et al. (2008)].

2.3 PWM control of multilevel multiphase drives

Multilevel multiphase inverters are a natural extension of two-level multiphase inverters, with an intention to provide the multiphase machines with a better quality of voltage supply. Besides that, the utilisation of multilevel multiphase inverters also offers a possibility to produce a higher output power than with the two-level multiphase inverters. The topology of multilevel multiphase drives is relatively new compared to its two-level counterpart; therefore the body of work that relates to the multilevel multiphase drives is limited at present. Nevertheless, considerations related to utilisation of multilevel multiphase inverters for high power applications have already been reported for several applications [Gritter et al. (2005), Lu and Corzine (2005), Neugebauer et al. (2004), Steiner et al. (2000)].

As explained in Chapter 1, multilevel multiphase drives can be realised in two ways, in single-sided supply and dual-inverter supply topologies. In the next sub-section, PWM techniques for the single-sided supply topology will be reviewed first. This is then followed by the dual-inverter supply topology. For the dual-inverter supply topology, if the scope of the discussion is restricted to six-phase phase drives, the number of available papers is rather limited. Therefore, the discussion of three-phase and other multiphase drives will also be included, so that the PWM techniques for a machine with open-end winding topology can be sufficiently reviewed.

2.3.1 Single-sided supply topology

The single-sided supply topology of multilevel inverter was initially reported for a three-phase drive in [Nabae et al. (1981)]. Since then, research related to this topology has been carried out continuously including multiphase drives in recent times.

For a multilevel three-phase VSI, the traditional carrier-based PWM techniques, developed for two-level inverters, have been successfully modified and implemented by

using multiple carriers to control different pairs of semiconductor devices. For multicell topologies, such as FC and CHB VSIs, each cell can be modulated independently by using sinusoidal bipolar or unipolar PWM techniques. Carrier-based technique can be modified by using phase-shifted PWM (PS-PWM) method. Here, the carrier signals are phase-shifted by 180°/*m* for CHB VSI and by 360°/*m* for FC VSI (*m* is the number of cells) across the cells to produce stepped multilevel output waveform with low distortion [Wu (2006)]. In contrast to PS-PWM, level-shifted PWM (LS-PWM) spreads the carriers' amplitude vertically across the whole amplitude range that can be generated by the inverter. Three different schemes are available, depending on the disposition of the carriers. First, in phase disposition scheme (PD-PWM), all carriers are in phase with each other. Second, for phase opposition disposition scheme (POD-PWM), all positive carriers are in phase with each other but in opposite phase with the negative carriers. Lastly, for alternate phase opposition disposition scheme (APOD-PWM), all carriers are alternately in phase opposition [Wu (2006)]. Although LS-PWM could be implemented for any multilevel topology, it is best suited to the NPC VSI since each carrier signal can be easily related to each pair of power semiconductors.

Just like with traditional carrier-based PWM, SVPWM algorithms that were initially introduced for two-level three-phase inverters have also been extended to multilevel three-phase inverters. SVPWM algorithms with reduced complexity and computational burden have been introduced in order to deal with an increasing number of space vectors for higher VSI level numbers [Celanovic and Boroyevich (2001), Prats et al. (2002)]. In addition to PWM for the linear modulation range, a number of papers have also presented SVPWM algorithms that can be extended into overmodulation range [Aneesh et al. (2009), Gupta and Khambadkone (2007), Shiny and Baiju (2010)]. Generalized three-dimensional (3D) SVPWM algorithms that alleviate various problems that cannot be solved by conventional two-dimensional SVPWM have also been reported [Franquelo et al. (2006), Prats et al. (2003)].

Besides all the mentioned papers which mostly report on generalised SVPWM strategies that can be applied for a three-phase VSI with any number of levels, there are also many other papers that are not included in this discussion, which address various SVPWM strategies that pursue various objectives such as minimising the switching frequency, simplifying calculation complexity, common mode voltage reduction (or elimination), voltage balancing, unbalanced system operation, etc.

In contrast to the multilevel three-phase VSIs, only a few papers related to multilevel six-phase drives are available. These are mostly related to asymmetrical six-phase drives, since the control can be made by phase-shifting the references of two three-phase VSIs by 30°. The multilevel multiphase PWM control for asymmetrical six-phase induction machine, proposed in [Oudjebour et al. (2004)], is basically developed based on carrier-based PWM technique for a multilevel three-phase VSI. The drive is operated by using two five-level NPC VSIs and the PWM strategy of each inverter is realised based on comparison of four phase-shifted carrier signals with reference signals that include zero-sequence injection. Experimental results of the indirect field oriented control of the drive are presented.

The implementation of the same PWM strategy has also been proposed for an asymmetrical six-phase induction machine fed by two three-phase five-level VSIs [Oudjebour and Berkouk (2005)]. Each leg of the three-phase inverter consists of four overlapped cells and each cell carries dc source(s) and two switches that work complementarily. Besides the carrier-based PWM with zero-sequence injection, the performance of the drive has also been investigated by implementing traditional SPWM method.

Implementation of SVPWM techniques for multilevel six-phase drives is reported for a six-phase synchronous machine [Yao et al. (2006)]. The machine is supplied by using two three-phase three-level NPC VSIs and each inverter is controlled separately by using SVPWM method that was initially developed for a three-phase VSI [Yao et al. (2004)]. For the SVPWM implementation, the (α-β) plane of the three-phase system is divided into six sectors and each sector is then split into six major triangular sectors. When the reference vector lies in one of the sectors, it will be synthesised by using three nearest space vectors. A strategy to tackle neutral-point unbalance, one of inherent problems in three-level NPC VSI, is also addressed based on the proposed space vector solution. Since the SVPWM technique is developed based on a three-phase inverter, the stator current contains harmonics, mainly the fifth and the seventh harmonics.

The SVPWM strategy can also be used for elimination of common mode voltage of a multilevel multiphase VSI. Such a method is targeted for asymmetrical six-phase traction drive system having two dc voltage sources which are regulated separately by using three-phase NPC VSI [Oleschuk and Griva (2010)]. In order to eliminate undesirable common mode voltages which are the main contributor to bearing problems in an induction machine, the SVPWM strategy that was initially developed for a three-level three-phase

VSI [Oleschuk and Blaabjerg (2002)] is successfully extended to the six-phase system. Six active space vectors with the largest magnitude are used in conjunction with a synchronised PWM technique, a method to provide synchronisation of the voltage waveform of the inverters which is necessary in order to avoid the occurrence of undesirable sub-harmonics.

In [Neugebauer et al. (2004)], a multilevel multiphase inverter for six-phase MEMS electrostatic induction micromotors is presented. To meet the stringent constrains of the power electronic converter for miniaturised motor, such as high voltage and high frequency operation, precise operating waveform and timing and also capacitive input impedance, a five-level VSI is used in conjunction with six identical transformer-coupled full-bridge inverters. This special inverter was developed because the conventional multilevel-multiphase inverters, such as NPC VSI, FC VSI and CHB VSI, are seen as not well suited for micromotor applications. Each phase of the inverter consists of four full-bridge inverters that are switched by comparing reference sinusoidal signal to a tuneable oscillator output, hence producing a three-level signal with different duty cycle on the primary side of the transformer. These signals are then summed into nine-level signals by connecting the secondary windings in series. The prototype of the drive system has been built in order to evaluate the performance.

2.3.2 Dual-inverter supply topology

The dual-inverter supply topology was initially introduced for open-end winding configuration of three-phase machines [Stemmler and Guggenbach (1993)]. Although the topology has been known for almost two decades, the extension towards the multiphase machines has only been reported in a very few papers, whereas the existing body of work is still mainly concentrated on the three-phase drives. Several papers related to PWM control of dual-inverter supply of open-end three-phase machine will be reviewed first, followed by the discussion of PWM strategies related to dual-inverter supply of open-end multiphase machines.

2.3.2.1 Open-end winding three-phase drives

In dual-inverter supply topology, both ends of the stator winding can be connected to either two-level or multilevel inverters. The two inverters that are connected at both ends of the open-end windings can also have an equal or different number of levels.

The dual-inverter supply system can be looked at from two different viewpoints. The first viewpoint is to consider the system as one unit that can produce an output voltage that has a number of levels which is the same as in output voltage produced by a traditional multilevel inverter (traditional inverter refers to a three-phase VSI in single-sided supply topology). For the open-end three-phase drives, with supply provided from two isolated dc sources, the utilisation of two two-level inverters produces the same output voltage as with a traditional three-level inverter, while the utilisation of two three-level inverters produces the same output voltage as with a traditional five-level inverter [Stemmler and Guggenbach (1993)]. This is achieved by modulating the two three-phase VSIs using carried-based SPWM technique.

Besides carrier-based PWM, the realisation of three-level output voltages from dual two-level inverter supplying an open-end three-phase winding can also be achieved by using SVPWM approach [Shivakumar et al. (2001a)]. The space vectors of the dual two-level three-phase VSIs are positioned at the same nineteen locations as for the traditional three-level VSI. However the number of redundant states is higher for the system with the dual-inverter supply since the space vectors are produced from $2^3 \times 2^3 = 64$ switching state combinations, compared to $3^3 = 27$ switching state combinations of the traditional three-level VSI. The (α-β) plane is divided into 24 equilateral triangles which can be grouped to form six hexagons plus one inner hexagon at the centre. The SVPWM strategy is implemented based on the defined hexagon areas and uses the same technique that was firstly proposed for traditional three-phase inverter [Kim and Sul (1995)]. The redundant switching states are beneficial to minimise the number of switchings per cycle and also to produce equal number of switchings for each inverter. Besides that, the required number of semiconductor devices is also fewer, compared to the traditional three-level inverter.

The number of levels of output voltage produced by the dual-inverter supply topology depends on the ratio of the two isolated dc source voltages that are used. For the two PWM strategies discussed above, the two isolated dc sources have an equal dc voltage. Different levels of output voltage can be produced if unequal ratio of dc voltages is utilised. Dual-inverter supply topology, with dc voltage ratio of 2:1, produces the same output voltage as the traditional four-level VSI [Corzine et al. (1999), Shivakumar et al. (2001b)]. Although the total number of switching states is still 64, the space vectors produced by the unequal dc source voltage ratio are now mapped at 37 locations, just like the space vector mapping produced by $4^3 = 64$ switching state combinations of the traditional four-level VSI. In [Corzine et al. (1999)], the performance of the supply is

compared with traditional four-level NPC VSI, both using SVPWM algorithm which utilises three space vectors that are the nearest to the reference vector [van der Broeck et al. (1988)]. The performance is identical, but the dual-inverter supply topology uses fewer switching devices, has simpler construction and can be implemented without problems associated with the capacitor voltage balancing. Meanwhile, the results presented in [Shivakumar et al. (2001b)] are basically an extension of the work reported in [Shivakumar et al. (2001a)] and just require a slight modification of the SVPWM technique used in the latter.

The ratio of dc supply voltages of the two inverters can be further varied if two multilevel inverters are used. For example, by using two three-level three-phase VSIs, the utilisation of 1:1, 2:1 and 3:1 voltage ratios can produce an output voltage that is equivalent to five-, seven- and nine-level traditional VSI [Corzine et al. (2003)]. In that investigation, one of the three-phase three-level NPC VSIs is supplied from one dc source while the other inverter is supplied by a capacitor voltage source (i.e capacitor bank). The voltage ratio of 3:1 is examined, and due to the usage of the capacitor as the voltage source, some voltage levels are sacrificed. However, there is enough state redundancy that has been used to regulate the capacitor voltage. The inverters are modulated by using nine-level SVPWM and a redundant switching state table and an output voltage that is equivalent to seven-level operation is produced. The proposed SVPWM technique is implemented based on the duty-cycle modulation, a discrete PWM technique that directly determines the nearest space vector selection and calculates their switching times based on per-phase duty cycles [Corzine and Baker (2002)].

This type of control is then further extended to voltage ratio of 4:1 [Xiaomin et al. (2006)]. Performance equivalent to eleven-level operation is practically achieved, except in the high modulation index region. Eleven-level duty-cycle modulation technique is used but some modifications are required with respect to the original strategy of redundant switching state selection, since some switching levels are missing due to the used dc voltage ratio.

Apart from considering the dual-inverter drives as one unit that produces multilevel output voltage for a given number of semiconductor devices, the operation of dual-inverter fed drives can also be viewed as combination of two separate inverters. This is also known as hybrid inverter drives, where the main inverter is known as bulk inverter and its function is to provide the required power to the machine. The second inverter is known as conditioning inverter and its function is to compensate the harmonics produced by the bulk

inverter. The bulk inverter is switched by using low-frequency PWM, while the conditioning inverter is switched by using high frequency PWM. Their operation is properly combined so that the machine is operated with the required power and also necessary power quality.

In Corzine et al. (2003), the control strategy for hybrid inverter control has been developed. The dc voltage ratio of 3:1 is, as noted, used where the conditioning inverter is supplied by a capacitor bank. The bulk inverter is supplied by using the higher voltage supply and is modulated by staircase or low frequency carrier-based PWM method. The conditioning inverter is powered by the lower voltage supply and is utilised as an active power filter, so that its function is to compensate the harmonics produced by the bulk inverter. The conditioning inverter is modulated by using high switching frequency PWM based on duty-cycle modulation technique reported in [Corzine and Baker (2002)]. In order to maintain the capacitor voltage at one third of the main inverter's dc source, a simple proportional-integral (PI) regulator is used to regulate active power flow into conditioning inverter. The implementation of this hybrid inverter control is then realised by using commercial-off-the shelf (COTS) inverter as the bulk inverter, leaving only the conditioning inverter as the one that has to be custom-made [Shuai et al. (2005)]. In order to achieve independent control of the conditioning inverter, an appropriate strategy to sense the bulk inverter voltages has been developed, so that harmonic compensation can be done, synchronised to the programmable bulk inverter staircase.

The hybrid inverter control can also be implemented by using two inverters that have different number of levels. Such an implementation has been reported for open-end three-phase winding machine fed by three-level and two-level inverter at the two winding sides. The dc voltage of the two-level inverter is half of the dc voltage of the three-level inverter [Kawabata et al. (2002)]. The two-level inverter operates as the conditioning inverter and is hence modulated at much higher switching frequency. When the reference voltage vector is small, the system will be operated by using the two-level inverter only, which is modulated by using conventional SVPWM strategy. When the reference voltage vector is high, the three-level inverter will be used to supply 2/3 of the total output power and the rest will be supplied by the two-level inverter. For operation with high reference voltage vector, the vectoral combination of the space vectors of both inverters is divided into thirteen areas. In each area, the reference vector can be synthesised by using a combination of predetermined switching states of the three-level inverter and conventional SVPWM

technique of the two-level inverter. By doing this, the output voltage can reach the same voltage level as the traditional four-level VSI.

2.3.2.2 Open-end winding multiphase drives

So far, the utilisation of dual-inverter supply for the open-end winding multiphase drives has only been reported in relatively few papers. It has to be noted that compared to the other drive configurations that have been discussed earlier, the SVPWM techniques for the open-end winding multiphase drives are much more difficult to develop due to the high number of switching states and space vectors that have to be considered.

The first implementation of dual-inverter supply for a multiphase machine is reported for an asymmetrical six-phase induction machine. The drive is constructed by using two sets of open-end three-phase windings supplied from four two-level three-phase VSIs [Mohapatra et al. (2002), Mohapatra and Gopakumar (2006)]. The inverters that are connected at two ends of the three-phase winding have unequal dc bus voltages. The goal of the research however, was to eliminate the low-order harmonics, and not to produce multilevel output voltage. The space vector switching strategy is appropriately executed so that the fundamental component in the (α-β) plane is added and the low-order harmonics in the (x-y) plane are cancelled. This goal is achieved by utilising 1:0.366 dc bus voltage ratio.

Another reported SVPWM strategy for an asymmetrical six-phase induction machine is also implemented by using quad (four) two-level three-phase VSIs having isolated dc sources [Grandi et al. (2010a), Grandi et al. (2010b)]. The machine is constructed by using two sets of open-end three-phase windings and the two ends of each three-phase winding are connected to two two-level VSIs which mean that the machine behaves as having two isolated neutrals. The two VSIs produce 64 switching state combinations that correspond to eighteen different active space vectors and a zero space vector. The space vectors are mapped into six sectors which are then further divided into four identical equilateral triangles. In each triangle, the reference vector is synthesized by using the nearest three vectors approach [Casadei et al. (2008)]. The reference vector for each three-phase winding is assigned based on the three-phase decomposition approach [Grandi et al. (2008)].The output voltage produced by each pair of two-level VSIs has the same form and number of levels as with the traditional three-level VSI. The power sharing algorithm between the four dc sources is also introduced. Besides that, the fault-tolerant capability of

the quad inverter fed six-phase drives have also been explored [Grandi et al. (2011), Grandi et al. (2012a), Grandi et al. (2012b)].

Dual-inverter supply topology, using two equal and isolated dc bus voltages, has initially been reported for an open-end five-phase drive system [Jones et al. (2010), Levi et al. (2010)]. In [Levi et al. (2010)], the reference vector is split into two halves and then phase-shifted by 180° for the two two-level five-phase VSIs. Two cases of carrier-based PWM with zero-sequence injection control are investigated. In the first case, the triangular carrier signals of the two inverters are phase-shifted by 180° while in the second case, the carrier signals are kept in phase. The PWM strategy with 180° phase-shifted carriers produces a nine-level phase voltage that is the same as with the traditional two-level five-phase VSI with twice the dc bus voltage value. The PWM strategy with carriers in phase also produces nine-level phase voltage, but the voltage is characterised with unequal voltage step size. The second case of carrier signals produces a phase voltage with better harmonic content. Here, the harmonics around the odd multiples of the switching frequency cancel out, hence pushing the switching harmonics to higher frequencies.

In [Jones et al. (2010)], the PWM strategy reported in [Levi et al. (2010)] is studied, but this time the two inverters are modulated using SVPWM approach. This strategy is referred to as equal reference sharing scheme (ERS), since the reference is divided equally between the two inverters. The two inverters are modulated by using the same SVPWM strategy that has been implemented for a single-sided supply of two-level five-phase inverter, which is based on utilisation of four active space vectors (two neighbouring large and two medium) per switching period. The performance is, as expected, the same as with the carrier-based counterpart. The unequal reference sharing scheme (URS) has also been proposed, where the reference between the two inverters is apportioned according to the total modulation index value. Only one inverter is used for operation up to half of the maximum modulation index and the drive is in two-level operation. Two inverters are operated for modulation index higher than half of the maximum, which then produces output voltage as in three-level operation. The same SVPWM strategy as in the ERS scheme is applied for the URS scheme, which is based on utilisation of four active space vectors per switching period. In both ERS and URS algorithms, the complexity of selecting the proper switching states and space vectors for a given reference is able to be reduced by considering the total modulation as a modulation of two independent inverters. These reference sharing algorithms are then extended to six [Patkar et al. (2012)], seven [Bodo et al. (2011a)] and nine-phase open-end winding drives [Bodo et al. (2013a)].

Another SVPWM strategy developed for the open-end winding five-phase drive fed by dual-inverter with isolated dc supplies is the decomposition method proposed in [Jones et al. (2011b)]. Again, in order to reduce the complexity of switching states selection, the overall system is decomposed into two sub-systems with lower complexity. In the developed method, the three-level space vector decagon produced by the dual-inverter supply topology is decomposed into a number of two-level decagons. For operation at less than half of the maximum achievable voltage, the reference is compounded only by the centre decagon. Therefore, the reference is met by operating one inverter only while the other inverter is put in zero state. The active inverter is once more modulated using the same SVPWM strategy initially developed for the single-sided two-level five-phase inverter hence producing two-level mode of operation. For operation at higher modulation index, a strategy similar to hybrid control is implemented where the reference is met by operating one of the inverters based on the ten-step mode while the other inverter is space vector modulated. The space vector modulated inverter is operated based on the multi-frequency operation since the selected space vectors are able not only to control the fundamental but also eliminated any unwanted any low-order harmonics. Some refinement of the developed modulation strategy which tackles the rise of the dc bus voltage for operation slightly higher than half of the modulation index is discussed in [Jones et al. (2012)].

Beside the SVPWM schemes, a modulation strategy that is based on the carrier-based PWM techniques, has also been implemented for the five-phase drives with dual-inverter supply [Bodo et al. (2011b), Bodo et al. (2013b)]. The modulation techniques are adopted from the traditional carrier-based PWM techniques well known for a single-sided three-level inverter which are PS-PWM and LS-PWM. In the developed modulation strategy, modulation signals for the equivalent single-sided topology are adjusted in order to enable their implementation for the dual-inverter supply. The similarities between the performance obtained from drive with the dual-inverter supply and single-sided three-level inverter are verified in [Bodo et al. (2012a)].

Finally, a modulation strategy for the five-phase drives fed by a dual two-level inverter with connected dc bus voltage has also been developed [Bodo et al. (2012b)]. Unlike the dual-inverter supply topology that utilised two isolated dc bus supplies (or four in [Grandi et al. (2010b), Grandi et al. (2012b)]), the utilisation of a single dc bus supply lead to the possibility of zero sequence current flow. Therefore, in order to stop the flow of the zero sequence current, the developed modulation strategies only considers a group of

switching states that produces zero common mode voltage. The switching sequence is then arranged in a manner such that the switching losses is minimised.

2.4 Summary

This chapter has presented a literature review in the area of PWM control for the six-phase drives. PWM techniques for the two-level six-phase drives are discussed first, followed by the PWM techniques for multilevel six-phase drives, covering both single-sided and dual-inverter supply topologies. With regard to the PWM techniques for the open-end winding configuration, the review also includes three-phase and other multiphase drives for the sake of completeness.

From the literature reviewed in this chapter, the references that are considered as strongly related to the research presented in this thesis are summarised in Tables 2.1 - 2.2. The material containing the PWM techniques for control of both asymmetrical and symmetrical six-phase drives with a single-sided supply topology are listed in Table 2.1. The lists are tabulated based on the type of modulation strategy being used and also the number of voltage levels being utilised.

Table 2.1, indicates that, between the two stator winding configurations, six-phase machine with asymmetrical winding configuration attracts more interest from researchers. The windings are commonly configured with two-isolated neutral points since the nonexistence of space vectors in the (0+-0-) plane leads to a formulation of simpler modulation strategy compared to configuration with a single neutral point.

Table 2.2 lists the literature related to PWM techniques for the control of open-end winding multiphase drives tabulated based on the number of phases. So far, for six-phase drives, the currently developed modulation strategies are all related to machine with asymmetrical winding configuration and supplied from four two-level three VSIs with isolated dc supplies. Modulation strategies for machine in the open-end winding configuration, supplied from two two-level six-phase VSIs with isolated dc supplies has not yet been addressed for both symmetrical and asymmetrical six-phase drives even though the utilisation of this particular topology has already been considered for five-, seven-, and nine-phase drives. From a practical point of view, two isolated dc supplies are easier to implement and more cost effective than four isolated dc supplies. However, the control becomes more complicated since the system behaves as having a single neutral point rather than two isolated neutral points.

Table 2.1: Literature related to PWM techniques for control of six-phase drives with a single-sided supply topology.

Modulation strategy	VSI level	Asymmetrical six-phase drives	Symmetrical six-phase drives
Carrier-based PWM	Two-level	Bojoi et al. (2002)	Not available
	Multilevel	Oudjebour et al. (2004) Neugebauer et al. (2004) Oudjebour and Berkouk (2005)	Not available
SVPWM	Two-level	Gopakumar et al. (1993) Zhao and Lipo (1995) Bakhshai et al. (1998) Shan et al. (2005) Hadiouche et al. (2006) Grandi et al. (2008) Marouani et al. (2008) Prieto et al. (2010) Yanhui et al. (2010)	von Jauanne and Haoran (1999) Correa et al. (2003b) Kianinezhad et al. (2005) Dujic et al. (2007a)
	Multilevel	Yao et al. (2006) Oleschuk and Griva (2010)	Not available

Table 2.2: Literature related to PWM techniques for control of open-end winding multiphase drives.

Modulation strategy	Six-phase drives (asymmetrical)	Other multiphase drives
Carrier-based PWM	Not available	Levi et al. (2010) - five-phase Bodo et al. (2011b) - five-phase Bodo et al. (2012a) - five-phase Bodo et al. (2013b) - five-phase
SVPWM	Mohapatra et al. (2002) Mohapatra and Gopakumar (2006) Grandi et al. (2010a) Grandi et al. (2010b) Grandi et al. (2011) Grandi et al. (2012a) Grandi et al. (2012b)	Jones et al. (2010) - five-phase Bodo et al. (2011a) - seven-phase Jones et al. (2011b) - five-phase Bodo et al. (2012b) - five-phase Bodo et al. (2013a) - seven- and nine-phase cases

Chapter 3

PWM TECHNIQUES FOR TWO-LEVEL ASYMMETRICAL SIX-PHASE DRIVES

3.1 Introduction

This chapter focuses on PWM techniques for a two-level asymmetrical six-phase drive. Two types of topology are discussed and their space vector models are explained. The most common topology is discussed first, which is two-level six-phase VSI supplying an asymmetrical machine with two isolated neutral points. This is followed by the second topology, which is an asymmetrical machine with a single neutral point. PWM techniques for the two-level six-phase VSI feeding asymmetrical machine with two isolated neutral points and single neutral point topologies are reviewed. Two groups of PWM techniques are discussed which are carrier-based PWM and SVPWM. The implementation of each technique is explained and simulations are conducted using MATLAB/Simulink in order to analyse their performance. The work presented in the later half of this chapter has been published in [Patkar and Jones (2013)].

3.2 Space vector model of two-level asymmetrical six-phase VSI

The asymmetrical six-phase machine has two sets of three-phase stator windings that are spatially shifted by 30°. The neutral of the stator windings can be configured in two different ways. The first is to connect the stator windings to two isolated neutral points while the second is to connect all the windings to a single neutral point [Zhao and Lipo (1995)].

In the next subsection, the drive configuration and space vector model for inverter supplying a machine with two isolated neutral points will be explained first. This will be followed by the drive configuration and space vector model for the inverter when the machine has a single neutral point.

3.2.1 Six-phase VSI feeding asymmetrical machine with two isolated neutral points

The power circuit topology of a two-level six-phase VSI supplying an asymmetrical machine with two isolated neutral points is shown in Fig. 3.1. It consists of two three-phase inverters sharing a common dc bus voltage, V_{dc}, while the machine's stator windings are connected in star with isolated neutrals, $n1$ and $n2$. A lower case symbol (*a, b, c, d, e, f*) denotes the machine output phases, while an upper case symbol (*A, B, C, D, E, F*) denotes the inverter legs. The dc bus voltage is assumed to be constant, and the negative rail of the dc bus is denoted by *N*. There are two switches for each inverter leg, where an upper switch and a lower switch work complementarily.

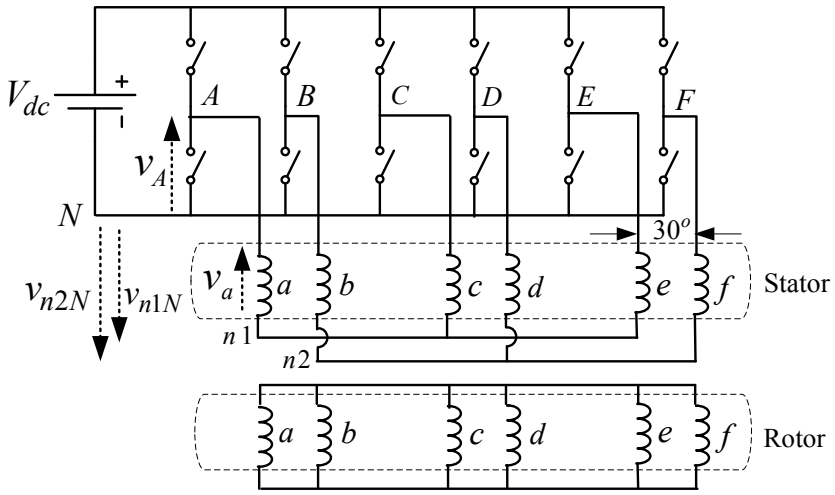

Fig. 3.1: Power circuit topology of two-level six-phase VSI supplying asymmetrical machine with two isolated neutral points.

There are six inverter legs in total; therefore the inverter has $2^6 = 64$ switching state combinations, which in turn determine space vectors. Based on the space vector theory, the switching states lead to 64 voltage space vectors. The space vector model of the inverter is developed with an assumption that the switches have an ideal commutation and zero forward voltage drop.

The correlation between phase voltages and leg voltages of the inverter can be given as follows:

$$\begin{aligned} v_A &= v_a + v_{nN} & v_D &= v_d + v_{nN} \\ v_B &= v_b + v_{nN} & v_E &= v_e + v_{nN} \\ v_C &= v_c + v_{nN} & v_F &= v_f + v_{nN} \end{aligned} \qquad (3.1)$$

Since the phases are star connected with isolated neutral points, then

$$v_a + v_c + v_e = 0 \qquad v_b + v_d + v_f = 0 \qquad (3.2)$$

and summation of (3.1) yields:

$$v_{n1N} = (1/3)(v_A + v_C + v_E) \qquad v_{n2N} = (1/3)(v_B + v_D + v_F) \tag{3.3}$$

The relationship between the phase voltages of the machine and leg voltages of the inverter is obtained by substituting (3.3) into (3.1). The result is as follows:

$$\begin{aligned} v_a &= (2/3)v_A - (1/3)(v_C + v_E) & v_b &= (2/3)v_B - (1/3)(v_D + v_F) \\ v_c &= (2/3)v_C - (1/3)(v_A + v_E) & v_d &= (2/3)v_D - (1/3)(v_B + v_F) \\ v_e &= (2/3)v_E - (1/3)(v_A + v_C) & v_f &= (2/3)v_F - (1/3)(v_B + v_D) \end{aligned} \tag{3.4}$$

The space vectors of the phase voltages can be projected into two orthogonal two-dimensional planes, known as (α-β) and (x-y), and a pair of zero-sequence components (0_+-0_-). By using power variant transformation, the space vectors in the stationary reference frame and zero-sequence components can be defined as follows:

$$\begin{aligned} \underline{v}_{\alpha\beta} &= v_\alpha + jv_\beta = 2/6(v_a + \underline{a}^4 v_c + \underline{a}^8 v_e + \underline{a} v_b + \underline{a}^5 v_d + \underline{a}^9 v_f) \\ \underline{v}_{xy} &= v_x + jv_y = 2/6(v_a + \underline{a}^8 v_c + \underline{a}^{16} v_e + \underline{a}^5 v_b + \underline{a} v_d + \underline{a}^9 v_f) \\ v_{0+} &= 2/6\,(v_a + v_c + v_e) \\ v_{0-} &= 2/6\,(v_b + v_d + v_f) \end{aligned} \tag{3.5}$$

where $\underline{a} = \exp(j\pi/6)$.

The mapping of the phase voltage space vectors into the (α-β) and (x-y) planes is shown in Fig. 3.2, where the value of V_{dc} has been taken as 1 p.u. The zero-sequence components in the (0_+-0_-) axes are equal to zero for all switching state combinations because of the isolated neutrals. The space vectors are labelled with decimal numbers. If converted into binary code, the numbers correspond to the state of an inverter leg in the sequence of (*A, B, C, D, E, F*). Value of "1" indicates that an upper switch in a particular leg is in "on" state, while a lower switch is in "off" state. On the other hand, value of "0" indicates that the upper switch is in "off" state, while the lower switch is in the opposite state.

In total, there are 48 distinct active space vectors in the (α-β) and (x-y) planes. Based on their magnitude, the active space vectors in the (α-β) and (x-y) planes can be categorised into four different groups, which are largest $\underline{v}_{l(k)}$, second largest $\underline{v}_{2l(k)}$, third largest $\underline{v}_{3l(k)}$, shortest $\underline{v}_{sh(k)}$, and zero $\underline{v}_0$ space vectors where index k denotes the k^{th} space vector for each group of space vectors. The groupings of space vectors are shown in Fig. 3.2 and can be expressed using equations presented in Table 3.1. Each group contains twelve distinct space vectors. The third largest space vectors have redundancy, each being produced by

two switching state combinations. On the other hand, the zero space vector is produced by four switching state combinations, which are V_0, V_{63}, V_{21}, and V_{42}.The largest space vectors in the (α-β) plane are mapped as the shortest space vectors in the (x-y) plane and vice versa. In the (α-β) and (x-y) planes, all redundant active space vectors have magnitude of the third largest space vectors.

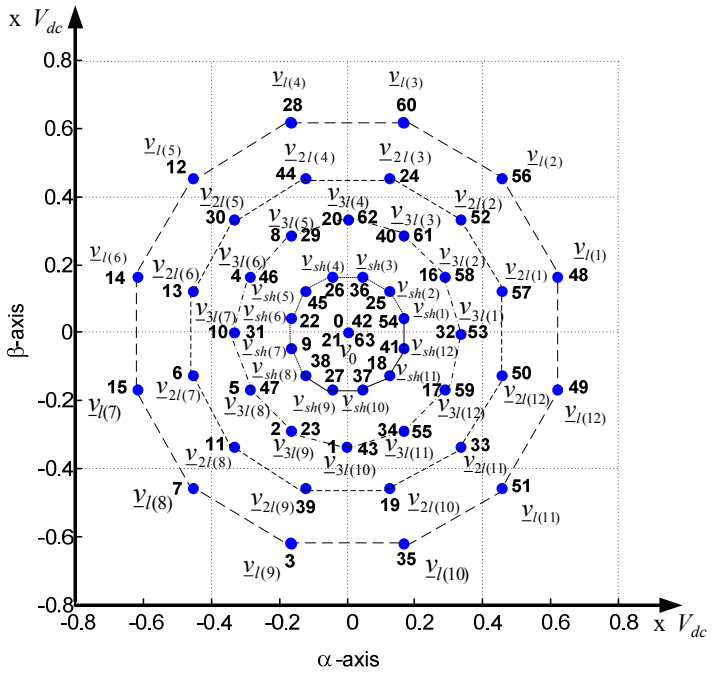

(a)

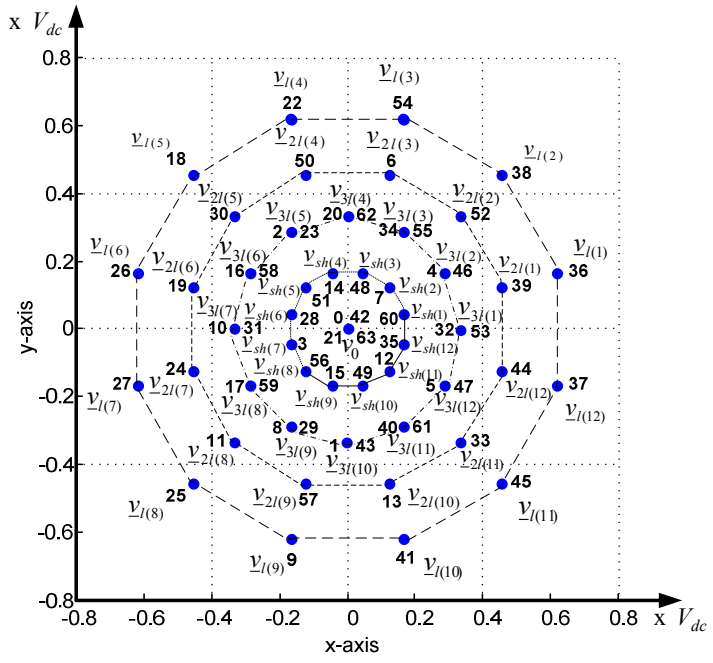

(b)

Fig. 3.2: Mapping of phase voltage space vectors for two-level six-phase VSI supplying asymmetrical machine with two isolated neutral points: (a) in (α-β) plane; (b) in (x-y) plane.

Table 3.1: Space vectors of two-level six-phase VSI supplying asymmetrical machine with two isolated neutral points in (α-β) and (x-y) planes.

Space vectors	Values of space vectors
Largest ($\underline{v}_{l(k)}$)	$\frac{\sqrt{2+\sqrt{3}}}{3} V_{dc} e^{j(2k-1)\frac{\pi}{12}}$ for k = 1, 2, ..., 12
Second largest ($\underline{v}_{2l(k)}$)	$\frac{\sqrt{2}}{3} V_{dc} e^{j(2k-1)\frac{\pi}{12}}$ for k = 1, 2, ..., 12
Third largest ($\underline{v}_{3l(k)}$)	$\frac{1}{3} V_{dc} e^{j(k-1)\frac{\pi}{6}}$ for k = 1, 2, ..., 12
Shortest ($\underline{v}_{sh(k)}$)	$\frac{\sqrt{2-\sqrt{3}}}{3} V_{dc} e^{j(2k-1)\frac{\pi}{12}}$ for k = 1, 2, ..., 12
Zero ($\underline{v}_0$)	0

3.2.2 Six-phase VSI feeding asymmetrical machine with a single neutral point

Two level six-phase VSI supplying asymmetrical machine with a single neutral point is used less frequently than with the machine with two isolated neutral points. The power circuit topology is shown in Fig. 3.3. The stator windings are connected to a single neutral, n.

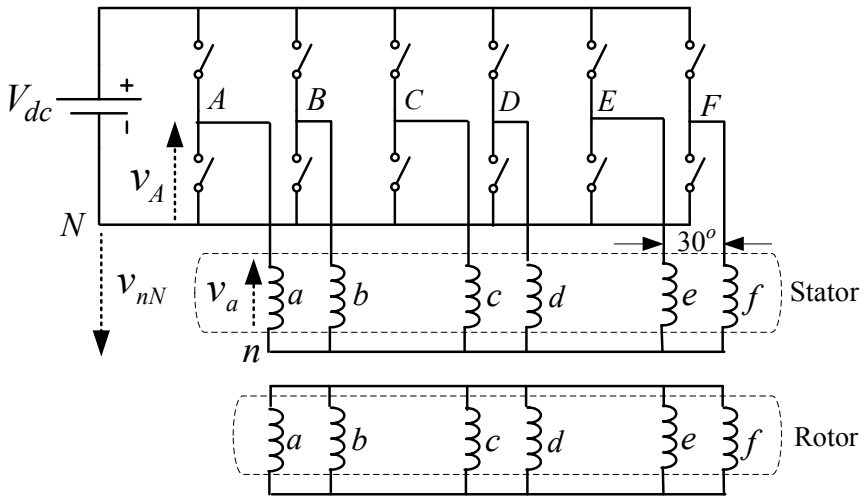

Fig. 3.3: Power circuit topology of two-level six-phase VSI feeding asymmetrical machine with a single neutral point.

The correlation between phase voltages and leg voltages can be given as follows:

$$\begin{aligned} v_A &= v_a + v_{nN} & \qquad v_D &= v_d + v_{nN} \\ v_B &= v_b + v_{nN} & \qquad v_E &= v_e + v_{nN} \\ v_C &= v_c + v_{nN} & \qquad v_F &= v_f + v_{nN} \end{aligned} \tag{3.6}$$

Since the stator windings are now star connected with single neutral,

$$v_a + v_b + v_c + v_d + v_e + v_f = 0 \qquad (3.7)$$

Summation of (3.6) yields:

$$v_{nN} = (1/6)(v_A + v_B + v_C + v_D + v_E + v_F) \qquad (3.8)$$

The relationship between the phase voltages of the machine and leg voltages of the inverter is obtained by substituting (3.8) into (3.6). The result is as follows:

$$\begin{aligned}
v_a &= (5/6)v_A - (1/6)(v_B + v_C + v_D + v_E + v_F) \\
v_b &= (5/6)v_B - (1/6)(v_A + v_C + v_D + v_E + v_F) \\
v_c &= (5/6)v_C - (1/6)(v_A + v_B + v_D + v_E + v_F) \\
v_d &= (5/6)v_D - (1/6)(v_A + v_B + v_C + v_E + v_F) \\
v_e &= (5/6)v_E - (1/6)(v_A + v_B + v_C + v_D + v_F) \\
v_f &= (5/6)v_F - (1/6)(v_A + v_B + v_C + v_D + v_E)
\end{aligned} \qquad (3.9)$$

The space vectors of phase voltages can again be projected into the (α-β) and (x-y) planes and also (0_+-0_-) axes using (3.5). The mapping of space vectors in the (α-β) and (x-y) planes is the same as for configuration with two isolated neutral points (Fig. 3.2 and Table 3.1). Additionally, there are now non-zero components in the (0_+-0_-) axes, such as shown in Fig. 3.4. The non-zero space vector in the (0_+-0_-) axes takes three different magnitudes and grouped as large $\underline{v}_{zl(k)}$, medium $\underline{v}_{zm(k)}$ and short $\underline{v}_{zsh(k)}$ space vectors. The grouping of the space vectors in the (0_+-0_-) axes is as presented in Table 3.2.

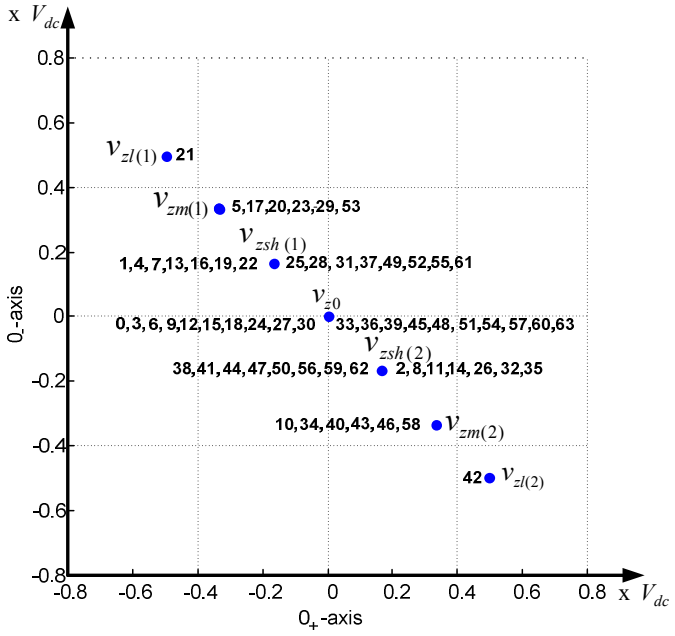

Fig. 3.4: Mapping of phase voltage space vectors for six-phase VSI feeding asymmetrical machine with single neutral point in (0_+-0_-) axes.

Table 3.2: Space vectors of two-level six-phase VSI feeding asymmetrical machine with a single neutral point in (0_+-0_-) axes.

Space vectors	Values of space vectors
Large ($v_{zl(k)}$)	$\frac{\sqrt{2}}{2}V_{dc}e^{(4k-1)\frac{\pi}{4}}$ for k = 1, 2
Medium ($v_{zm(k)}$)	$\frac{\sqrt{2}}{3}V_{dc}e^{(4k-1)\frac{\pi}{4}}$ for k = 1, 2
Short ($v_{zsh(k)}$)	$\frac{\sqrt{2}}{6}V_{dc}e^{(4k-1)\frac{\pi}{4}}$ for k = 1, 2
Zero (v_{z0})	0

3.3 Control of two-level six-phase VSI feeding asymmetrical machine with two isolated neutral points

The most efficient way to control the VSI is by using PWM techniques. Several techniques are available, and, in general can be categorised into two groups: carrier-based PWM and space vector PWM (SVPWM). Each technique is discussed in the following sub-sections, and MATLAB/Simulink simulations are undertaken in order to evaluate their performance.

Simulations are performed by setting the dc bus voltage to 300V and using a switching frequency, f_s, of 2 kHz. Reference frequency is 50 Hz. The modulation index M is set to the maximum value ($M_{\max}$) in the linear PWM region. The modulation index is defined as:

$$M = V_1 / 0.5V_{dc} \qquad (3.10)$$

where V_1 is the peak of the sinusoidal reference, which equals the desired output voltage fundamental. The machine parameters used for the simulation are specified in Table 3.3. These parameters correspond to the machine used later in the experiments.

Table 3.3: Parameters of asymmetrical six-phase machine.

Machine parameter	Value
Stator resistance, R_s [Ω]	12.5
Rotor resistance, R_r [Ω]	12.6
Stator leakage inductance of (α-β) plane, $L_{ls\_\alpha\beta}$ [H]	0.061
Rotor leakage inductance of (α-β) plane, $L_{lr\_\alpha\beta}$ [H]	0.010
Stator leakage inductance of (x-y) plane, L_{ls_xy} [H]	0.005
Stator leakage inductance of (0_+-0_-) plane, L_{ls_0+0-}[H]	0.061
Magnetising inductance, L_m [H]	0.580

3.3.1 Carrier-based PWM

Implementation of carrier-based PWM requires two sets of three-phase sinusoidal waveforms as reference signals. The two sets of reference signals are phase-shifted by 30°. Two types of carrier-based PWM can be implemented. The first one is pure sinusoidal PWM while the second is sinusoidal PWM with two zero-sequence injections (which is sometimes called double zero-sequence injection).

3.3.1.1 Pure sinusoidal PWM

In this technique, two sets of three-phase pure sinusoidal waveforms are generated as reference signals. The range of modulation index for this technique is $0 \le M \le 1$. The reference signals for M_{max} = 1 are as shown in Fig. 3.5. The signals are stated in p.u. where 1 p.u. = V_{dc}. Fig. 3.6 shows phase voltage components of the machine and their frequency spectra. The phase voltage contains fundamental component with 106.066 Vrms magnitude and no low-order harmonics. The fundamental component of α-component voltage has the same magnitude as in the phase voltage, while frequency spectrum of x-component voltage contains only switching frequency associated harmonics.

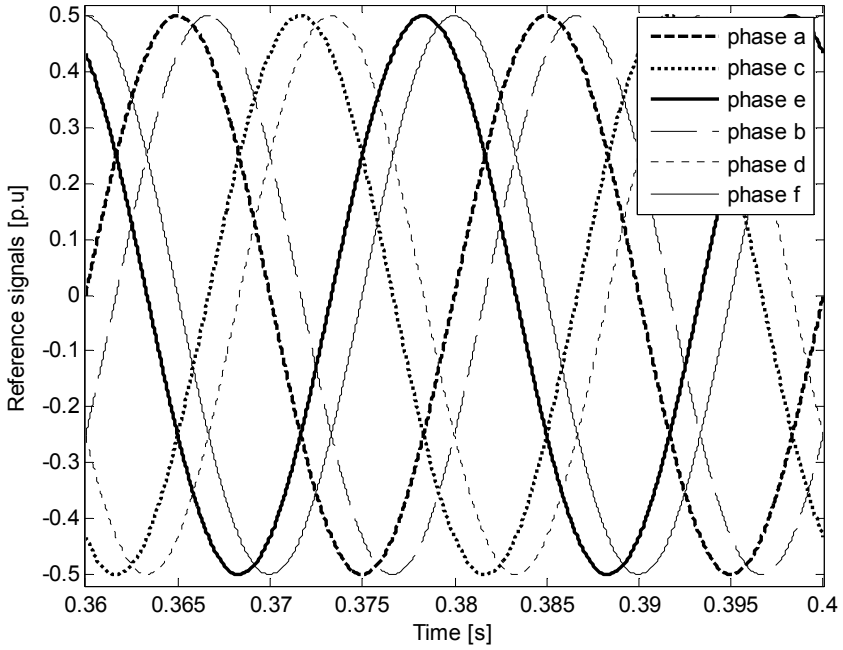

Fig. 3.5: Reference signals for pure sinusoidal PWM technique.

Current components of the machine and their frequency spectra are as shown in Fig. 3.7. The fundamental component of the current is mapped into the α-axis while the current ripple is mapped into the x-axis.

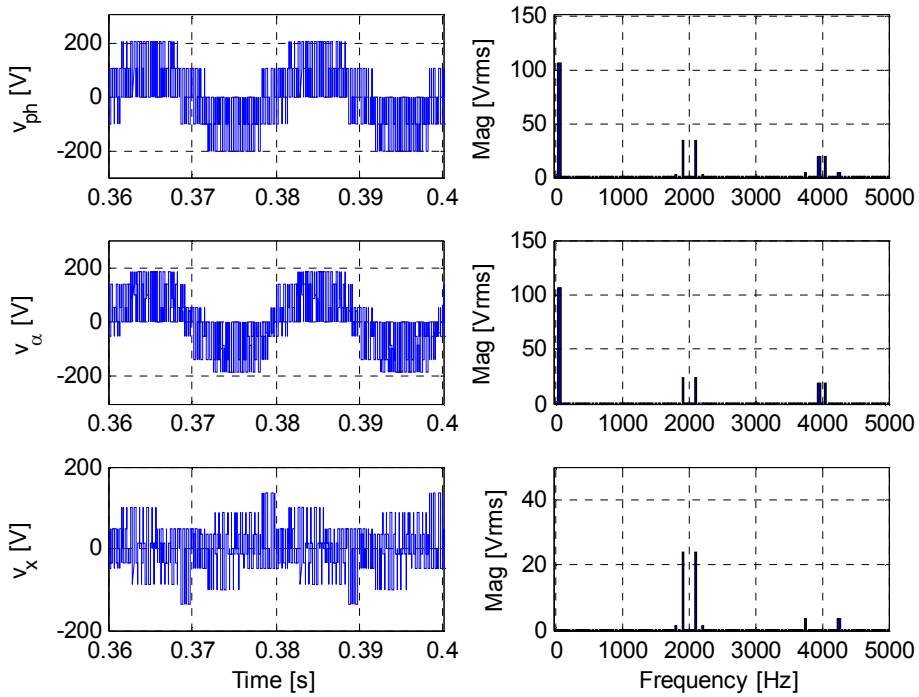

Fig. 3.6: Phase voltage components and frequency spectra for pure sinusoidal PWM technique. From top to bottom: phase voltage, α-component voltage, and x-component voltage.

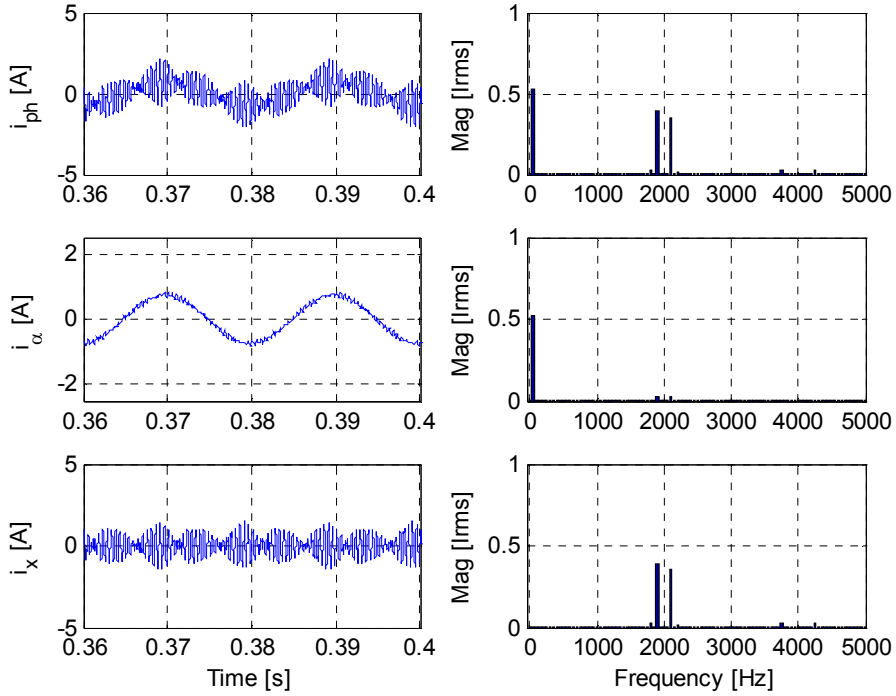

Fig. 3.7: Current components and frequency spectra for pure sinusoidal PWM technique. From top to bottom: phase current, α-component current, and x-component current.

3.3.1.2 Double zero-sequence injection

A zero-sequence signal (third or all triplen harmonics) can be injected into the reference signals of a three-phase inverter in order to increase the dc bus utilisation [Blasko (1996), Houldsworth and Grant (1984)]. The same strategy can be applied here; however it requires an injection of two zero-sequence signals (v_{01} and v_{02}) into the reference signals [Bojoi et al. (2002)], as follows (with *i = a, c, e* and *j = b, d, f*):

$$\begin{aligned} &v_i(t) = v_i{}^*(t) + v_{01} \quad ; \quad v_j(t) = v_j{}^*(t) + v_{02} \\ &v_{01} = -0.5\,[\min(v_a{}^*, v_c{}^*, v_e{}^*) + \max(v_a{}^*, v_c{}^*, v_e{}^*)] \\ &v_{02} = -0.5\,[\min(v_b{}^*, v_d{}^*, v_f{}^*) + \max(v_b{}^*, v_d{}^*, v_f{}^*)]) \end{aligned} \qquad (3.11)$$

The range of modulation index for this technique is $0 \le M \le 1.154$. The reference signals for M_{max} = 1.154 are shown in Fig. 3.8. Phase voltage components and their frequency spectra are shown in Fig. 3.9. Due to the higher maximum modulation index, this technique produces higher maximum fundamental component magnitude than the pure sinusoidal PWM technique. The magnitude of fundamental component for phase voltage and α-component voltage is now 122.4745 Vrms.

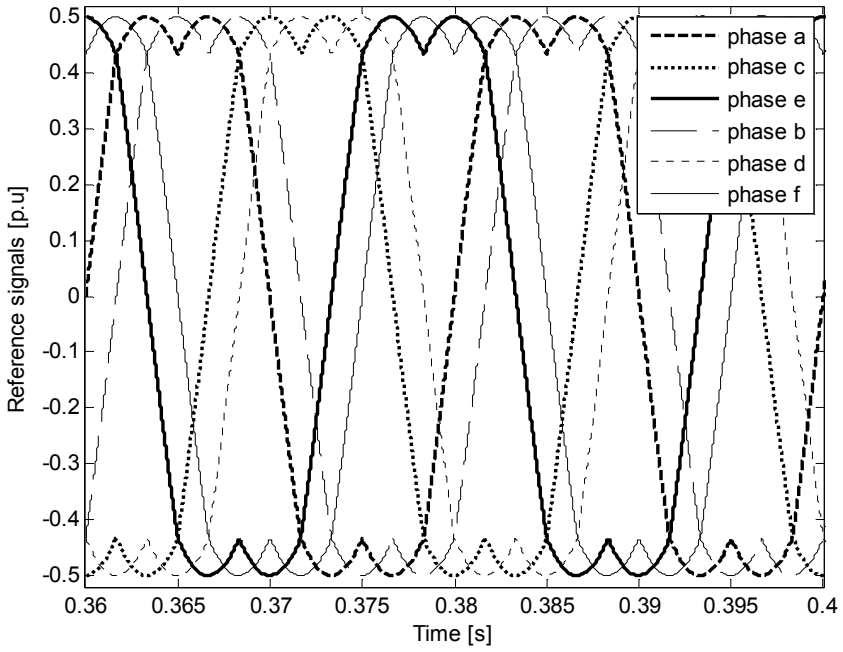

Fig. 3.8: Reference signals for double zero-sequence injection technique.

Current components of the inverter machine and their frequency spectra are as shown in Fig. 3.10. Compared to the pure sinusoidal PWM technique, this technique generates

more sidebands around multiple of switching frequency and increasing current ripple in the *x*-axis.

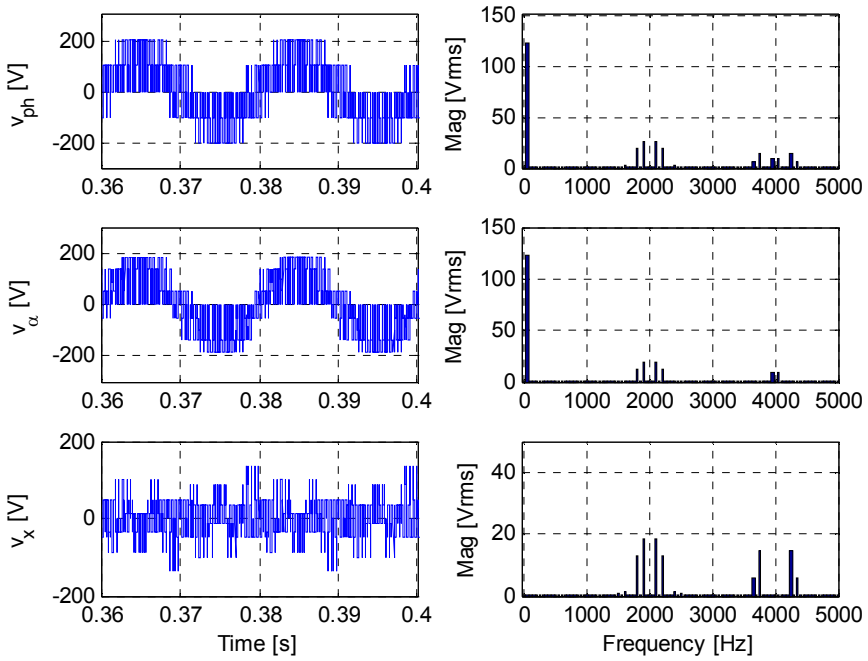

Fig. 3.9: Phase voltage components and frequency spectra for double zero-sequence injection technique. From top to bottom: phase voltage, α-component voltage, and x-component voltage.

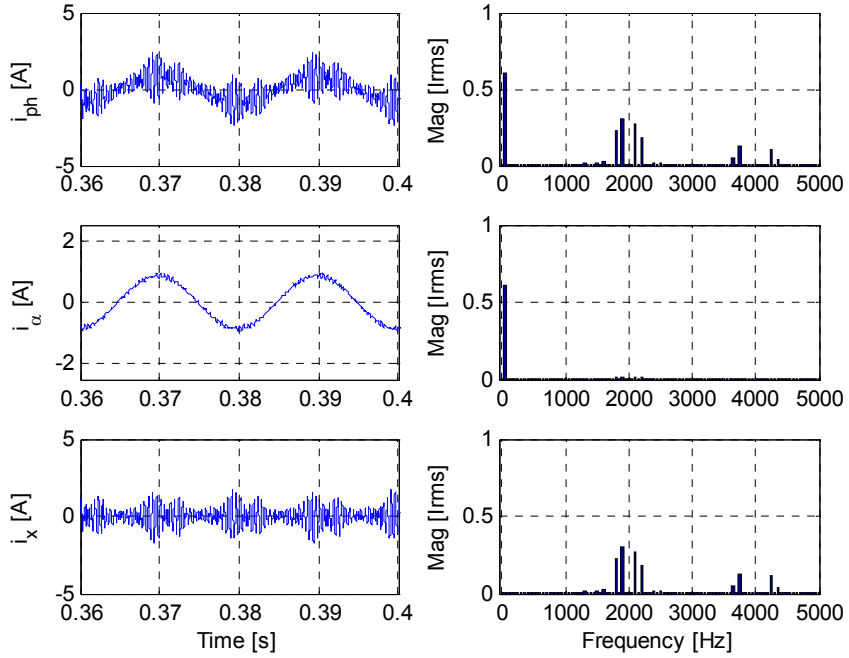

Fig. 3.10: Current components and frequency spectra for double zero-sequence injection technique. From top to bottom: phase current, α-component current, and x-component current.

3.3.2 Space vector PWM

Space vector PWM (SVPWM) is a control algorithm where a reference signal, which is in the (α-β) plane, is synthesized by using several space vectors (combination of active and zero space vectors). The space vectors are appropriately selected and applied for a fraction of time (called dwell time) of a switching period. The space vectors can be selected and applied in many ways, but the main idea is to select the space vectors that produce the highest fundamental component amplitude in the (α-β) plane, while minimising (or zeroing, ideally) all harmonic components in the other plane(s). In this way, the utilisation of dc bus voltage can be maximised, while at the same time minimising the losses generated by harmonics. Two main SVPWM techniques will be discussed here, namely the conventional and the vector space decomposition (VSD) based techniques.

3.3.2.1 Conventional SVPWM

Conventional SVPWM is a modulation technique that is widely applied to three-phase inverters, where in each sector, the reference vector is synthesized by using three space vectors [Wu (2006)]. For a six-phase inverter feeding an asymmetrical machine with two isolated neutrals points, two of the utilised vectors are active space vectors with the largest amplitude, while the third is one of the four switching state combinations of the zero space vector [Gopakumar et al. (1993)]. The selection of the voltage vectors is based on space vector mapping in (α-β) plane. Here, the (α-β) plane is equally divided into twelve 30° sectors (I to XII), as shown in Fig. 3.11. The selected active space vectors for sector I are indicated by thick arrows.

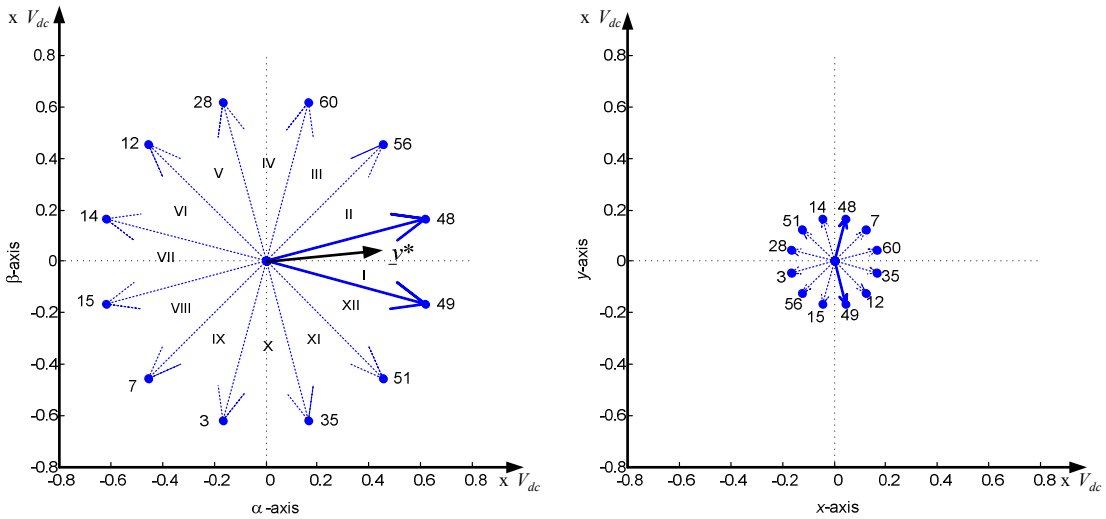

Fig. 3.11: Space vector selection for sector I for conventional SVPWM technique in (α-β) plane (left) and in (x-y) plane (right).

The calculation of dwell times for selected space vectors is done based on Fig. 3.12. The two active space vectors are represented by V_1 and V_2. During a switching period T_s, the reference vector $\underline{v}^*$ is synthesised by means of V_1, V_2 and zero voltage vector, applied for time intervals T_1, T_2 and T_0 respectively.

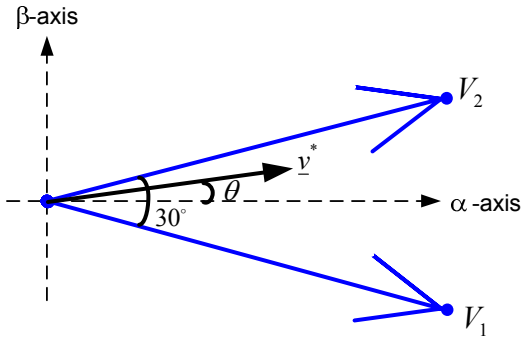

Fig. 3.12: Principle of calculation of dwell time for conventional SVPWM technique.

Based on the volt-second balance principle, the dwell time corresponding to each space vector can be expressed as follows:

$$\begin{aligned} T_1 V_{1\alpha} + T_2 V_{2\alpha} &= V_\alpha^* T_s \\ T_1 V_{1\beta} + T_2 V_{2\beta} &= V_\beta^* T_s \\ T_1 + T_2 + T_0 &= T_s \end{aligned} \qquad (3.12)$$

where α-β subscripts indicate the (α-β) components of the space vector. It can be shown that T_1 and T_2 can be calculated as follows:

$$\begin{aligned} T_1 &= 2\frac{|\underline{v}^*|}{|V|} T_s \sin(30^\circ - \theta) \\ T_2 &= 2\frac{|\underline{v}^*|}{|V|} T_s \sin\theta \end{aligned} \qquad (3.13)$$

$|V|$ is the amplitude of V_1 and V_2 (i.e. the magnitude of the large space vector) and θ is angular position of the reference.

The switching sequences of inverter legs for all twelve sectors are as shown in Fig. 3.13. The selected space vectors for each sector are also listed. The four switching state combinations of the zero space vector are alternately used, so that during the switching period each switch is being switched on and off once only.

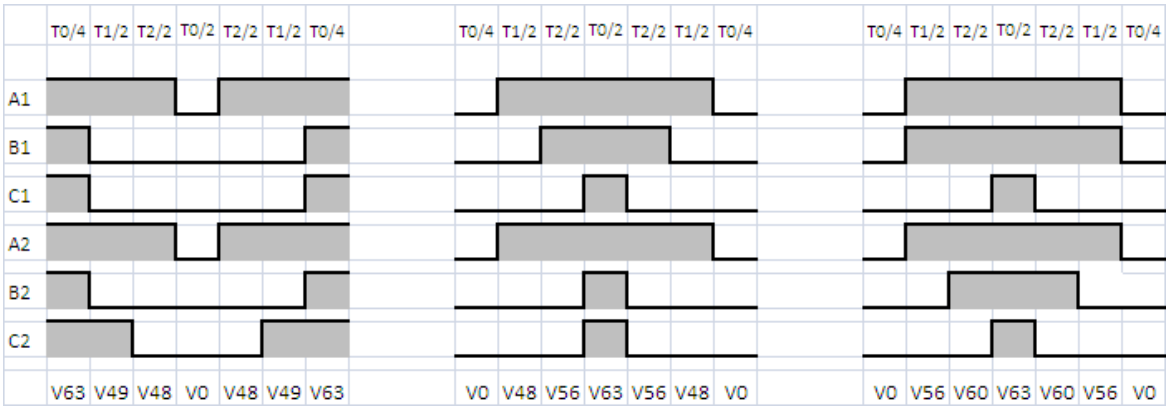

Sector I

Sector II

Sector III

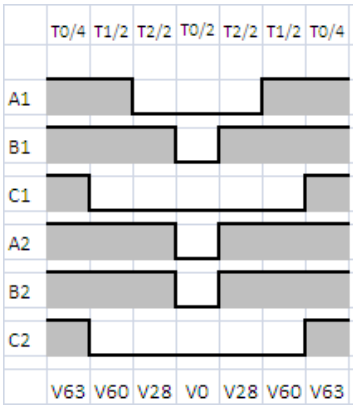

Sector IV

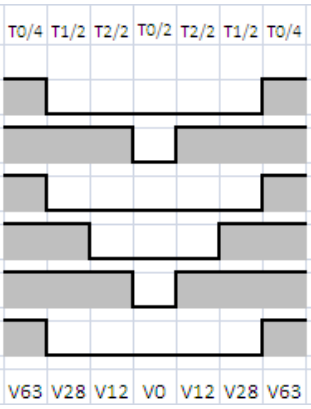

Sector V

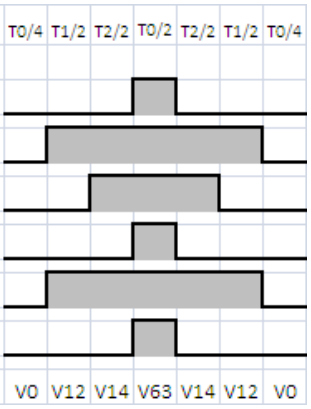

Sector VI

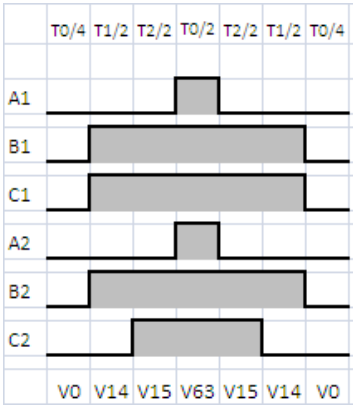

Sector VII

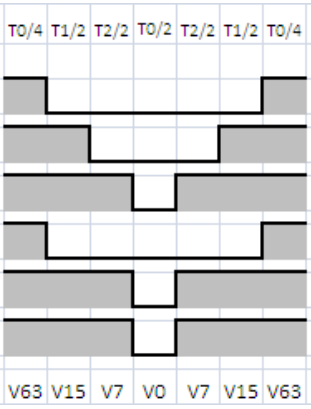

Sector VIII

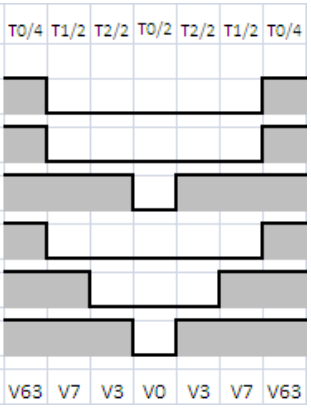

Sector IX

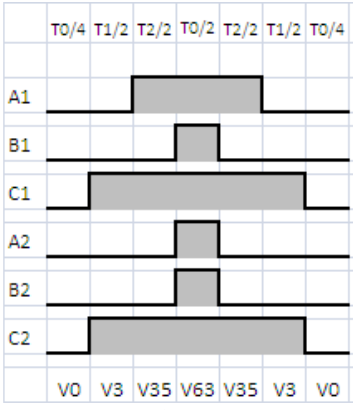

Sector X

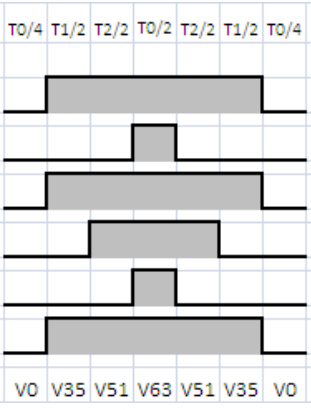

Sector XI

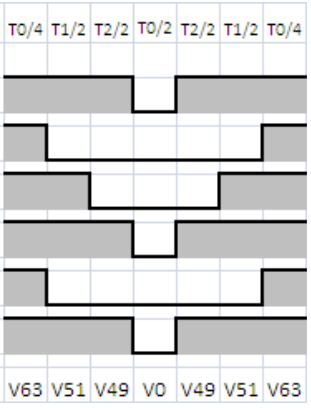

Sector XII

Fig. 3.13: Switching sequences of inverter legs for conventional SVPWM technique.

The range of modulation index for the conventional SVPWM technique is $0 \le M \le 1.243$ .The average leg voltages (in p.u. value) with respect to *N*, produced by applying M_{max} = 1.243 to the reference signal, are as shown in Fig. 3.14. The increase in the maximum modulation index value over the value of 1.154 is achieved at the expense of low-order harmonics which now appear in the (*x*-*y*) plane. This is the consequence of lack of control of the harmonics in the (*x*-*y*) plane since, according to (3.12), only reference in the (*α*-*β*) plane is controlled. In simple words, one has to use four active space vectors in order to achieve on average desired reference in the (*α*-*β*) plane and zero the low-order harmonics in the (*x*-*y*) plane, (i.e. reference for (*x*-*y*) plane is zero).

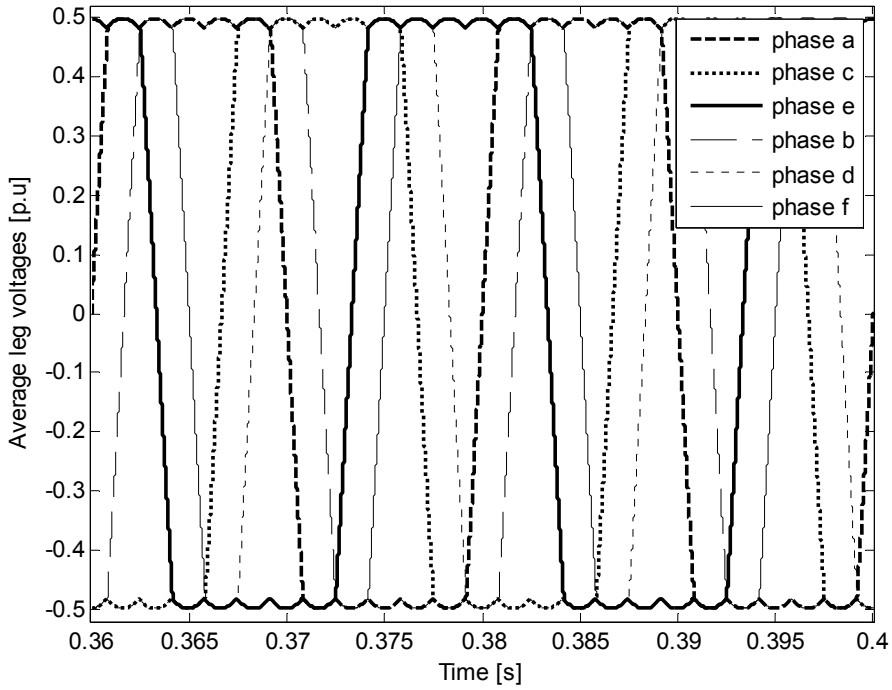

Fig. 3.14: Average leg voltages for conventional SVPWM technique.

Fig. 3.15 shows the phase voltage components of the machine and their frequency spectra, while the current components of the machine and their frequency spectra are shown in Fig. 3.16. There are low order voltage harmonics (5^{th}, 7^{th}, etc) in the (*x*-*y*) plane. As a result, these harmonics are reflected in the current in the machine. For this technique, the magnitude of the fundamental component of phase voltage is 131.8401 Vrms which is higher than the value obtained by the two previous PWM techniques. The phase current has a very high ripple and the ripple is mainly contributed by the 5^{th} and 7^{th} harmonics.

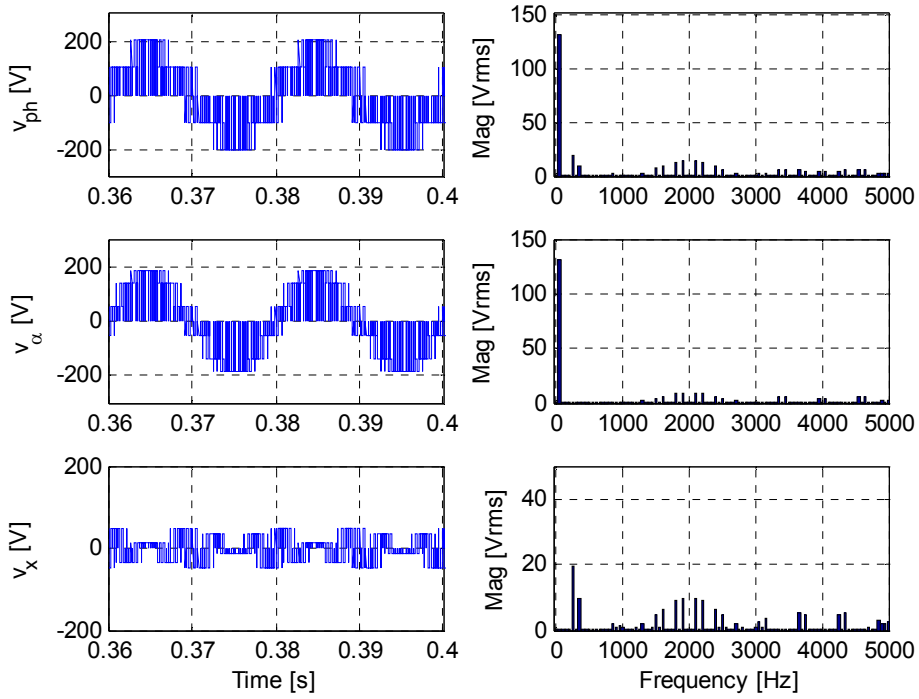

Fig. 3.15: Phase voltage components and frequency spectra for conventional SVPWM technique. From top to bottom: phase voltage, α-component voltage, and x-component voltage.

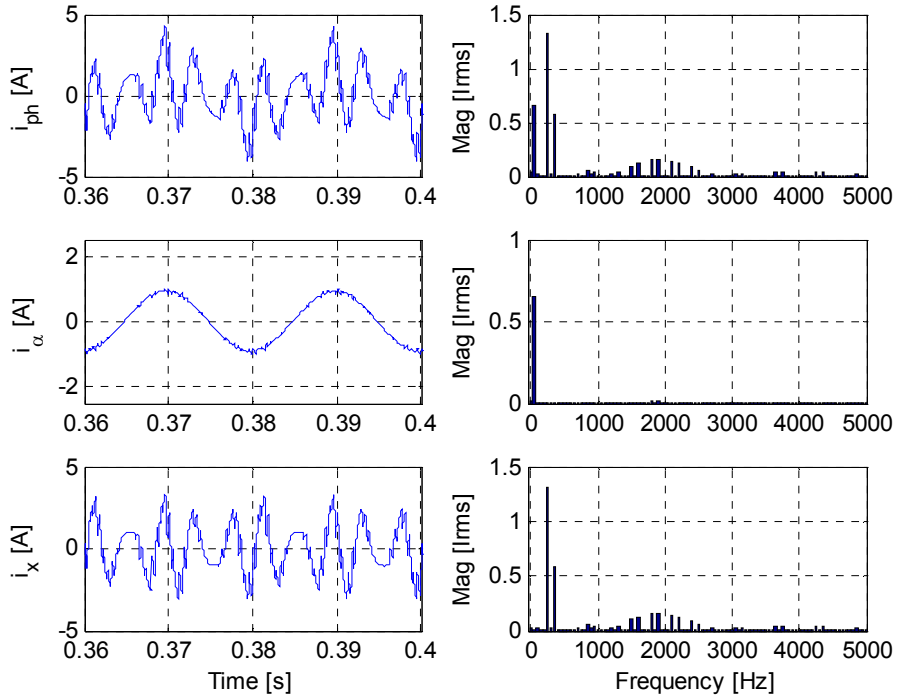

Fig. 3.16: Machine current components and frequency spectra for conventional SVPWM technique. From top to bottom: phase current, α-component current, and x-component current.

3.3.2.2 Vector Space Decomposition (VSD)

In the vector space decomposition (VSD) technique, the reference vector is synthesised by using five space vectors during a switching period [Hadiouche et al. (2006), Zhao and Lipo (1995)]. Four of the space vectors are the active space vectors with the largest amplitude while the fifth is one of the four switching state combinations of the zero space vector. The four active space vectors are adjacent in (α-β) plane but in (x-y) plane they are practically opposite in phase. The selected active space vectors for sector I are shown by thick arrows in Fig. 3.17.

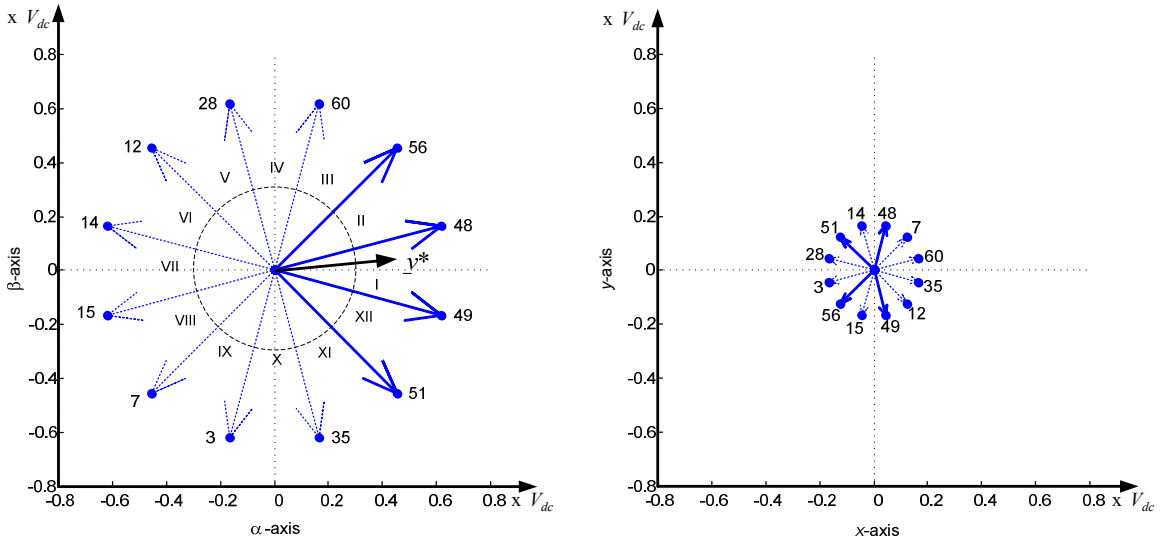

Fig. 3.17: Selected space vectors of VSD technique for sector I in (α-β) plane (left) and in (x-y) plane (right).

Based on the volt-second principle, the time of application (dwell time) for each space vector can be determined as follows:

$$\begin{aligned}
&T_1V_{1\alpha}+T_2V_{2\alpha}+T_3V_{3\alpha}+T_4V_{4\alpha}+T_5V_{5\alpha}=V_\alpha^*T_s\\
&T_1V_{1\beta}+T_2V_{2\beta}+T_3V_{3\beta}+T_4V_{4\beta}+T_5V_{5\beta}=V_\beta^*T_s\\
&T_1V_{1x}+T_2V_{2x}+T_3V_{3x}+T_4V_{4x}+T_5V_{5x}=0\\
&T_1V_{1y}+T_2V_{2y}+T_3V_{3y}+T_4V_{4y}+T_5V_{5y}=0\\
&T_1+T_2+T_3+T_4+T_5=T_s
\end{aligned} \qquad (3.14)$$

where α-β and x-y subscripts indicate the (α-β) and (x-y) components of the space vectors. V_1 to V_4 are used to represent the four adjacent active space vectors, while V_5 is the zero space vector. T_1 to T_5 are dwell times corresponding to the applied space vectors.

The switching sequences of inverter legs for all twelve sectors are as shown in Fig. 3.18(a) and Fig. 3.18(b). The selected active and zero space vectors for each sector are also

listed. Compared to the conventional SVPWM technique, in the VSD technique, the switches in one of the inverter legs are switched on and off three times during a switching period. The switches in the other legs are switched once only.

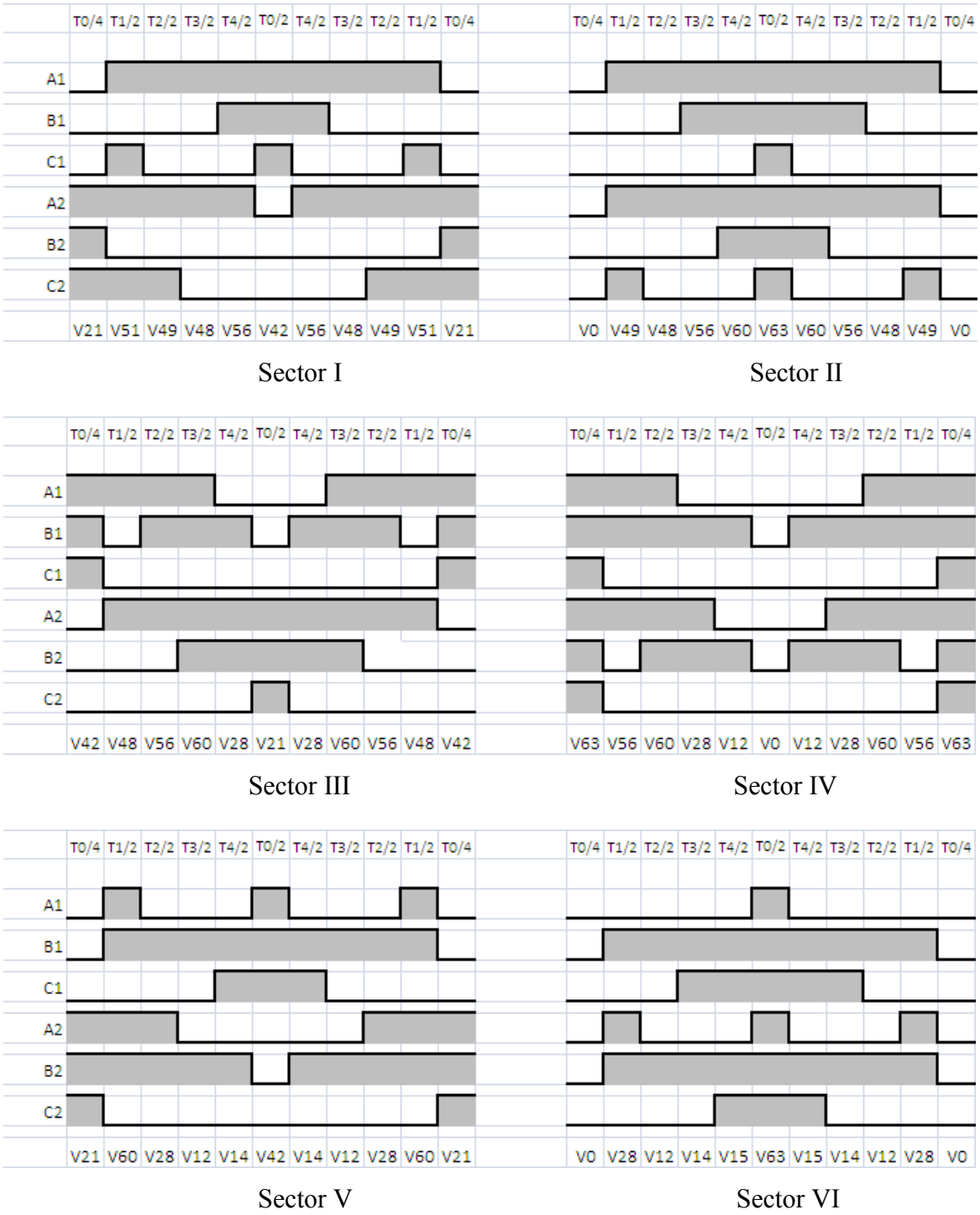

Fig. 3.18(a): Switching sequences of inverter legs for VSD technique for sectors I-VI.

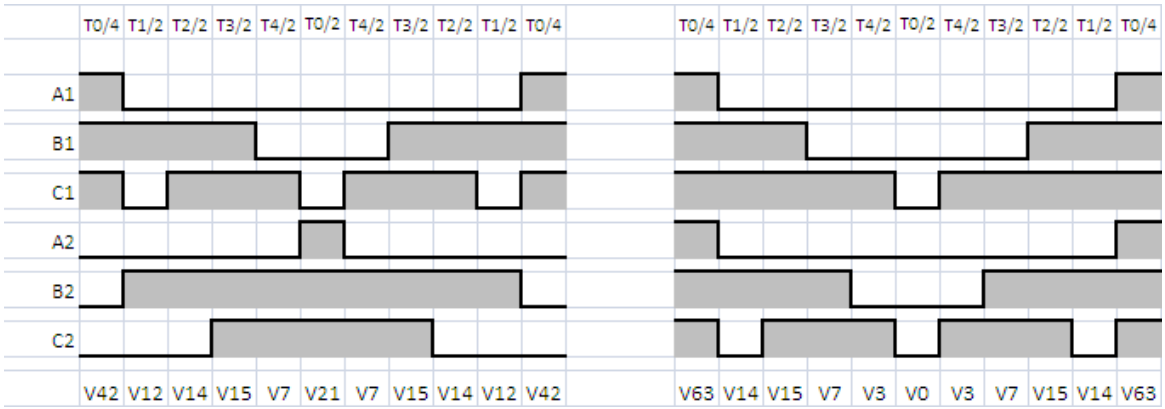

Sector VII Sector VIII

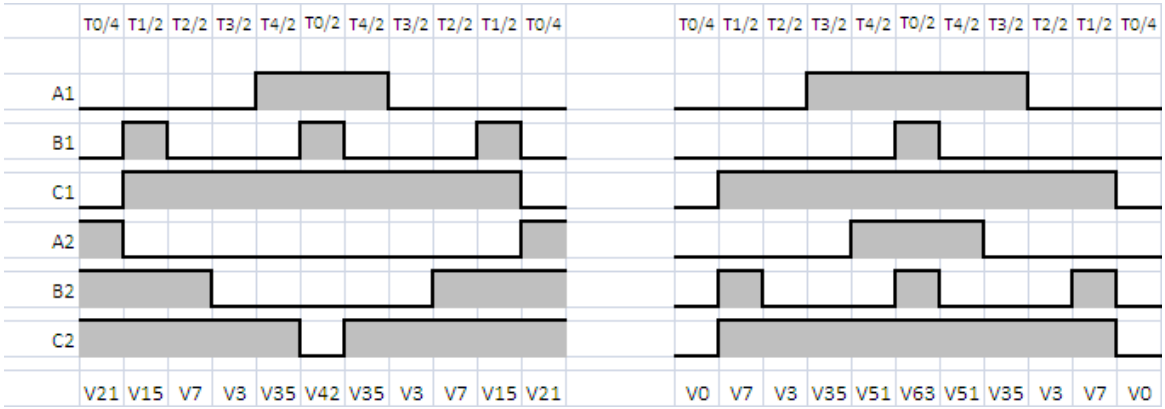

Sector IX Sector X

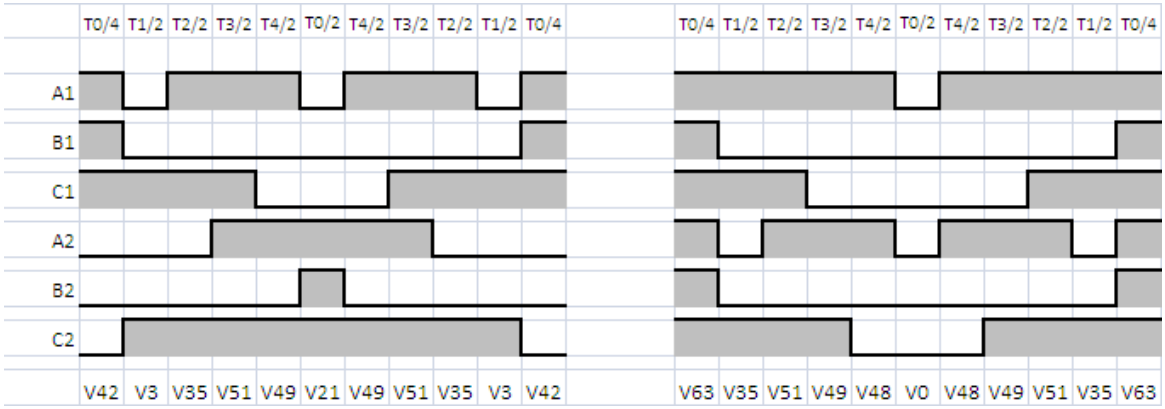

Sector XI Sector XII

Fig. 3.18(b): Switching sequences of inverter legs for VSD technique for sectors VII-XII.

The range of modulation index for the VSD technique is $0 \le M \le 1.1547$. The average leg voltages, produced by applying M_{max} = 1.154 to the reference signal, are as shown in Fig. 3.19. Fig. 3.20 shows phase voltage components of the machine and their frequency spectra, while machine current components of the inverter and their frequency spectra are as shown in Fig. 3.21. Compared to the conventional SVPWM technique, there

are no low-order harmonics created in the (*x*-*y*) plane. However, it produces a lower magnitude of fundamental component of phase voltage, which is 122.4745 Vrms.

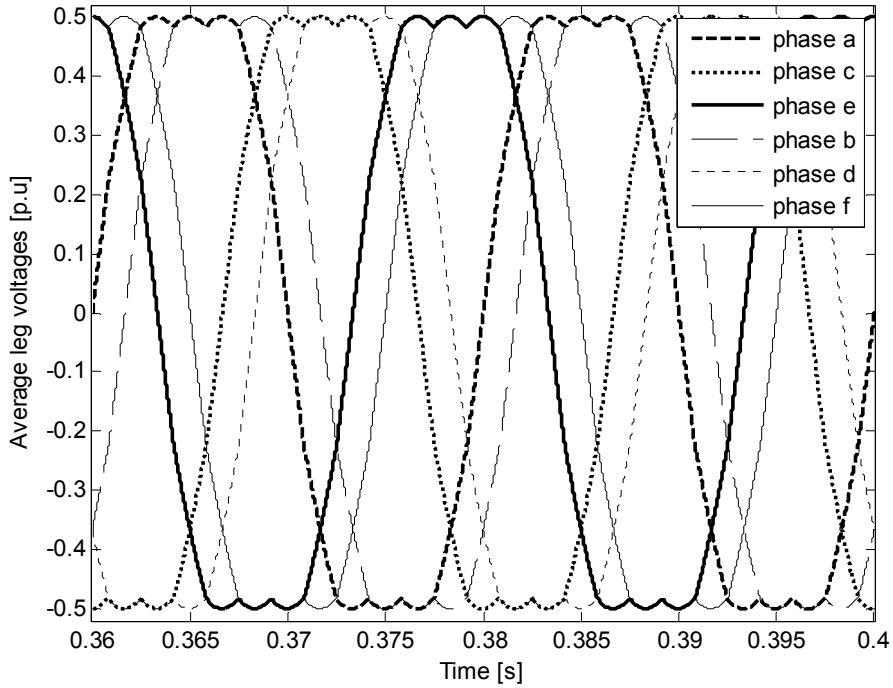

Fig. 3.19: Average leg voltages for VSD technique.

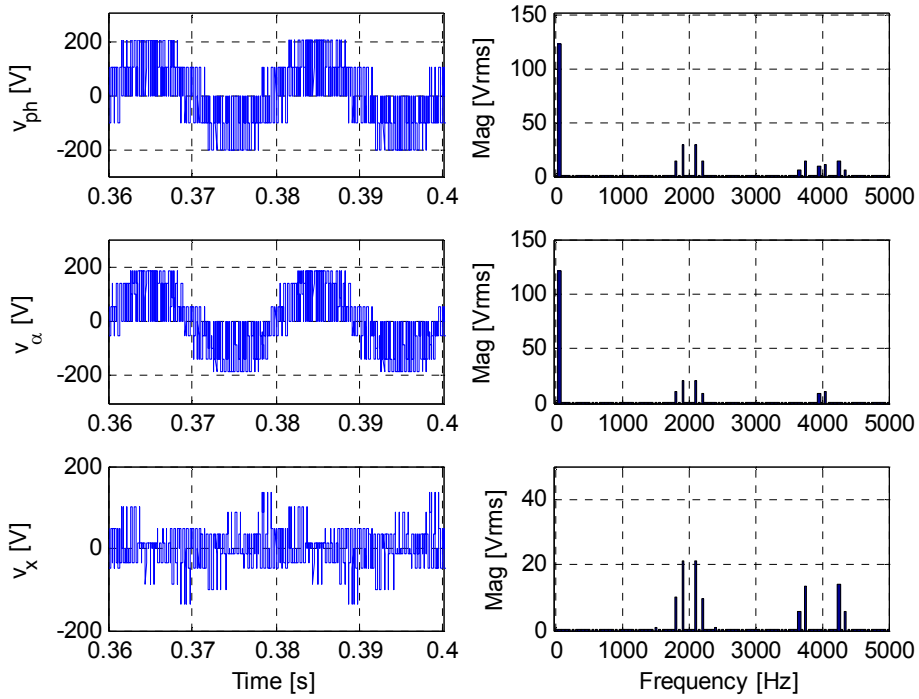

Fig. 3.20: Phase voltage components and frequency spectra for VSD technique. From top to bottom: phase voltage, α-component voltage, and x-component voltage.

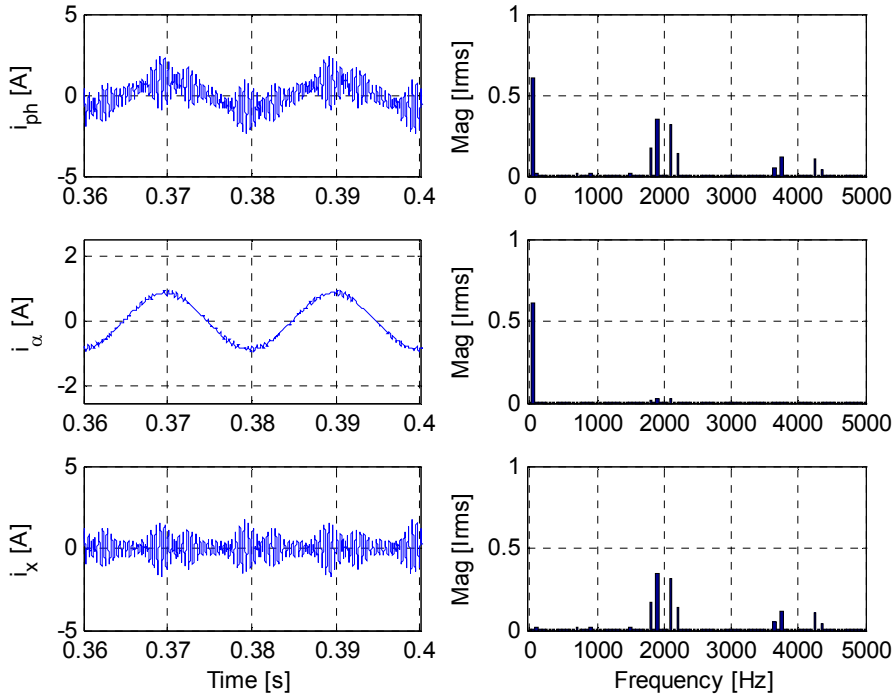

Fig. 3.21: Current components and their frequency spectra for VSD technique. From top to bottom: phase current, α-component current, and x-component current.

3.4 Control of two-level six-phase VSI feeding asymmetrical machine with a single neutral point

As stated before, asymmetrical machine with a single neutral point is rarely found in the literature. One of the reasons is it operates at lower maximum modulation index value (in the linear PWM region) than a machine with two isolated neutral points [Dujic et al. (2010)]. As a result the maximum dc bus voltage utilisation is reduced.

Besides that, the utilisation of asymmetrical machine with a single neutral point also leads to the occurrence of non-zero space vectors in (0_+-0_-) axes and the flow of zero-sequence current is now possible. Therefore, besides zeroing the lower order harmonics in (x-y) plane, the applied PWM control techniques must also be able to zero (on average) the zero-sequence components too. To avoid the flow of the zero-sequence current, it becomes necessary to modify the PWM techniques that were previously discussed for the two-level six-phase VSI feeding an asymmetrical machine with two isolated neutral points. Obviously for the SVPWM techniques, this requires a complex modulation algorithm. Therefore only carrier based PWM techniques will be considered here due to the simplicity of implementation.

Two carrier-based PWM control strategies will be implemented. The first is pure sinusoidal PWM and the second is sinusoidal PWM with zero-sequence injection. The same simulation settings and machine parameters as stated in Section 3.3 are used to evaluate the performance.

3.4.1 Pure sinusoidal PWM (SPWM)

For implementation of the SPWM technique, no modification is required for the generation of the reference signals. The reference signals that are used here are same as those described in Section 3.3.1.1. The range of modulation index is also $0 \le M \le 1$.

The phase voltage components of the machine and their frequency spectra are shown in Fig. 3.22 while the current components and their frequency spectra are shown in Fig. 3.23. Additionally, the 0-component of phase voltage and machine current, together with their spectra, are now included in order to show the characteristics of the zero-sequence component. The phase voltage contains fundamental component of 106.066 Vrms with no low-order harmonics. The fundamental component of α-component voltage has the same magnitude as the phase voltage, while frequency spectrum of x- and 0-component voltages contains only switching frequency associated harmonics.

3.4.2 Sinusoidal PWM with zero-sequence injection

Since the machine is connected to a single neutral point, the reference signals are required to be injected with single zero-sequence signal only, as follows ($i = a, b, c, d, e, f$):

$$\begin{aligned} v_i(t) &= v_i{}^*(t) + v_0 \\ v_0 &= -0.5[\min(v_a{}^*, v_b{}^*, v_c{}^*, v_d{}^*, v_e{}^*, v_f{}^*) + \max(v_a{}^*, v_b{}^*, v_c{}^*, v_d{}^*, v_e{}^*, v_f{}^*)] \end{aligned} \quad (3.15)$$

The injection of zero sequence signal leads to a higher maximum modulation index than the SPWM technique, i.e., $0 \le M \le 1.0354$. The reference signals for maximum modulation index are shown in Fig. 3.24. The phase voltage components and the current components of the inverter machine are shown in Fig. 3.25 and Fig. 3.26 respectively, together with their frequency spectra. With the sinusoidal PWM with zero sequence injection technique, the fundamental component of the phase voltage and α-component voltage is increased to 109.8208 Vrms. No low order harmonics are observed and the harmonics that are plotted on frequency spectrum of both x- and 0-component voltage are once again only associated with the switching frequency.

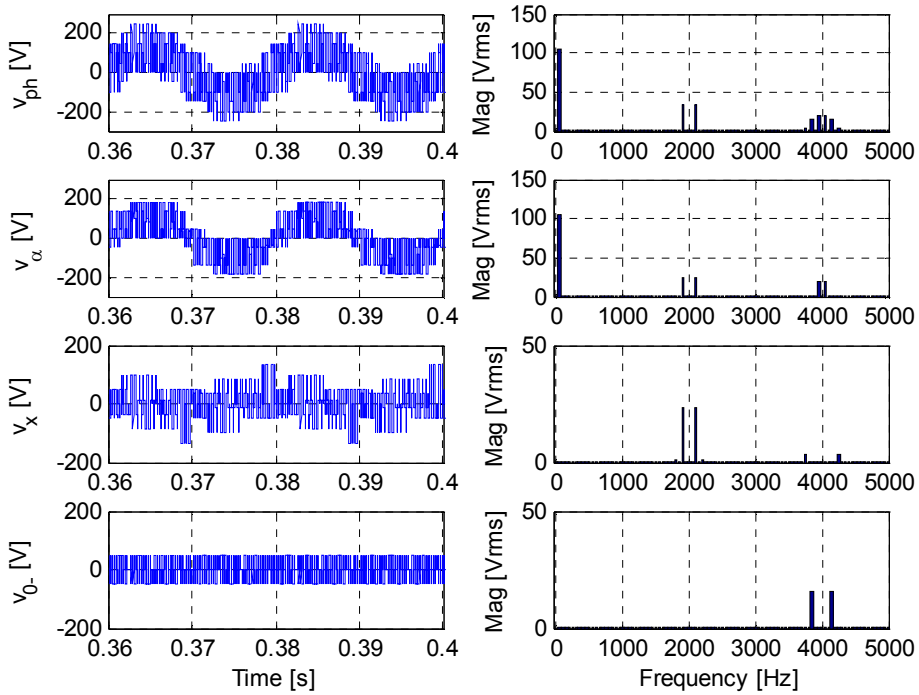

Fig. 3.22: Phase voltage components and frequency spectra for pure sinusoidal PWM technique. From top to bottom: phase voltage, α-component voltage, x-component voltage and 0-component voltage.

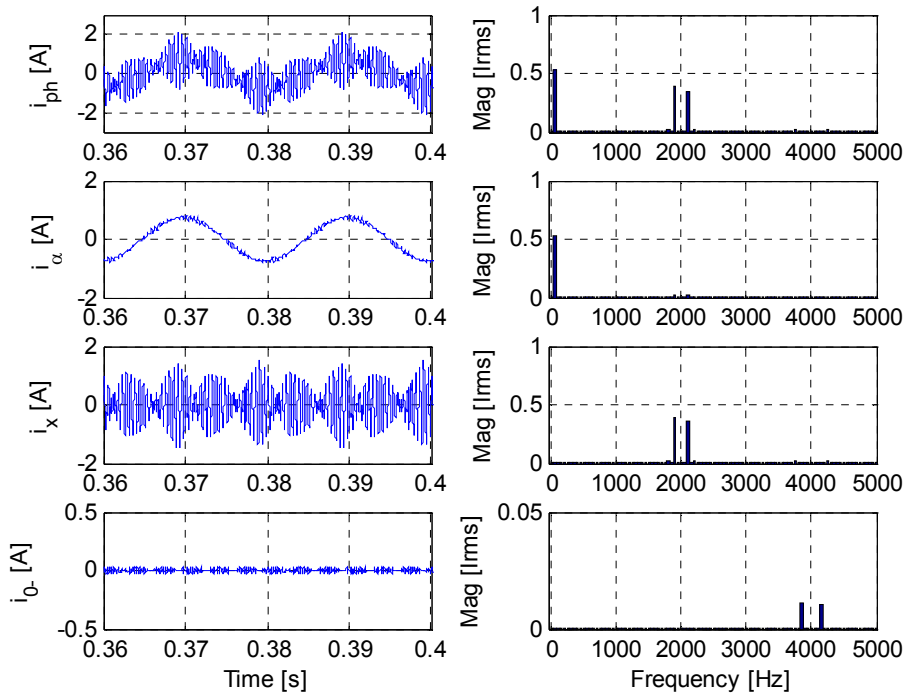

Fig. 3.23: Current components and frequency spectra for pure sinusoidal PWM technique. From top to bottom: phase current, α-component current, x-component current and 0-component current.

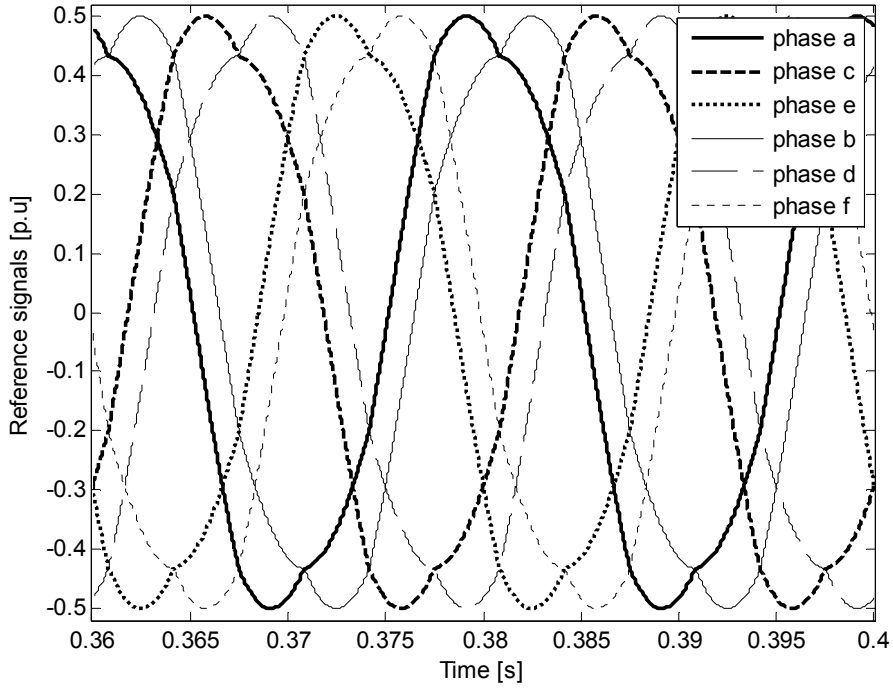

Fig. 3.24: Reference signals for sinusoidal PWM with zero-sequence injection technique.

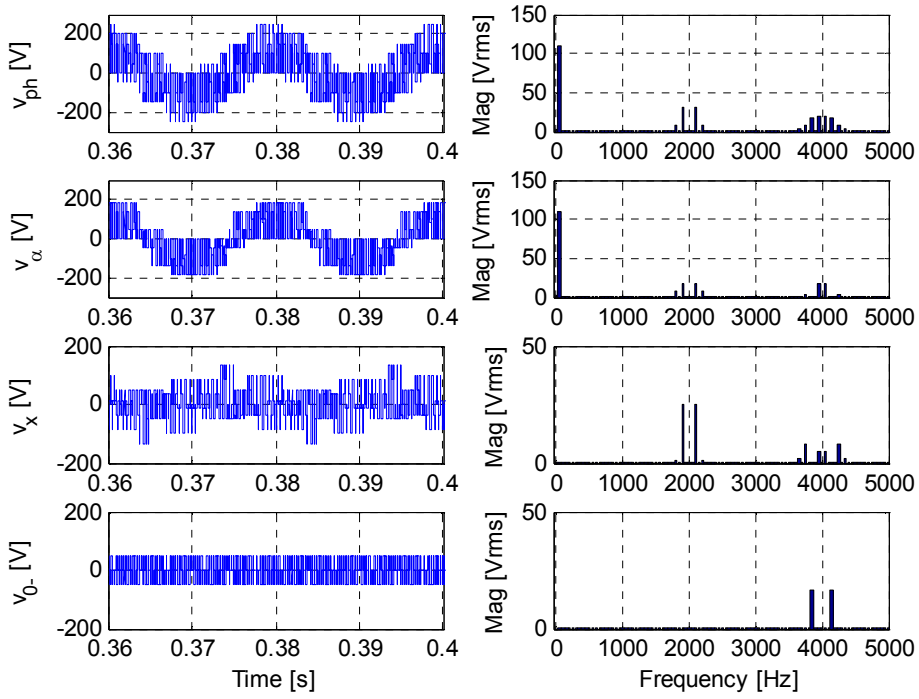

Fig. 3.25: Phase voltage components and frequency spectra for sinusoidal PWM with zero sequence injection technique. From top to bottom: phase voltage, α-component voltage, x-component voltage and 0_-component voltage.

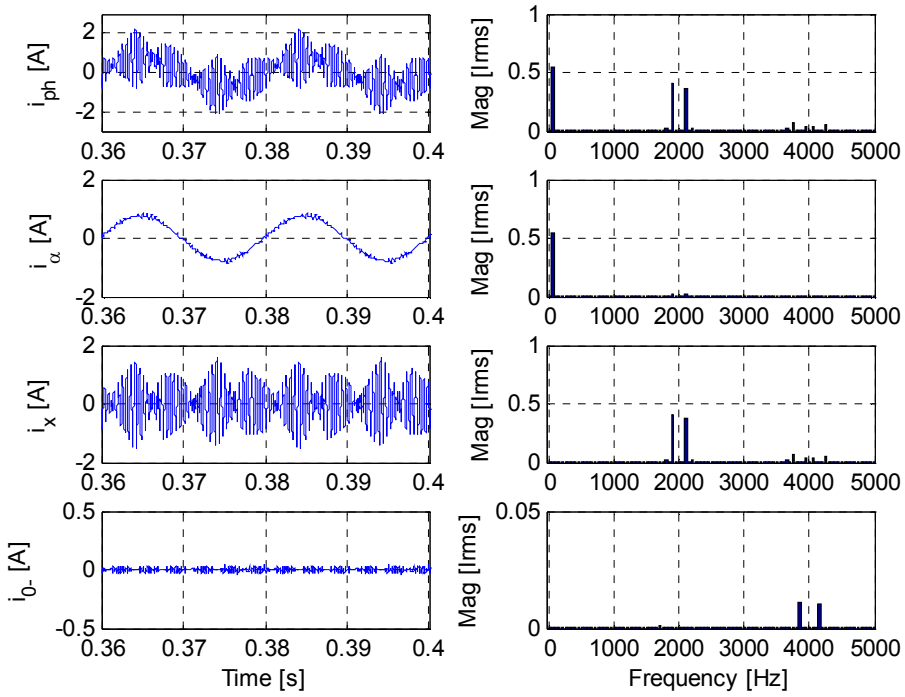

Fig. 3.26: Current components and frequency spectra for sinusoidal PWM with zero sequence injection technique. From top to bottom: phase current, α-component current, x-component current and 0_-component current.

3.5 Performance comparison of the considered PWM techniques

PWM technique that permits operation at a higher modulation index in the linear PWM region will produce a higher fundamental component magnitude for a given dc voltage. This situation leads to a better dc bus voltage utilisation.

For the two-level six-phase VSI feeding an asymmetrical machine with two isolated neutral points, the conventional SVPWM technique produces the highest dc bus voltage utilisation. However this improvement is achieved at the expense of existence of low-order harmonics that map into (x-y) plane, which is highly undesirable. This is followed by the double zero-sequence injection and VSD techniques, while the lowest maximum modulation index is for the pure sinusoidal PWM technique. As noted, the conventional SVPWM technique generates low-order harmonics in the (x-y) plane that will contribute to losses. The other techniques produce no low-order harmonics in the (x-y) plane.

Only carrier-based PWM techniques are investigated for the two-level six-phase VSI feeding an asymmetrical machine with a single neutral point. For this drive topology, the zero sequence injection technique enables higher dc bus voltage utilisation than the sinusoidal PWM technique. The dc bus voltage utilisation is lower compared to the value

achieved in the case of two isolated neutral points using PWM techniques such as the double zero-sequence injection and VSD techniques.

Besides the dc bus voltage utilisation, the performance of the PWM techniques for drive with two isolated neutral points and a single neutral point topologies can also be compared based on the total harmonic distortion (THD) of phase voltage and current. In order to do so, for each drive topology, one PWM technique that produce the highest dc bus voltage utilisation without generating low order harmonics in the (x-y) plane and (0_+-0_-) axes is selected. For a machine with two isolated neutral points, double zero sequence injection is chosen while for a machine with a single neutral point, the zero sequence injection technique is selected.

A series of MATLAB/Simulink simulations and experimental works are conducted in order to compare the performance of each machine configuration of the two-level asymmetrical six-phase drive. In the simulation, a SimPowerSystem toolbox is used to model the two level six-phase VSI. The inverter model includes IGBTs and reverse diodes that have a forward voltage of 1.2 V and 1.6 V respectively. The inverter is also modelled with 6 μs dead time. In brief, the simulations are carried out in a manner that it imitates the non-ideal characteristics of the experimental tools.

As for the experimental works, the related PWM techniques are implemented using a dSPACE DS1006 processor board. A custom-made two-level multiphase VSI is used and the dSPACE module is connected to the VSI via the dSPACE DS5101 Digital Waveform Output Board. The phase voltage and current waveforms are captured using a Tektronix MSO 2014 Mixed Signal Oscilloscope through a Tektronix P5205A High Voltage Differential Probe and a Tektronix TCP0030 Current Probe. The captured waveforms are then post-processed using MATLAB program for plotting and FFT analysis. The detailed explanation of the simulation and experimental set-up is presented in the Appendix 1.

The drive operation is based on open-loop constant V/f control (300 V peak phase voltage at 50 Hz with M = 1) without voltage boost. The simulations were conducted for modulation index value spanning from M = 0.1 to the maximum achievable modulation index value M_{max} in 0.1 increments. The THDs are calculated as follows:

$$THD = \sqrt{\frac{\sum_{n=1,2,3\ldots}^{r} X_n^2 - X_1^2}{X_1^2}} \qquad (3.16)$$

where X_n is the rms value of the n^{th} harmonic component of the voltage or current, X_1 is the

rms of the fundamental, n is the harmonic order used for calculation and r is the maximum harmonic order which is taken into account. The THDs are calculated up to the 41 kHz. The calculated THD is in p.u. value and this unit is utilised throughout this thesis whenever the THD value of any voltage/current waveform is considered in the discussion. The value of 41 kHz is chosen as a high enough value that takes into account the first 20 side bands of the spectrum. Used switching frequency is f_{sw}=2 kHz.

Tables 3.4 - 3.5 present the simulation results regarding the fundamental component of phase voltage and current and also their THDs for machine configured with two isolated neutral points and modulated using the double zero-sequence injection technique. In addition, the THDs of α-, x- and 0-component of phase voltage and current are also included. For a machine with a single neutral point topology and modulated using the zero-sequence injection technique, the obtained results are presented in Tables 3.6 - 3.7. The number of phase voltage levels is also stated in the tables. For a machine with two isolated neutral points the number of phase voltage levels is five, which is similar to a three-phase drive. For a machine with a single neutral point the number of phase voltage levels is eleven.

From Tables 3.4 - 3.7, it can be observed that the zero-sequence components are equal to zero for the machine with two isolated neutral points. For the machine with a single neutral point, the THDs of 0-component of phase voltage and current are contributed by the harmonics that are associated with the switching frequency. The experimental results regarding the fundamental component of phase voltage and current and also their THDs for each machine configuration are presented in Tables 3.8 - 3.9. As can be observed, the experimental results match quite closely with the simulation results presented in Tables 3.4 - 3.7. The small deviation between the magnitude of fundamental component of phase voltage obtained through simulation and experiment is most likely due to the variation of dc link voltage during the experiment.

The performance comparison between the two asymmetrical six-phase drive topologies in terms of phase voltage and current THDs are presented in Fig. 3.27. Both simulation and experimental results are compared. It can be observed from the figures that the phase voltage THDs of the machine with a single and two isolated neutral points are almost identical. On the other hand, the current THDs of the machine with a single neutral point is higher than with two isolated neutral points due to excitation of the (x-y) plane and zero-sequence components in the (0_+-0_-) axes. Fig. 3.28 shows the i_{s0+} and i_{s0-} current components for the single neutral point case when $M = 1$. The single neutral point

Table 3.4: Simulation results - phase voltage fundamental component and THDs, along with THDs of α-, x- and 0-component voltage for machine with two isolated neutral points.

M	v_{ph}		v_α	v_x	v_{0-}	v_{ph} level
	V_1(rms)	THD	THD	THD	THD	
0.1	7.9213	3.7048	3.6402	0.7031	0	5
0.2	19.3289	2.5171	2.3778	0.8112	0	5
0.3	30.7235	1.9399	1.8122	0.6771	0	5
0.4	41.4751	1.6049	1.4875	0.5964	0	5
0.5	52.1588	1.3661	1.2548	0.5386	0	5
0.6	62.7009	1.1805	1.0740	0.4937	0	5
0.7	73.2918	1.0289	0.9209	0.4610	0	5
0.8	84.1055	0.8937	0.7848	0.4315	0	5
0.9	94.9154	0.7723	0.6583	0.4081	0	5
1.0	105.1217	0.6672	0.5447	0.3889	0	5
1.1547	121.5861	0.5090	0.3557	0.3656	0	5

Table 3.5: Simulation results - phase current fundamental component and THDs, along with THDs of α-, x- and 0-component current for machine with two isolated neutral points.

M	i_{ph}		i_α	i_x	i_{0-}
	I_1(rms)	THD	THD	THD	THD
0.1	0.3092	0.1714	0.0300	0.1709	0
0.2	0.4568	0.1404	0.0385	0.1401	0
0.3	0.4967	0.1766	0.0499	0.1738	0
0.4	0.5089	0.2365	0.0589	0.2301	0
0.5	0.5119	0.3146	0.0655	0.3076	0
0.6	0.5146	0.3994	0.0709	0.3945	0
0.7	0.5215	0.4912	0.0717	0.4869	0
0.8	0.5224	0.5935	0.0714	0.5899	0
0.9	0.5271	0.6954	0.0697	0.6922	0
1.0	0.5231	0.8152	0.0691	0.8121	0
1.1547	0.5198	1.0122	0.0726	1.0079	0

configuration allows the third harmonic to flow in each three-phase winding set. The currents flowing through the three-phase winding sets have opposing phase shifts and so sum to zero as evident from Fig. 3.28. Zero-sequence currents cannot flow in the two isolated neutral points configuration and this leads to the superior current THD.

Table 3.6: Simulation results - phase voltage fundamental component and THDs, along with THDs of α-, x- and 0-component voltage for machine with a single neutral point.

M	v_{ph}		v_α	v_x	v_{0-}	v_{ph} level
	V_1(rms)	THD	THD	THD	THD	
0.1	8.0271	3.7158	3.5954	0.8083	0.4521	11
0.2	19.2362	2.5572	2.3658	0.8464	0.4911	11
0.3	30.2917	2.0022	1.7995	0.7556	0.4590	11
0.4	41.0147	1.6664	1.4682	0.6748	0.4123	11
0.5	51.7380	1.4229	1.2309	0.6097	0.3746	11
0.6	62.2980	1.2369	1.0468	0.5623	0.3493	11
0.7	72.6507	1.0863	0.8945	0.5274	0.3284	11
0.8	83.4199	0.9522	0.7583	0.4913	0.3065	11
0.9	93.9161	0.8341	0.6329	0.4658	0.2892	11
1.0	104.2791	0.7316	0.5139	0.4442	0.2751	11
1.0353	108.0870	0.6934	0.4660	0.4382	0.2721	11

Table 3.7: Simulation results - phase current fundamental component and THDs, along with THDs of α-, x- and 0-component current for machine with a single neutral point.

M	i_{ph}		i_α	i_x	i_{0-}
	I_1(rms)	THD	THD	THD	THD
0.1	0.3129	0.2076	0.0393	0.1371	0.1667
0.2	0.4520	0.1748	0.0400	0.1481	0.1020
0.3	0.4889	0.2142	0.0499	0.1981	0.0794
0.4	0.5020	0.2899	0.0585	0.2780	0.0648
0.5	0.5138	0.3777	0.0641	0.3677	0.0572
0.6	0.5151	0.4863	0.0700	0.4780	0.0694
0.7	0.5194	0.6036	0.0719	0.5950	0.0730
0.8	0.5265	0.7163	0.0705	0.7090	0.0716
0.9	0.5316	0.8396	0.0687	0.8335	0.0709
1.0	0.5368	0.9684	0.0685	0.9639	0.0669
1.0353	0.5402	1.0210	0.0688	1.0182	0.0598

For the phase voltage THDs, the results obtained from the experiments match very closely with the simulation. For the phase current THDs, there is a small differences between the results obtained from the simulations and experiments. The difference is likely due to rotor leakage inductances value which in practice is frequency-dependent [Dujic et al. (2011), Jones et al. (2011a)], while in the simulations a constant value of rotor leakage inductance is used.

Table 3.8: Experiment results - fundamental component and THD of phase voltage and current for machine with two isolated neutral points.

	v_{ph}		I_{ph}	
M	V_1(rms)	THD	I_1(rms)	THD
0.1	8.0254	3.8594	0.3068	0.0947
0.2	19.2897	2.5544	0.4519	0.1228
0.3	29.8520	1.9830	0.4857	0.1840
0.4	40.7488	1.6302	0.5105	0.2538
0.5	51.3963	1.3878	0.5159	0.3392
0.6	62.1466	1.1954	0.5243	0.4282
0.7	72.2507	1.0449	0.5310	0.5217
0.8	83.8120	0.9100	0.5336	0.6301
0.9	94.0316	0.7911	0.5321	0.7428
1.0	104.4925	0.6835	0.5342	0.8525
1.0353	120.3962	0.5247	0.5464	1.0234

Table 3.9: Experiment results - fundamental component and THD of phase voltage and current for machine with a single neutral point.

	v_{ph}		I_{ph}	
M	V_1(rms)	THD	I_1(rms)	THD
0.1	8.2432	0.2990	0.2990	3.7419
0.2	19.2408	0.4344	0.4344	2.5557
0.3	29.7600	0.4732	0.4732	2.0130
0.4	40.5530	0.4922	0.4922	1.6743
0.5	51.1492	0.5051	0.5051	1.4317
0.6	61.3524	0.5099	0.5099	1.2488
0.7	71.7117	0.5187	0.5187	1.0940
0.8	82.2390	0.5227	0.5227	0.9613
0.9	92.9455	0.5320	0.5320	0.8414
1.0	102.7734	0.5324	0.5324	0.7385
1.0353	105.6717	0.5353	0.5353	0.7037

Figs. 3.29 - 3.30 depict the simulation and experimental results of phase voltage and current waveforms, their spectra and THDs, for machine with two isolated neutral points. On the other hand, the results obtained with a single neutral point configuration are shown in Figs. 3.31 - 3.32. A strong correspondence between the simulation and experimental results can be observed where the phase voltage and current waveforms, FFTs and THDs match quite closely. A small amount of low order harmonics in both simulations and experimental results is contributed by the dead-time effect of the VSIs.

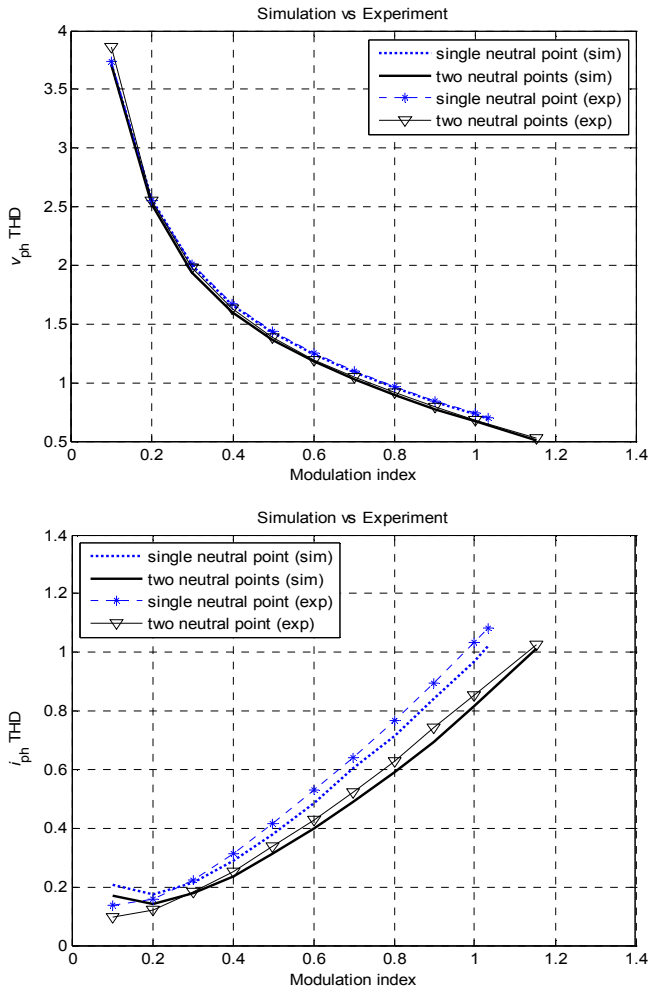

Fig. 3.27: Performance of machine with two isolated neutral points and a single neutral point: phase voltage THD against modulation index (top), load current THD against modulation index (bottom).

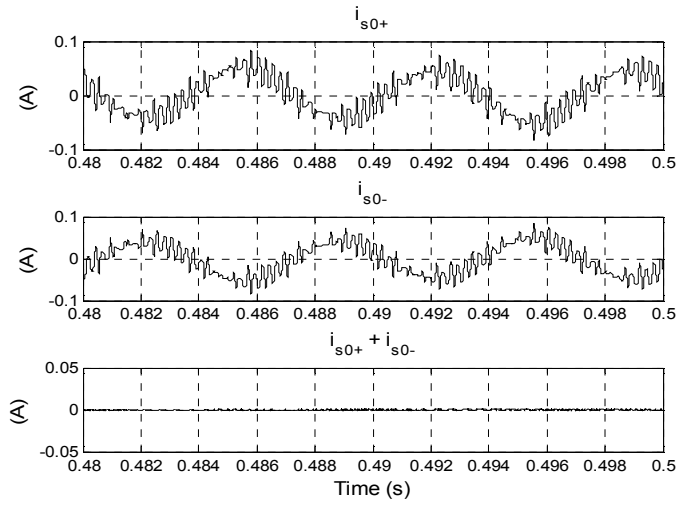

Fig. 3.28: Simulation of a single neutral point.configuration with $M = 1$: i_{s0+} current (top), i_{s0-} current (middle) and $i_{s0+} + i_{s0-}$ (bottom).

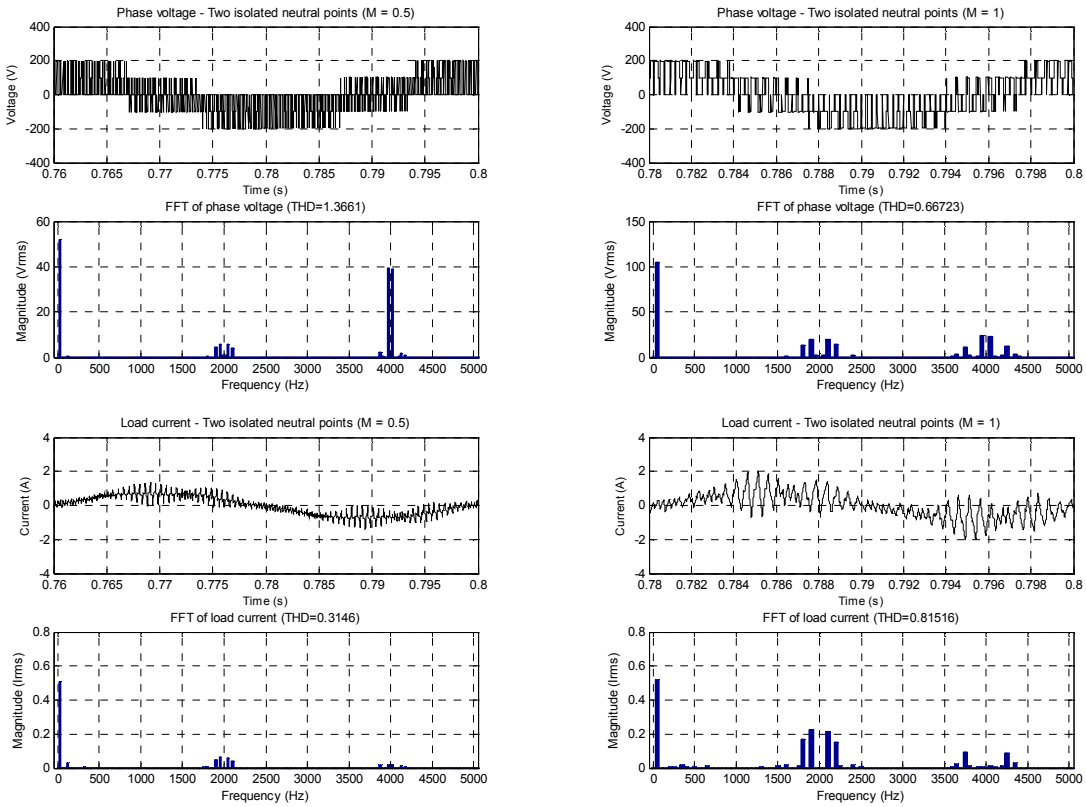

Fig. 3.29: Simulation results with $M = 0.5$ (left) and $M = 1$ (right) for machine with two isolated neutral points. Top: Phase voltage waveform and spectra. Bottom: Phase current waveform and spectra.

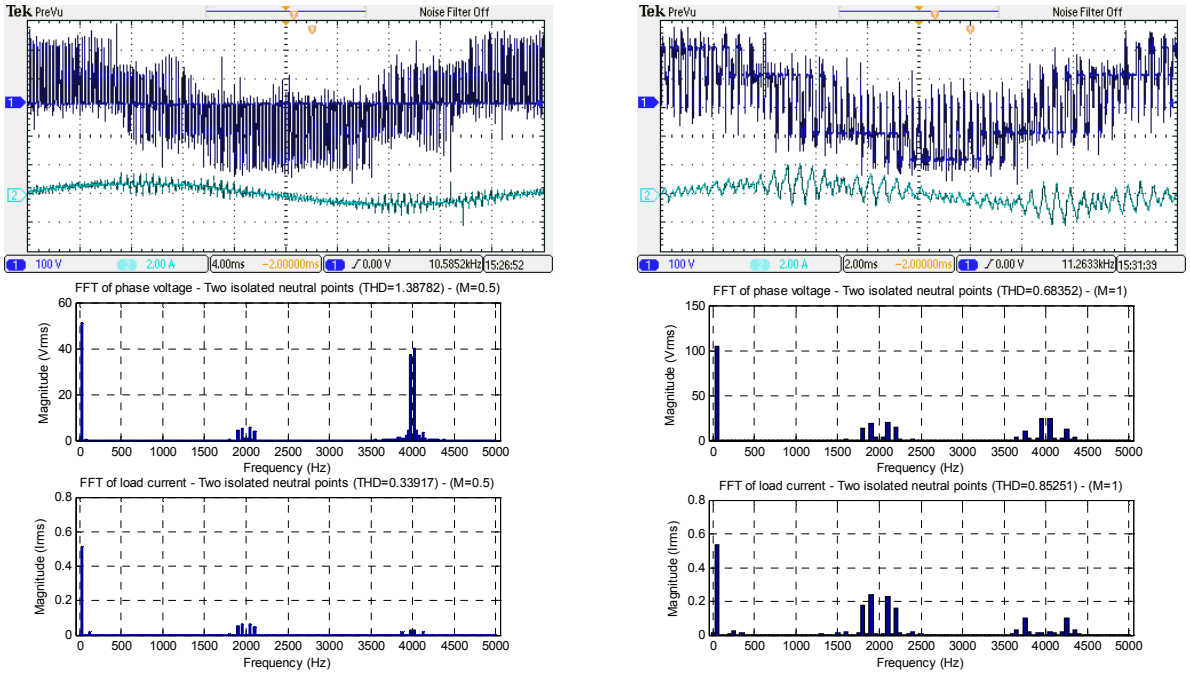

Fig. 3.30: Experimental results with $M = 0.5$ (left) and $M = 1$ (right) for machine with two isolated neutral points. Top: Phase voltage and current waveforms. Bottom: Phase voltage and current spectra.

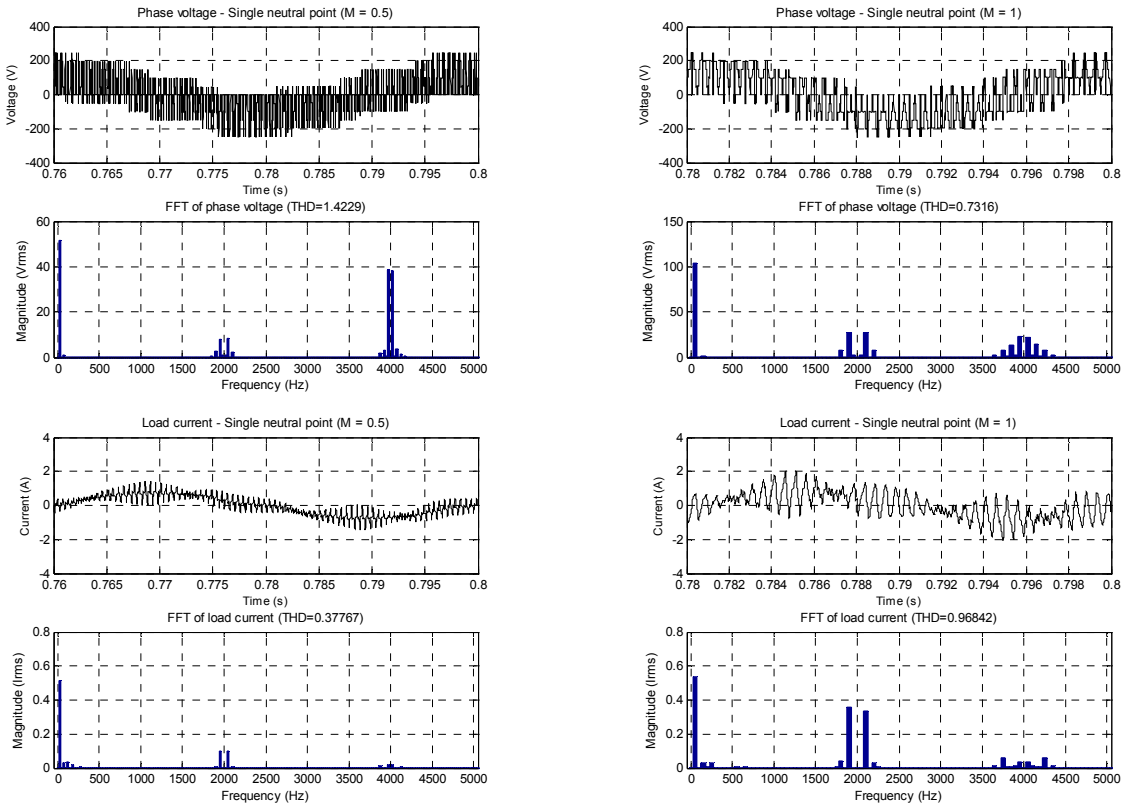

Fig. 3.31: Simulation results with $M = 0.5$ (left) and $M = 1$ (right) for machine with a single neutral point. Top: Phase voltage waveform and spectra. Bottom: Phase current waveform and spectra

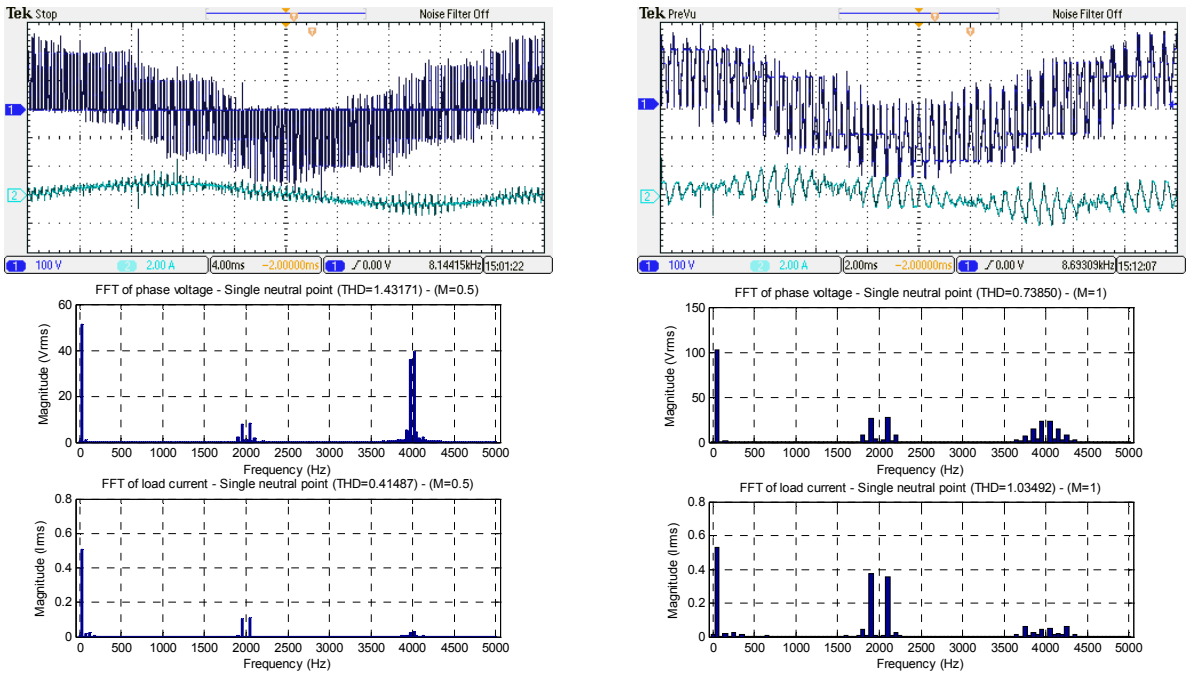

Fig. 3.32: Experimental results with $M = 0.5$ (left) and $M = 1$ (right) for machine with a single neutral point. Top: Phase voltage and current waveforms. Bottom: Phase voltage and current spectra.

Fig. 3.33 shows the FFT of the α- axis, x- axis and 0_-- components of the phase voltage produced by each configuration of neutral point connection with $M = 1$. The figure reveals that the machine with a single neutral point produces harmonics in the (0+-0-) axes while machine with two isolated neutral points does not. The third harmonic component is largely due to the inverter dead-time. Due to the dead time effect, the performance of machine with a single neutral point is degraded compared to the configuration with two isolated neutral points.

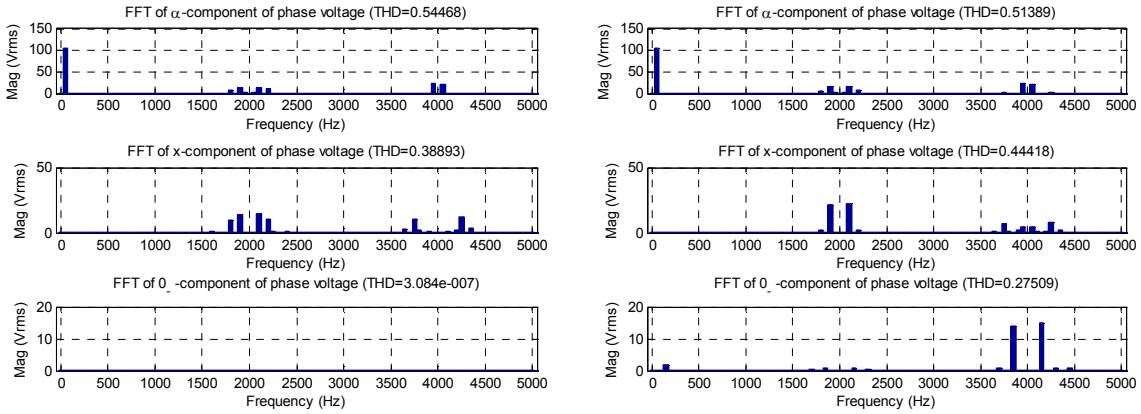

Fig. 3.33: Simulation results with $M = 1$ for machine with two isolated neutral points (right) and with a single neutral point (left). From top to bottom: FFT of α- axis, x- axis and 0_-- components of the phase voltage.

3.6 Summary

This chapter has discussed two types of topology for two-level asymmetrical six-phase drive, which are asymmetrical machines with two isolated neutral points and with a single neutral point. The drive configuration and the space vector model for the two topologies are explained. The topologies produce the same space vector mapping in the (α-β) and (x-y) planes. The components in the (0_+-0_-) axes are always equal to zero for the machine with two isolated neutral points, but, for the machine with a single neutral point, there are non-zero components in the (0_+-0_-) axes.

Several modulation techniques covering both carrier-based PWM and SVPWM have been reviewed. The performance of each technique has also been investigated and compared based on results of MATLAB/Simulink simulation. For the machine with two isolated neutral points, two PWM techniques; double zero-sequence injection and VSD techniques; produce the best overall performance in terms of elimination of low-order harmonics and utilisation of the dc bus voltages. For the machine with a single neutral

point, only the carrier based PWM technique is considered and the utilisation of zero-sequence produces superior results to the pure sinusoidal PWM technique.

The performance of the two types of topology has also been compared. The performance of the machine with two isolated neutral points is superior compared to the machine with a single neutral point in term of dc bus voltage utilisation and also the THDs of phase voltage and current.

However, as has been discussed in the previous chapter the machine with a single neutral point possess advantage in term of offering better post-fault operation due to higher degree of freedom compared to configuration with two-isolated neutral points. Therefore during the occurrence of fault, it is beneficial to connect the neutrals together (into a single neutral point configuration) so that improved post-fault operation can be achieved.

Chapter 4

PWM TECHNIQUES FOR TWO-LEVEL SYMMETRICAL SIX-PHASE DRIVE

4.1 Introduction

This chapter focuses on PWM techniques for a two-level symmetrical six-phase drive. The space vector model for the inverter is elaborated first, and then several PWM techniques based on SVPWM strategy are discussed. The implementation of each technique is explained and simulations are conducted by using MATLAB/Simulink in order to analyse their performance. Only the case of machine with a single neutral point is considered.

4.2 Space vector model of two-level symmetrical six-phase VSI

The power circuit topology of two-level symmetrical six-phase drive is shown in Fig. 4.1. The dc bus voltage V_{dc} is assumed to be constant and the negative rail is denoted by *N*. The stator windings of the machine are star connected with a single neutral point, *n*. The upper and lower switches for each leg work complementarily. An upper case symbol (*A, B, C, D, E, F*) again denotes the inverter legs while a lower case symbol (*a, b, c, d, e, f*) once more denotes the machine output phases.

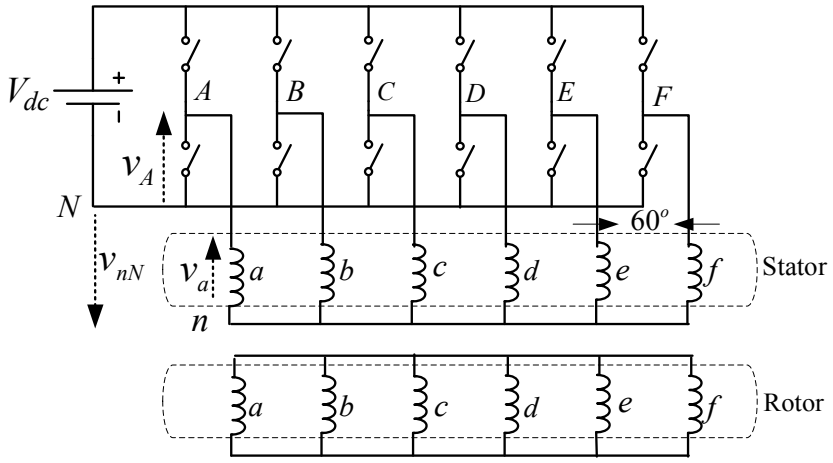

Fig. 4.1: Power circuit topology of two-level six-phase VSI feeding a symmetrical machine.

The correlation between the phase voltages and leg voltages can be again given as follows:

$$\begin{aligned} v_A &= v_a + v_{nN} & v_D &= v_d + v_{nN} \\ v_B &= v_b + v_{nN} & v_E &= v_e + v_{nN} \\ v_C &= v_c + v_{nN} & v_F &= v_f + v_{nN} \end{aligned} \qquad (4.1)$$

Since the phases are star-connected with a single neutral point,

$$v_a + v_b + v_c + v_d + v_e + v_f = 0 \qquad (4.2)$$

Using (4.2), summation of (4.1) yields:

$$v_{nN} = (1/6)(v_A + v_B + v_C + v_D + v_E + v_F) \qquad (4.3)$$

The relationship between the phase voltages and the leg voltages is obtained by substituting (4.3) into (4.1). The relationship is in essence the same as in (3.9).

$$\begin{aligned} v_a &= (5/6)v_A - (1/6)(v_B + v_C + v_D + v_E + v_F) \\ v_b &= (5/6)v_B - (1/6)(v_A + v_C + v_D + v_E + v_F) \\ v_c &= (5/6)v_C - (1/6)(v_A + v_B + v_D + v_E + v_F) \\ v_d &= (5/6)v_D - (1/6)(v_A + v_B + v_C + v_E + v_F) \\ v_e &= (5/6)v_E - (1/6)(v_A + v_B + v_C + v_D + v_F) \\ v_f &= (5/6)v_F - (1/6)(v_A + v_B + v_C + v_D + v_E) \end{aligned} \qquad (4.4)$$

In total there are again 2^6 = 64 switching state combinations for the two-level symmetrical six-phase VSI. Based on space vector theory, the switching states lead to 64 voltage space vectors. Projection of space vectors of the phase voltages into (α-β) and (x-y) planes, and 0_+ and 0_--axes is performed by using the following equations:

$$\begin{aligned} \underline{v}_{\alpha\beta} &= \frac{2}{6}\left(v_a + \underline{a}v_b + \underline{a}^2 v_c + \underline{a}^3 v_d + \underline{a}^4 v_e + \underline{a}^5 v_f\right) \\ \underline{v}_{xy} &= \frac{2}{6}\left(v_a + \underline{a}^2 v_b + \underline{a}^4 v_c + \underline{a}^6 v_d + \underline{a}^8 v_e + \underline{a}^{10} v_f\right) \\ v_{0_+} &= \frac{2}{6}\left(\frac{1}{2}\right)(v_a + v_b + v_c + v_d + v_e + v_f) \\ v_{0_-} &= \frac{2}{6}\left(\frac{1}{2}\right)(v_a - v_b + v_c - v_d + v_e - v_f) \end{aligned} \qquad (4.5)$$

where $\underline{a} = \exp(j2\pi/6)$.

The mapping of the space vectors is shown in Fig. 4.2. The space vectors are again labelled with decimal numbers. If converted into six-digit binary code, the numbers

correspond to the state of the upper inverter leg switches in the sequence of (*A, B, C, D, E, F*). Value of "1" indicates once more that an upper switch in a particular leg is in "on" state, while the value of "0" indicates that the switch is in "off" state.

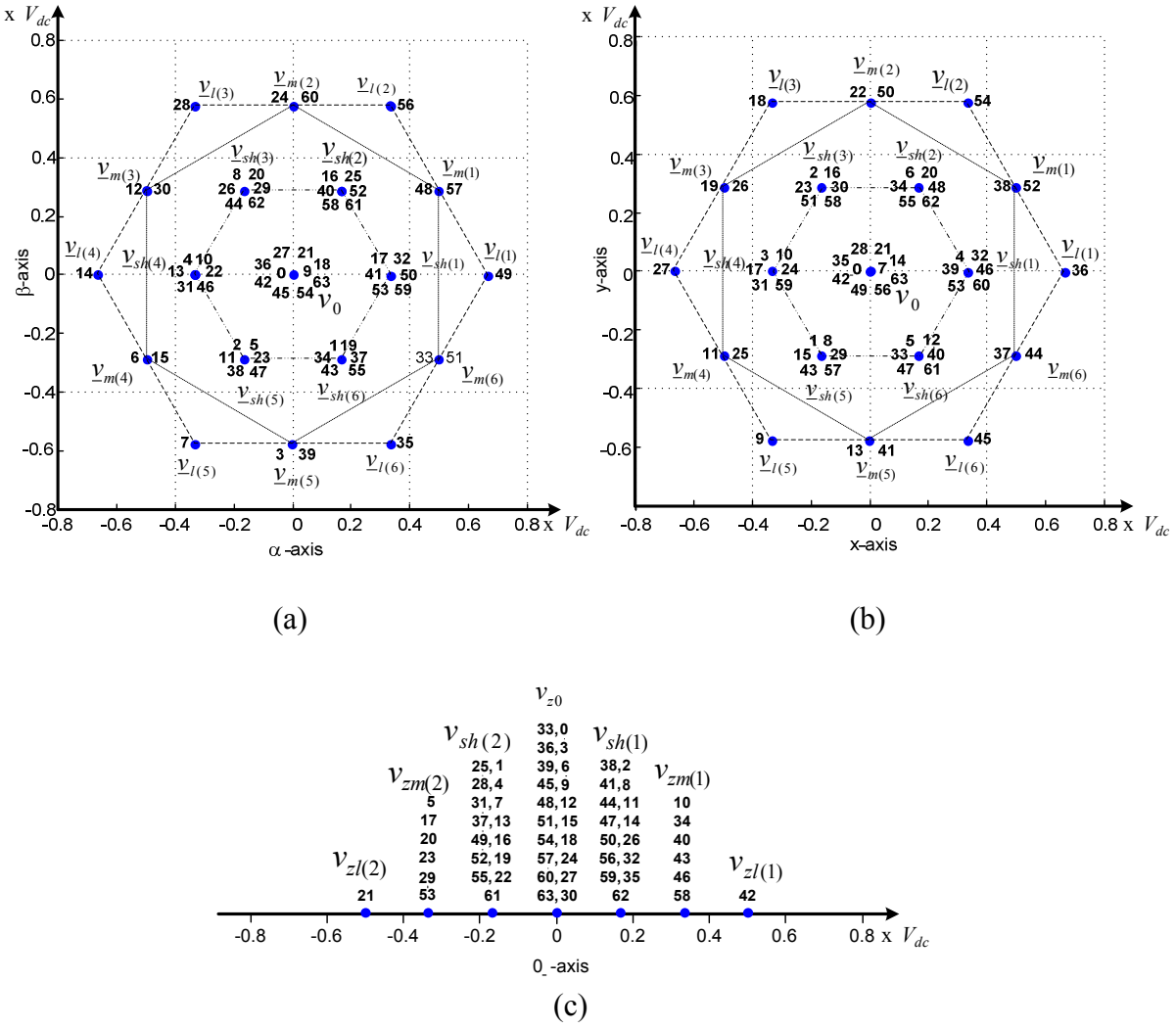

Fig. 4.2: Mapping of phase voltage space vectors for six-phase VSI feeding symmetrical machine: (a) in (*α-β*) plane; (b) in (*x-y*) plane; (c) in 0_-axis.

In the (*α-β*) and (*x-y*) planes, the 64 space vectors are positioned at nineteen locations. Based on their magnitude, the space vectors can be categorised into four different groups, which are large ($\underline{v}_{l(k)}$), medium ($\underline{v}_{m(k)}$), short ($\underline{v}_{sh(k)}$) and zero space vectors (v_0) where the index k once more denotes the k^{th} space vector for each group of space vectors. The groupings of the space vectors are shown in Figs. 4.2(a) - (b) and can be expressed using equations presented in Table 4.1. There is no state redundancy for the large space vectors. The medium space vectors have a double redundancy while the short space vectors have six-fold redundancy. The zero space vector in the (*α-β*) and (*x-y*) planes is produced by ten switching states.

The 0_+-component is equal to zero for all space vectors but this is not the case for the 0_--component. The 0_--components are positioned in seven locations. They are positioned on the straight line of 0_--axis, and have four different magnitudes, which are $\pm 1/2\, V_{dc}$, $\pm 1/3\, V_{dc}$, $\pm 1/6\, V_{dc}$ and zero. The groupings of the 0_--component are shown in Fig. 4.2(c) and can be expressed using equations presented in Table 4.2.

Table 4.1: Space vectors of a six-phase VSI feeding symmetrical machine in (α-β) and (x-y) planes.

Space vectors	Values of space vectors
Large ($\underline{v}_{l(k)}$)	$\frac{2}{3}V_{dc}e^{j(k-1)\frac{\pi}{3}}$ for k = 1, 2, ..., 6
Medium ($\underline{v}_{m(k)}$)	$\frac{1}{\sqrt{3}}V_{dc}e^{j(2k-1)\frac{\pi}{6}}$ for k = 1, 2, ..., 6
Short ($\underline{v}_{sh(k)}$)	$\frac{1}{3}V_{dc}e^{j(k-1)\frac{\pi}{3}}$ for k = 1, 2, ..., 6
Zero ($\underline{v}_0$)	0

Table 4.2: 0_--components.

Space vectors	Values of space vectors
Large ($v_{zl(k)}$)	$\frac{1}{2}V_{dc}e^{j(k-1)\pi}$ for k = 1, 2.
Medium ($v_{zm(k)}$)	$\frac{1}{3}V_{dc}e^{j(k-1)\pi}$ for k = 1, 2.
Short ($v_{zsh(k)}$)	$\frac{1}{6}V_{dc}e^{j(k-1)\pi}$ for k = 1, 2.
Zero (v_{z0})	0

4.3 SVPWM control of two-level symmetrical six phase drive

In order to develop the SVPWM control of two-level symmetrical six-phase drive, the (α-β) plane can again be divided into twelve 30° sectors such as shown in Fig. 4.3. Each sector is bounded by one large, one medium (with two switching states), one short (with six switching states), and one zero space vector (with ten switching states). For SVPWM control, the reference vector $\underline{v}^*$ can be synthesised by using various combinations of those space vectors. Consider further, use of vectors from each group in one switching period.

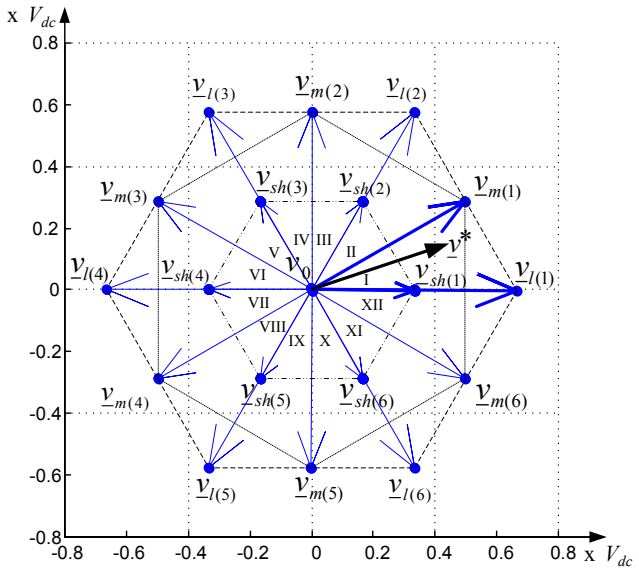

Fig. 4.3: Region of twelve 30° sectors in (α-β) plane.

By using volt-second balance principle, the reference vector in each sector can be synthesised as follows:

$$\begin{aligned} \underline{v}^* T_s &= \underline{v}_l T_l + \underline{v}_m T_m + \underline{v}_{sh} T_{sh} + \underline{v}_0 T_0 \\ T_s &= T_l + T_m + T_{sh} + T_0 \end{aligned} \qquad (4.6)$$

where T_l, T_m , T_{sh} and T_0 represent the dwell times of large, medium, short and zero space vectors. Splitting each space vector into real (α) and imaginary (β) component yields:

$$\begin{aligned} v_\alpha^* T_s &= v_l^\alpha T_l + v_m^\alpha T_m + v_{sh}^\alpha T_{sh} + v_0^\alpha T_0 \\ v_\beta^* T_s &= v_l^\beta T_l + v_m^\beta T_m + v_{sh}^\beta T_{sh} + v_0^\beta T \end{aligned} \qquad (4.7)$$

Since $\underline{v}_{sh} = (1/2)\,\underline{v}_l$ and $\underline{v}_0 = 0$, (4.7) can be re-arranged as [Correa et al. (2003a)]:

$$T_l + \frac{T_{sh}}{2} = \frac{v_\alpha^* v_m^\beta - v_\beta^* v_m^\alpha}{v_l^\alpha v_m^\beta - v_l^\beta v_m^\alpha} T_s \qquad T_m = \frac{v_\beta^* v_l^\alpha - v_\alpha^* v_l^\beta}{v_l^\alpha v_m^\beta - v_l^\beta v_m^\alpha} T_s \qquad (4.8)$$

By introducing a control variable, defined as $\rho = \dfrac{T_l}{T_l + \dfrac{T_{sh}}{2}}$, (4.8) can be re-written as:

$$\begin{aligned} T_l &= \rho \frac{v_\alpha^* v_m^\beta - v_\beta^* v_m^\alpha}{v_l^\alpha v_m^\beta - v_l^\beta v_m^\alpha} T_s \qquad T_{sh} = 2(1-\rho) \frac{v_\alpha^* v_m^\beta - v_\beta^* v_m^\alpha}{v_l^\alpha v_m^\beta - v_l^\beta v_m^\alpha} T_s \\ T_m &= \frac{v_\beta^* v_l^\alpha - v_\alpha^* v_l^\beta}{v_l^\alpha v_m^\beta - v_l^\beta v_m^\alpha} T_s \end{aligned} \qquad (4.9)$$

The range of ρ is $0 \le \rho \le 1$. Note that the value of ρ can be used to regulate the ratio of the dwell time of the large and short space vector.

In the following subsections, several SVPWM techniques that utilise different value of ρ will be discussed. The techniques are simulated by MATLAB/Simulink using the machine parameters presented in Table 4.3. The parameters are estimated using the symmetrical machine that will be used in the experiments later on. The simulations are conducted using the dc bus voltage of 200 V and switching frequency f_s of 2 kHz. Reference frequency is 50 Hz.

Table 4.3: Parameters of symmetrical six-phase machine.

Machine parameter	Value
Stator resistance, R_s [Ω]	3
Rotor resistance, R_r [Ω]	3
Stator leakage inductance, L_{ls} [H]	0.005
Rotor leakage inductance, L_{lr} [H]	0.005
Magnetising inductance, L_m [H]	0.185

The switching sequences for all twelve sectors are as shown in Fig. 4.4. Selected space vectors for each sector are also listed. Seven switching states are used during a switching half-period, which produce once large, twice medium, twice short, and twice zero space vector. Each switch is being switched on and off once only.

4.3.1 SVPWM for $\rho = 1$

From (4.9), when the control variable is chosen to be ρ = 1, it can be seen that $T_{sh} = 0$. Short space vector is not used. Therefore, this technique only utilises five switching states (i.e. one for large, two for medium, and two for zero space vector) during a switching period. The range of modulation index for this technique is $0 \le M \le 2/\sqrt{3}$.

The reference sinusoidal signals are taken with maximum modulation index $M_{\max} = 2/\sqrt{3}$. The setting of ρ = 1 leads to the third harmonic injection with SVPWM and produces average leg voltages shown in Fig. 4.5. The components of phase voltage and current, accompanied by their frequency spectra, are shown in Fig. 4.6 and Fig. 4.7, respectively. The phase voltage and current contain low frequency harmonics where the third harmonic is the most dominant. The low-order harmonics are contained within the 0-component, which contains the harmonics of the order $3n$ (n = 1, 3, 5...). By choosing ρ = 1, the low frequency harmonics are eliminated in (x-y) components, but not in 0-component since the average value during a switching period is not equal to zero. The

magnitude of the fundamental component of phase voltage is V_1 = 81.6497 Vrms and the third harmonics is V_3 = 17 Vrms.

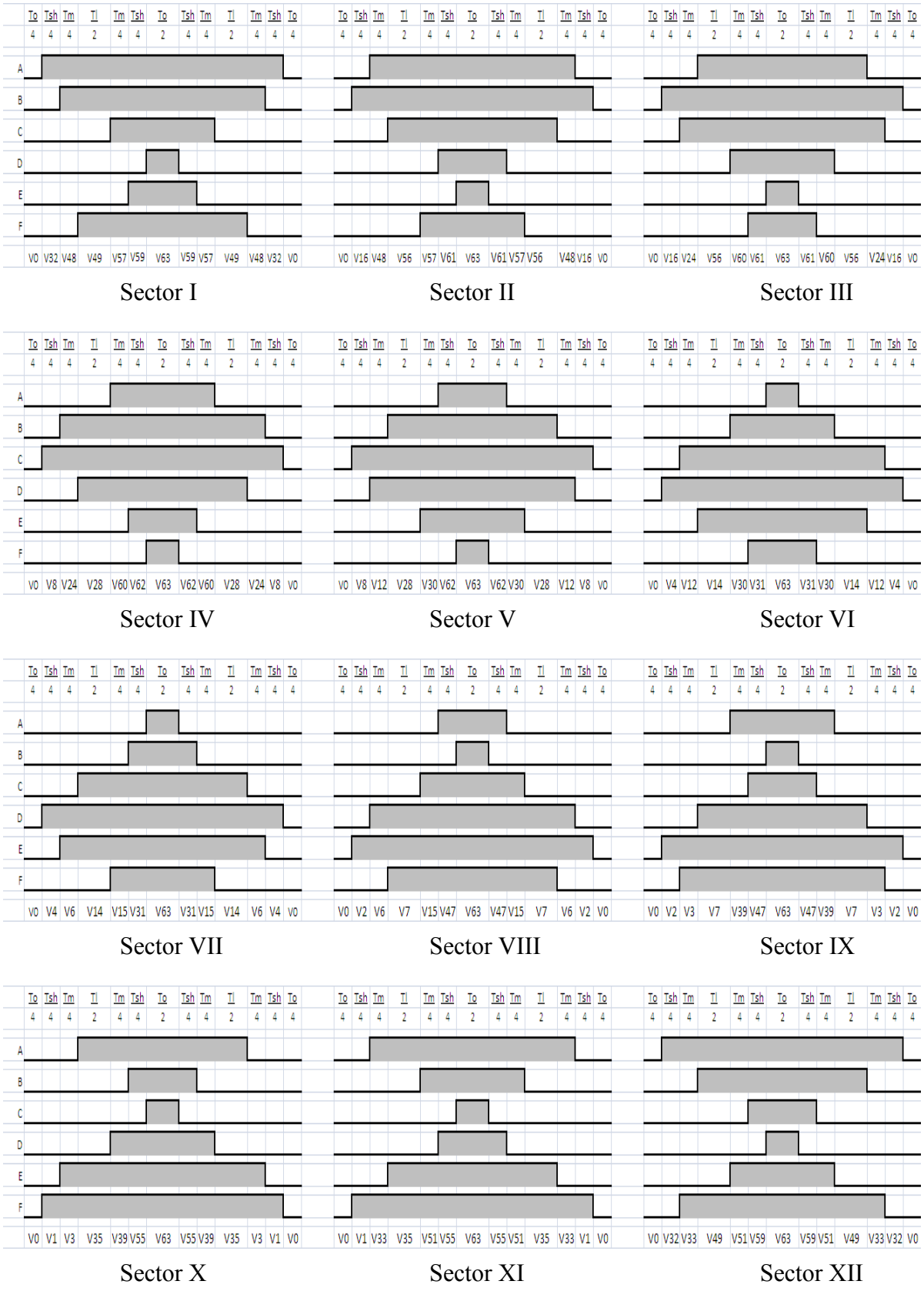

Fig. 4.4: Switching sequences of SVPWM for two-level symmetrical six-phase VSI.

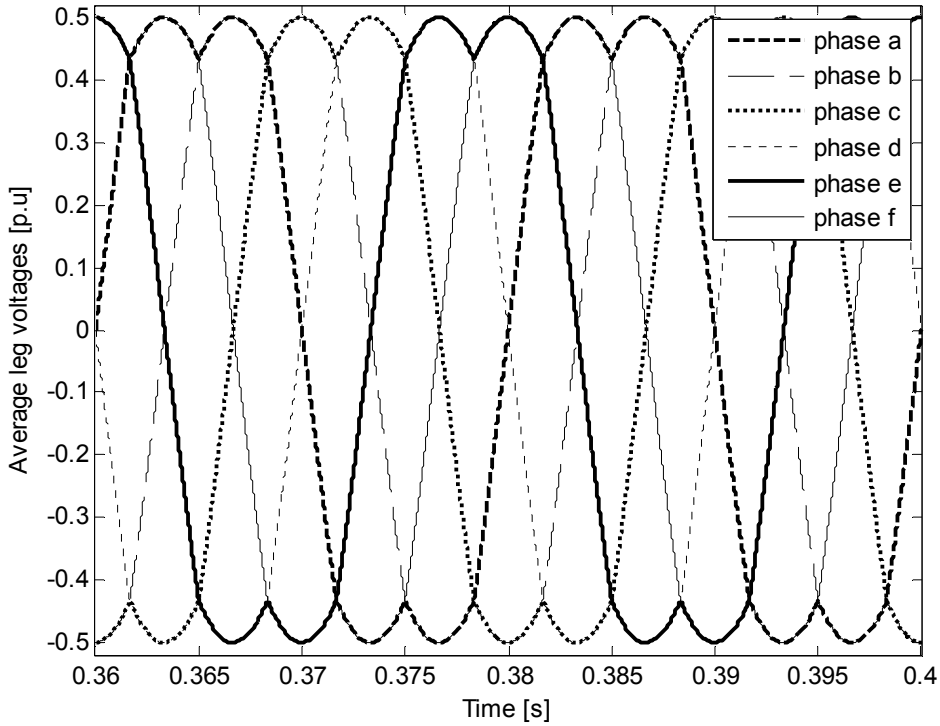

Fig. 4.5: Average leg voltages for SVPWM technique for $\rho = 1$ and $M = 2/\sqrt{3}$.

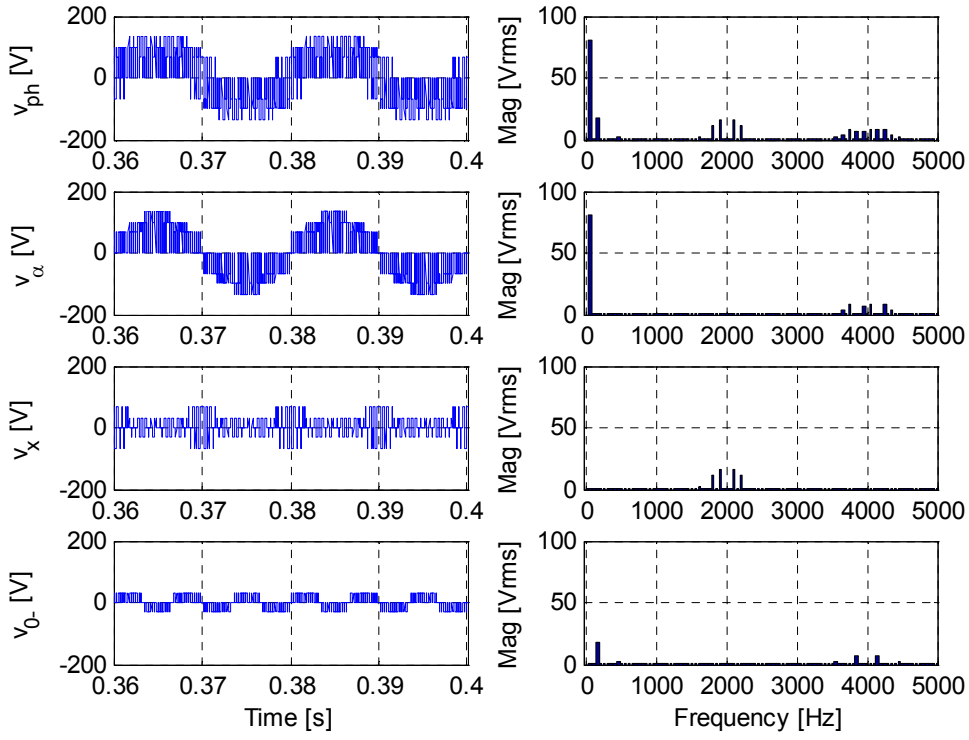

Fig. 4.6: Phase voltage components and frequency spectra for $\rho = 1$ and $M = 2/\sqrt{3}$. From top to bottom: phase voltage, α-component, x-component, and 0-component.

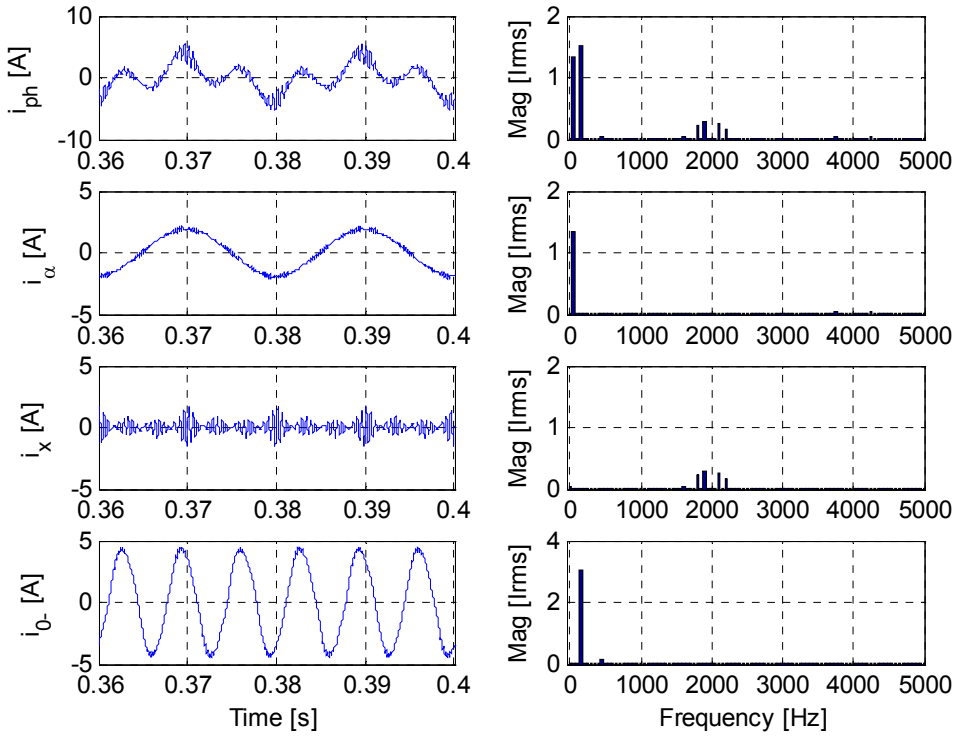

Fig. 4.7: Current components and frequency spectra for $\rho = 1$ and $M = 2/\sqrt{3}$.
From top to bottom: phase current, α-component, x-component, and 0-component.

4.3.2 SVPWM for $\rho = 2/3$

As the control variable is chosen to be ρ = 2/3, it can be seen from (4.9) that $T_l = T_{sh}$. Therefore, the SVPWM technique with ρ = 2/3 utilises seven switching states (i.e. one for large, two for medium, two for short, and two for zero space vector) during a switching period. The range of modulation index for this technique is $0 \le M \le 1$.

The average leg voltages for $M_{\max} = 1$ are shown in Fig. 4.8. The filtered leg voltages are purely sinusoidal without any low-order harmonic injection. The inverter's phase voltage and current components, accompanied by their frequency spectra, are shown in Figs. 4.9 - 4.10.

There are no low-order harmonics in the phase voltage and current since the low-order harmonics in the (x-y) plane and 0-components are all eliminated. The nearest harmonics of the 0-components are located in the side-band around twice the switching frequency. The amplitude of the fundamental component of phase voltage for $M = 1$ is $V_1 = 70.7107$ Vrms, which is lower compared to the value obtained for $\rho = 1$.

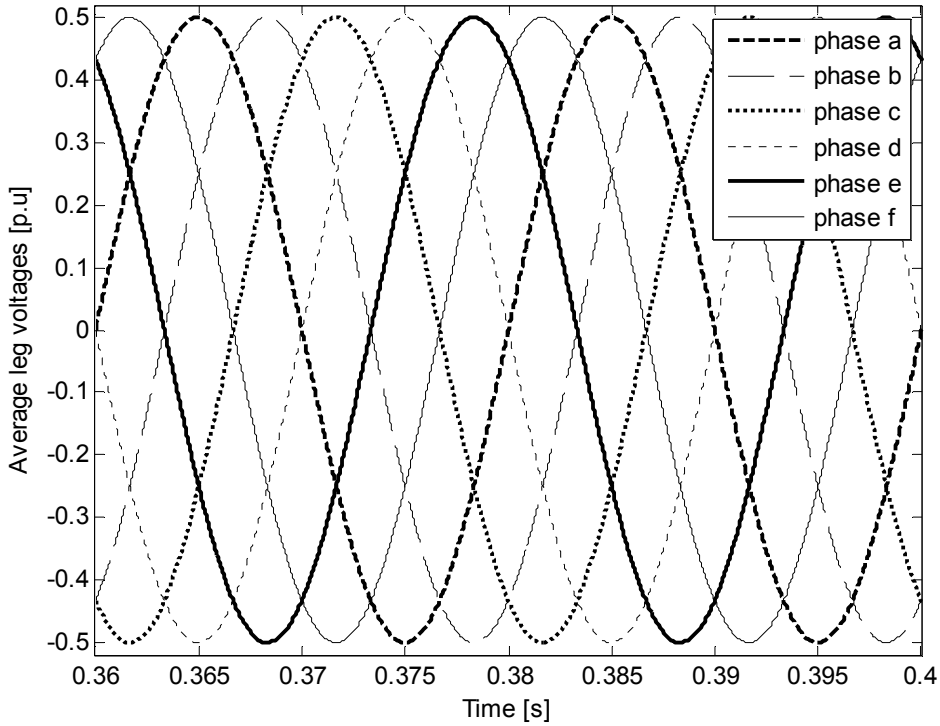

Fig. 4.8: Average leg voltages for SVPWM technique for $\rho = 2/3$ and $M_{\max} = 1$.

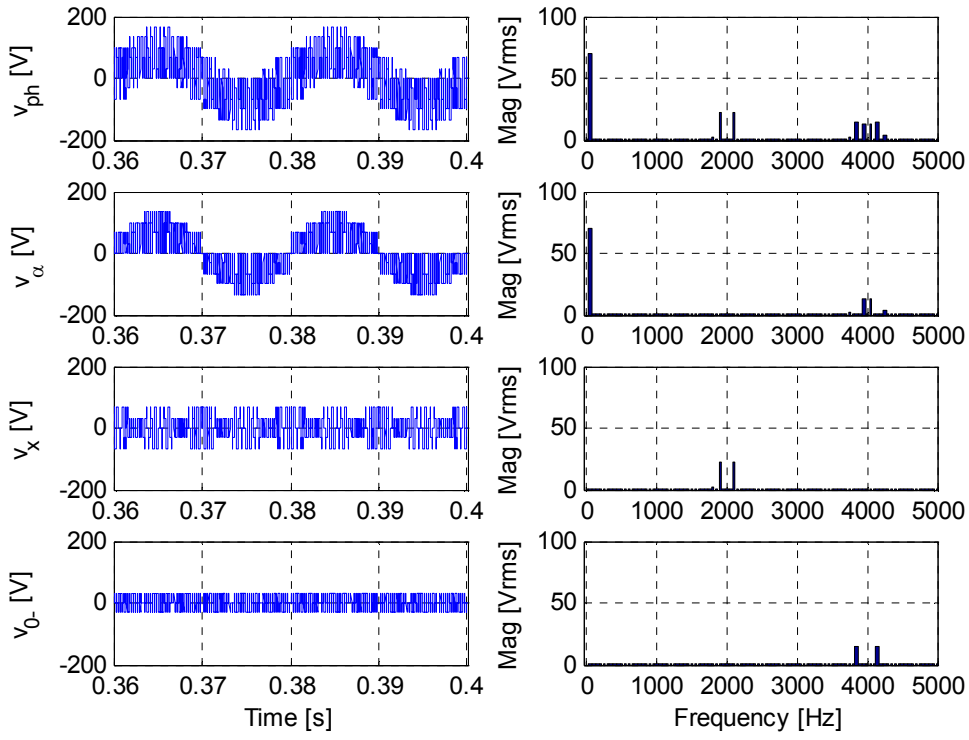

Fig. 4.9: Voltage components and frequency spectra for $\rho = 2/3$ and $M_{\max} = 1$.
From top to bottom: phase voltage, α-component, x-component, and 0-component.

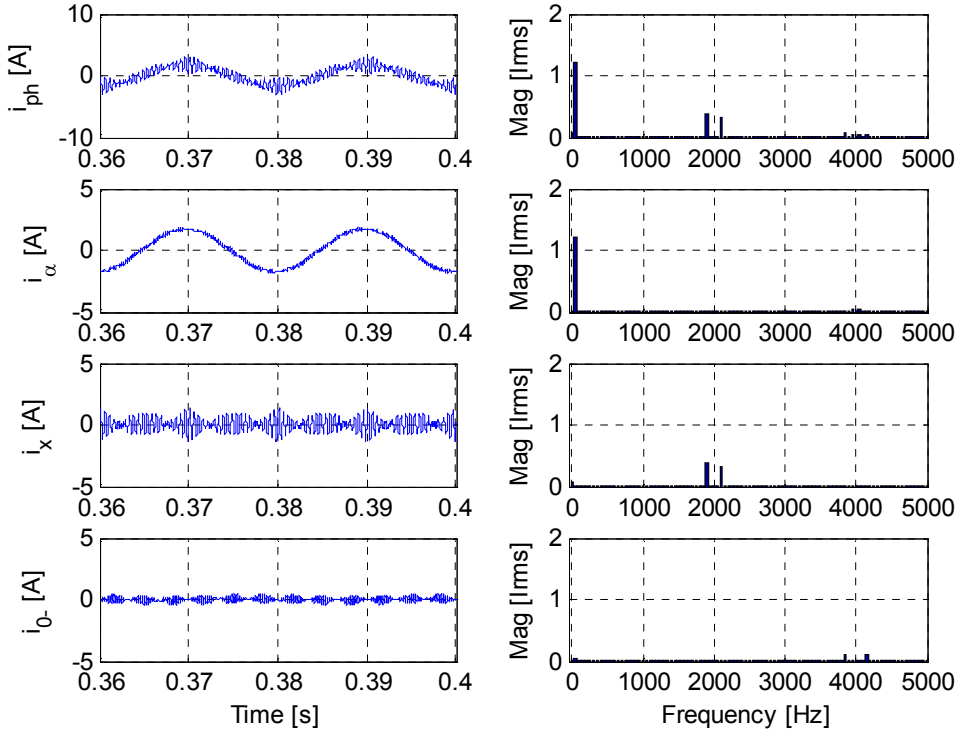

Fig. 4.10: Current components and frequency spectra for $\rho = 2/3$ and $M_{\max} = 1$.
From top to bottom: phase current, α-component, x-component, and 0-component.

For the purpose of performance comparison later on, the THD of the phase voltage and current and also their α-, x-, and 0-component is calculated using (3.16) for values of modulation index spanning from $M = 0.1$ to $M_{\max} = 1$ in 0.1 increments. Similar to Section 3.5, the simulations are again conducted by considering the non-ideal characteristics of the semiconductor devices and also the dead-time requirement of the inverter. The results are shown in Tables 4.4 - 4.5. The THDs of 0-component are mainly contributed by the harmonics around nf_s multiples, where n = 2, 4, 6... and f_s is the switching frequency (2 kHz).

4.3.3 SVPWM for linear variation of ρ

Another SVPWM technique can be applied by varying the value of ρ. As ρ is linearly increased in the range of $2/3 < \rho < 1$ [Dujic et al. (2007a)], the utilisation of the dc bus voltage is gradually improved. The low-order harmonics are also kept to a minimum in the lower part of the range and only attain maximum amplitude when $\rho = 1$. This technique is only applied for modulation index range of $1 \le M \le 2/\sqrt{3}$. The variation of ρ, as function of the modulation index, is expressed as follows:

$$\rho = -\frac{1}{3-2\sqrt{3}}M + \frac{3\sqrt{3}-4}{3\sqrt{3}-6} \qquad (4.10)$$

Table 4.4: Phase voltage fundamental component and THDs, along with THDs of α-, x- and 0-component voltage for SVPWM technique with $\rho = 2/3$.

M	v_{ph}		v_α	v_x	v_{0-}	
	V_1(rms)	THD	THD	THD	THD	v_{ph} level
0.1	5.5777	3.5814	3.3523	1.1030	0.5973	11
0.2	12.6565	2.6278	2.2840	1.1171	0.6651	11
0.3	20.1309	2.0366	1.7166	0.9447	0.5588	11
0.4	26.9549	1.7089	1.3998	0.8382	0.5046	11
0.5	34.2026	1.4551	1.1573	0.7583	0.4521	11
0.6	41.2921	1.2642	0.9718	0.6951	0.4151	11
0.7	48.2129	1.1125	0.8160	0.6499	0.3864	11
0.8	55.3096	0.9786	0.6751	0.6084	0.3623	11
0.9	62.5271	0.8573	0.5374	0.5724	0.3422	11
1.0	69.7365	0.7489	0.3947	0.5476	0.3267	11

Table 4.5: Load current fundamental component and THDs, along with THDs of α-, x- and 0-component current for SVPWM technique with $\rho = 2/3$.

M	i_{ph}		i_α	i_x	i_{0-}
	I_1(rms)	THD	THD	THD	THD
0.1	0.7301	0.3346	0.0664	0.0238	0.3268
0.2	1.0154	0.2761	0.0918	0.0416	0.2539
0.3	1.1985	0.2788	0.1754	0.0663	0.2047
0.4	1.1446	0.4003	0.3468	0.1064	0.1991
0.5	1.1493	0.3564	0.2686	0.1514	0.1810
0.6	1.1516	0.3379	0.2050	0.1993	0.1781
0.7	1.1124	0.3470	0.1353	0.2615	0.1806
0.8	1.1541	0.3757	0.1178	0.3084	0.1809
0.9	1.1573	0.4273	0.1005	0.3684	0.1886
1.0	1.1666	0.4770	0.0752	0.4341	0.1830

From (4.9), as ρ is linearly increased, the T_{sh} is decreased and becomes zero at $\rho = 1$. Seven switching states are utilised during a switching period except when $\rho = 1$. The average leg voltages for $M = 1.0392$ (90% of $M_{\max}$) are illustrated in Fig. 4.11 and they are again non-sinusoidal due to the generation of the 0-component harmonics. The phase voltage and current components are shown in Fig. 4.12 and Fig. 4.13, respectively. The amplitude of the fundamental component of phase voltage is 73.4825 Vrms, which is

higher than the value obtained for $\rho = 2/3$. Meanwhile, the amplitude of the third harmonic is 3.6 Vrms, which is lower than when $\rho = 1$. This situation can continuously be observed as ρ linearly varies within the mentioned range.

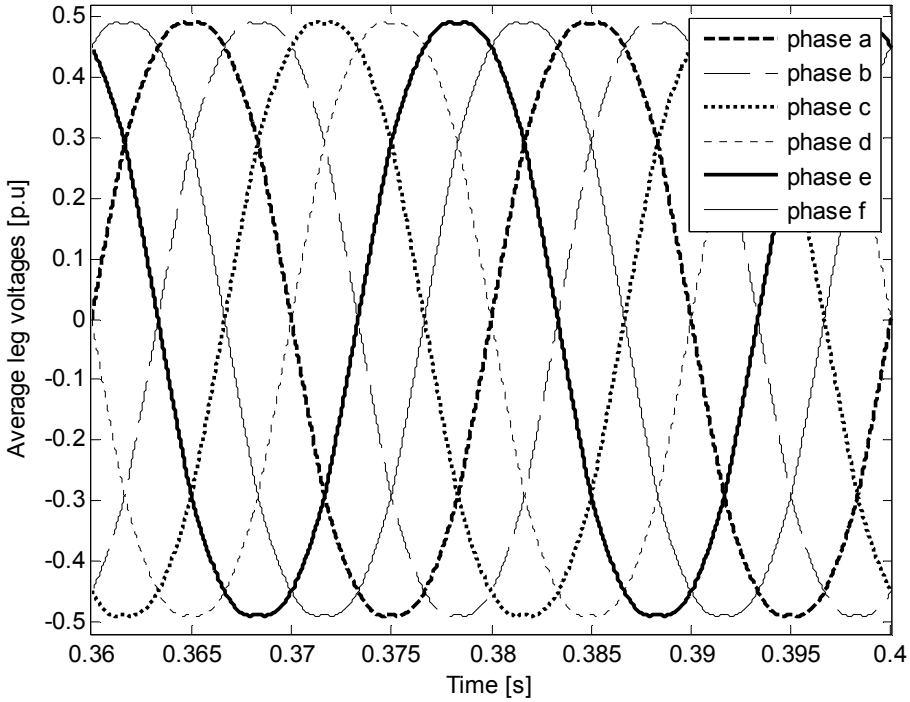

Fig. 4.11: Average leg voltages for SVPWM with linear variation of ρ ($M = 1.0392$).

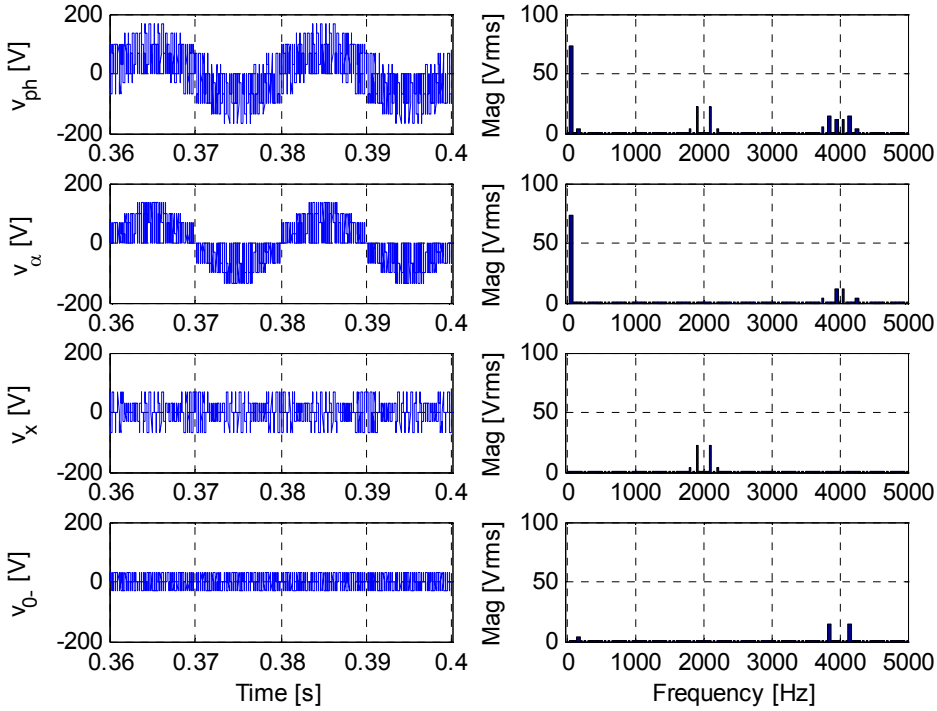

Fig. 4.12: Voltage components and frequency spectra for linear variation of ρ ($M = 1.0392$). From top to bottom: phase voltage, α-component, x-component, and 0-component.

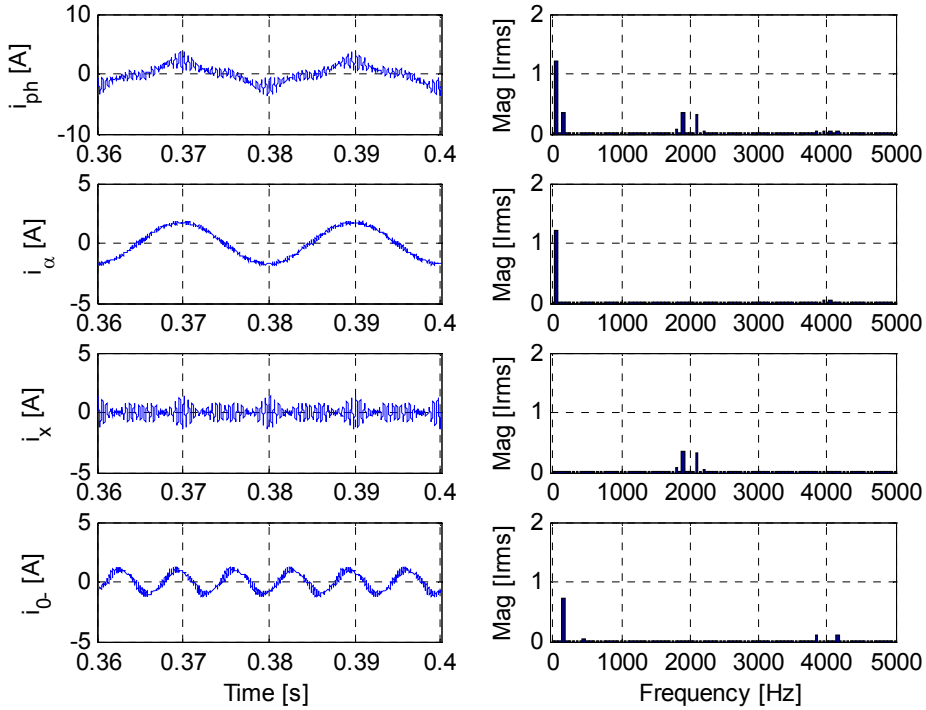

Fig. 4.13: Current components and frequency spectra for linear variation of ρ (M = 1.0392). From top to bottom: phase current, α-component, x-component, and 0-component.

4.4 Performance comparison of SVPWM techniques

Based on the discussion of the three SVPWM techniques for the two-level six-phase VSI having symmetrical machine connected to a single neutral point, it can be seen that the low-order harmonics can be eliminated by choosing ρ = 2/3. However, the maximum amplitude of fundamental component of phase voltage is limited to V_1 = 70.7107 Vrms. On the other hand, with ρ = 1, the maximum fundamental component of phase voltage can be increased to V_1 = 81.6497 Vrms. The amplitude of fundamental component of phase voltage is higher, which reflects the better utilisation of dc bus, but unfortunately with the presence of some undesired low-order harmonics. The compromise of the two situations is possible by chosing ρ value that can be linearly varied in the range of $2/3 < \rho < 1$. As the value of ρ is increased within that range, the utilisation of the dc bus is also improved while at the same time minimising the presence of low-order harmonics.

4.5 Summary

This chapter has elaborated the phase voltage space vector model for the two-level six-phase VSI with a symmetrical machine connected to a single neutral point. Then, three

SVPWM techniques for the inverter control are discussed, each utilising a different value of control variable ρ. MATLAB/Simulink simulations have also been carried out in order to analyse and compare their performance.

It has been found that, by using $\rho = 2/3$, the low-order harmonics are all eliminated. Since further on only the pure sinusoidal output voltage will be considered, the SVPWM technique for $\rho = 2/3$ will be used. This limits the maximum modulation index to 1, as with pure sinusoidal PWM of a three-phase VSI. The THD of phase voltage and its components for $\rho = 2/3$ has also been calculated for $0 \le M \le 1$ and will be used for performance comparison later on.

Chapter 5

VOLTAGE SPACE VECTORS FOR SIX-PHASE DRIVES WITH DUAL-INVERTER SUPPLY

5.1 Introduction

This chapter discusses voltage space vectors for the symmetrical and asymmetrical six-phase drives with dual-inverter supply. The topology of the dual-inverter supplied drive is at first explained. This is followed by an analysis of the voltage space vectors produced by the dual-inverter supplied symmetrical and asymmetrical six-phase drives.

5.2 Drive topology

The dual-inverter supply topology comprises an open-end structure of stator winding which is then supplied from both ends by a VSI. Two two-level VSIs are most commonly utilised, but the windings can also be supplied using higher level VSIs [Shuai and Corzine (2007), Stemmler and Guggenbach (1993)] or even by two VSIs that operate with a different number of levels [Kawabata et al. (2002), Lakshminarayanan et al. (2007)] . The existing body of work for a machine with open-end structure is mainly focused on a three-phase drive, while only a few papers investigate this topology in conjunction with multiphase machines.

The structure of an open-end winding six-phase drive, supplied by two two-level VSIs, is shown in Fig. 5.1. The structure for both open end winding symmetrical and asymmetrical drive configurations is the same. The only difference is the machine structure. For both symmetrical and asymmetrical six-phase machine, the stator windings are opened at both ends, and each end is supplied using a two-level six-phase inverter. This arrangement will be referred to further on as a dual-inverter supply topology. The two inverters are identified with indices 1 and 2. The upper case symbol (*A, B, C, D, E, F*) is again used to denote the inverter legs while the machine phases are once more denoted by a lower case symbol (*a, b, c, d, e, f*). The negative rails of the dc bus are identified as $N1$ and $N2$.

The inverters are supplied by isolated dc bus voltages, labelled as V_{dc1} and V_{dc2}. The value of the dc bus voltages is set to half of the dc voltage that is used by the six-phase drive when one end of the winding is connected to the two-level VSI while the other end is connected into neutral point (termed further on as a single-sided supply topology). The relationship between the dc bus voltages is written as follows:

$$V_{dc1} = V_{dc2} = 0.5V_{dc} \tag{5.1}$$

where V_{dc} stands for the equivalent dc supply in single-sided supply topology.

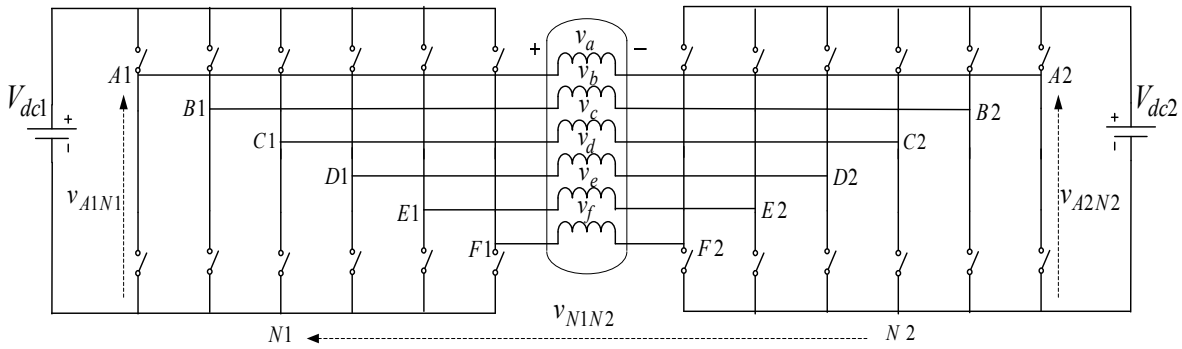

Fig. 5.1: Drive topology of dual two-level VSI supply for open-end winding six-phase drive.

For the dual-inverter supply topology, the phase voltages across the open-end windings can be given as follows:

$$\begin{aligned}
v_a &= v_{A1N1} + v_{N1N2} - v_{A2N2} \\
v_b &= v_{B1N1} + v_{N1N2} - v_{B2N2} \\
v_c &= v_{C1N1} + v_{N1N2} - v_{C2N2} \\
v_d &= v_{D1N1} + v_{N1N2} - v_{D2N2} \\
v_e &= v_{E1N1} + v_{N1N2} - v_{E2N2} \\
v_f &= v_{F1N1} + v_{N1N2} - v_{F2N2}
\end{aligned} \tag{5.2}$$

Since the two dc bus voltages are assumed to be isolated and the sum of phase voltages is equal to zero, one can write:

$$v_a + v_b + v_c + v_d + v_e + v_f = 0 \tag{5.3}$$

Using (5.3), the summation of (5.2) yields:

$$\begin{aligned}
v_{N1N2} = -\frac{1}{6}\left(v_{A1N1} + v_{B1N1} + v_{C1N1} + v_{D1N1} + v_{E1N1} + v_{F1N1}\right) + \frac{1}{6}(v_{A2N2} + \\
v_{B2N2} + v_{C2N2} + v_{D2N2} + v_{E2N2} + v_{F2N2})
\end{aligned} \tag{5.4}$$

The relationship between the phase voltages and leg voltages can be obtained by substituting (5.4) into (5.2). The relationship can be written (in matrix form) as follows:

$$\begin{bmatrix} v_a \\ v_b \\ v_c \\ v_d \\ v_e \\ v_f \end{bmatrix} = \frac{1}{6} \begin{bmatrix} 5 & -1 & -1 & -1 & -1 & -1 \\ -1 & 5 & -1 & -1 & -1 & -1 \\ -1 & -1 & 5 & -1 & -1 & -1 \\ -1 & -1 & -1 & 5 & -1 & -1 \\ -1 & -1 & -1 & -1 & 5 & -1 \\ -1 & -1 & -1 & -1 & -1 & 5 \end{bmatrix} \begin{bmatrix} v_{A1N1} - v_{A2N2} \\ v_{B1N1} - v_{B2N2} \\ v_{C1N1} - v_{C2N2} \\ v_{D1N1} - v_{D2N2} \\ v_{E1N1} - v_{E2N2} \\ v_{F1N1} - v_{F2N2} \end{bmatrix} \quad (5.5)$$

5.3 Voltage space vectors for dual-inverter six-phase supply

The dual-inverter supply topology provides a much higher number of switching state combinations, compared to the single-sided supply topology. Here, the two inverters can be controlled independently; therefore in total, 64 x 64 = 4096 switching state combinations are available for both symmetrical and asymmetrical configurations.

Since the dual-inverter supply topology has much higher number of switching state combinations than the single-sided supply, the topology also produces more space vectors. In the next subsection, the voltage space vectors generated by the topology are discussed.

5.3.1 Voltage space vectors for the dual-inverter symmetrical six-phase drive

For the dual two-level VSI supplying open-end symmetrical six-phase machine, the projections of space vectors for the phase voltages in the (α-β) and (x-y) planes, and 0_+- and 0_--axes can be obtained by using (4.5) and (5.5). The projections of space vectors in the (α-β) and (x-y) planes and 0_--axis are as shown in Fig. 5.2. As can be seen in the (α-β) and (x-y) planes, the space vectors are mapped into 61 locations. The space vectors are mapped with nine different magnitudes, which are $2/3\,V_{dc}$, $3/5\,V_{dc}$, $1/\sqrt{3}\,V_{dc}$, $1/2\,V_{dc}$, $0.441V_{dc}$, $1/3\,V_{dc}$, $1/\sqrt{12}\,V_{dc}$, $1/6\,V_{dc}$ and zero.

Regarding mapping on the 0_+- and 0_--axes, the 0_+-components are all equal to zero, which is similar to the single-sided supply topology. Meanwhile, the components along the 0_--axis are positioned at thirteen locations. The components are on the straight line of 0_--axis and take seven different magnitudes, which are $\pm 1/2\,V_{dc}$, $\pm 5/12\,V_{dc}$, $\pm 1/3\,V_{dc}$, $\pm 1/4\,V_{dc}$, $\pm 1/6\,V_{dc}$, $\pm 1/12\,V_{dc}$ and zero.

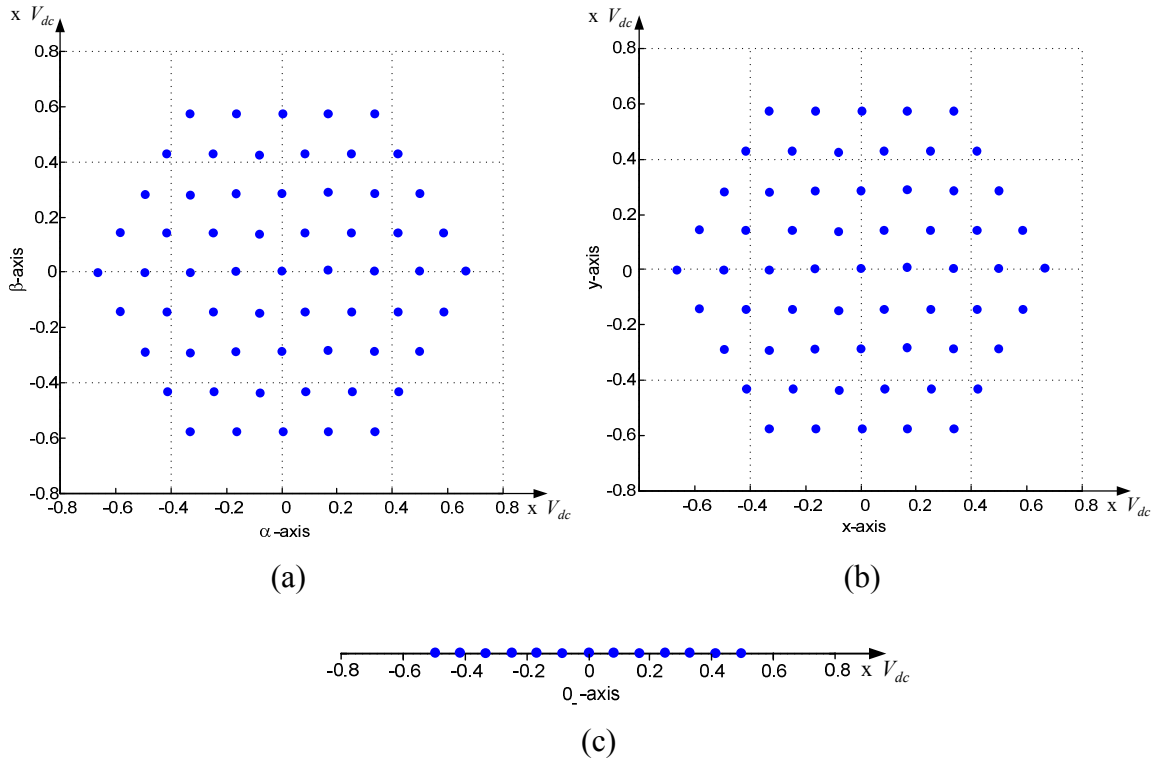

Fig. 5.2: Mapping of phase voltage space vectors for the dual-inverter symmetrical six-phase drive: (a) in (α-β) plane; (b) in (x-y) plane; (c) in 0_-axis.

5.3.1.1 Analysis of the voltage space vectors for the dual-inverter symmetrical six-phase drive

The space vectors are produced by the interactions of space vectors developed by the two inverters. In order to determine the space vectors for the dual-inverter supply topology, the space vectors which are obtained by individually operating the inverters as a single-sided supply topology with 0.5 V_{dc} (5.1), are considered first. Then the mapping of space vectors for the dual-inverter supply topology can be determined by analysing the interactions between various groups of space vectors.

For a symmetrical six-phase drive configured with the single-sided supply topology, the space vectors with 0.5 V_{dc} supply, are shown in Fig. 5.3. The groups of space vectors that are mapped in the (α-β) and (x-y) planes can be represented by the equations given in Tables 5.1 - 5.2. On the other hand, the groups of 0_-components can be represented by equations shown in Tables 5.3 - 5.4. The symbols k and l denote the k^{th} and the l^{th} space vector for each group of space vectors for inverter 1 and inverter 2, respectively.

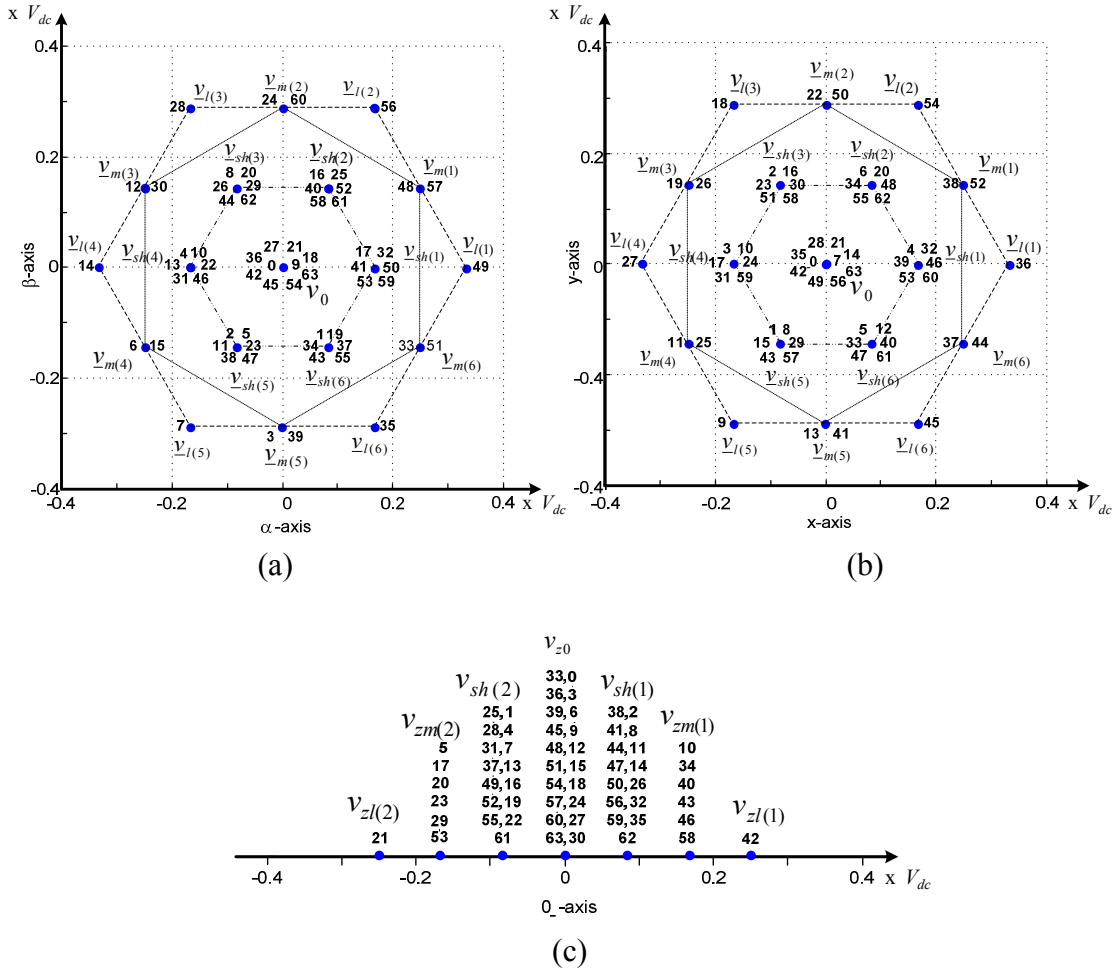

Fig. 5.3: Symmetrical six-phase drive - space vectors mapping for inverter 1 and 2 operated as a single-sided supply topology with 0.5 V_{dc} supply: (a) in (α-β) plane; (b) in (x-y) plane; (c) in 0_-axis.

The interaction between the large, medium, short and zero space vectors of inverter 1 with the large, medium, short and zero space vectors of inverter 2 is analysed based on the following equations:

$$\begin{aligned} \underline{v}_{\alpha\beta} &= \underline{v}_{\alpha\beta(INV\,1)} - \underline{v}_{\alpha\beta(INV\,2)} \\ \underline{v}_{xy} &= \underline{v}_{xy(INV\,1)} - \underline{v}_{xy(INV\,2)} \\ v_{0_+} &= v_{0_+(INV\,1)} - v_{0_+(INV\,2)} \\ v_{0\_} &= v_{0\_(INV\,1)} - v_{0\_(INV\,2)} \end{aligned} \qquad (5.6)$$

The analysis leads to the expressions presented in Tables 5.5 - 5.6.

Table 5.1: Symmetrical six-phase drive - space vectors in (α-β) and (x-y) planes (inverter 1).

Space vectors	Value of space vectors	Angular position
Large ($\underline{v}_{l(k)}$)	$\frac{1}{3}V_{dc}e^{j(k-1)\frac{\pi}{3}}$ for k = 1, 2, ..., 6	$(k-1)\pi/3$
Medium ($\underline{v}_{m(k)}$)	$\frac{1}{\sqrt{12}}V_{dc}e^{j(2k-1)\frac{\pi}{6}}$ for k = 1, 2, ..., 6	$(2k-1)\pi/6$
Short ($\underline{v}_{sh(k)}$)	$\frac{1}{6}V_{dc}e^{j(k-1)\frac{\pi}{3}}$ for k = 1, 2, ..., 6	$(k-1)\pi/3$
Zero ($\underline{v}_0$)	0	0

Table 5.2: Symmetrical six-phase drive - space vectors in (α-β) and (x-y) planes (inverter 2).

Space vectors	Value of space vectors	Angular position
Large ($\underline{v}_{l(l)}$)	$\frac{1}{3}V_{dc}e^{j(l-1)\frac{\pi}{3}}$ for l = 1, 2, ..., 6	$(l-1)\pi/3$
Medium ($\underline{v}_{m(l)}$)	$\frac{1}{\sqrt{12}}V_{dc}e^{j(2l-1)\frac{\pi}{6}}$ for l = 1, 2, ..., 6	$(2l-1)\pi/6$
Short ($\underline{v}_{sh(l)}$)	$\frac{1}{6}V_{dc}e^{j(l-1)\frac{\pi}{3}}$ for l = 1, 2, ..., 6	$(l-1)\pi/3$
Zero ($\underline{v}_0$)	0	0

Table 5.3: Symmetrical six-phase drive - 0-components (inverter 1).

Space vectors	Value of space vectors	Angular position
Large ($v^1_{zl(k)}$)	$\frac{1}{4}V_{dc}e^{j(k-1)\pi}$ for k = 1, 2.	$(k-1)\pi$
Medium ($v^1_{zm(k)}$)	$\frac{1}{6}V_{dc}e^{j(k-1)\pi}$ for k = 1, 2.	$(k-1)\pi$
Short ($v^1_{zsh(k)}$)	$\frac{1}{12}V_{dc}e^{j(k-1)\pi}$ for k = 1, 2.	$(k-1)\pi$
Zero(v^1_{z0})	0	0

Table 5.4: Symmetrical six-phase drive - 0-components (inverter 2).

Space vectors	Value of space vectors	Angular position
Large ($v^2_{zl(k)}$)	$\frac{1}{4}V_{dc}e^{j(l-1)\pi}$ for l = 1, 2.	$(l-1)\pi$
Medium ($v^2_{zm(k)}$)	$\frac{1}{6}V_{dc}e^{j(l-1)\pi}$ for l = 1, 2.	$(l-1)\pi$
Short ($v^2_{zsh(k)}$)	$\frac{1}{12}V_{dc}e^{j(l-1)\pi}$ for l = 1, 2.	$(l-1)\pi$
Zero(v^2_{z0})	0	0

Table 5.5: Symmetrical six-phase drive - space vectors in (α-β) and (x-y) planes for the dual-inverter supply topology.

		Inverter 2			
		$\underline{v}_{l(l)}$	$\underline{v}_{m(l)}$	$\underline{v}_{sh(l)}$	v_0
Inverter 1	$\underline{v}_{l(k)}$	$\frac{1}{3}V_{dc}(e^{j(k-1)\frac{\pi}{3}} - e^{j(l-1)\frac{\pi}{3}})$	$\frac{1}{3}V_{dc}e^{j(k-1)\frac{\pi}{3}} - \frac{1}{\sqrt{12}}V_{dc}e^{j(2l-1)\frac{\pi}{6}}$	$\frac{1}{3}V_{dc}(e^{j(k-1)\frac{\pi}{3}} - 0.5e^{j(l-1)\frac{\pi}{3}})$	$\frac{1}{3}V_{dc}e^{j(k-1)\frac{\pi}{3}}$
	$\underline{v}_{m(k)}$	$\frac{1}{\sqrt{12}}V_{dc}e^{j(2k-1)\frac{\pi}{6}} - \frac{1}{3}V_{dc}e^{j(l-1)\frac{\pi}{3}}$	$\frac{1}{\sqrt{12}}V_{dc}(e^{j(2k-1)\frac{\pi}{6}} - e^{j(2l-1)\frac{\pi}{6}})$	$\frac{1}{\sqrt{12}}V_{dc}e^{j(2k-1)\frac{\pi}{6}} - \frac{1}{6}V_{dc}e^{j(l-1)\frac{\pi}{3}}$	$\frac{1}{\sqrt{12}}V_{dc}e^{j(2k-1)\frac{\pi}{6}}$
	$\underline{v}_{sh(k)}$	$\frac{1}{3}V_{dc}(0.5e^{j(k-1)\frac{\pi}{3}} - e^{j(l-1)\frac{\pi}{3}}$	$\frac{1}{6}V_{dc}e^{j(k-1)\frac{\pi}{3}} - \frac{1}{\sqrt{12}}V_{dc}e^{j(2l-1)\frac{\pi}{6}}$	$\frac{1}{6}V_{dc}(e^{j(k-1)\frac{\pi}{3}} - e^{j(l-1)\frac{\pi}{3}})$	$\frac{1}{6}V_{dc}e^{j(k-1)\frac{\pi}{3}}$
	$\underline{v}_0$	$-\frac{1}{3}V_{dc}e^{j(l-1)\frac{\pi}{3}}$	$-\frac{1}{\sqrt{12}}V_{dc}e^{j(2l-1)\frac{\pi}{6}}$	$-\frac{1}{6}V_{dc}e^{j(l-1)\frac{\pi}{3}}$	0

Table 5.6: Symmetrical six-phase drive - 0-components for the dual-inverter supply topology.

		Inverter 2			
		$v^2_{zl(l)}$	$v^2_{zm(l)}$	$v^2_{zsh(l)}$	v^2_{z0}
Inverter 1	$v_{zl(k)}$	$\frac{1}{4}V_{dc}(e^{j(k-1)\pi} - e^{j(l-1)\pi})$	$\frac{1}{4}V_{dc}e^{j(k-1)\pi} - \frac{1}{6}V_{dc}e^{j(l-1)\pi}$	$\frac{1}{4}V_{dc}e^{j(k-1)\pi} - \frac{1}{12}V_{dc}e^{j(l-1)\pi}$	$\frac{1}{4}V_{dc}e^{j(k-1)\pi}$
	$v_{zm(k)}$	$\frac{1}{6}V_{dc}e^{j(k-1)\pi} - \frac{1}{4}V_{dc}e^{j(l-1)\pi}$	$\frac{1}{6}V_{dc}(e^{j(k-1)\pi} - e^{j(l-1)\pi})$	$\frac{1}{6}V_{dc}e^{j(k-1)\pi} - \frac{1}{12}V_{dc}e^{j(l-1)\pi}$	$\frac{1}{6}V_{dc}e^{j(k-1)\pi}$
	$v_{zsh(k)}$	$\frac{1}{12}V_{dc}e^{j(k-1)\pi} - \frac{1}{4}V_{dc}e^{j(l-1)\pi}$	$\frac{1}{12}V_{dc}e^{j(k-1)\pi} - \frac{1}{6}V_{dc}e^{j(l-1)\pi}$	$\frac{1}{12}V_{dc}(e^{j(k-1)\pi} - e^{j(l-1)\pi})$	$\frac{1}{12}V_{dc}e^{j(k-1)\pi}$
	v_{z0}	$-\frac{1}{4}V_{dc}e^{j(l-1)\pi}$	$-\frac{1}{6}V_{dc}e^{j(l-1)\pi}$	$-\frac{1}{12}V_{dc}e^{j(l-1)\pi}$	0

5.3.2 Voltage space vectors for the dual-inverter asymmetrical six-phase drive

For the dual two-level VSI supplying an open-end asymmetrical six-phase machine, the projections of space vectors for the phase voltages in the (α-β) and (x-y) planes, and in the (0_+ -0_-) axes can be obtained by using (3.5) and (5.5). Figs. 5.4(a) - (b) show the projections of phase voltage space vectors in the (α-β) and (x-y) planes while the distribution of the vectors in the (0_+ -0_-) axes are plotted in Fig. 5.4(c).

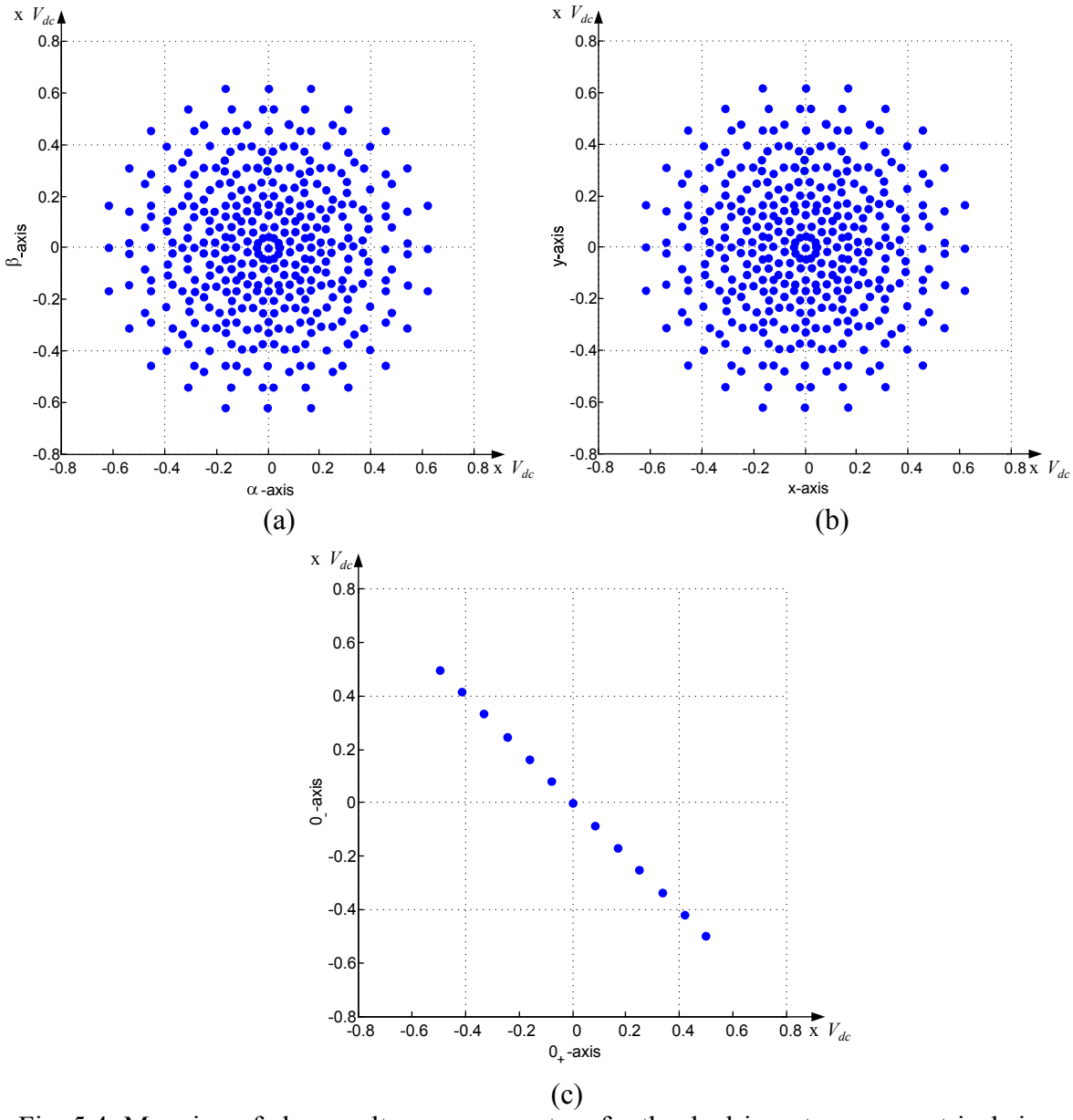

Fig. 5.4: Mapping of phase voltage space vectors for the dual-inverter asymmetrical six-phase drive: (a) in (α-β) plane; (b) in (x-y) plane; (c) in (0_+-0_-) axes.

The non-zero space vectors in the (α-β) and (x-y) planes are mapped into 361 locations with 23 different magnitudes and the magnitude of the largest and shortest space vectors are $0.6440V_{dc}$ and $0.0447V_{dc}$. respectively For the (0_+-0_-) components, the space

vectors occupy thirteen locations with six different non-zero magnitudes which are $\sqrt{2}/12\,V_{dc}$, $\sqrt{2}/6\,V_{dc}$, $\sqrt{2}/4\,V_{dc}$, $\sqrt{2}/3\,V_{dc}$, $0.5893V_{dc}$, $\sqrt{2}/2\,V_{dc}$ and zero.

5.3.2.1 Analysis of the voltage space vectors for the dual-inverter asymmetrical six-phase drive

The space vectors of the inverter when they are individually operated as a single-sided supply topology with 0.5 V_{dc} supply, are shown in Fig. 5.5.The groups of space vectors that are mapped in the (α-β) and (x-y) planes are represented by the equations given in Tables 5.7 - 5.8. On the other hand, the groups of (0_+-0_-) components are represented by equations shown in Tables 5.9 - 5.10.

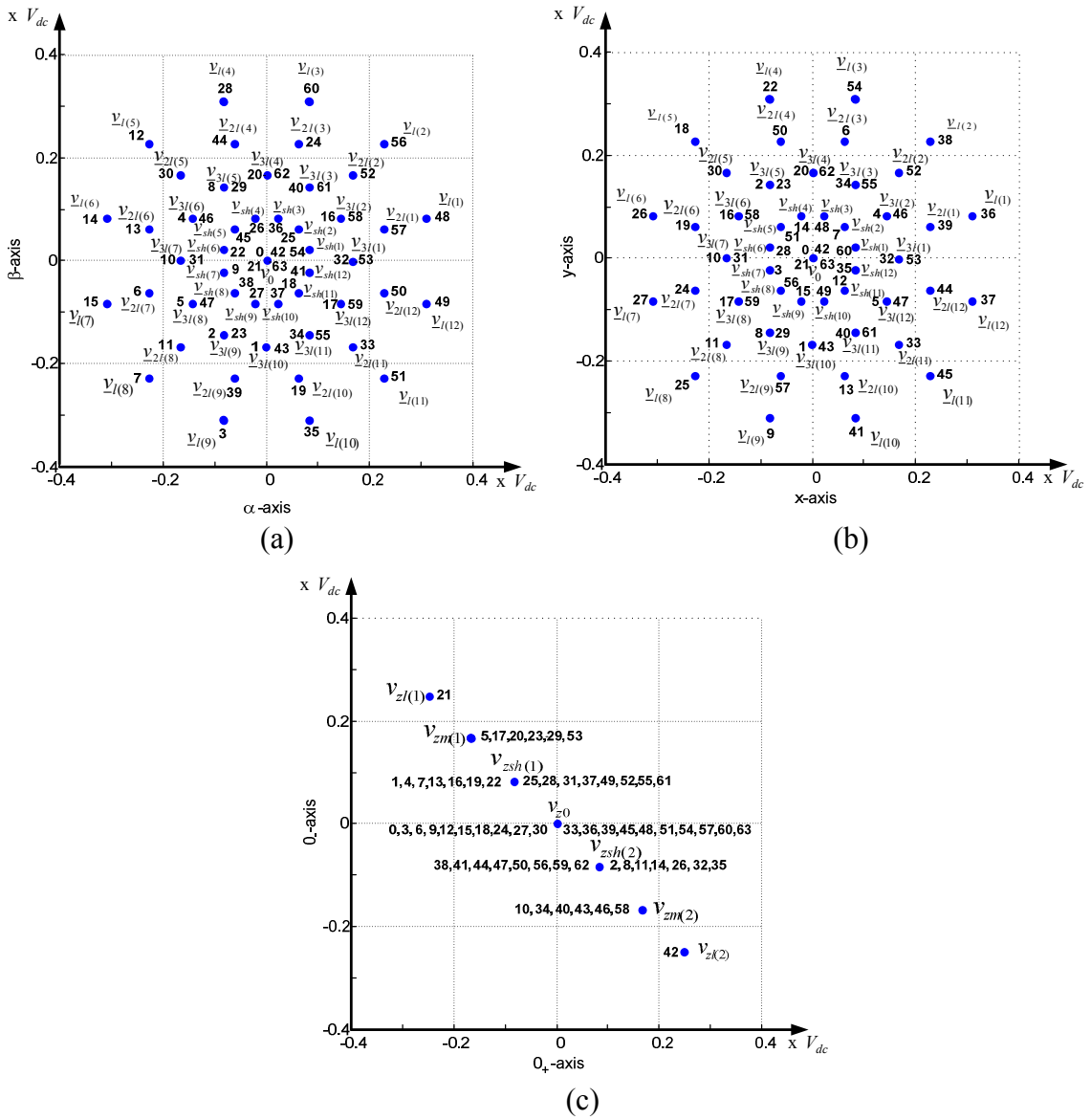

Fig. 5.5: Asymmetrical six-phase drive - space vectors mapping for inverter 1 and 2 operated as a single-sided supply topology with 0.5 V_{dc} supply: (a) in (α-β) plane; (b) in (x-y) plane; (c) in (0_+-0_-) axes.

Table 5.7: Asymmetrical six-phase drive - space vectors in (α-β) and (x-y) planes (inverter 1).

Space vectors	Value of space vectors	Angular position
Largest ($\underline{v}_{l(k)}$)	$\frac{\sqrt{2+\sqrt{3}}}{6}V_{dc}e^{j(2k-1)\frac{\pi}{12}}$ for k = 1, 2, ..., 12	$(2k-1)\pi/12$
Second largest ($\underline{v}_{2l(k)}$)	$\frac{\sqrt{2}}{6}V_{dc}e^{j(2k-1)\frac{\pi}{12}}$ for k = 1, 2, ..., 12	$(2k-1)\pi/12$
Third largest ($\underline{v}_{3l(k)}$)	$\frac{1}{6}V_{dc}e^{j(k-1)\frac{\pi}{6}}$ for k = 1, 2, ..., 12	$(k-1)\pi/6$
Shortest ($\underline{v}_{sh(k)}$)	$\frac{\sqrt{2-\sqrt{3}}}{6}V_{dc}e^{j(2k-1)\frac{\pi}{12}}$ for k = 1, 2, ..., 12	$(2k-1)\pi/12$
Zero ($\underline{v}_0$)	0	0

Table 5.8: Asymmetrical six-phase drive - space vectors in (α-β) and (x-y) planes (inverter 2).

Space vectors	Value of space vectors	Angular position
Largest ($\underline{v}_{l(l)}$)	$\frac{\sqrt{2+\sqrt{3}}}{6}V_{dc}e^{j(2l-1)\frac{\pi}{12}}$ for l = 1, 2, ..., 12	$(2l-1)\pi/12$
Second largest ($\underline{v}_{2l(l)}$)	$\frac{\sqrt{2}}{6}V_{dc}e^{j(2l-1)\frac{\pi}{12}}$ for l = 1, 2, ..., 12	$(2l-1)\pi/12$
Third largest ($\underline{v}_{3l(l)}$)	$\frac{1}{6}V_{dc}e^{j(l-1)\frac{\pi}{6}}$ for l = 1, 2, ..., 12	$(l-1)\pi/6$
Shortest ($\underline{v}_{sh(l)}$)	$\frac{\sqrt{2-\sqrt{3}}}{6}V_{dc}e^{j(2l-1)\frac{\pi}{12}}$ for l = 1, 2, ..., 12	$(2l-1)\pi/12$
Zero ($\underline{v}_0$)	0	0

Table 5.9: Asymmetrical six-phase drive - space vectors in (0_+-0_-) axes. (inverter 1).

Space vectors	Value of space vectors	Angular position
Large ($v^1_{zl(k)}$)	$\frac{\sqrt{2}}{4}V_{dc}e^{(4k-1)\frac{\pi}{4}}$ for k = 1, 2	$(4k-1)\pi/4$
Medium ($v^1_{zm(k)}$)	$\frac{\sqrt{2}}{6}V_{dc}e^{(4k-1)\frac{\pi}{4}}$ for k = 1, 2	$(4k-1)\pi/4$
Short ($v^1_{zsh(k)}$)	$\frac{\sqrt{2}}{12}V_{dc}e^{(4k-1)\frac{\pi}{4}}$ for k = 1, 2	$(4k-1)\pi/4$
Zero(v^1_{z0})	0	0

Table 5.10: Asymmetrical six-phase drive - space vectors in (0_+-0_-) axes. (inverter 2).

Space vectors	Value of space vectors	Angular position
Large ($v^2_{zl(l)}$)	$\frac{\sqrt{2}}{4}V_{dc}e^{(4l-1)\frac{\pi}{4}}$ for l = 1, 2	$(4l-1)\pi/4$
Medium ($v^2_{zm(l)}$)	$\frac{\sqrt{2}}{6}V_{dc}e^{(4l-1)\frac{\pi}{4}}$ for l = 1, 2	$(4l-1)\pi/4$
Short ($v^2_{zsh(l)}$)	$\frac{\sqrt{2}}{12}V_{dc}e^{(4l-1)\frac{\pi}{4}}$ for l = 1, 2	$(4l-1)\pi/4$
Zero(v^2_{z0})	0	0

The interaction between the large, medium, short and zero space vectors of inverter 1 with the large, medium, short and zero space vectors of inverter 2 is also analysed based on (5.6). The analysis leads to the expressions of the space vectors for the dual-inverter supply topology, presented in Tables 5.11 - 5.12.

Table 5.11: Asymmetrical six-phase drive - space vectors in (0_+-0_-) axes for dual-inverter supply topology .

		Inverter 2			
		$v^2_{zl(k)}$	$v^2_{zm(k)}$	$v^2_{zsh(k)}$	v^2_{z0}
Inverter 1	$v_{zl(k)}$	$\frac{\sqrt{2}}{4}V_{dc}(e^{(4k-1)\frac{\pi}{4}} - e^{(4l-1)\frac{\pi}{4}})$	$\frac{\sqrt{2}}{4}V_{dc}e^{(4k-1)\frac{\pi}{4}} - \frac{\sqrt{2}}{6}V_{dc}e^{(4l-1)\frac{\pi}{4}}$	$\frac{\sqrt{2}}{4}V_{dc}e^{(4k-1)\frac{\pi}{4}} - \frac{\sqrt{2}}{12}V_{dc}e^{(4l-1)\frac{\pi}{4}}$	$\frac{\sqrt{2}}{4}V_{dc}e^{(4k-1)\frac{\pi}{4}}$
	$v_{zm(k)}$	$\frac{\sqrt{2}}{6}V_{dc}e^{(4k-1)\frac{\pi}{4}} - \frac{\sqrt{2}}{4}V_{dc}e^{(4l-1)\frac{\pi}{4}}$	$\frac{\sqrt{2}}{6}V_{dc}(e^{(4k-1)\frac{\pi}{4}} - e^{(4l-1)\frac{\pi}{4}})$	$\frac{\sqrt{2}}{6}V_{dc}e^{(4k-1)\frac{\pi}{4}} - \frac{\sqrt{2}}{12}V_{dc}e^{(4l-1)\frac{\pi}{4}}$	$\frac{\sqrt{2}}{6}V_{dc}e^{(4k-1)\frac{\pi}{4}}$
	$v_{zsh(k)}$	$\frac{\sqrt{2}}{12}V_{dc}e^{(4k-1)\frac{\pi}{4}} - \frac{\sqrt{2}}{4}V_{dc}e^{(4l-1)\frac{\pi}{4}}$	$\frac{\sqrt{2}}{12}V_{dc}e^{(4k-1)\frac{\pi}{4}} - \frac{\sqrt{2}}{6}V_{dc}e^{(4l-1)\frac{\pi}{4}}$	$\frac{\sqrt{2}}{12}V_{dc}(e^{(4k-1)\frac{\pi}{4}} - e^{(4l-1)\frac{\pi}{4}})$	$\frac{\sqrt{2}}{12}V_{dc}e^{(4k-1)\frac{\pi}{4}}$
	v_{z0}	$-\frac{\sqrt{2}}{4}V_{dc}e^{(4l-1)\frac{\pi}{4}}$	$-\frac{\sqrt{2}}{6}V_{dc}e^{(4l-1)\frac{\pi}{4}}$	$-\frac{\sqrt{2}}{12}V_{dc}e^{(4l-1)\frac{\pi}{4}}$	0

5.4 Summary

This chapter has explained the topology of dual-inverter supply for both asymmetrical and symmetrical six-phase drives. The space vectors generated by the dual-inverter supply are then plotted and analysed. The space vectors of the dual inverter supplied drive are basically produced due to the interactions of groups of space vectors of the two inverters.

Table 5.12: Asymmetrical six-phase drive - space vectors in (α-β) and (x-y) planes for dual-inverter supply topology.

		Inverter 2				
		$\underline{v}_{l(l)}$	$\underline{v}_{2l(l)}$	$\underline{v}_{3l(l)}$	$\underline{v}_{sh(l)}$	v_0
Inverter 1	$\underline{v}_{l(k)}$	$\frac{\sqrt{2+\sqrt{3}}}{6}V_{dc}(e^{j(2k-1)\frac{\pi}{12}} - e^{j(2l-1)\frac{\pi}{12}})$	$\frac{\sqrt{2+\sqrt{3}}}{6}V_{dc}e^{j(2k-1)\frac{\pi}{12}} - \frac{\sqrt{2}}{6}V_{dc}e^{j(2l-1)\frac{\pi}{12}}$	$\frac{\sqrt{2+\sqrt{3}}}{6}V_{dc}e^{j(2k-1)\frac{\pi}{12}} - \frac{1}{6}V_{dc}e^{j(l-1)\frac{\pi}{6}}$	$\frac{\sqrt{2+\sqrt{3}}}{6}V_{dc}e^{j(2k-1)\frac{\pi}{12}} - \frac{\sqrt{2-\sqrt{3}}}{6}V_{dc}e^{j(2l-1)\frac{\pi}{12}}$	$\frac{\sqrt{2+\sqrt{3}}}{6}V_{dc}e^{j(2k-1)\frac{\pi}{12}}$
	$\underline{v}_{2l(k)}$	$\frac{\sqrt{2}}{6}V_{dc}e^{j(2k-1)\frac{\pi}{12}} - \frac{\sqrt{2+\sqrt{3}}}{6}V_{dc}e^{j(2l-1)\frac{\pi}{12}}$	$\frac{\sqrt{2}}{6}V_{dc}(e^{j(2k-1)\frac{\pi}{12}} - e^{j(2l-1)\frac{\pi}{12}})$	$\frac{\sqrt{2}}{6}V_{dc}e^{j(2k-1)\frac{\pi}{12}} - \frac{1}{6}V_{dc}e^{j(l-1)\frac{\pi}{6}}$	$\frac{\sqrt{2}}{6}V_{dc}e^{j(2k-1)\frac{\pi}{12}} - \frac{\sqrt{2-\sqrt{3}}}{6}V_{dc}e^{j(2l-1)\frac{\pi}{12}}$	$\frac{\sqrt{2}}{6}V_{dc}e^{j(2k-1)\frac{\pi}{12}}$
	$\underline{v}_{3l(k)}$	$\frac{1}{6}V_{dc}e^{j(k-1)\frac{\pi}{6}} - \frac{\sqrt{2+\sqrt{3}}}{6}V_{dc}e^{j(2l-1)\frac{\pi}{12}}$	$\frac{1}{6}V_{dc}e^{j(k-1)\frac{\pi}{6}} - \frac{\sqrt{2}}{6}V_{dc}e^{j(2l-1)\frac{\pi}{12}}$	$\frac{1}{6}V_{dc}(e^{j(k-1)\frac{\pi}{6}} - e^{j(l-1)\frac{\pi}{6}})$	$\frac{1}{6}V_{dc}e^{j(k-1)\frac{\pi}{6}} - \frac{\sqrt{2-\sqrt{3}}}{6}V_{dc}e^{j(2l-1)\frac{\pi}{12}}$	$\frac{1}{6}V_{dc}e^{j(k-1)\frac{\pi}{6}}$
	$\underline{v}_{sh(k)}$	$\frac{\sqrt{2-\sqrt{3}}}{6}V_{dc}e^{j(2k-1)\frac{\pi}{12}} - \frac{\sqrt{2+\sqrt{3}}}{6}V_{dc}e^{j(2l-1)\frac{\pi}{12}}$	$\frac{\sqrt{2-\sqrt{3}}}{6}V_{dc}e^{j(2k-1)\frac{\pi}{12}} - \frac{\sqrt{2}}{6}V_{dc}e^{j(2l-1)\frac{\pi}{12}}$	$\frac{\sqrt{2-\sqrt{3}}}{6}V_{dc}e^{j(2k-1)\frac{\pi}{12}} - \frac{1}{6}V_{dc}e^{j(l-1)\frac{\pi}{6}}$	$\frac{\sqrt{2-\sqrt{3}}}{6}V_{dc}(e^{j(2k-1)\frac{\pi}{12}} - e^{j(2l-1)\frac{\pi}{12}})$	$\frac{\sqrt{2-\sqrt{3}}}{6}V_{dc}e^{j(2k-1)\frac{\pi}{12}}$
	$\underline{v}_0$	$-\frac{\sqrt{2+\sqrt{3}}}{6}V_{dc}e^{j(2l-1)\frac{\pi}{12}}$	$-\frac{\sqrt{2}}{6}V_{dc}e^{j(2l-1)\frac{\pi}{12}}$	$-\frac{1}{6}V_{dc}e^{j(l-1)\frac{\pi}{6}}$	$-\frac{\sqrt{2-\sqrt{3}}}{6}V_{dc}e^{j(2l-1)\frac{\pi}{12}}$	0

Chapter 6

REFERENCE SHARING ALGORITHMS FOR SIX-PHASE DRIVES WITH DUAL-INVERTER SUPPLY

6.1 Introduction

This chapter discusses two reference sharing algorithms for a six-phase drive with dual-inverter supply, which are Equal Reference Sharing (ERS) and Unequal Reference Sharing (URS) algorithms. The algorithm for the ERS is elaborated first, followed by the URS. The algorithms, which were previously implemented for five-phase [Jones et al. (2010)] and seven-phase drives [Bodo et al. (2011a)] are extended and implemented for both symmetrical and asymmetrical configurations of a dual-inverter supplied six-phase drive. The performance of the algorithms is evaluated based on the THD of the phase voltage and current, and also their axes components (which are α-, x-, and 0-component). The original results of the URS algorithm applied with the dual-inverter supplied symmetrical six-phase drive have been published in [Patkar et al. (2012)].

6.2 Reference sharing algorithms for dual-inverter six-phase supply

As discussed in Chapter 5, the dual-inverter six-phase supply topology generates a much higher number of voltage space vectors compared to the single-sided supply configuration. As a consequence, the implementation of SVPWM technique for the dual-inverter six-phase supply topology is also challenging. This is due to the large number of voltage space vectors that have to be considered. In order to reduce the complexity level, the dual-inverter supply topology can be decomposed into two sub-systems. One of the ways to do this is by splitting the total reference into two individual references so that the individual inverter can be controlled independently [Jones et al. (2010), Levi et al. (2012)]. Two reference splitting algorithms are considered, which are ERS and URS algorithms. These two algorithms are discussed in the next section, followed by detailed simulations and experimental verifications for both symmetrical and asymmetrical machine configurations.

6.2.1 Equal reference sharing (ERS) algorithm

A block diagram of the ERS algorithm is shown in Fig. 6.1. In order to control the inverters independently, the algorithm utilises two two-level six-phase space vector modulators. Equal but phase-opposing voltage references v_1^* and v_2^* are applied to the modulators by multiplying the phase voltage reference v_{ph}^* with 0.5 and -0.5, respectively. As a result, the two modulators are always operated in phase opposition and generate complementary leg voltages at the output of the two inverters. The leg voltages of the inverter are then connected as a dual-inverter supply to each side of the open-end winding.

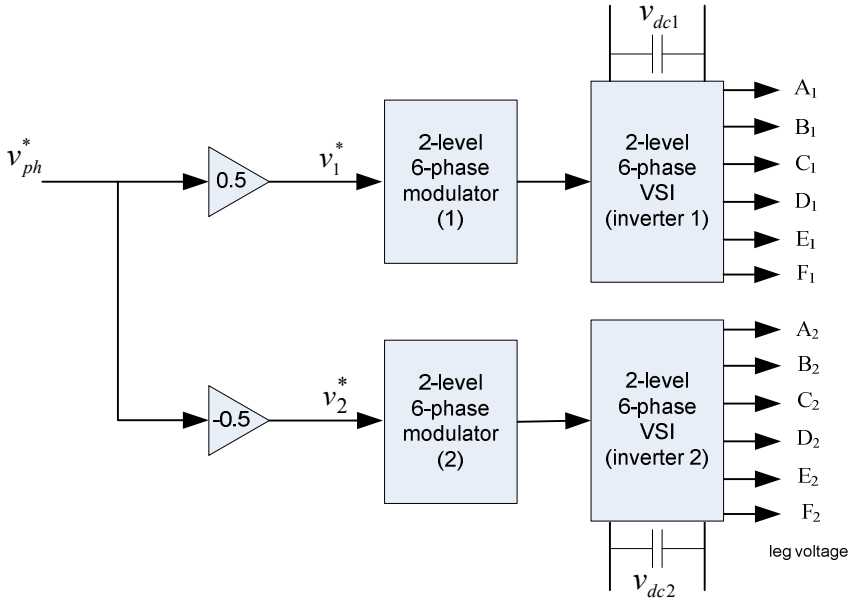

Fig. 6.1: Equal Reference Sharing (ERS) algorithm.

6.2.2 Unequal reference sharing (URS) algorithm

The URS algorithm is illustrated in the block diagram shown in Fig. 6.2. The algorithm also utilises two independent two-level six-phase modulators, but the phase voltage reference v_{ph}^* is divided unequally between the two modulators. The v_{ph}^* and the reference of the first and second modulator (v_1^* and v_2^*) are defined as (6.1) where M is the overall modulation index and M_1 and M_2 are the modulation indices for inverters 1 and 2.

$$\begin{aligned} v_{ph}^* &= M(0.5)V_{dc} \\ v_1^* &= M_1(0.5)V_{dc1} \\ v_2^* &= M_2(0.5)V_{dc2} \end{aligned} \qquad (6.1)$$

The v_{ph}^{*} is then split between each modulator based on the constraints in (6.2). Basically, for $M \le M_{\max}/2$, only one inverter is used, which is inverter 1. Inverter 2 is only operated when $M \ge M_{\max}/2$ and in this situation inverter 1 operates with $M_1 = M_{\max}$. It has to be noted that the value of $M_{\max}$ is dictated by the machine's stator winding configuration [Dujic et al. (2010)].

$$\begin{aligned} 0 \le M \le \frac{M_{\max}}{2} \qquad & \begin{cases} M_1 = 2M \\ M_2 = 0 \end{cases} \\ \frac{M_{\max}}{2} \le M \le M_{\max} \qquad & \begin{cases} M_1 = M_{\max} \\ M_2 = 2M - M_{\max} \end{cases} \end{aligned} \tag{6.2}$$

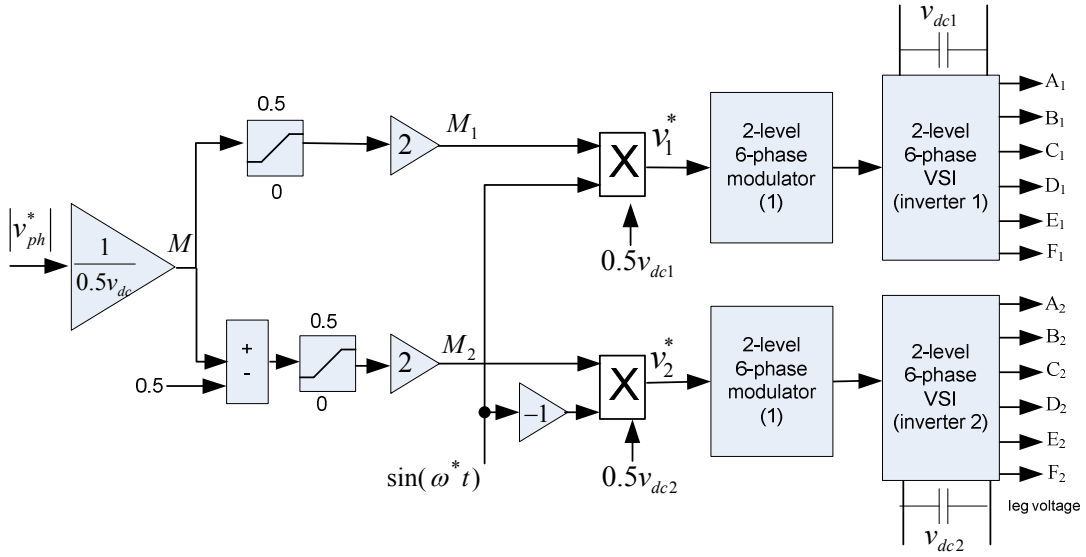

Fig. 6.2: Unequal Reference Sharing (URS) algorithm.

In the next section, the implementation of ERS and URS algorithms for symmetrical and asymmetrical six-phase drive with dual-inverter supply will be discussed. The performance of each algorithm will also be analysed and compared.

6.3 ERS and URS algorithms for the dual-inverter symmetrical six-phase drive

In order to develop a suitable PWM/SVPWM algorithm for the dual-inverter six-phase drive, one of the possible approaches is to adopt a suitable PWM/SVPWM technique initially implemented for a single-sided supply configuration. In Chapter 4, it has been demonstrated that the SVPWM technique with ρ = 2/3 produces a satisfactory result for symmetrical six-phase drive with a single-sided supply configuration. Therefore, in what follows, SVPWM technique with ρ = 2/3 will be used in the ERS and URS algorithms for dual-inverter supply of symmetrical six-phase drive.

6.3.1 Performance of ERS algorithm for symmetrical six-phase drive

In order to evaluate the performance of the ERS algorithm, a series of MATLAB/Simulink simulation is conducted for drive operation based on the open-loop constant *V*/*f* control (200 V peak phase voltage at 50 Hz with $M = 1$) without voltage boost operation. The simulations are carried out for values of modulation index spanning from $M = 0.1$ to $M_{\max} = 1$ with 0.1 increments. For each inverter, the dc bus voltage is set to 100 V (which is equivalent to 200 V supply of a single-sided supply topology). The machine parameters used in the simulations are as stated in Table 4.3 and similar to Section 3.5 and 4.3, the simulations are conducted by considering the non-ideal characteristics of the inverter such as the forward voltage drop of the power switches (1.2 V for the IGBTs and 1.6 V for the reverse diodes) and also the dead-time requirement of the inverter (6 μs). The switching frequency is set to 2 kHz. It has to be noted that the settings and parameters used in the simulations correspond to the values used in the experimental works carried out later on.

The results obtained from the simulations are tabulated in Tables 6.1 - 6.2. The performance of the ERS algorithm is evaluated based on the THD (3.16) of the phase voltage and current, and also their axes component (α-, x- and 0-component) which are again based on the same performance indicators used in Section 3.5 and 4.3. The THDs are calculated up to 41 kHz. Besides that, the level of phase voltage obtained for operation with every modulation index value is also stated.

Based on the results presented in Tables 6.1 - 6.2, it can be seen that for operation with every modulation index value, the fundamental component of phase voltage reaches the expected magnitude calculated from (3.10) except for small differences due to effect of voltage drop on the semiconductor devices and also dead-time requirement of the inverter. Also, for operation with every modulation index value also, the number of levels of the phase voltage is eleven. For the load current, the magnitude of the fundamental component is almost constant around 1.1 A (rms).

The space vectors that are applied by the modulator of each inverter for sector I and $M = 0.5$ are shown in Fig. 6.3. In this sector, the sequence of applied space vectors by the modulator of inverter 1 is V_0-V_{32}-V_{48}-V_{49}-V_{57}-V_{59}-V_{63}-V_{59}-V_{57}-V_{49}-V_{48}-V_{32}-V_0 while the modulator of inverter 2 applies V_{63}-V_{31}-V_{15}-V_{14}-V_6-V_4-V_0-V_4-V_6-V_{14}-V_{15}-V_{31}-V_{63}. By referring to the space vector mapping of the inverter that is operated in the single-sided supply topology with 0.5 V_{dc} supply (Fig. 5.3), it can be seen that the space vectors that are

Table 6.1: Symmetrical six-phase drive - Phase voltage fundamental component and THDs, along with THDs of α-, x- and 0-component voltages for ERS algorithm.

M	v_{ph}		v_α	v_x	v_{0-}	
	V_1(rms)	THD	THD	THD	THD	v_{ph} level
0.1	5.5110	3.4599	3.2291	1.1847	0.7269	11
0.2	12.7719	2.5894	2.2403	1.1046	0.6837	11
0.3	19.6902	2.0936	1.7624	0.9669	0.5852	11
0.4	27.0305	1.7228	1.4122	0.8441	0.5117	11
0.5	34.2435	1.4687	1.1695	0.7631	0.4568	11
0.6	41.4119	1.2743	0.9807	0.6989	0.4191	11
0.7	48.6054	1.1153	0.8210	0.6486	0.3873	11
0.8	55.6656	0.9834	0.6811	0.6095	0.3622	11
0.9	63.0640	0.8603	0.5431	0.5728	0.3414	11
1.0	70.3273	0.7515	0.3985	0.5483	0.3264	11

Table 6.2: Symmetrical six-phase drive - Load current fundamental component and THDs, along with THDs of α-, x- and 0-component currents for ERS algorithm.

M	i_{ph}		i_α	i_x	i_{0-}
	I_1(rms)	THD	THD	THD	THD
0.1	0.5770	0.4258	0.7269	0.0301	0.4172
0.2	0.9788	0.3219	0.6837	0.0432	0.3055
0.3	1.0832	0.3063	0.5852	0.0730	0.2582
0.4	1.1278	0.3444	0.5117	0.1093	0.2419
0.5	1.1720	0.3511	0.4568	0.1489	0.2200
0.6	1.1196	0.3809	0.4191	0.2060	0.2128
0.7	1.1761	0.3494	0.3873	0.2485	0.2051
0.8	1.1568	0.3885	0.3622	0.3040	0.2012
0.9	1.1662	0.4352	0.3414	0.3674	0.2077
1.0	1.1755	0.4829	0.3264	0.4341	0.1973

applied by each modulator at any time instant are phase-shifted by 180°. These space vectors are also applied for equal dwell times. If the combinations of the applied space vectors from two winding sides are examined in more detail, it is easy to show that the effective space vectors applied in dual-inverter supply topology, are exactly those used in the single-sided supply topology.

Simulation results of phase voltage and current waveforms and spectra for M = 0.5 and M = 1 are shown in Fig. 6.4. By comparing the results in Tables 4.4 - 4.5 and Tables 6.1 - 6.2, it can be seen that the ERS algorithm practically produces an identical

performance as the SVPWM technique for the single-sided supply topology, with $\rho = 2/3$. The waveforms and frequency spectra for phase voltage and current for $M = 1$ (Fig. 6.4) and are also in essence identical to the results shown in Figs. 4.9 - 4.10. Slight discrepancies are understandable since the URS algorithm needs to cope with the dead time effect of the two inverters. Therefore, in the ERS algorithm, the two inverters are modulated in such a way that they effectively operate as one two-level inverter in single-sided supply mode.

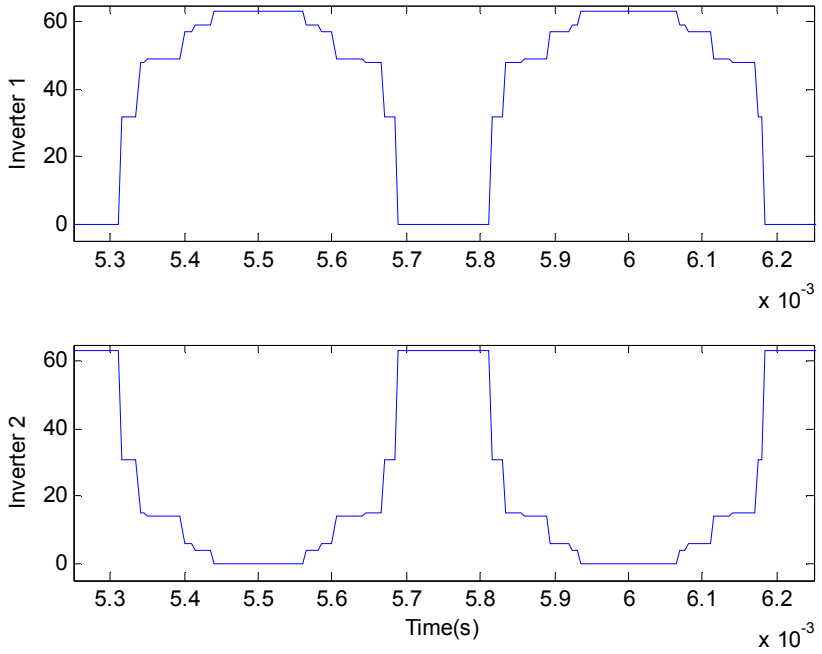

Fig. 6.3: Applied space vectors in sector I with $M = 0.5$ (ERS algorithm).

6.3.2 Performance of URS algorithm for symmetrical six-phase drive

The performance of the URS algorithm for the symmetrical six-phase drive is shown in Tables 6.3 - 6.4 where the same performance indicators as the ERS algorithm are being used. The results are obtained using the same simulation settings and machine parameters used for the ERS algorithm.

From the tables, it can be seen again that the fundamental component of phase voltage reaches the expected magnitude for operation at every modulation index value (except for small differences due to non-ideal model of the inverter) and the fundamental component of the load current is also almost constant around 1.1 A (rms). Regarding the phase voltage level, it can be noticed that the number of phase voltage levels is eleven for operation at less than half of the maximum modulation index ($M \leq 0.5$). For $M \geq 0.5$, the level increases up to 21 levels before reverting back to eleven levels for M_{max}= 1.

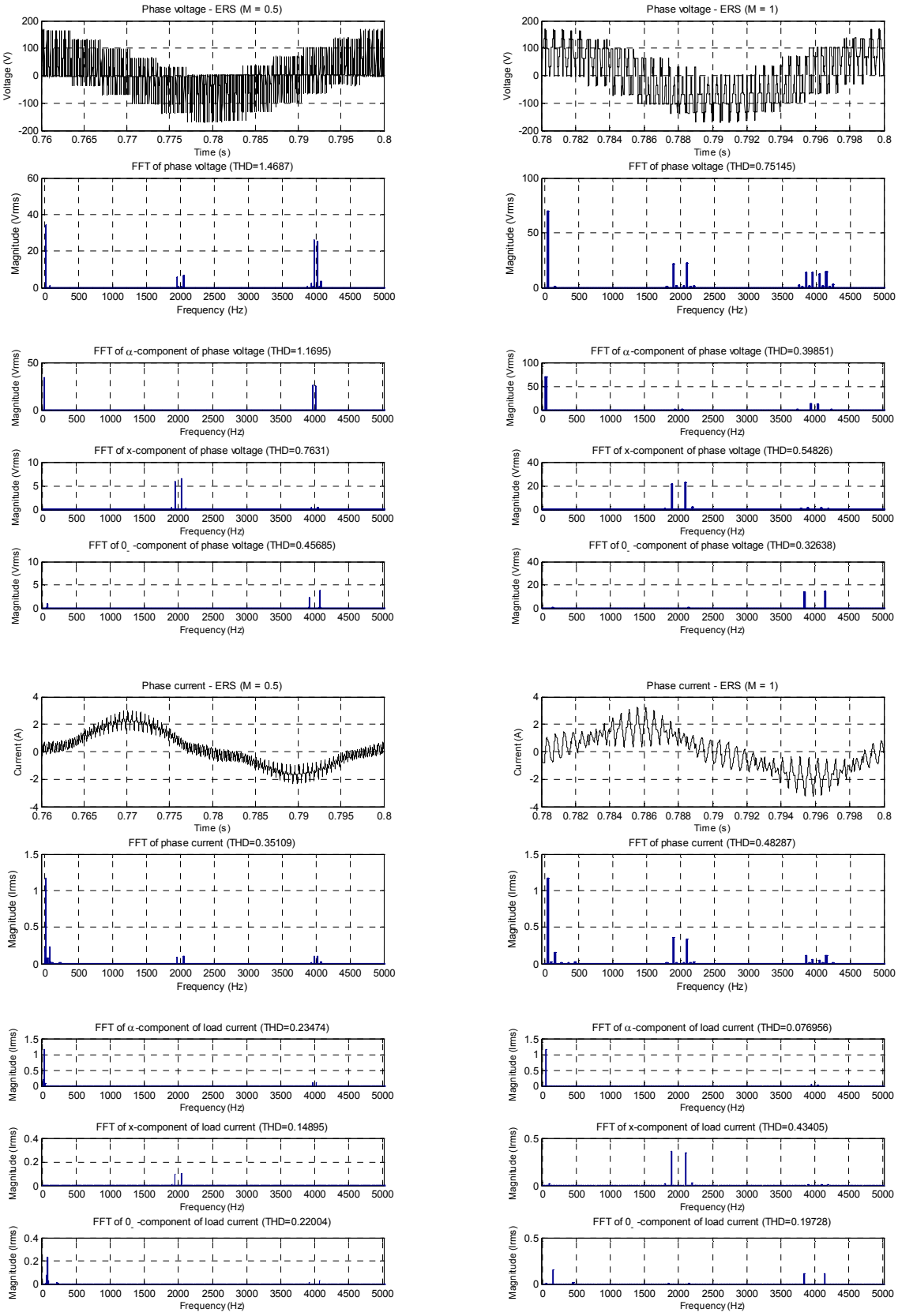

Fig. 6.4: Simulation results with $M = 0.5$ (left) and $M = 1$ (right) using the ERS algorithm with the symmetrical six-phase drive. Top: Phase voltage waveform and spectra. Bottom: Phase current waveform and spectra.

Table 6.3: Symmetrical six-phase drive - Phase voltage fundamental component and THDs, along with THDs of α-, x- and 0-component voltages for the URS algorithm.

	v_{ph}		v_α	v_x	v_{0-}	
M	V_1(rms)	THD	THD	THD	THD	v_{ph} level
0.1	6.3156	2.5011	2.1260	1.1406	0.6562	11
0.2	12.7138	1.8226	1.4944	0.8883	0.5472	11
0.3	20.1012	1.3114	1.0116	0.7141	0.4306	11
0.4	27.2641	1.0031	0.6967	0.6193	0.3702	11
0.5	34.6778	0.7617	0.4074	0.5530	0.3296	11
0.6	41.4412	0.8243	0.5694	0.5139	0.3026	19
0.7	48.7267	0.8345	0.5903	0.5131	0.2915	19
0.8	55.9323	0.8191	0.6369	0.6020	0.3425	21
0.9	63.0860	0.7927	0.4932	0.5370	0.3118	21
1.0	70.3274	0.7514	0.0770	0.4342	0.1974	11

Table 6.4: Symmetrical six-phase drive - Load current fundamental component and THDs, along with THDs of α-, x- and 0-component currents for the URS algorithm.

	i_{ph}		i_α	i_x	i_{0-}
M	I_1(rms)	THD	THD	THD	THD
0.1	0.7134	0.3466	0.0610	0.0299	0.3387
0.2	1.0289	0.2809	0.0824	0.0581	0.2615
0.3	1.0929	0.3117	0.1704	0.1032	0.2375
0.4	1.1385	0.3969	0.2975	0.1555	0.2120
0.5	1.1590	0.4043	0.2816	0.2184	0.1892
0.6	1.1223	0.3781	0.2036	0.2360	0.2157
0.7	1.1736	0.3459	0.1080	0.2585	0.2058
0.8	1.1696	0.3811	0.1021	0.3090	0.1994
0.9	1.1707	0.4290	0.0993	0.3665	0.2001
1.0	1.1750	0.4831	0.0770	0.4342	0.1974

Simulation results showing the phase voltage and current waveforms, along with their spectra for M = 0.5 and M = 0.8 are presented in Fig. 6.5. For $M \leq 0.5$, the drive is effectively operated in two-level single-sided supply mode since only inverter 1 is active. The space vectors that are used by the modulators in sector I with M = 0.5 are shown in Fig. 6.6 (top). The sequence of applied space vectors by the modulator of inverter 1 is the same as the ERS algorithm, while the modulator of inverter 2 is switched between space vectors V_0 and V_{63} only. The phase voltage waveform has eleven levels which are the same as with the ERS algorithm, but its THD is significantly lower than with the ERS

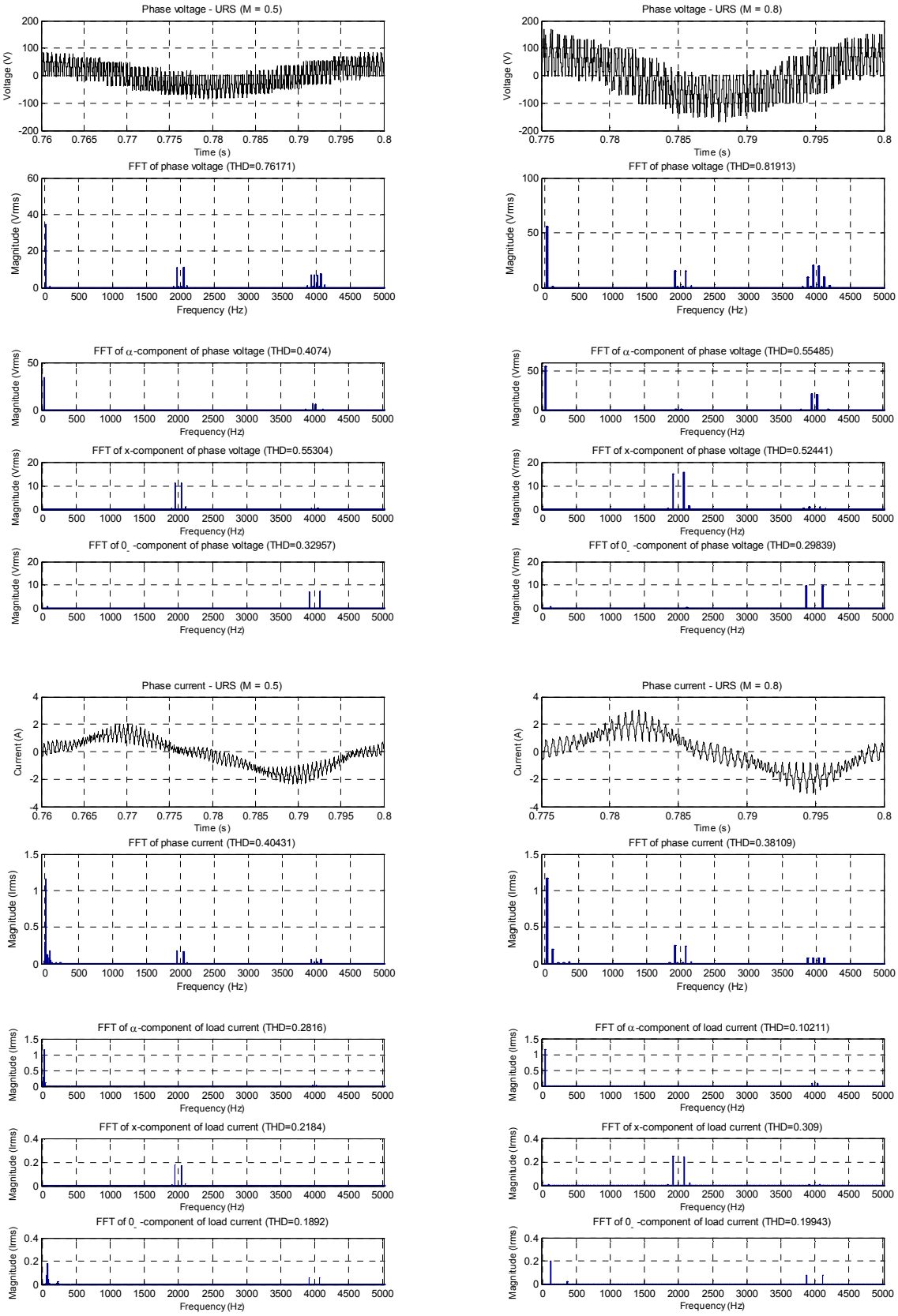

Fig. 6.5: Simulation results with $M = 0.5$ (left) and $M = 0.8$ (right) using the URS algorithm with the symmetrical six-phase drive. Top: Phase voltage waveform and spectra. Bottom: Phase current waveform and spectra.

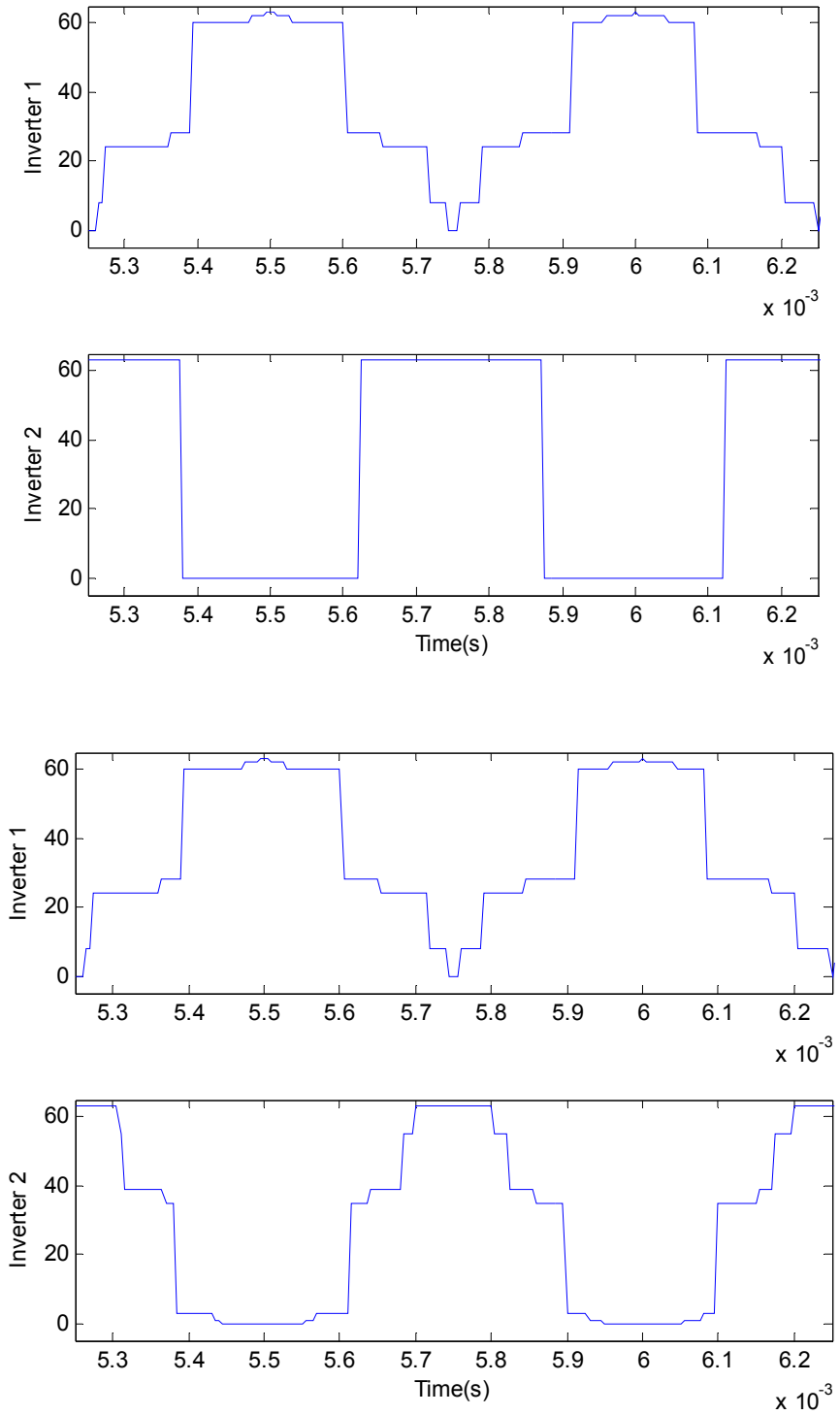

Fig. 6.6: ERS algorithm for symmetrical six-phase drive - applied space vectors in sector I with $M = 0.5$ (top) and $M = 0.8$ (bottom).

algorithm. The improvement of THD is caused by the reduced dc bus voltage, which is switched across the winding. The winding effectively sees half of dc voltage with the URS algorithm, while for ERS algorithm a full dc voltage (200 V) is switched across the winding.

For $M \geq 0.5$, the modulation of inverter 1 is locked to $M_1 = 1$ while inverter 2 is modulated independently according to M_2. As inverter 2 starts to operate, the URS algorithm produces a multilevel phase voltage waveform. The space vectors that are used by the modulators for M = 0.8 are shown in Fig. 6.6 (bottom). The inverters generate the same space vectors as with the ERS algorithm, but they are now applied at different time instants due to different dwell times. Therefore, the applied space vectors by the two modulators are not always opposing each other. This means that the total number of space vectors, generated by the URS algorithm, is significantly higher than the number available with the ERS algorithm. As a result, higher number of levels in phase voltage waveform can be produced and this contributes to the reduction of THD. Once when the URS algorithm is operated at M = 1, both inverters work with the same modulation index and the drive behaviour is identical as with the ERS algorithm.

Based on the simulation results presented in Tables 6.1 - 6.4, for operation with every modulation index value, a small deviation from the expected value of the phase voltage fundamental component is witnessed as a consequence of the voltage drop on the semiconductor devices and also the dead-time requirement of the inverter. Besides that, the device voltage drops and inverter dead time also become the source of low-order harmonics [Jones et al. (2009)] , as can be seen in the spectra shown in Figs. 6.4 - 6.5. The transformation of the phase voltage into the (α-β) and (x-y) planes, and also (0_+-0_-) axes reveals that the fundamental component maps into the (α-β) plane alongside the two largest switching harmonics around twice of the switching frequency (4 kHz). On the other hand, the two largest switching harmonics around the switching frequency (2 kHz) are mapped into the (x-y) plane. Finally, the largest low-order harmonic (i.e. 3rd harmonic) maps into the (0_+-0_-) axes.

Experimental results of the phase voltage and current waveforms for the URS algorithm, together with their spectra for M = 0.5 and M = 0.8 are shown in Fig. 6.7. The results are obtained from experimental works that are conducted based on the settings and machine parameters described earlier for the simulation. The detailed explanation of the experimental set-up is available in the Appendix 1. By comparing the respective figures, it can be seen that simulation and experiment produce phase voltage waveforms, FFTs and THDs that are matched quite closely. For the load current, small differences are observed. These differences are mainly due to mismatch between machine parameters values that are being used in the simulations and experiments. Besides that, a small amount of low order

harmonics also appears in the experimental results, again with small disagreements with the simulation. It is verified by extensive simulations that the amount of dead time and semiconductors voltage drops influence the amplitudes of these harmonics.

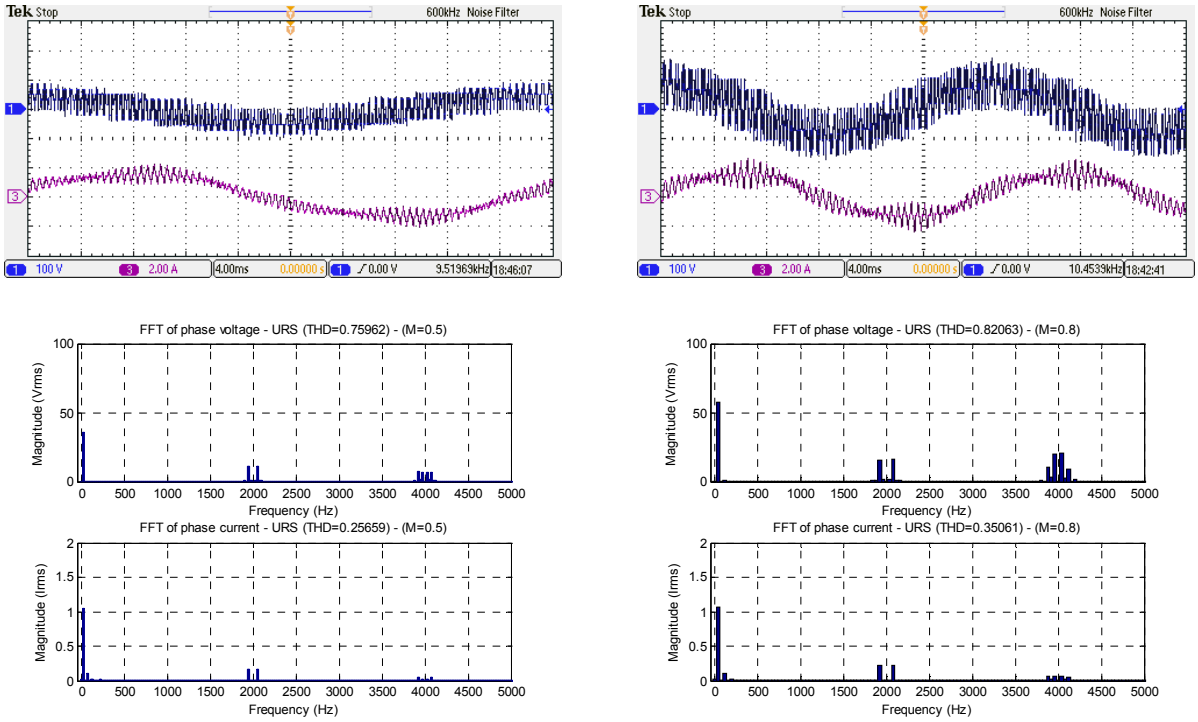

Fig. 6.7: Experimental results with $M = 0.5$ (left) and $M = 0.8$ (right) using the URS algorithm with the symmetrical six-phase drive. Top: Phase voltage waveform and spectra. Bottom: Phase current waveform and spectra

6.3.3 Performance comparison of URS and ERS algorithms for symmetrical six-phase drive

The performance comparison of the ERS and URS algorithms based on THD of phase voltage and current, along with their axes components, over the entire linear range of modulation index, is shown in Fig. 6.8. By referring to the simulation results, for the phase voltage THD, performance of the URS algorithm is considerably better than the ERS algorithm for the whole range of modulation index due to reason that has been explained earlier. Besides that, the THD of URS algorithm for each component of phase voltage is also always better than the ERS algorithm. For the URS algorithm, the change of operation from two-level to multilevel such as shown in the last column of Table 6.3 can also be observed from Fig. 6.8 where the change of trend of voltage and current THD curves starts at $M > 0.5$.

The THD of load current is understandably smaller than phase voltage due to the filtering effect provided by the machine impedance. For the load current THD, the

performance of ERS and URS algorithms is almost the same, especially for operation at higher range of modulation index ($M \geq 0.6$). For operation at around half of M_{max}, the current THD of ERS is better than URS. By comparing the simulation result shown in Fig. 6.4 and Fig. 6.5 with M = 0.5, it can be observed that the magnitude of the two largest switching harmonics around the switching frequency (2 kHz) for the URS is slightly larger than the ERS. Since these harmonics map into the (x-y) plane, URS algorithm has THD of x-component that is larger than ERS which consequently affects the overall THD of the load current.

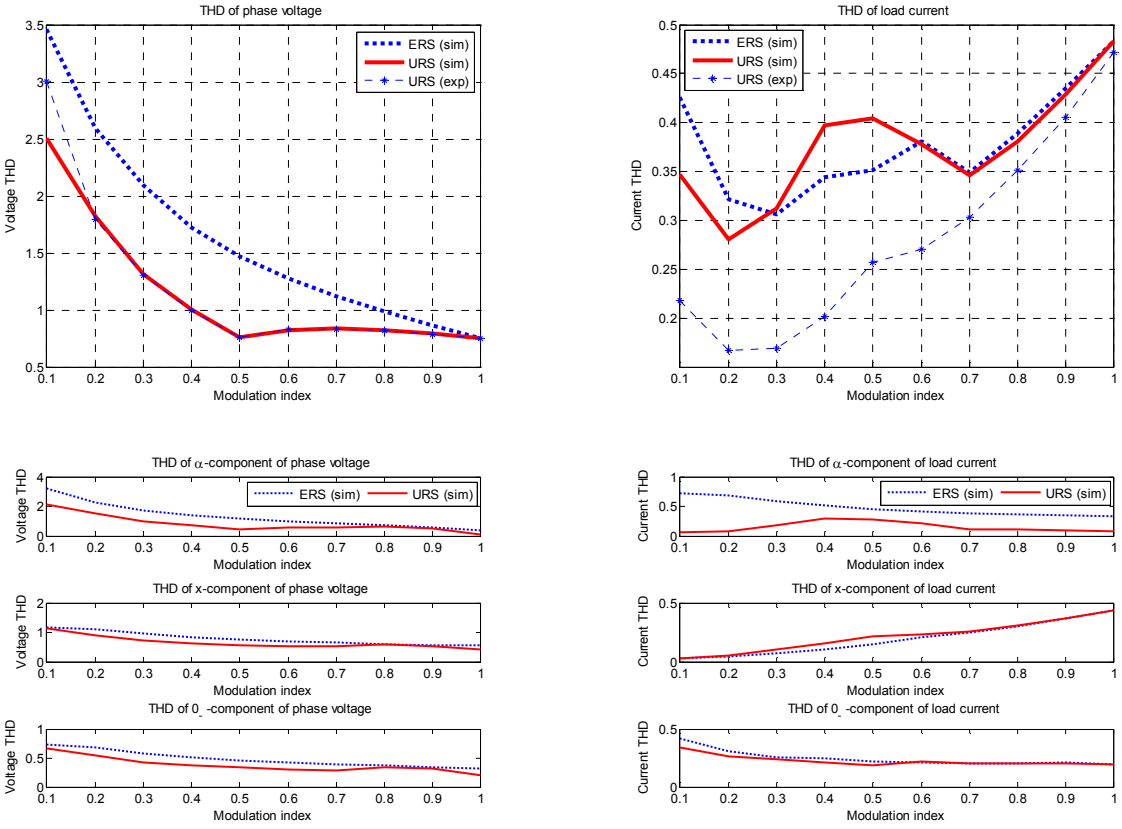

Fig. 6.8: Comparison of voltage and current THDs for ERS and URS algorithms for symmetrical six-phase drive. Phase voltage and its axes component (left), load current and its axes components (right).

It has been clearly demonstrated that the ERS modulation method produces identical performance to that of a single-sided two-level inverter supplied drive. Since the performance of the single-sided drive has been verified many times in the literature, for the purposes of brevity the experimental verification of the ERS method is not provided in this chapter.

Regarding to the experimental results of the URS algorithm, for the phase voltage THDs, the results obtained from the experiments match very closely with the simulation.

On the other hand, some disaggrement between the simulations and experiments are observed for the phase current THD. The disagreement is mostly contributed by the mismatch between the machine parameters that is being used in simulations with the actual parameters of the machine. Nevertheless, across the whole range of modulation index, almost similar trend of phase current THD is obtained from the simulations and experiments.

6.4 ERS and URS algorithms for dual-inverter asymmetrical six-phase drive

For the open-end asymmetrical six-phase drive, the case that would correspond to the situation with two neutral points would require four isolated dc supplies, which is very inconvenient from the practical point of view [Grandi et al. (2010b)]. Therefore, a topology with two equal and isolated dc supplies is considered, and this corresponds in terms of a single-sided supply, to existence of a single neutral point. Therefore, based on the results and discussion of PWM techniques for an asymmetrical six-phase drive with a single neutral point in Chapter 3 (Section 3.4), the sinusoidal PWM with zero-sequence injection technique is chosen to be utilised for the URS and ERS algorithms.

6.4.1 Performance of ERS algorithm for asymmetrical six-phase drive

In order to investigate the performance of the ERS algorithm for the asymmetrical six-phase drive a series of MATLAB/Simulink simulations are once more conducted for drive operation based on the open-loop constant *V/f* control (without voltage boost operation) for range of modulation index spanning from $M = 0.1$ to $M_{\max}$ in 0.1 increments. For this drive configuration, $M_{\max} = 1.0353$. Therefore simulation for operation with half of maximum modulation index value ($M = 0.5176$) is also carried out in order to thoroughly investigate the performance of the ERS algorithm. The parameters of the asymmetrical machine used in the simulations are as depicted in Table 3.3. For each inverter, the dc bus voltage is set to 150 V (which is equivalent to 300 V supply of a single-sided supply topology). 2 kHz is again utilised as the switching frequency.

The performance of the ERS algorithm for the asymmetrical six-phase drive is presented in Tables 6.5 - 6.6. Similar to the symmetrical six-phase drive, the performance are measured based on the THD of the phase voltage and current, and also their axes component (α-, x- and 0.-component). Besides that, the number of phase voltage level is again presented for operation with every modulation index value.

Table 6.5: Asymmetrical six-phase drive - phase voltage fundamental component and THDs, along with THDs of α-, *x*- and 0-component voltages for the ERS algorithm.

	v_{ph}		v_α	v_x	v_{0-}	
M	V_1(rms)	THD	THD	THD	THD	v_{ph} level
0.1	7.6577	3.7354	3.6288	0.8336	0.4338	11
0.2	18.5034	2.6159	2.4256	0.8556	0.5005	11
0.3	29.6759	2.0217	1.8222	0.7588	0.4599	11
0.4	40.4308	1.6757	1.4798	0.6764	0.4129	11
0.5	51.1491	1.4287	1.2381	0.6110	0.3752	11
0.5176	52.9100	1.3943	1.2048	0.6028	0.3706	11
0.6	61.6661	1.2411	1.0516	0.5632	0.3498	11
0.7	72.0021	1.0892	0.8983	0.5276	0.3289	11
0.8	82.7141	0.9546	0.7616	0.4914	0.3068	11
0.9	93.1840	0.8358	0.6356	0.4654	0.2893	11
1.0	103.5066	0.7328	0.5163	0.4435	0.2751	11
1.0353	107.2863	0.6942	0.4684	0.4373	0.2719	11

Table 6.6: Asymmetrical six-phase drive - load current fundamental component and THDs, along with THDs of α-, *x*- and 0-component currents for the ERS algorithm.

	i_{ph}		i_α	i_x	i_{0-}
M	I_1(rms)	THD	THD	THD	THD
0.1	0.2563	0.2620	0.0551	0.1667	0.2287
0.2	0.4345	0.1920	0.0427	0.1568	0.1257
0.3	0.4785	0.2206	0.0512	0.1998	0.0967
0.4	0.4958	0.2914	0.0592	0.2771	0.0782
0.5	0.5096	0.3750	0.0644	0.3640	0.0666
0.5176	0.5067	0.3960	0.0661	0.3859	0.0654
0.6	0.5114	0.4832	0.0704	0.4742	0.0758
0.7	0.5159	0.6000	0.0724	0.5909	0.0785
0.8	0.5212	0.7149	0.0717	0.7073	0.0758
0.9	0.5276	0.8355	0.0697	0.8291	0.0741
1.0	0.5309	0.9677	0.0698	0.9630	0.0692
1.0353	0.5343	1.0192	0.0702	1.0166	0.0618

From the results, it can be noticed that the ERS algorithm produces eleven levels of phase voltage for the whole range of modulation index value which is the same phase voltage level obtained from the ERS algorithm applied to symmetrical six-phase drive. Regarding the fundamental component of the load current, the value is fluctuated around 0.5 A(rms). The value of the fundamental component of phase voltage reaches the

expected value (3.5), and again it is slightly reduced by the non-ideal condition of the inverter.

Fig. 6.9 depicts simulation results of phase voltage and current waveforms, their spectra and THDs for M = 0.5 and M = 1. Based on the previous analysis of the ERS algorithm for the symmetrical six-phase drive and also comparison of the results presented in Tables 6.5 - 6.6 with the results obtained from the zero-sequence injection technique (Section 3.4.2), it can be concluded that the performance of ERS algorithm of asymmetrical six-phase drive is identical to the zero-sequence injection technique. Slight discrepancies are again due to effect of the dead-time for the two inverters of the ERS, where for the zero-sequence injection technique only single inverter is used. Other than that, it can be said that the drive effectively operates as one two-level inverter in a single-sided supply mode.

6.4.2 Performance of URS algorithm for asymmetrical six-phase drive

The performance of the URS algorithm for asymmetrical six-phase drive is tabulated in Table 6.7 for the THD of phase voltage and its axes components and in Table 6.8 for the THD of phase current and its axes components. The results are obtained from MATLAB/Simulink simulations which are carried out using the same simulation setting and machine parameters described earlier for the ERS algorithm. For the clarity of results, the simulation is again carried out for modulation index of half of the maximum ($M = 0.5176$).

Similar to the URS algorithm of symmetrical six-phase drive, the drive is again effectively operated in two-level single-sided supply mode when the modulation index less than half of the maximum ($M \leq 0.5176$) with the number of phase voltage levels being eleven. Then, for operation at modulation index higher than half of the maximum ($M > 0.5176$), the drive operates in multilevel mode and generates up to 21 levels of phase voltage. Finally for operation at M_{max} (M = 1.0353), the drive reverts back to two-level mode. The value of phase voltage fundamental component increases steadily with the increases of modulation index value. Further, the fundamental component of the load current is maintained around 0.5 A(rms), the same value obtained for the ERS algorithm.

Simulation results showing the phase voltage and current waveforms, together with their spectra for the URS algorithm with M = 0.5 and M = 0.8 are presented in Fig. 6.10. By comparing the results obtained for the ERS (Fig. 6.9) and URS (Fig. 6.10), it can be

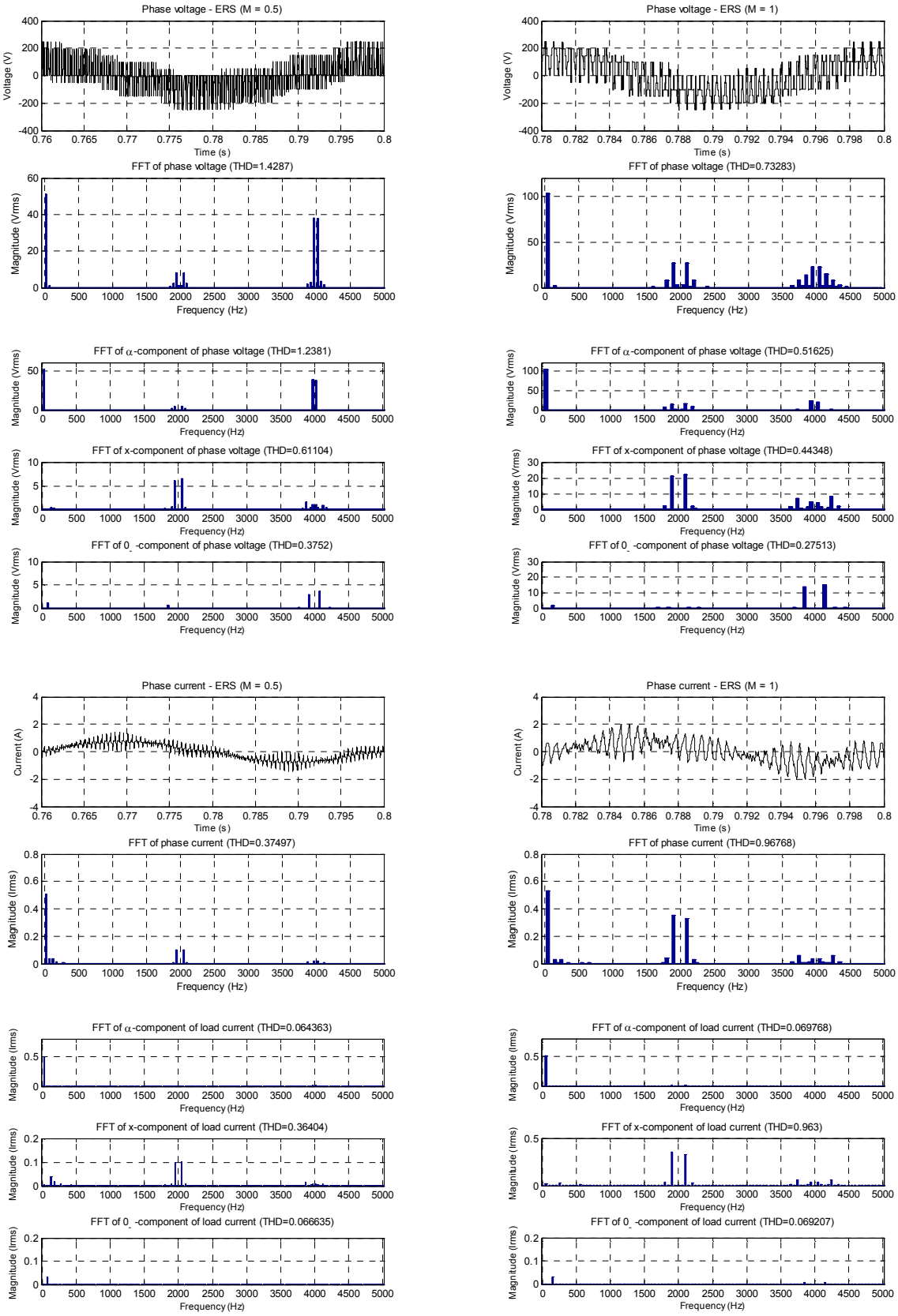

Fig. 6.9: Simulation results with $M = 0.5$ (left) and $M = 1$ (right) using the ERS algorithm with the asymmetrical six-phase drive. Top: Phase voltage waveform and spectra. Bottom: Phase current waveform and spectra.

Table 6.7: Asymmetrical six-phase drive - phase voltage fundamental component and THDs, along with THDs of α-, *x*- and 0-component voltages for the URS algorithm.

	v_{ph}		v_α	v_x	v_{0-}	
M	V_1(rms)	THD	THD	THD	THD	v_{ph} level
0.1	8.8612	2.6415	2.4355	0.8723	0.5331	11
0.2	19.4060	1.7370	1.5345	0.6971	0.4274	11
0.3	30.2927	1.2619	1.0691	0.5738	0.3549	11
0.4	40.8637	0.9667	0.7674	0.5012	0.3113	11
0.5	51.3537	0.7382	0.5153	0.4502	0.2800	11
0.5176	53.3578	0.7002	0.4646	0.4441	0.2777	11
0.6	61.5493	0.7517	0.5825	0.4081	0.2537	19
0.7	71.8313	0.7785	0.6264	0.3952	0.2429	19
0.8	82.5964	0.7658	0.6139	0.3943	0.2383	19
0.9	93.1539	0.7440	0.5687	0.4106	0.2486	21
1.0	103.5681	0.7186	0.5049	0.4346	0.2688	21
1.0353	107.2853	0.6942	0.4684	0.4373	0.2719	11

Table 6.8: Asymmetrical six-phase drive - load current fundamental component and THDs, along with THDs of α-, *x*- and 0-component currents for the URS algorithm.

	i_{ph}		i_α	i_x	i_{0-}
M	I_1(rms)	THD	THD	THD	THD
0.1	0.3242	0.1949	0.0325	0.1419	0.1454
0.2	0.4576	0.1868	0.0331	0.1690	0.0911
0.3	0.4921	0.2628	0.0362	0.2525	0.0717
0.4	0.5044	0.3770	0.0361	0.3708	0.0588
0.5	0.5128	0.5108	0.0354	0.5076	0.0490
0.5176	0.5138	0.5422	0.0366	0.5403	0.0409
0.6	0.5127	0.5569	0.0452	0.5546	0.0467
0.7	0.5136	0.6195	0.0587	0.6146	0.0577
0.8	0.5217	0.7147	0.0659	0.7090	0.0625
0.9	0.5236	0.8433	0.0696	0.8373	0.0667
1.0	0.5316	0.9692	0.0701	0.9651	0.0655
1.0353	0.5344	1.0191	0.0702	1.0165	0.0618

concluded that the fundamental component of phase voltage reaches the expected magnitude. The same harmonics mapping as the symmetrical six-phase drive are also obtained. The fundamental component and the two largest harmonics around twice of the switching frequency (4 kHz) are mapped into the (α-β) plane while the two largest harmonics around the switching frequency (2 kHz) are mapped into the (*x*-*y*) plane. Some

low order harmonics can again be observed in the phase voltage and current spectra as the consequence of the non- ideal nature of the inverters (devices voltage drop and dead-time requirement). The largest low order harmonic (3^{rd} harmonic) is mapped into the (0_+-0_-) axis.

Fig. 6.11 depicts experimental results obtained for the URS algorithm with M = 0.5 and M = 0.8. A strong correspondence between simulations and experiments can be observed by comparing the results presented in Fig. 6.10 and Fig. 6.11. The phase voltage and current waveforms, FFTs and THDs match quite closely thus verifying that the practical implementation performs as expected. A small amount of low order harmonics that appears in both simulations and experimental results are, again, a consequence of semiconductor voltage drop and the effect of dead time.

6.4.3 Performance comparison of URS and ERS algorithms for asymmetrical six-phase drive

The voltage and current THDs comparison of the ERS and URS algorithms, for operation in the linear range of modulation index are shown in Fig. 6.12. By comparing the respective simulation results obtained from symmetrical (Fig. 6.8) and asymmetrical six-phase drives (Fig. 6.12), similar outcome can be concluded. The URS algorithm produces a better phase voltage THD than the ERS algorithm for the whole range of modulation index. The THD for each axis component of phase voltage produced by the URS algorithm is also always better than the ERS algorithm.

For the load current THD, the performance of the ERS algorithm is better than that of the URS algorithm for operation at $M < 0.7$. The reason is the magnitude of the dominant harmonics (in particular, the largest two) around the switching frequency (2 kHz) for URS algorithm is larger than ERS algorithm. As a result, URS algorithm produces a worst x-component and load current THDs than ERS algorithm. This situation can be observed by comparing the spectra shown in Fig. 6.9 (ERS) and Fig. 6.10 (URS) with $M = 0.5$. For $M \geq 0.7$, the load current THD of ERS and URS algorithms are almost identical.

For the phase voltage THD of the URS algorithm, the results obtained from the experiments match very closely with simulations. For the current THDs, the results obtained using simulations and experiments produce satisfactory but imperfect match. The trends are the same in the experimental and simulation results, while minor discrepancies in numerical values are hardly surprising, considering that the simulation was based on the

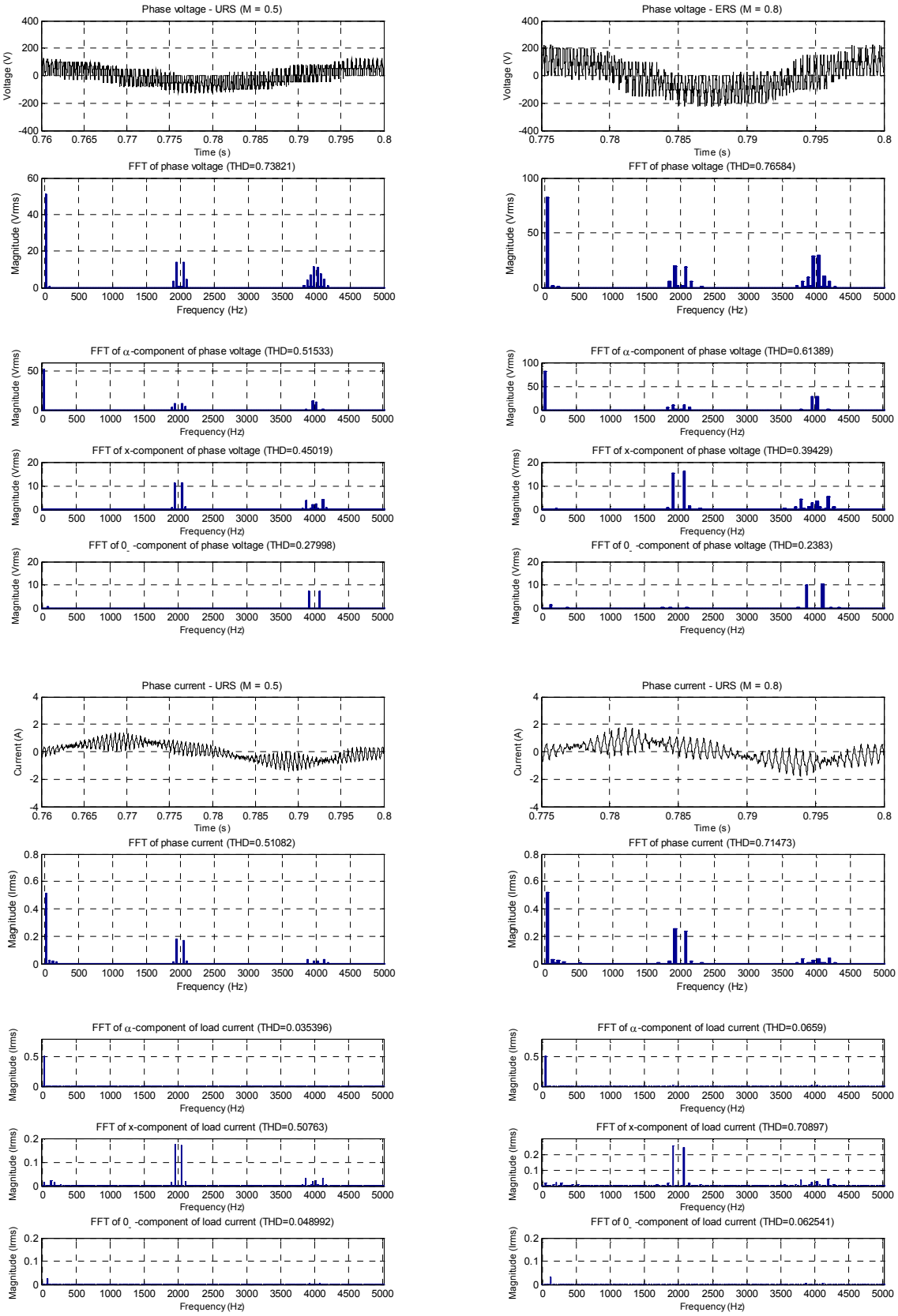

Fig. 6.10: Simulation results with $M = 0.5$ (left) and $M = 0.8$ (right) using the URS algorithm with the asymmetrical six-phase drive. Top: Phase voltage waveform and spectra. Bottom: Phase current waveform and spectra.

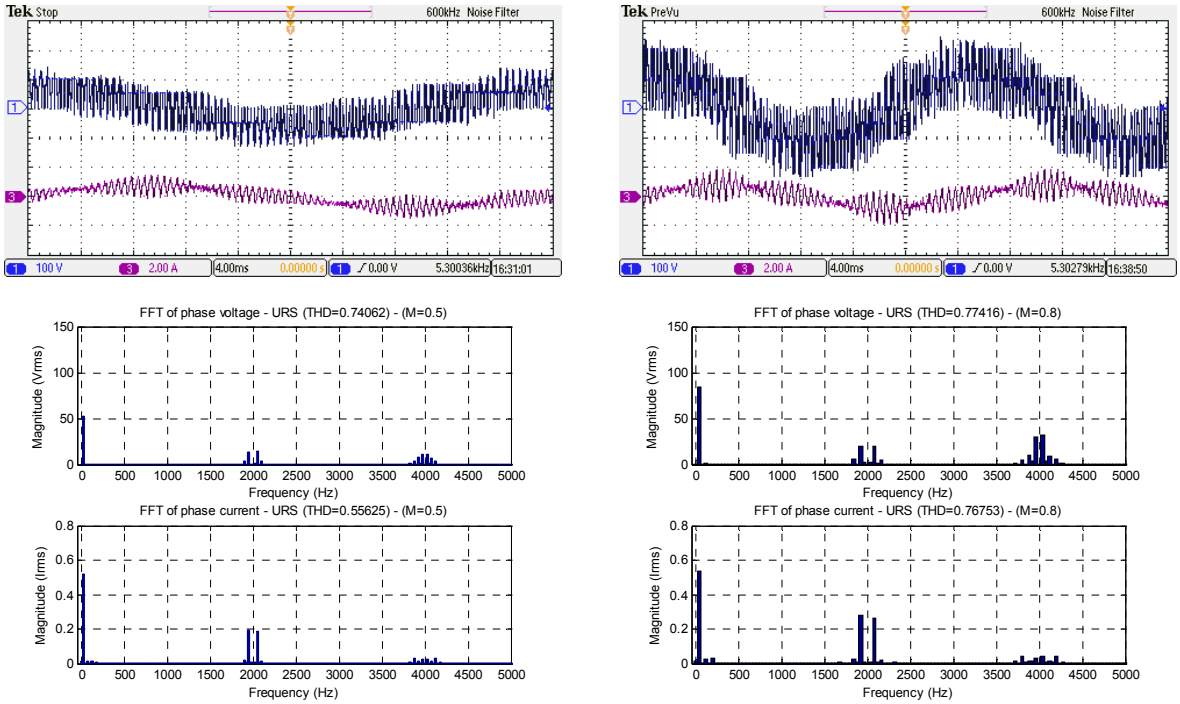

Fig. 6.11: Experimental results with $M = 0.5$ (left) and $M = 0.8$ (right) for URS algorithm for asymmetrical six-phase drive. Top: Phase voltage waveform and spectra. Bottom: Phase current waveform and spectra.

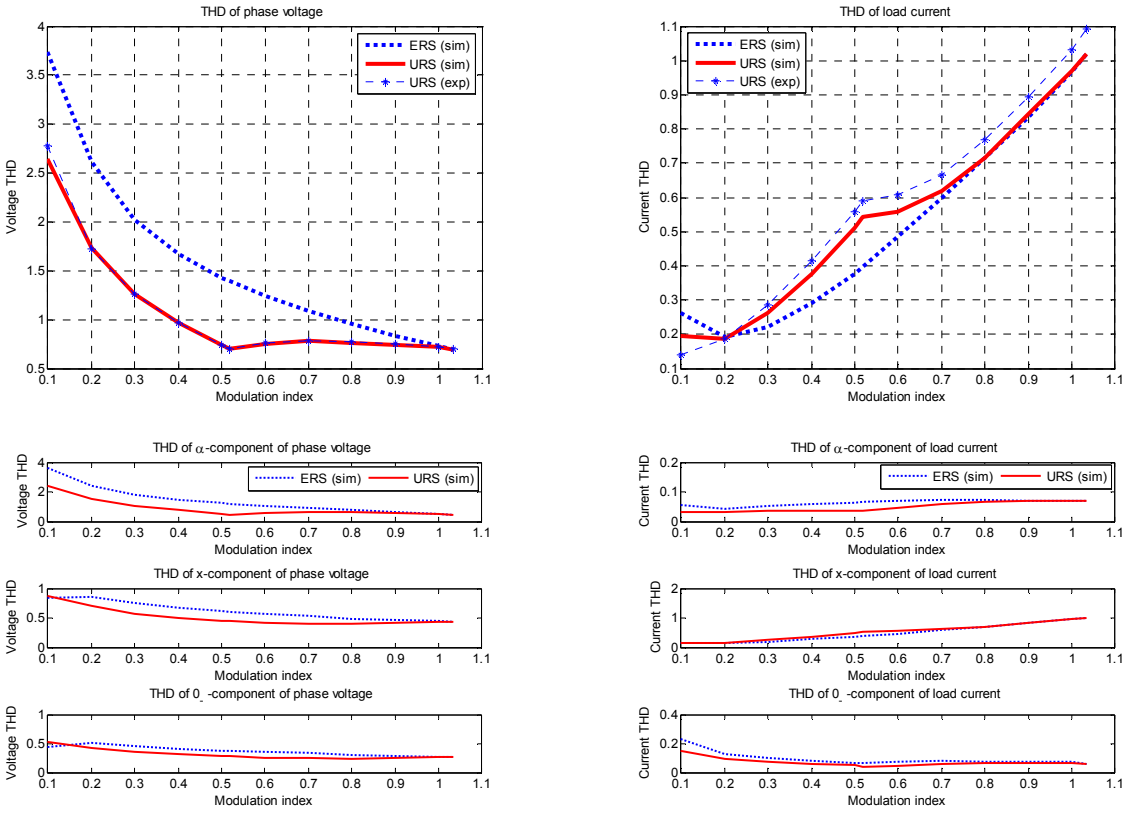

Fig. 6.12: Comparison of voltage and current THDs for ERS and URS algorithms for asymmetrical six-phase drive. Phase voltage and its axes component (left), load current and its axes components (right).

constant-parameter machine model. Moreover, rotor skin effect means that the rotor leakage inductance has a different value at each frequency. This issue has been discussed in more detail in recent studies related to the current ripple characterisation in five-phase drives [Dujic et al. (2011), Jones et al. (2011a), Prieto et al. (2011)].

For the sake of brevity, the experimental result for ERS algorithm is again not included. However, the result is more or less similar to the one depicted in Fig. 3.27 because the performance of the ERS algorithm is in essence identical to a two-level six-phase inverter supplying machine with a single neutral point.

6.5 Summary

Two PWM algorithms (ERS and URS) for the dual-inverter supplied symmetrical and asymmetrical six-phase drives are elaborated. The performances of ERS and URS algorithms for both symmetrical and asymmetrical configurations of six-phase drives are analysed and their performances are in agreement with the analysis of the reference sharing algorithms implemented for five-phase and seven-phase drives.

ERS algorithm produces phase voltage level and THD that are identical to a six-phase drive supplied by a single-sided two-level VSI. For the URS algorithm, in term of phase voltage THD, it produces performance that is considerably better than the ERS, except when the modulation index is equal to one, where the performance is the same. For modulation index greater than half of the maximum, the URS algorithm also produces multilevel phase voltage waveform. Meanwhile, in terms of load current THD, the performance of the URS algorithm is worse than the ERS algorithm for operation around modulation index less than half of the maximum. For the rest of the linear range of modulation index operation, their performance is almost identical.

Based on the results obtained from the implementation of ERS and URS algorithm, it can be concluded that the performance of dual-inverter fed six-phase drive with both symmetrical and asymmetrical winding configurations is comparable in term of phase voltage THD. With regards to load current THD, it can be observed that the machine with asymmetrical windings produce a higher current THDs than the machine with symmetrical windings, especially for operation at modulation index higher than half of the maximum. For drive with machine configured with symmetrical winding, the current THD obtained from ERS and URS algorithm is limited to around 0.5, while for machine with asymmetrical winding configuration, the current THD reaches a value around 1. Therefore, if current THD is taken as figure of merit, it can be concluded that the performance of the

ERS and URS algorithms is slightly better if it is implemented with machine configured with symmetrical winding.

Chapter 7

CARRIER-BASED PWM TECHNIQUES FOR SIX-PHASE DRIVES WITH DUAL-INVERTER SUPPLY

7.1 Introduction

This chapter discusses carrier-based PWM techniques for the six-phase drive with dual-inverter supply. The considered modulation techniques are phase disposition (PD-PWM) and alternate phase opposition disposition (APOD-PWM), which are classified as level-shifted PWM (LS-PWM) methods, and phase-shifted PWM (PS-PWM) method. Each modulation technique is implemented for both symmetrical and asymmetrical configurations of dual-inverter supplied six-phase drive. The THD of the phase voltage and current, and also their axes component (α-, x- and 0-component) are once more used as the performance indicator to the considered modulation techniques. The results of the carrier-based PWM techniques applied to the asymmetrical six-phase drive have been published in [Jones et al. (2013)].

7.2 Multilevel carrier-based PWM techniques

Fig. 7.1 shows the three carrier-based PWM techniques commonly utilised in the single-sided three-level VSIs, classified as PS-PWM and LS-PWM. The PS-PWM and the LS-PWM have appeared as a natural extension of the traditional carrier-based PWM for two-level inverters and they will be examined here. Similarly to the dual-inverter supply topology, the single-sided multilevel inverter such as FC topology can be represented as a series connection of several two-level inverter cells. In the PS-PWM a phase shift is introduced between the carrier signals that command the cells belonging to the same inverter leg, forcing them to switch at different instants. A stepped multilevel waveform is created in this way. The three-level structure consists of two such cells. The lowest THD is achieved in this case when the carriers are in anti-phase. Since all the cells are effectively controlled with the same carrier that is altered only in terms of phase, i.e. the carriers occupy the same vertical position (Fig. 7.1), the switch utilisation and the average power handled are evenly distributed among the cells at all times. With a topology with k cells,

the output phase voltage has a switching pattern with k times the frequency of the pattern of each cell. Thus, the first higher frequency harmonics will appear at the frequencies around k (here $k = 2$) times the carrier frequency [Rodriguez et al. (2009)].

With the LS-PWM, the comparison of the carrier signals with the reference decides between the upper and lower voltage levels. These voltage levels correspond to the positive and negative dc-link rails in the case of a two-level VSI. For a multilevel inverter, there are (m-1) carriers, where m is the number of voltage levels. They are now vertically shifted rather than phase-shifted, as shown in the mid and lower parts of Fig. 7.1. Since each carrier determines a border between two voltage levels, the notion 'level-shifted' is used. Depending on the controlled topology, additional logic has to be implemented to generate gating signals that produce the desired voltage levels.

There are several forms of the LS-PWM method. When all the positive carriers are in phase with each other and in phase opposition with the negative carriers, the method is known as phase opposition disposition (POD-PWM). The APOD-PWM is obtained by having opposite phase for each two adjacent carriers. In the three-level case, POD-PWM and APOD-PWM result in identical phase voltages and so only APOD-PWM is addressed further. When all carriers are in phase with each other, the method is PD-PWM. For the five-phase case it has already been confirmed using simulations and experimentally that PD-PWM leads to less distorted voltages and currents, compared to PS-PWM [Bodo et al. (2013b)].

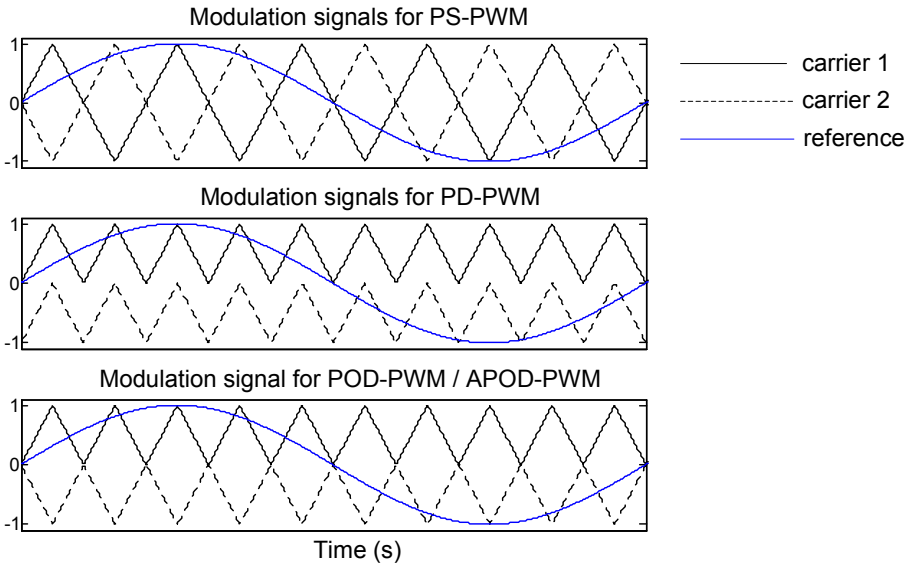

Fig. 7.1: Three-level carrier and modulating signals (without zero-sequence injection) for PS-PWM and LS-PWM (PD-PWM and POD-PWM/APOD-PWM) modulation methods of a single-sided three-level VSI.

7.3 Carrier-based PWM for the open-end configuration

In the single-sided three-level inverters the available leg voltage levels are $V_{dc}/2$, zero and $-V_{dc}/2$. The boundaries between the levels are determined according to Fig. 7.1 so that the converter is switched to $V_{dc}/2$ when the reference is greater than both carriers. The converter is switched to $-V_{dc}/2$ when the reference is less than both carriers. The zero voltage level is generated when the reference is in between the two carriers. This means that this level can be generated in two different ways with PS-PWM depending on which carrier has the larger value.

In the dual-inverter supply topology, as a consequence of the inverters being connected on opposite sides of the machine windings, the modulation rules for the inverter 2 should be inverted in order to make the single-sided PWM methods applicable. This is achieved by changing the sign of the reference and carrier 2 waveforms shown in Fig. 7.1. The new modulation signals for each modulation method that are to be used in conjunction with the dual-inverter supply topology are as depicted in Fig. 7.2.

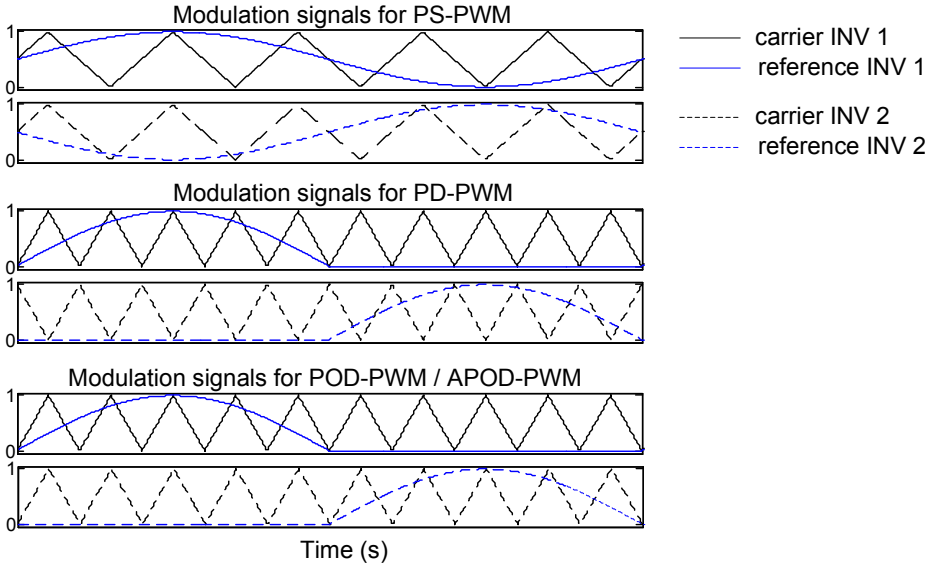

Fig. 7.2: Three-level carrier and modulating signals (without zero-sequence injection) for PS-PWM and LS-PWM (PD-PWM and POD-PWM/APOD-PWM) modulation methods of dual-inverter supply topology.

The three-level PS-PWM has an effective switching frequency which is twice higher than the frequency at which the semiconductors are switched. With the idea of comparing the results for the same average switching frequency, the carrier frequency of the PS-PWM is taken further on, in the simulations and experiments, as one half of the carrier frequency of the PD-PWM and APOD-PWM. This makes the total number of switchings in a modulation period for all three considered techniques the same, so that the average

switching frequency is equalised. However, the instantaneous switching frequency in PD-PWM and APOD-PWM is twice higher in one half-period, since switching occurs only when the modulation signal intersects the corresponding carrier signal. The PD-PWM is in this respect the same as APOD-PWM. Thus the applied carriers for these two methods will have the same frequency.

In the next section, the three considered carrier based PWM techniques for the dual-inverter supplied symmetrical six-phase drive are to be discussed. The implementation of the modulation techniques for the dual-inverter supplied asymmetrical six-phase drive is carried out in the subsequent section.

7.4 Carrier-based PWM methods for symmetrical six-phase drive

In order to investigate the performance of the carrier-based PWM methods, the same MATLAB/Simulink simulation setting and parameters described for the URS and ERS algorithms for symmetrical six-phase drive (Section 6.3) is followed where the simulations are again carried out in a manner that it imitates the non-ideal condition of the experimental set-up. The two inverters are modulated using signals shown in Fig. 7.2 and operated up to $M_{\max} = 1$. In order to compare the performance of each modulation technique using the same average switching frequency, the frequency for the carrier signals of the PS-PWM is set to 1 kHz while for the PD-PWM and APOD-PWM the frequency is set to 2 kHz. The performance indicators described in Chapter 3 are again being used to measure the performance of the three considered carrier-based PWM methods. The performance for each modulation method is presented in Tables 7.1 - 7.6.

Table 7.1: Symmetrical six-phase drive - phase voltage fundamental component and THDs, along with THDs of α-, x- and 0-component voltages for PS-PWM method.

	v_{ph}		v_α	v_x	v_{0-}	v_{ph} level
M	V_1(rms)	THD	THD	THD	THD	
0.1	6.4655	3.2423	3.1156	0	0.8983	3
0.2	13.1515	2.3571	2.2342	0	0.7515	3
0.3	19.8974	1.8528	1.7437	0	0.6228	3
0.4	27.0737	1.4974	1.3982	0	0.5361	3
0.5	34.2050	1.2512	1.1566	0	0.4787	3
0.6	41.1622	1.0666	0.9719	0	0.4374	3
0.7	47.9971	0.9155	0.8178	0	0.4053	3
0.8	55.0785	0.7759	0.6780	0	0.3775	3
0.9	61.8489	0.6572	0.5526	0	0.3530	3
1.0	68.9983	0.5253	0.4140	0	0.3343	3

Table 7.2: Load current fundamental component and THDs, along with THDs of α-, x- and 0-component currents for PS-PWM method.

	i_{ph}		i_α	i_x	i_{0-}
M	I_1(rms)	THD	THD	THD	THD
0.1	0.7112	0.3428	0.1204	0	0.3203
0.2	1.0253	0.2702	0.1620	0	0.2170
0.3	1.1150	0.2870	0.2285	0	0.1777
0.4	1.1233	0.3328	0.2898	0	0.1637
0.5	1.1270	0.3486	0.3058	0	0.1675
0.6	1.1369	0.3439	0.2866	0	0.1874
0.7	1.1615	0.3285	0.2501	0	0.2119
0.8	1.1487	0.3447	0.2332	0	0.2529
0.9	1.1503	0.3629	0.2034	0	0.2975
1.0	1.1559	0.3701	0.1669	0	0.3306

Table 7.3: Symmetrical six-phase drive - phase voltage fundamental component and THDs, along with THDs of α-, x- and 0-component voltages for APOD-PWM method.

	v_{ph}		v_α	v_x	v_{0-}	v_{ph} level
M	V_1(rms)	THD	THD	THD	THD	
0.1	6.4510	3.2377	3.1136	0	0.8894	3
0.2	13.0971	2.3636	2.2425	0	0.7482	3
0.3	20.0614	1.8389	1.7319	0	0.6177	3
0.4	27.1272	1.4945	1.3966	0	0.5330	3
0.5	34.2298	1.2501	1.1562	0	0.4757	3
0.6	41.4035	1.0586	0.9658	0	0.4339	3
0.7	48.3941	0.9031	0.8105	0	0.4010	3
0.8	55.1774	0.7720	0.6753	0	0.3747	3
0.9	62.2309	0.6448	0.5405	0	0.3502	3
1.0	69.1512	0.5243	0.4066	0	0.3329	3

Table 7.4: Load current fundamental component and THDs, along with THDs of α-, x- and 0-component currents for APOD-PWM method.

	i_{ph}		i_α	i_x	i_{0-}
M	I_1(rms)	THD	THD	THD	THD
0.1	0.7054	0.3246	0.1219	0	0.3015
0.2	1.0251	0.2661	0.1622	0	0.2104
0.3	1.1084	0.2852	0.2272	0	0.1785
0.4	1.1279	0.3314	0.2901	0	0.1609
0.5	1.1317	0.3433	0.3003	0	0.1644
0.6	1.1381	0.3319	0.2777	0	0.1807
0.7	1.1500	0.3239	0.2487	0	0.2075
0.8	1.1501	0.3334	0.2263	0	0.2438
0.9	1.1542	0.3434	0.1915	0	0.2859
1.0	1.1569	0.3478	0.1466	0	0.3137

Table 7.5: Symmetrical six-phase drive - phase voltage fundamental component and THDs, along with THDs of α-, x- and 0-component voltages for PD-PWM method.

	v_{ph}		v_α	v_x	v_{0-}	v_{ph} level
M	V_1(rms)	THD	THD	THD	THD	
0.1	6.2393	2.4986	2.1271	1.1274	0.6685	11
0.2	12.6183	1.8109	1.4732	0.9009	0.5465	11
0.3	19.9425	1.3024	0.9925	0.7188	0.4374	11
0.4	27.0397	0.9952	0.6801	0.6212	0.3770	11
0.5	34.1083	0.7629	0.4029	0.5539	0.3368	11
0.6	41.1785	0.6030	0.2426	0.4163	0.3629	15
0.7	48.1031	0.5345	0.2738	0.3404	0.3085	17
0.8	55.1680	0.4800	0.2950	0.2907	0.2425	17
0.9	62.3137	0.4217	0.2878	0.2556	0.1705	17
1.0	69.3599	0.3596	0.2582	0.2386	0.0819	17

Table 7.6: Load current fundamental component and THDs, along with THDs of α-, x- and 0-component currents for PD-PWM method.

	i_{ph}		i_α	i_x	i_{0-}
M	I_1(rms)	THD	THD	THD	THD
0.1	0.6972	0.3330	0.0630	0.0900	0.3151
0.2	1.0206	0.2817	0.0724	0.1230	0.2427
0.3	1.1089	0.2863	0.1251	0.1549	0.2123
0.4	1.1260	0.3160	0.1745	0.1804	0.1933
0.5	1.1324	0.3162	0.1615	0.1893	0.1940
0.6	1.1339	0.2836	0.0913	0.1783	0.1988
0.7	1.1449	0.2569	0.0446	0.1575	0.1971
0.8	1.1522	0.2397	0.0571	0.1416	0.1844
0.9	1.1617	0.2311	0.0626	0.1497	0.1631
1.0	1.1674	0.2456	0.0590	0.1935	0.1368

From the tables, it can be seen that for all considered modulation methods, the expected value of phase voltage fundamental component is reached for operation at every modulation index value. The value increases linearly with an increase of modulation index while the load current fundamental component is maintained around 1.1 A (rms). Regarding the number of phase voltage level, PS-PWM and APOD-PWM produce three levels of phase voltage for the entire modulation index range. For PD-PWM, the number of levels is eleven for $M \leq 0.5$ while for $M > 0.5$, up to seventeen levels of phase voltage is obtained.

To complete the analysis, the simulation results consisting of the phase voltage and current waveforms, their spectra, and THDs for $M = 0.5$ and $M = 1$ are also provided for all three modulation methods. These results are presented in Figs. 7.3 - 7.5.

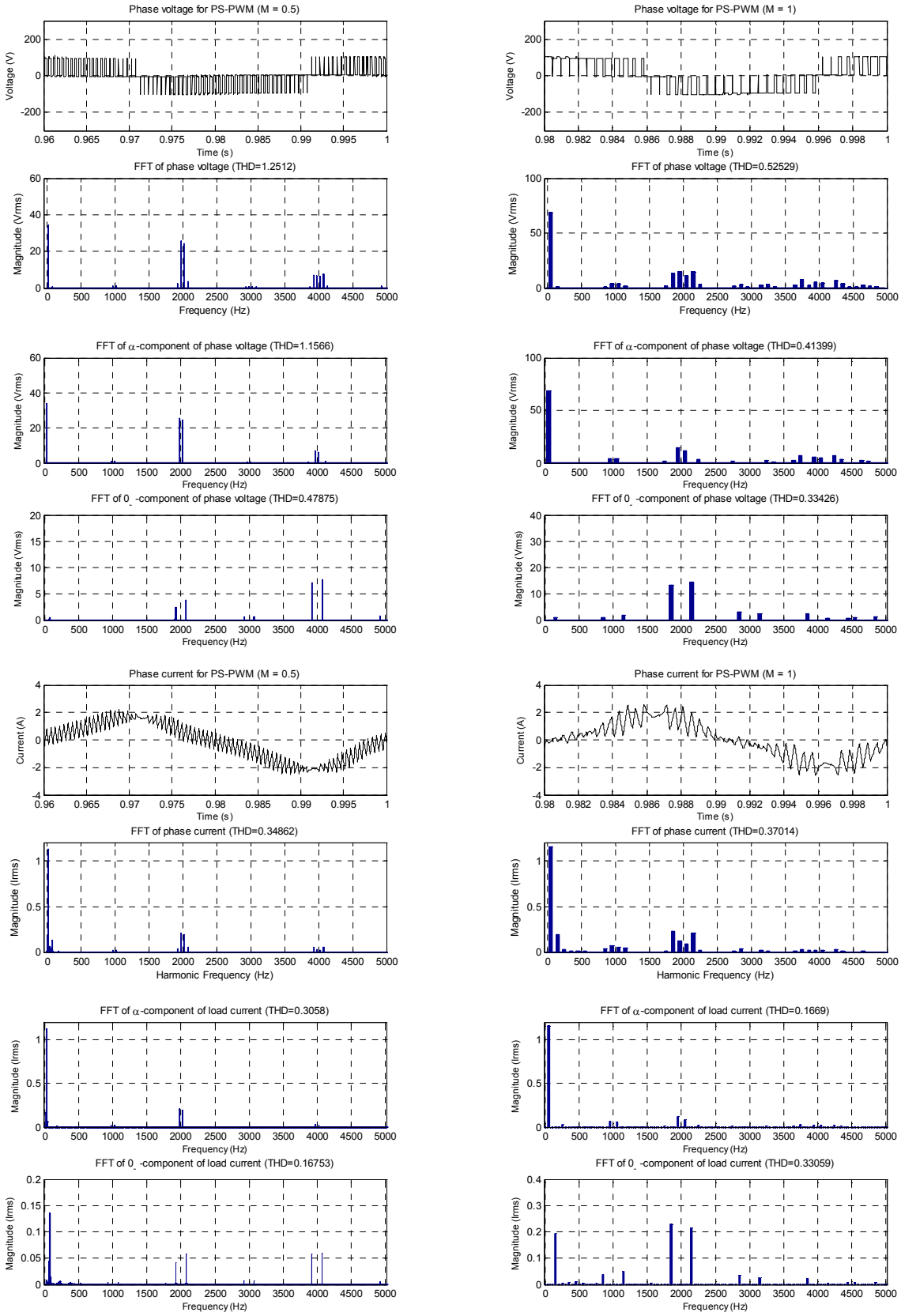

(a) (b)

Fig. 7.3: Simulation result for PS-PWM technique applied to a symmetrical six-phase drive: phase voltage and current waveforms along with their α-component, x-component and 0_-component FFTs for (a) $M = 0.5$ (b) $M = 1$.

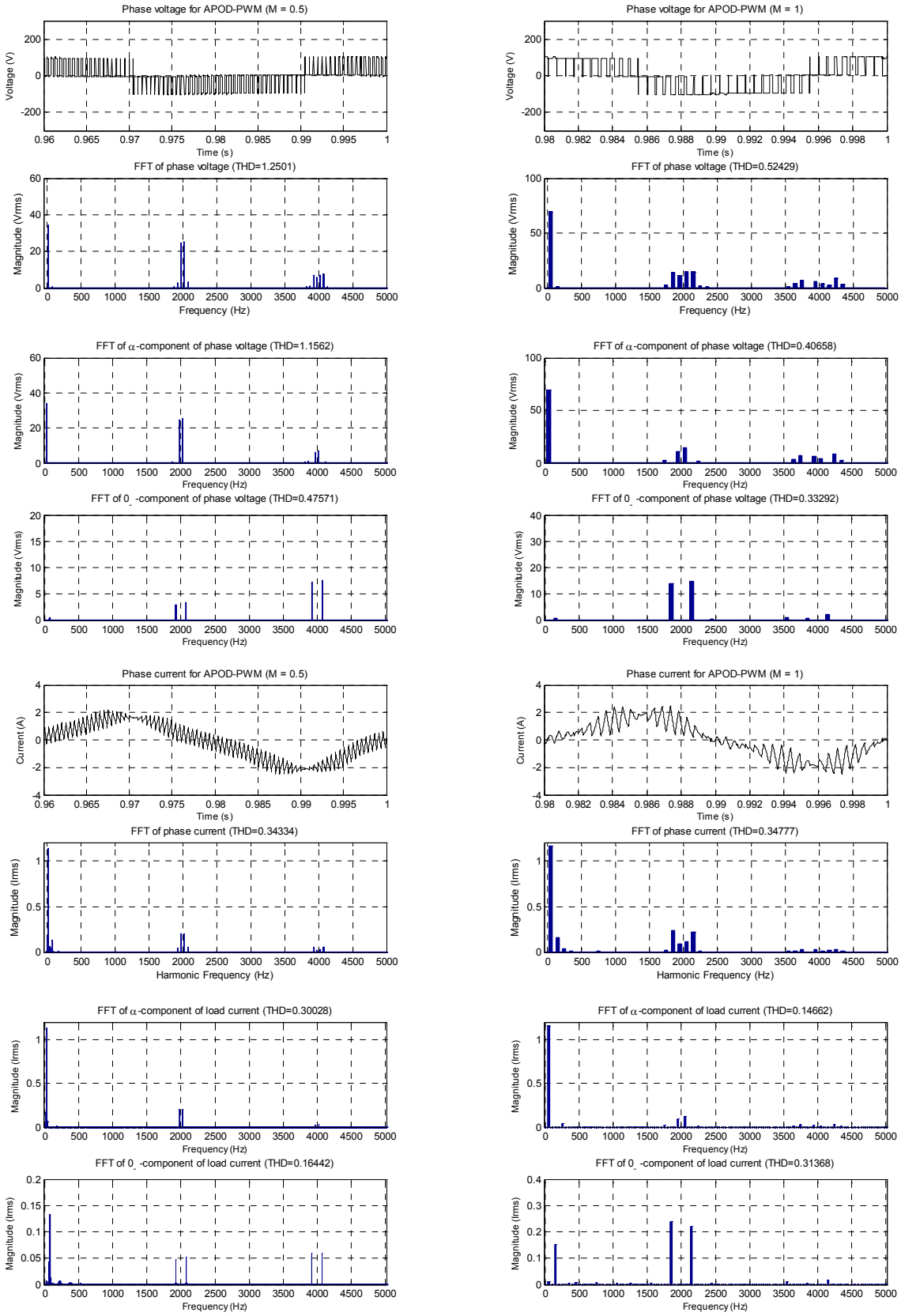

(a) (b)

Fig. 7.4: Simulation result for APOD-PWM technique applied to symmetrical six-phase drive: phase voltage and current waveforms along with their α-component, x-component and 0_-component FFTs for (a) $M = 0.5$ (b) $M = 1$.

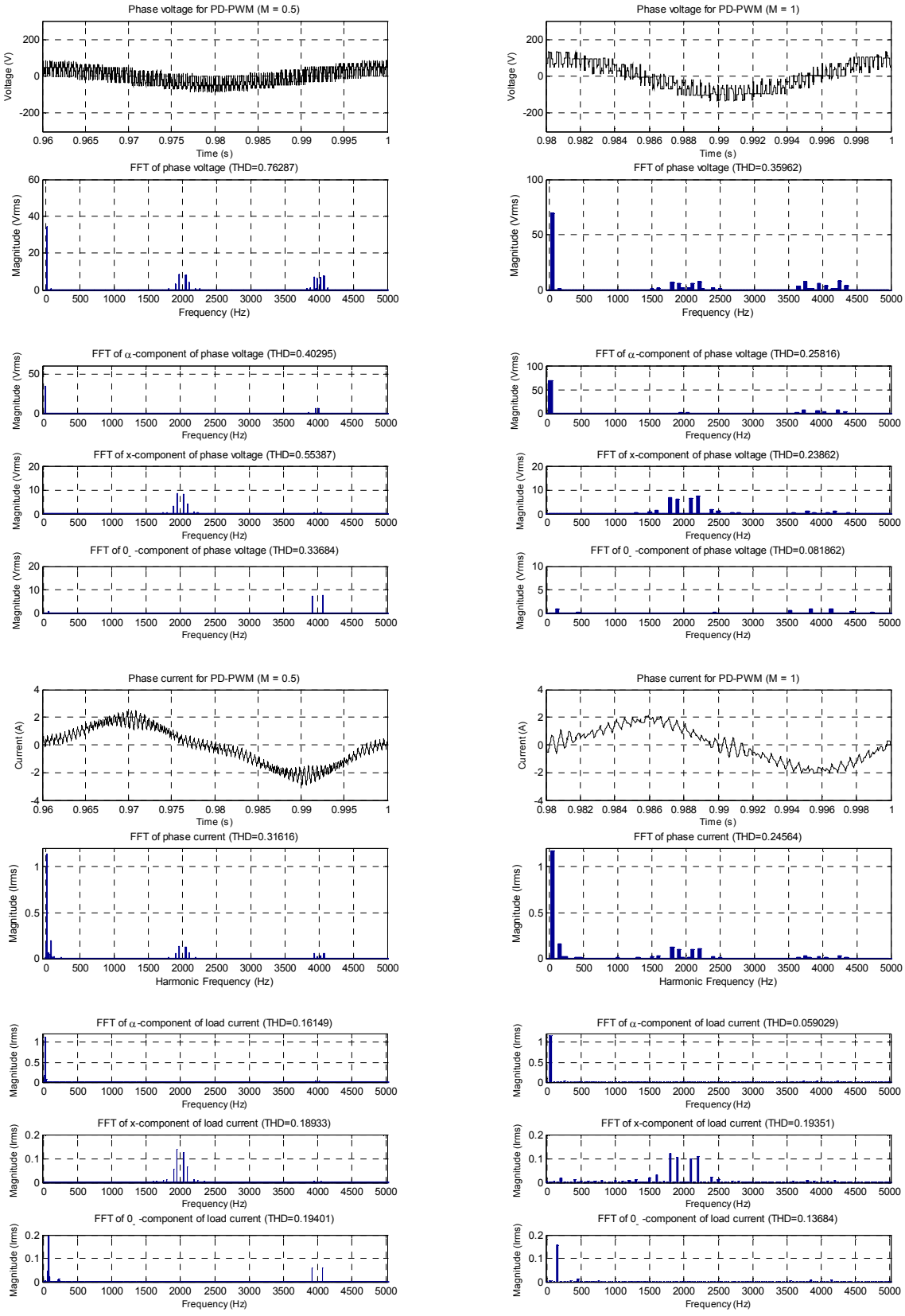

(a) (b)

Fig. 7.5: Simulation result for PD-PWM technique applied to symmetrical six-phase drive: phase voltage and current waveforms along with their α-component, x-component and 0-component FFTs for (a) $M = 0.5$ (b) $M = 1$.

The phase voltage and current waveforms and spectra for PS-PWM are presented in Fig. 7.3. From the figure, it can be seen that the phase voltage waveform comprises only three phase voltage levels where their values alternates between zero and $\pm V_{\mathrm{dc}}$. The spectra of the α- and 0-component of the phase voltage and current are also provided in Fig. 7.3. The x-component of phase voltage and current are not presented since no harmonic is mapped in the (x-y) plane. The fundamental component of phase voltage maps into the (α-β) plane while the dead-time generated low order harmonics can be seen in the 0-axis.

Despite the effective switching frequency of the PS-PWM being twice the inverter switching frequency, it can be seen from Fig. 7.3 that some additional harmonics appear around 1 kHz in the voltage. This is expected, since the two individual inverters do switch at 1 kHz frequency. In theory, the harmonics around 1 kHz should have phase shifts and magnitudes which cancel each other. However, due to the dead-time implemented in the simulation, the switching instants vary slightly and these harmonics do not cancel completely. A small amount of low-order harmonics can be seen in the current spectrum; again, these harmonics are a consequence of the inverter dead time and device voltage drops.

Fig. 7.4 presents simulation results for the APOD-PWM. Comparison of Fig. 7.3 and Fig. 7.4 reveals that APOD-PWM and PS-PWM produce very similar phase voltage and current waveforms. On the other hand, since the APOD-PWM device switching frequency is 2 kHz, there are no residual sideband harmonics around 1 kHz. As expected, the harmonics mapping is similar to the PS-PWM method.

The performance of the PD-PWM technique is illustrated in Fig. 7.5. Here, the phase voltage comprises of harmonics that are mapped into the (x-y) plane also. The stator phase voltage has 11 voltage levels for M = 0.5 with the maximum level being $5/12(V_{dc})$. For M = 1, the voltage level increases to seventeen levels with maximum level being $2/3(V_{dc})$. The switching harmonics appear at sidebands around multiples of the switching frequency (2 kHz). Again, the inverter dead time and device voltage drops generate low order harmonic that map into the (x-y) plane and 0-axis.

Comparison of the harmonic performance of the three carrier-based PWM methods over the entire linear modulation range is provided in Fig. 7.6 where the THD is shown for the phase voltage and current, as well as for their axes components. It can be seen that the PD-PWM method offers the lowest voltage THD while the PS-PWM and APOD-PWM methods produce almost identical THDs. The same conclusion can also be applied for the

current THD. Current THD of PD-PWM is the lowest among the three considered methods especially for operation at higher modulation index value ($M > 0.5$). These results are in agreement with analysis of the performance of three-phase [McGrath and Holmes (2002)] and five-phase multilevel drives [Bodo et al. (2013b)].

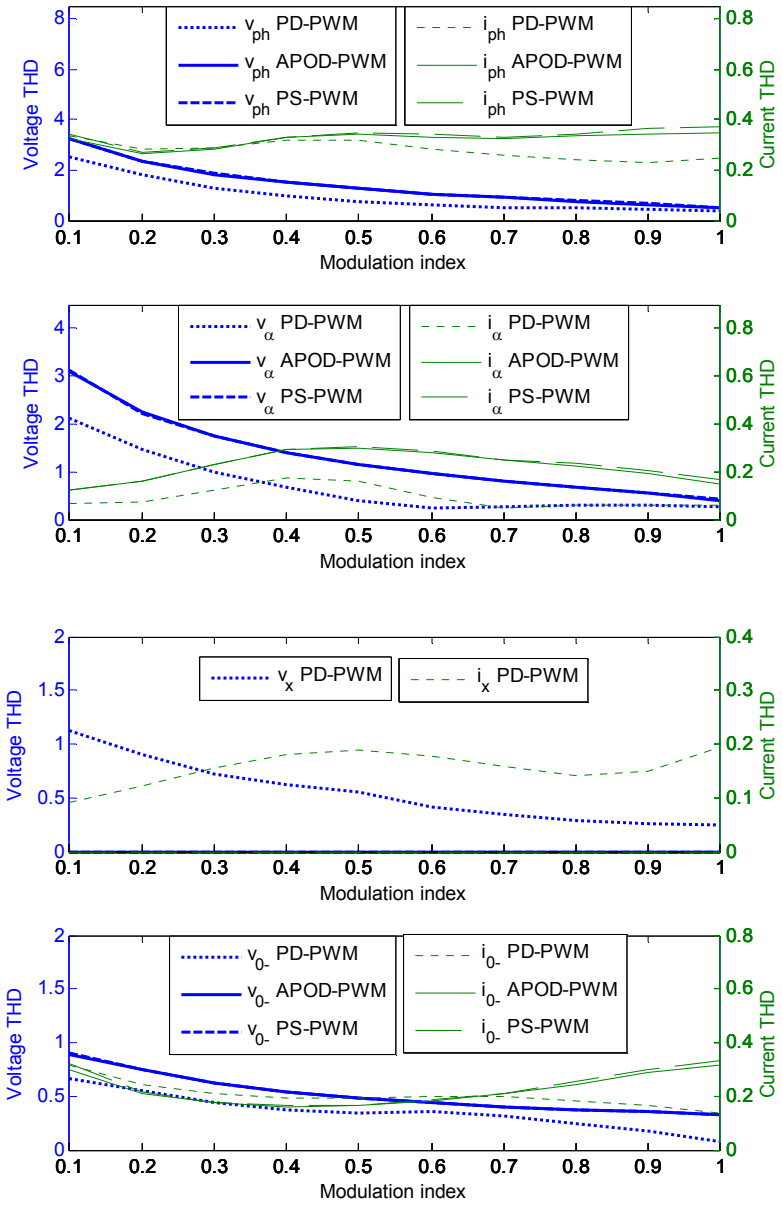

Fig. 7.6: Simulation results for symmetrical six-phase drives: phase voltage and current, their α-, x- and 0-component THDs against modulation index for the PS-PWM, APOD-PWM and PD-PWM methods.

Experimental results obtained for all the three carrier-based PWM methods are presented in Figs. 7.7 - 7.9. By comparing the respective figures for all three modulation methods, it can be seen that the simulation and experiment works produce voltage waveforms, FFTs and THDs that are matched quite closely. For the phase current, there is

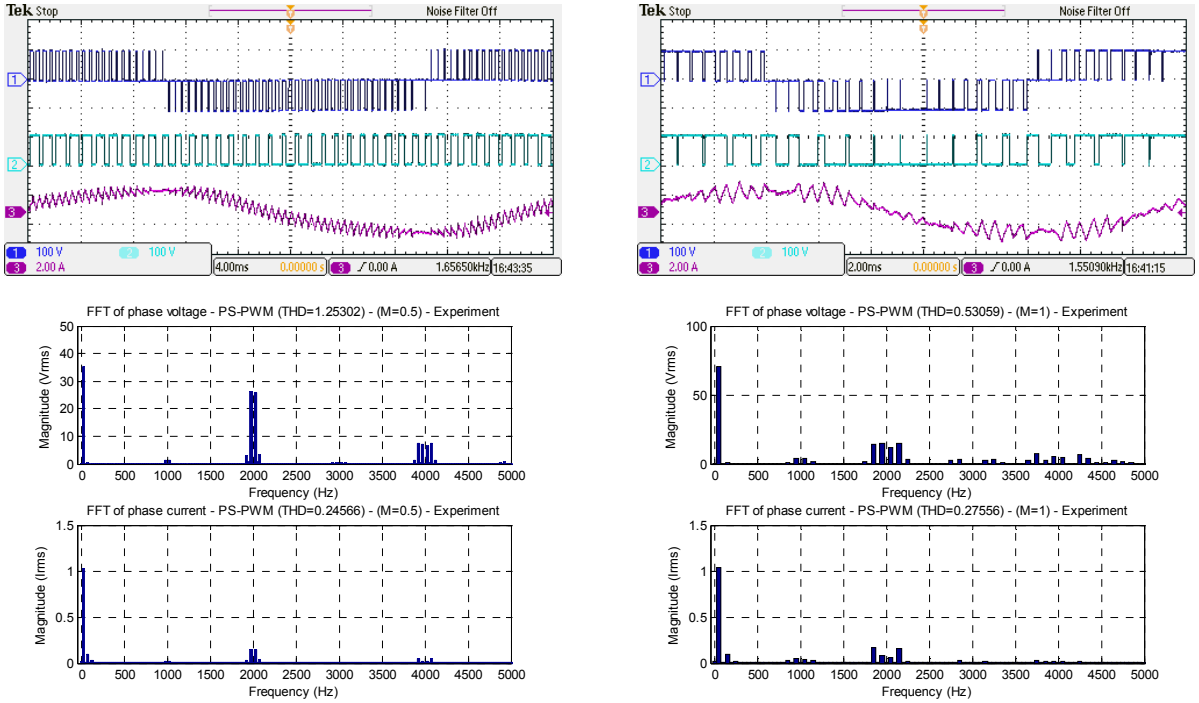

(a) (b)

Fig. 7.7: Experiment results, PS-PWM: phase voltage/current and leg A1 voltage waveforms, and spectra for (a) $M = 0.5$ (b) $M = 1$.

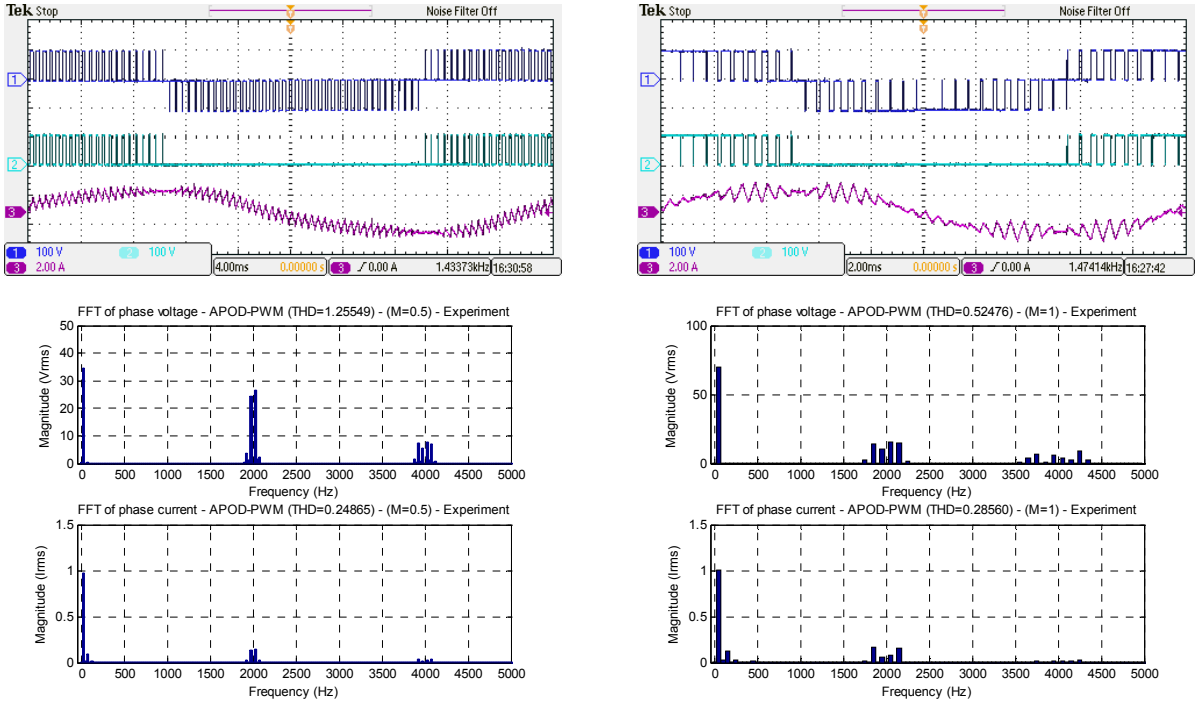

(a) (b)

Fig. 7.8: Experiment results, APOD-PWM: phase voltage/current and leg A1 voltage waveforms, and spectra for (a) $M = 0.5$ (b) $M = 1$.

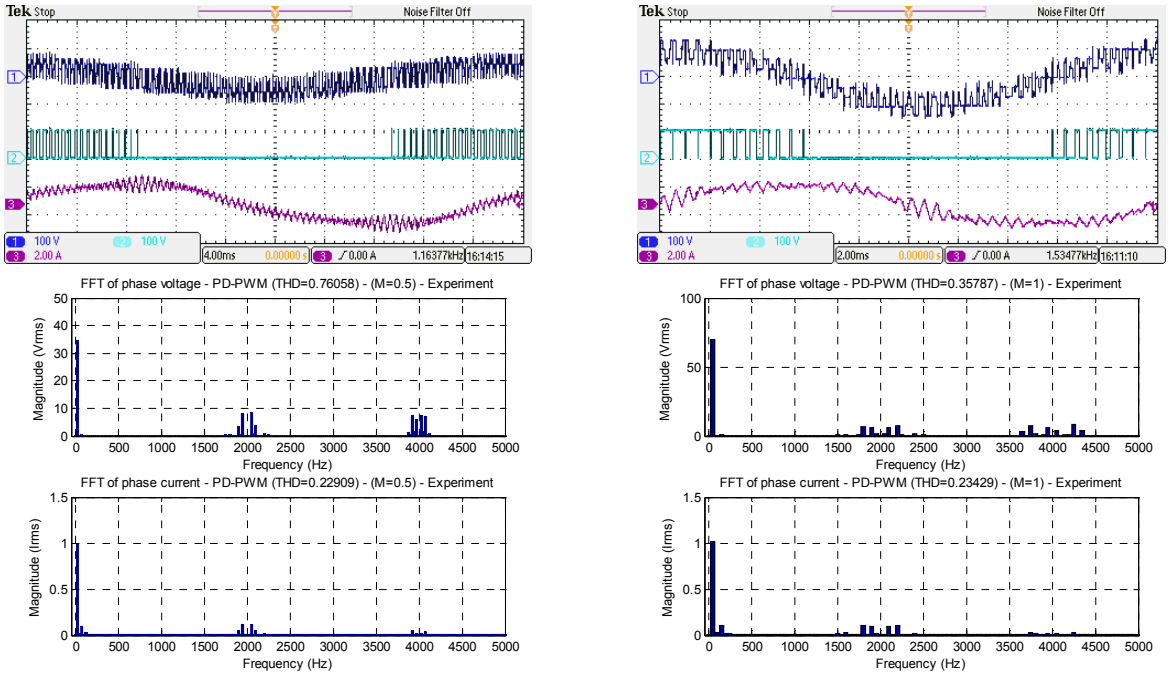

(a) (b)

Fig. 7.9: Experiment results, PD-PWM: phase voltage/current and leg A1 voltage waveforms, and spectra for (a) $M = 0.5$ (b) $M = 1$.

a small differences between the results obtained from simulations and experiments. The differences are again likely due to mismatch between the value of machine parameters that is being used in the simulation with the exact machine parameters value. Besides that, a small amount of low order harmonics also appears in both simulations and experimental results where their amplitudes is influenced by the amount of dead time and voltage drops on the semiconductor devices. The leg A1 voltage waveforms clearly show the PS-PWM switching at half the frequency of the other methods; however, over one fundamental period the average switching frequency is equal for the three methods and hence the switching losses of the inverter are practically the same.

7.5 Performance comparison

The THDs of phase voltage and current, obtained from simulation and experiments for the linear modulation range are plotted in Fig. 7.12. For the phase voltage THDs, the results obtained from experiments match very closely with simulations. The PD-PWM produces the best performance while APOD-PWM and PS-PWM perform equally. Similar conclusion is also obtained for the current THD. There are however, some disaggrements between the simulations and experiments results. These disagreements are mostly contributed by the lack of knowledge of the exact machine parameters. Nevertheless, similar trends of current THD are obtained for each individual PWM technique. For PD-

PWM, the trend on the current THD curve is changing when $M > 0.5$ as a consequence of the increase in the number of phase voltage levels from eleven to seventeen, such as shown in the last column of Table 7.5. For the PS-PWM and APOD-PWM, no change of trend on the THD curve is observed since the number of phase voltage levels is always equal to three for the whole linear modulation range as indicated in Table 7.1 and 7.3, respectively.

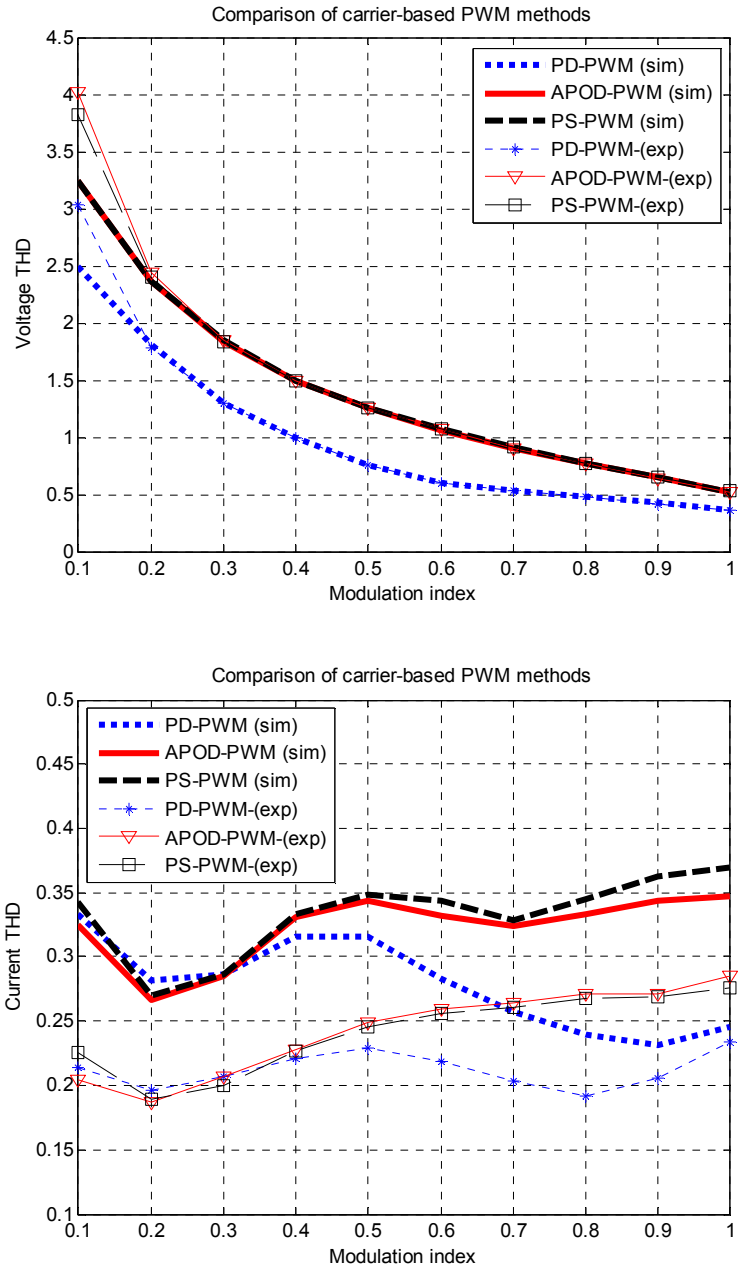

Fig. 7.10: Simulation and experimental THD plotted against the modulation index for the carrier-based PWM techniques. Phase voltage (top), load current (bottom).

7.6 Carrier-based PWM methods for asymmetrical six-phase drive

The performance of carrier-based PWM methods for the asymmetrical six-phase drive with dual-inverter supply is investigated using the same MATLAB/Simulink simulation set-up for the URS and ERS algorithms for asymmetrical six-phase drives explained in Section 6.4. In order to maximise the dc bus voltage utilisation, the zero-sequence injection signals are added to the reference so that M_{max} = 1.0353 is obtained. Similar to the symmetrical six-phase drive, the frequency of carrier signals for each PWM method is also averaged to 2 kHz. The performance of each modulation method in term of THDs of the phase voltage and current and also their axes components are presented in Tables 7.7 - 7.12, together with the number of phase voltage level obtained for every modulation index operation.

Again, similar to the symmetrical six-phase drive, the rms of the phase voltage fundamental component reaches the expected level for operation with every modulation index value while the rms of the load current fundamental component is maintained around 0.5 A. The PS-PWM and APOD-PWM generate thirteen phase voltage levels for operation with every modulation index value. For the PD-PWM, there are eleven phase voltage levels for $M \leq 0.5$, while for $M > 0.5$, the level increases steadily up to nineteen.

Further, the phase voltage and current waveforms, their spectra, and THDs are presented for modulation index M = 0.5 and M = 1 for each modulation method. Simulation results for the all three modulation methods are provided in Figs. 7.11 - 7.13

The PS-PWM phase voltage and current waveforms and spectra are presented in Fig. 7.11 along with their α-, x- and 0$_-$-component. The load phase voltage waveform comprises thirteen levels, the maximum being $(2/3)V_{dc}$. Again, due to the dead-time implementation, some additional harmonics appear around 1 kHz, in ideal conditions, these harmonics should not be present. A small amount of low-order harmonics can also be seen in the voltage and current spectra, once more, these harmonics are a consequence of the inverter dead time and semiconductors voltage drops. As expected, the transformation of the stator phase voltage into (α-β) and (x-y) planes and (0$_+$-0$_-$) axes reveals that the fundamental maps into the (α-β) plane. The largest switching harmonics map into the (α-β) plane while the dead-time generated low order harmonics can be seen in the (x-y) plane and also 0$_-$-axis.

Table 7.7: Asymmetrical six-phase drive - phase voltage fundamental component and THDs, along with THDs of α-, x- and 0-component voltages for PS-PWM method.

	v_{ph}		v_α	v_x	v_{0-}	v_{ph}
M	V1(rms)	THD	THD	THD	THD	level
0.1	9.1418	3.4771	3.3721	0.5246	0.6750	13
0.2	19.4291	2.3879	2.2846	0.4942	0.5255	13
0.3	30.2417	1.8145	1.7213	0.4062	0.4376	13
0.4	41.1748	1.4688	1.3791	0.3530	0.3820	13
0.5	51.8650	1.2285	1.1405	0.3173	0.3439	13
0.6	62.6235	1.0407	0.9528	0.2905	0.3148	13
0.7	72.5612	0.8959	0.8040	0.2707	0.2945	13
0.8	83.4452	0.7554	0.6590	0.2530	0.2755	13
0.9	93.7269	0.6353	0.5278	0.2383	0.2606	13
1.0	104.2884	0.5103	0.3875	0.2246	0.2480	13
1.0353	108.0510	0.4725	0.3361	0.2185	0.2452	13

Table 7.8: Load current fundamental component and THDs, along with THDs of α-, x- and 0-component currents for PS-PWM method.

	i_{ph}		i_α	i_x	i_{0-}
M	I1(rms)	THD	THD	THD	THD
0.1	0.3239	0.1935	0.0583	0.1331	0.1439
0.2	0.4572	0.1553	0.0757	0.1084	0.0932
0.3	0.4927	0.1594	0.0965	0.1118	0.0716
0.4	0.5047	0.1861	0.1123	0.1384	0.0575
0.5	0.5116	0.2189	0.1216	0.1784	0.0507
0.6	0.5130	0.2596	0.1251	0.2248	0.0476
0.7	0.5155	0.3031	0.1218	0.2760	0.0476
0.8	0.5130	0.3566	0.1134	0.3360	0.0523
0.9	0.5095	0.4126	0.0992	0.3974	0.0584
1.0	0.5216	0.4658	0.0790	0.4552	0.0636
1.0353	0.5175	0.4812	0.0734	0.4698	0.0666

Table 7.9: Asymmetrical six-phase drive - phase voltage fundamental component and THDs, along with THDs of α-, x- and 0-component voltages for APOD-PWM method.

	v_{ph}		v_α	v_x	v_{0-}	v_{ph}
M	V1(rms)	THD	THD	THD	THD	level
0.1	9.1144	3.4782	3.3751	0.5067	0.6743	13
0.2	19.4276	2.3862	2.2859	0.4920	0.5238	13
0.3	30.4717	1.8026	1.7117	0.4036	0.4335	13
0.4	41.1706	1.4681	1.3789	0.3536	0.3810	13
0.5	51.8611	1.2282	1.1404	0.3171	0.3422	13
0.6	62.1900	1.0473	0.9586	0.2912	0.3150	13
0.7	73.2718	0.8843	0.7943	0.2686	0.2912	13
0.8	83.6223	0.7497	0.6548	0.2520	0.2736	13
0.9	94.3536	0.6195	0.5153	0.2379	0.2588	13
1.0	104.6165	0.5017	0.3770	0.2259	0.2459	13
1.0353	108.2337	0.4601	0.3238	0.2211	0.2430	13

Table 7.10: Load current fundamental component and THDs, along with THDs of α-, x- and 0-component currents for APOD-PWM method

	i_{ph}		i_α	i_x	i_{0-}
M	I1(rms)	THD	THD	THD	THD
0.1	0.3234	0.1869	0.0608	0.1334	0.1362
0.2	0.4579	0.1557	0.0754	0.1115	0.0925
0.3	0.4923	0.1617	0.0965	0.1123	0.0725
0.4	0.5044	0.1870	0.1120	0.1415	0.0579
0.5	0.5107	0.2208	0.1211	0.1811	0.0495
0.6	0.5150	0.2603	0.1236	0.2277	0.0460
0.7	0.5160	0.3062	0.1195	0.2806	0.0460
0.8	0.5179	0.3556	0.1087	0.3364	0.0489
0.9	0.5203	0.4094	0.0913	0.3960	0.0555
1.0	0.5180	0.4715	0.0688	0.4624	0.0620
1.0353	0.5131	0.4933	0.0608	0.4850	0.0652

Table 7.11: Asymmetrical six-phase drive - phase voltage fundamental component and THDs, along with THDs of α-, x- and 0-component voltages for PD-PWM method.

	v_{ph}		v_α	v_x	v_{0-}	v_{ph}
M	V1(rms)	THD	THD	THD	THD	level
0.1	9.0165	2.6140	2.4154	0.8598	0.5454	11
0.2	19.3619	1.7497	1.5426	0.7019	0.4380	11
0.3	30.2711	1.2683	1.0698	0.5758	0.3576	11
0.4	40.9489	0.9680	0.7619	0.5040	0.3141	11
0.5	51.6173	0.7370	0.5028	0.4550	0.2832	11
0.6	62.0262	0.5676	0.3249	0.3543	0.3033	15
0.7	72.4601	0.4977	0.3072	0.3044	0.2460	17
0.8	83.2150	0.4575	0.3011	0.2806	0.2011	17
0.9	93.8327	0.4217	0.2759	0.2677	0.1766	19
1.0	104.3578	0.3809	0.2315	0.2593	0.1582	19
1.0353	108.1034	0.3654	0.2104	0.2573	0.1524	19

Table 7.12: Load current fundamental component and THDs, along with THDs of α-, x- and 0-component currents for PD-PWM method.

	i_{ph}		i_α	i_x	i_{0-}
M	I1(rms)	THD	THD	THD	THD
0.1	0.3271	0.2415	0.0373	0.2076	0.1373
0.2	0.4617	0.2814	0.0420	0.2701	0.0873
0.3	0.4967	0.3479	0.0438	0.3403	0.0656
0.4	0.5087	0.3982	0.0402	0.3934	0.0509
0.5	0.5104	0.4199	0.0357	0.4180	0.0381
0.6	0.5174	0.3923	0.0300	0.3897	0.0413
0.7	0.5123	0.3675	0.0285	0.3643	0.0411
0.8	0.5179	0.3722	0.0289	0.3688	0.0364
0.9	0.5185	0.4418	0.0283	0.4384	0.0340
1.0	0.5176	0.5613	0.0252	0.5587	0.0335
1.0353	0.5192	0.6171	0.0254	0.6148	0.0360

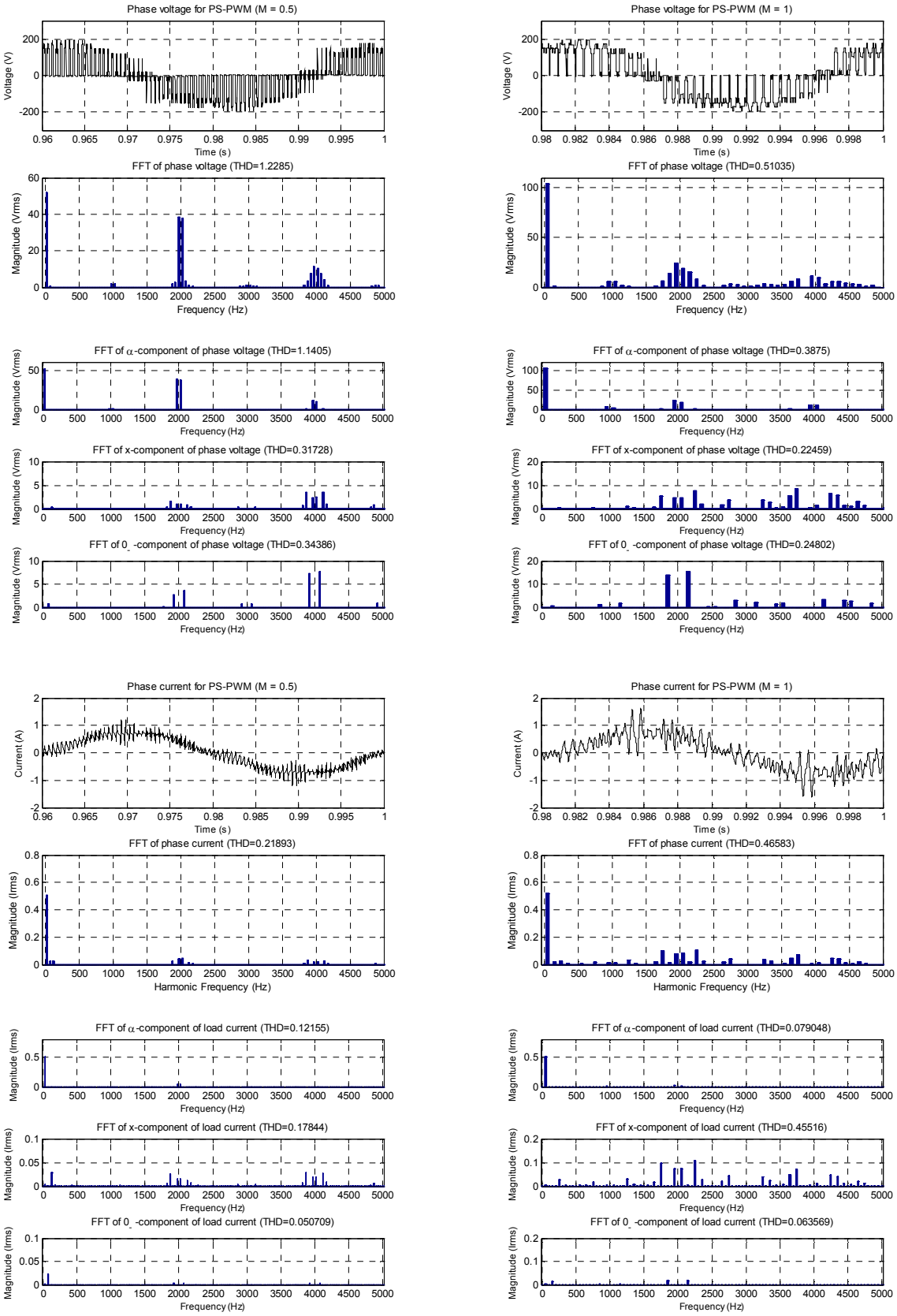

(a) (b)

Fig. 7.11: Simulation result for PS-PWM technique applied to an asymmetrical six-phase drive: phase voltage and current waveforms along with their α-component, x-component and 0-component FFTs for (a) $M = 0.5$ (b) $M = 1$.

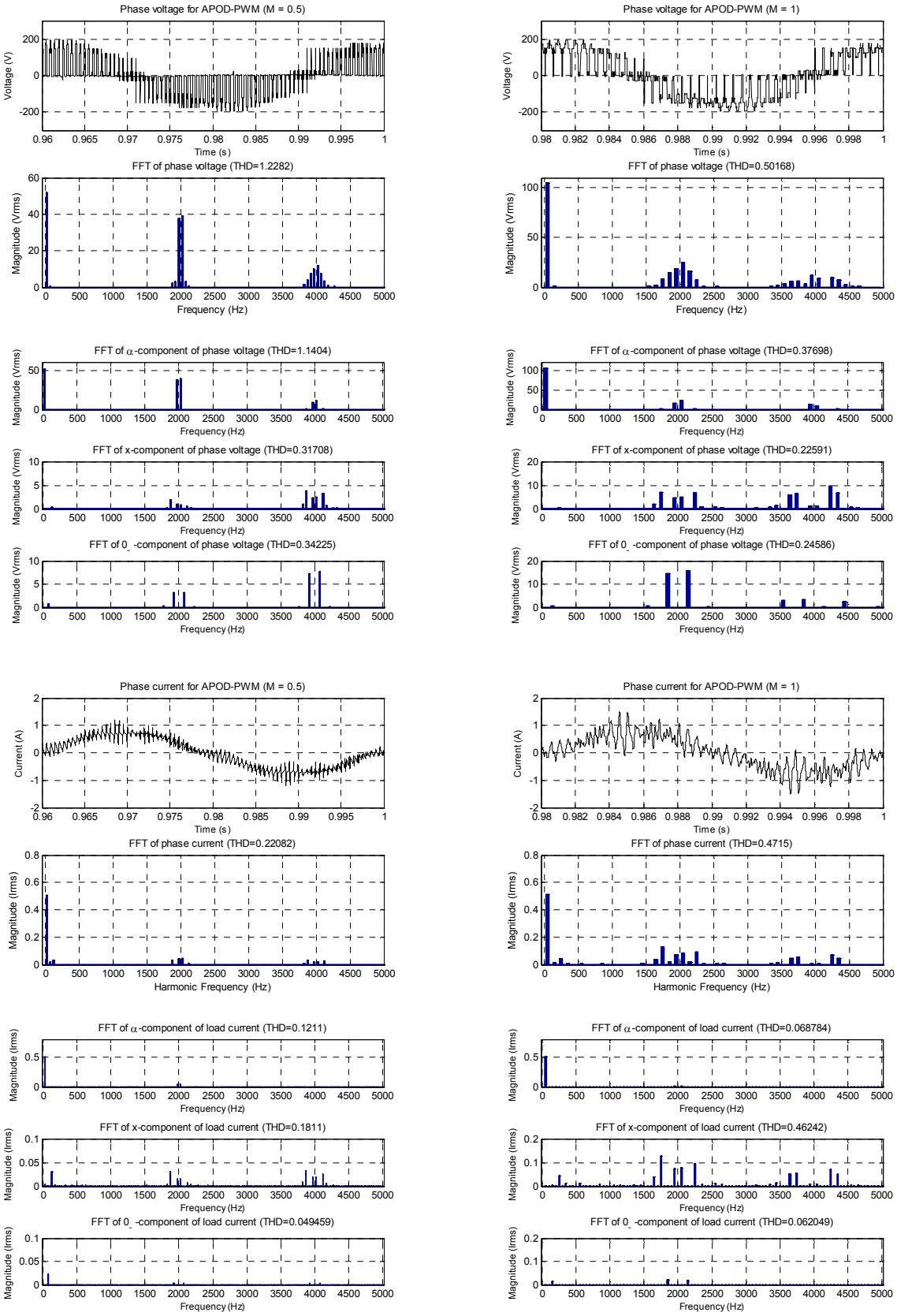

(a) (b)

Fig. 7.12: Simulation result for APOD-PWM technique applied to an asymmetrical six-phase drive: phase voltage and current waveforms along with their α-component, x-component and 0-component FFTs for (a) $M = 0.5$ (b) $M = 1$.

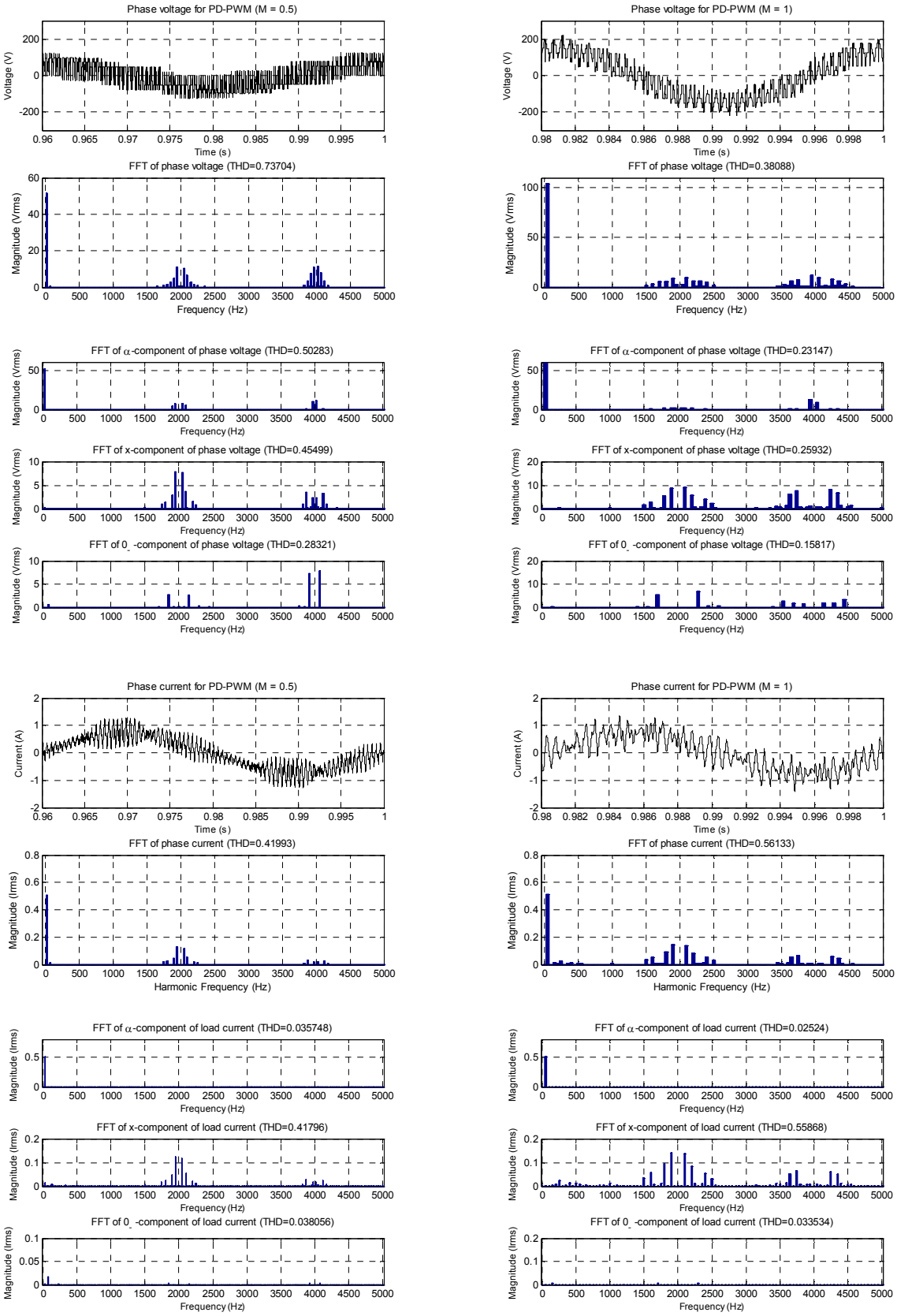

(a) (b)

Fig. 7.13: Simulation result for PD-PWM technique applied to an asymmetrical six-phase drive: phase voltage and current waveforms along with their α-component, x-component and 0_-component FFTs for (a) $M = 0.5$ (b) $M = 1$.

Fig. 7.12 presents simulation results for the APOD-PWM. Again, as observed for the symmetrical six-phase drive, APOD-PWM produces phase voltage and current waveforms that is almost identical to the PS-PWM. The harmonic mapping is also very similar to the PS-PWM method except that there are no residual sideband harmonics around 1 kHz.

The performance of the PD-PWM technique is illustrated in Fig. 7.13. The phase voltage has eleven voltage levels for $M = 0.5$, the maximum level being $(5/12)V_{dc}$. For $M = 1$, the number of phase voltage level is nineteen with the maximum level being $(3/4)V_{dc}$. The switching harmonics appear at sidebands around multiples of the switching frequency (2 kHz) and the low order harmonics are visible on the (x-y) plane and 0-axis. The first sideband harmonics (2 kHz) are significantly smaller than in the other two methods while the second sideband harmonics have approximately the same magnitude. Importantly, the dominant first sideband harmonics map into the (x-y) plane and so have a more detrimental effect on the current waveform than for the other methods, resulting in a significantly larger current THD.

All PWM schemes are capable of matching the voltage reference and produce a multilevel load phase voltage waveform with a low level of low-order harmonic content.

Comparison of the harmonic performance of the considered methods over the entire linear modulation range is provided in Fig. 7.14 where THD is shown for the phase voltage and current, as well as for their axes components. As observed, the PD-PWM method offers the lowest voltage THD while the PS-PWM and APOD-PWM methods produce almost identical THDs. This trend is in agreement with analysis of the performance of three-phase [McGrath and Holmes (2002)] and five-phase multilevel drives [Bodo et al. (2013b)]. However, the current THD of the PD-PWM is significantly worse than for the APOD-PWM and PS-PWM, which is quite different from the situation encountered in three-phase [McGrath and Holmes (2002)] and five-phase [Bodo et al. (2013b)] drives. The reason is revealed by inspecting the THDs of individual planes of the three methods, included in Fig. 7.14. The voltage and current axis THDs show that the PD-PWM has the lowest THD in the (α-β) plane and (0_+-0-) axes and the highest THD in the (x-y) plane. However, since the dominant first sideband voltage harmonics map into the (x-y) plane, which offers very low impedance to the current, the x-axis, and hence phase current as well, have significantly higher current THD than the other methods. This can also be seen in the current ripple of the PD-PWM and APOD-PWM methods (Fig. 7.13 and Fig. 7.12, respectively).

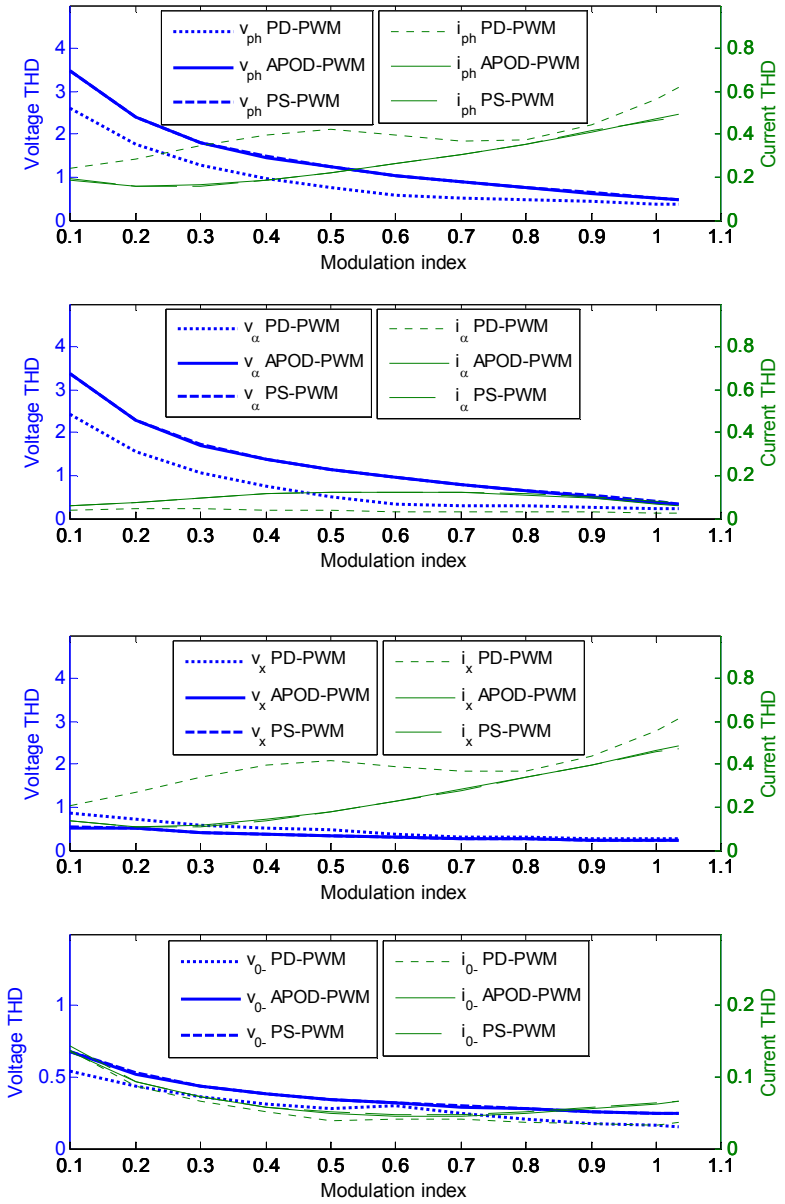

Fig. 7.14: Simulation results: phase voltage and current, their α-component x-component and 0.-component THDs against modulation index for the PS-PWM, APOD-PWM and PD-PWM methods.

Figs. 7.15 - 7.17 depict experimental results obtained for the three modulation methods for M = 0.5 and M = 1. A strong correspondence between simulations and experiments can be observed by comparing the respective figures for all three methods. The voltage and current waveforms, FFTs and THDs match quite closely. A small amount of low order harmonics appears in both simulations and experimental results and the rms of the fundamental reaches the expected level.

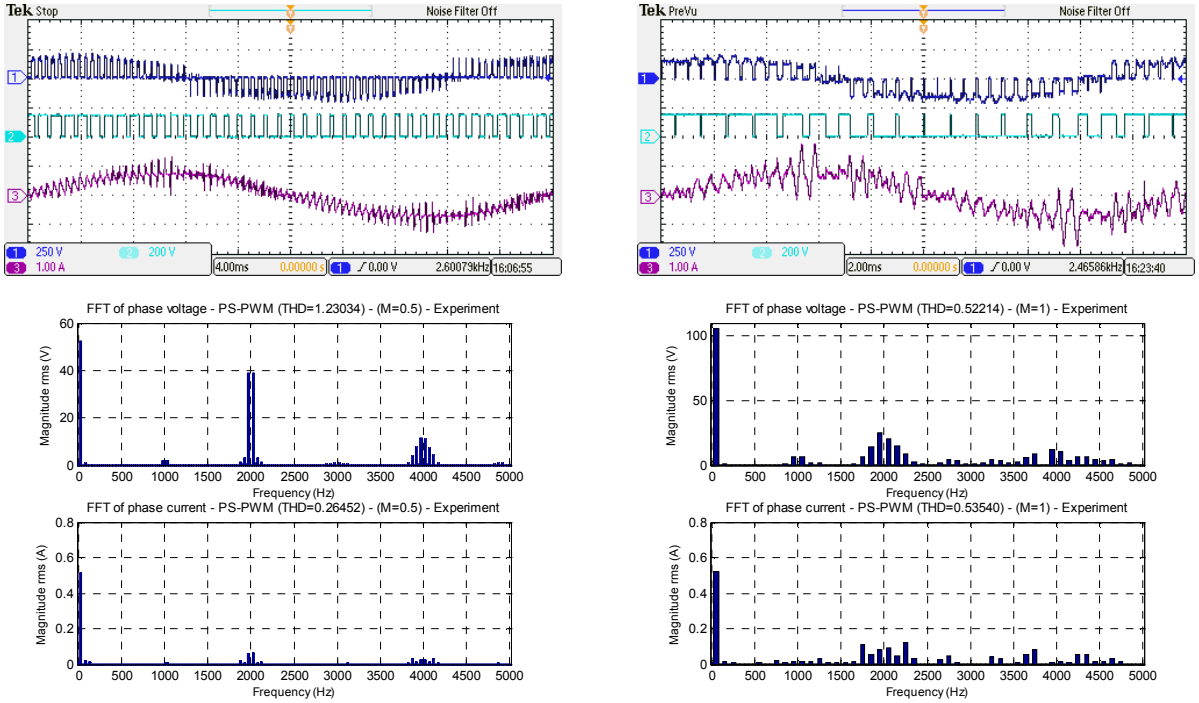

(a) (b)

Fig. 7.15: Experiment results for PS-PWM: phase voltage/current and leg A1 voltage waveforms, and spectra for (a) $M = 0.5$ (b) $M = 1$.

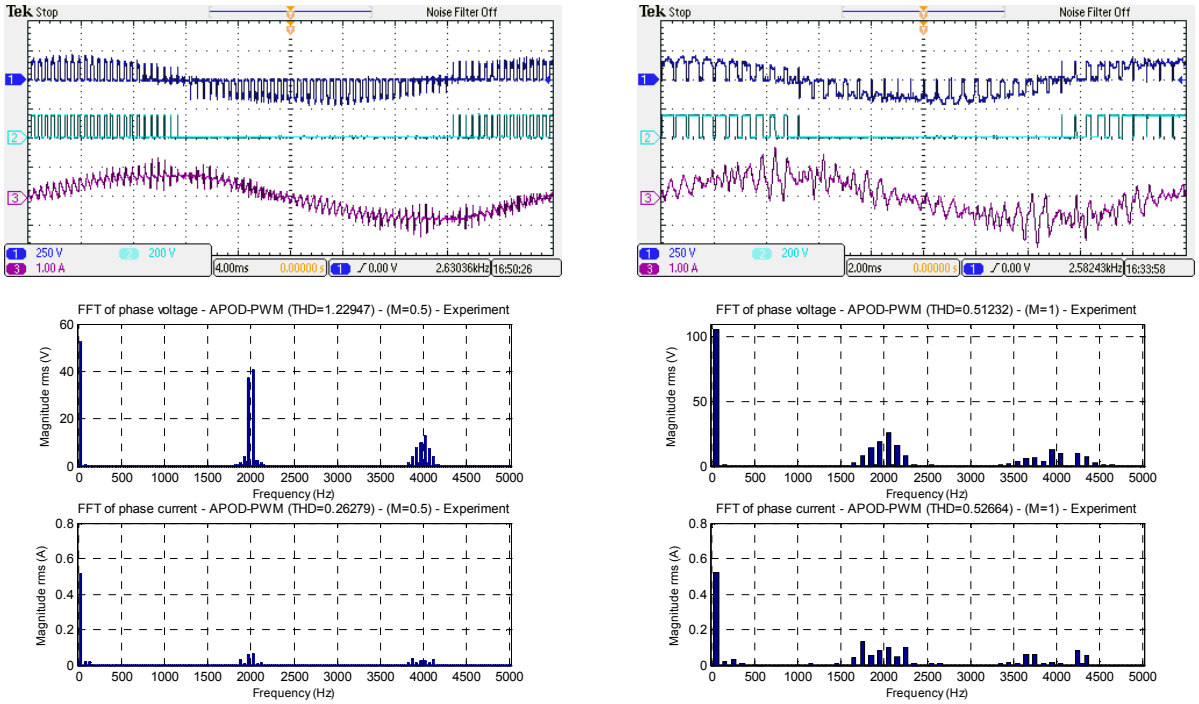

(a) (b)

Fig. 7.16: Experiment results for APOD-PWM: phase voltage/current and leg A1 voltage waveforms, and spectra for (a) $M = 0.5$ (b) $M = 1$.

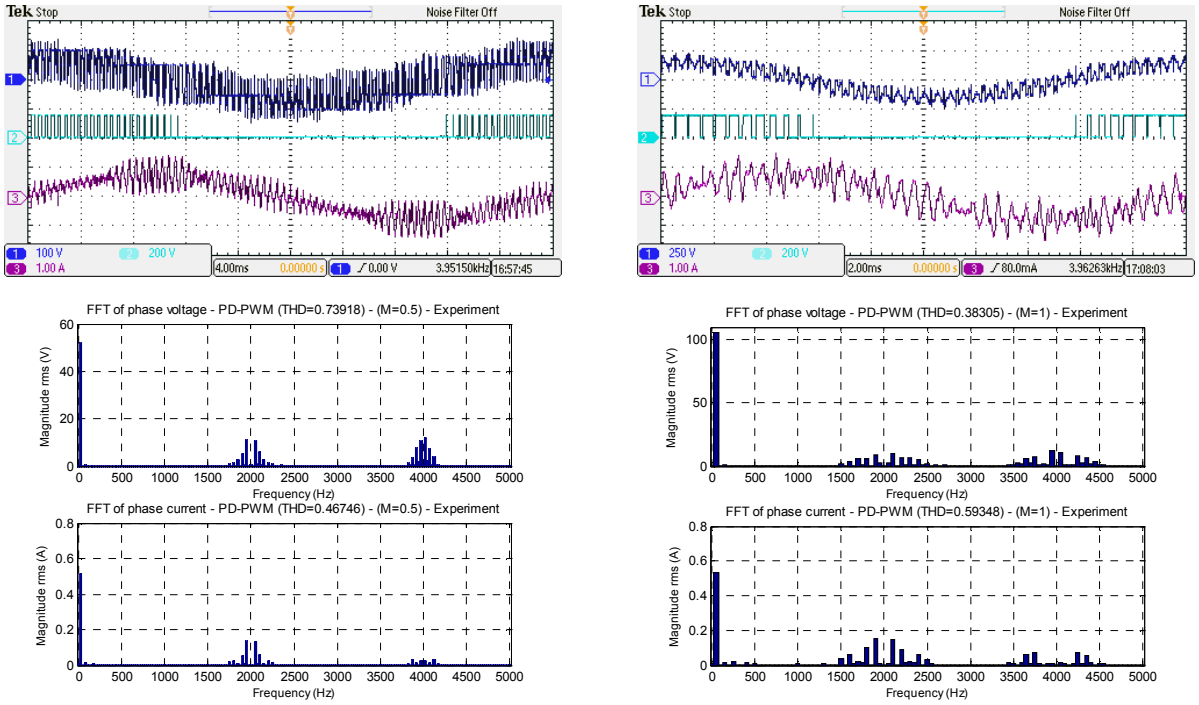

(a) (b)

Fig. 7.17: Experiment results for PD-PWM: phase voltage/current and leg A1 voltage waveforms, and spectra for (a) $M = 0.5$ (b) $M = 1$.

As both experimental and simulation results clearly show, PD-PWM yields superior quality of the output voltage waveform, compared to the other carrier-based methods, since the resultant voltage THDs are smaller. However, the current waveform has a higher ripple content as reflected by the higher current THDs. The improvement in phase voltage is in accordance with the increase of the number of phase voltage levels with PD-PWM (eleven at M = 0.5 to nineteen at M = 1), while for PS-PWM and APOD-PWM the number of levels remains at thirteen throughout the modulation range. Furthermore, the PS-PWM and APOD-PWM can be considered as quasi-multilevel methods since the voltage waveforms show that the zero space vector is applied during each switching period, regardless of the modulation index. This is in contrast to the PD-PWM. When M = 0.5 the currents generated by the PD-PWM clearly contain a higher degree of ripple than the other methods. When M = 1 these differences are more difficult to observe in the current waveforms. The leg A1 voltage waveforms again show that the PS-PWM is switched at half the frequency of the other methods. However, over one fundamental period the average switching frequency is equal for the three methods and hence practically producing the same switching losses.

7.7 Performance comparison

The THD of phase voltage and current, obtained from simulation and experiments for the entire linear range of the modulation index are plotted in Fig. 7.18. In terms of phase voltage THD, the results obtained from the experiments match very closely with the simulation. Performance of APOD-PWM and PS-PWM is equal while PD-PWM produces the best performance among the three methods.

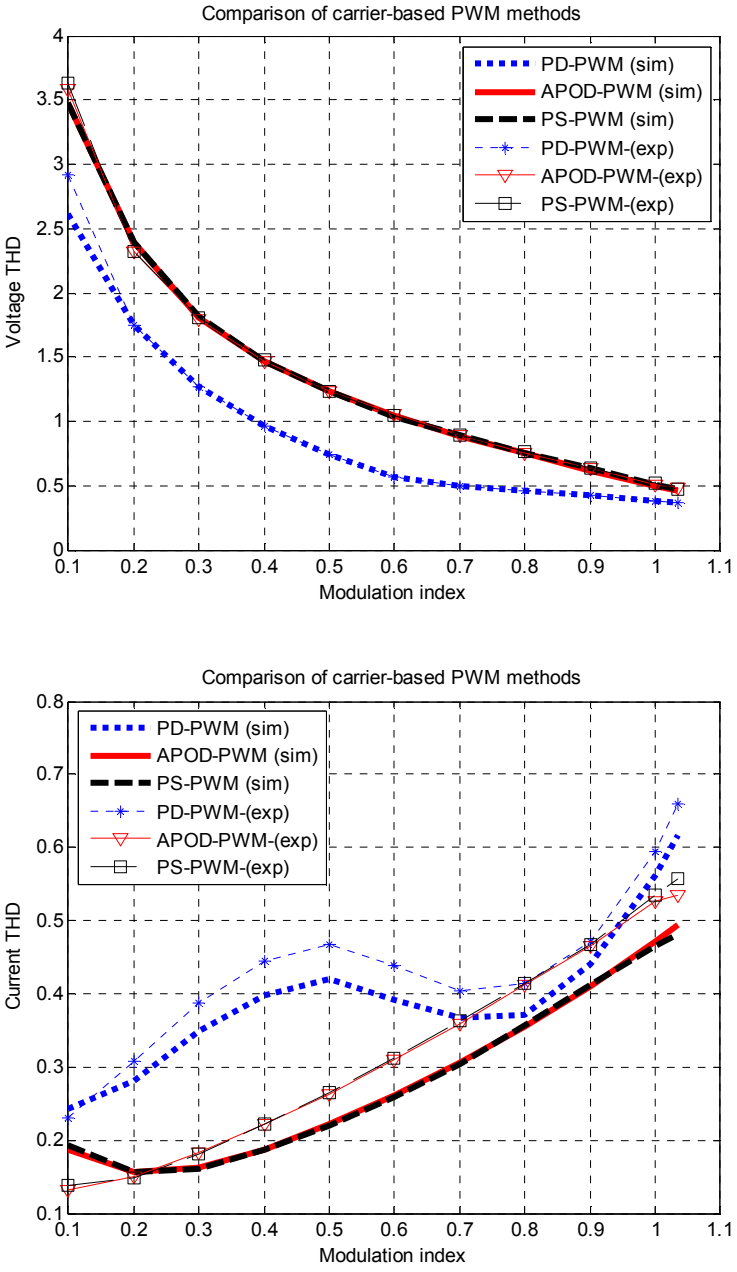

Fig. 7.18: Simulation and experimental THD plotted against the modulation index for the carrier-based PWM methods. Phase voltage (top), load current (bottom).

Examination of the current THD reveals that the PS-PWM and APOD-PWM produce almost identical profiles while the PD-PWM offers the worst performance. The current THD obtained using simulations and experiments show satisfactory but imperfect match. The trends are the same in the experimental and simulation results for each individual PWM technique. Minor discrepancies in the numerical values are again expected since the simulation was based on the constant-parameter machine model and rotor skin effect means that the rotor leakage inductance has a different value at each frequency [Dujic et al. (2011), Jones et al. (2011a), Prieto et al. (2011)]. Besides that, similar to symmetrical six-phase drive, the change of trend on the current THD curve for the PD-PWM begins at half of the maximum modulation index value as a consequence of the increase in number of phase voltage levels. For the PS-PWM and APOD-PWM, the number of phase voltage level is always the same for the whole linear modulation range, therefore no changes of trend in the current THD curves is observed.

7.8 Summary

This chapter has discussed the carrier-based PWM techniques for multilevel six-phase inverters. It is shown that an open-end multiphase winding topology with dual two-level inverter supply and equal and isolated dc-link voltages can be approached, from the PWM point of view, as a three-level single-sided supply topology. In order to achieve this, a set of gating signals is used for realising the required inverter states. These gating signals are related to the ones that are used to modulate the output of the FC VSI topology.

Since the open-end configuration, considered here, does not have capacitors that require voltage balancing, both the PS-PWM and all the LS-PWM techniques are applicable to the topology. It is shown that for a symmetrical six-phase drive, the PD-PWM method produces better phase voltage and load current THDs than the APOD-PWM and PS-PWM, where the performance of the APOD-PWM and PS-PWM is identical. The APOD-PWM yields the same output waveforms as the PS-PWM when the frequencies of the carrier signals are properly adjusted. This outcome is very similar to the three-phase and five-phase systems.

For the asymmetrical six-phase drive, the situation is very different. Despite the PD-PWM modulation producing better results in terms of voltage THD, the same does not apply to the current THD. APOD-PWM and PS-PWM offer superior performance in terms of current THD, when compared to the PD-PWM.

Unlike the outcome in the previous chapter where similar voltage and current THD performances were obtained with a symmetrical and asymmetrical six-phase machine (for each of the reference sharing algorithms URS and ERS), the situation is different for the analysed carrier-based PWM techniques. Based on the current THD results, which are responsible for the stator copper losses, one can see that the performances depend on whether a symmetrical or asymmetrical drive is used. The best performance for the asymmetrical drive is obtained by PS- and APOD-PWM, while for the symmetrical case the lowest current THD is obtained for PD-PWM.

Chapter 8

CONCLUSION

8.1 Summary and conclusion

This thesis presents development of PWM techniques for control of dual-inverter supplied six-phase machine configured in an open-end winding configuration. Both asymmetrical and symmetrical winding arrangement of six-phase machine, are covered. So far, PWM strategies for the dual-inverter fed multiphase drives have only been investigated for the drives with an odd number of phases, such as five- [Satiawan (2012)], seven-, and nine-phase [Bodo (2013)]. An investigation of a PWM strategy for an open-end winding asymmetrical six-phase drive has also been conducted, but the drive is supplied from four isolated dc supplies [Grandi et al. (2010b)].

The thesis commences with an extensive literature review in the areas relevant to the research project. The emphasis of the review is placed on the multiphase drives that have a composite number of phases, where six is the most common one. After that, PWM strategies for multiphase drives with a composite number of phases are discussed. PWM strategies for multiphase drives supplied from a two-level inverter are elaborated first, followed by PWM strategies for multiphase drives supplied by a multilevel inverter, covering both single-sided and dual-inverter supply configurations.

Next, space vector modelling for a single-sided supply configuration using two-level six-phase VSI is elaborated. This is followed by an analysis and MATLAB/Simulink simulation study of several PWM techniques applicable to the two configurations of six-phase winding arrangement. For asymmetrical winding arrangement, the discussion covers PWM techniques for both single and two-isolated neutral points configuration of asymmetrical six-phase machine. For symmetrical winding arrangement, only the case of machine with a single neutral point is considered.

Further, the thesis elaborates a space vector modelling for an open-end winding six-phase drive supplied by two two-level six-phase VSIs having equal dc bus voltages. The resulting space vectors are generated from interactions of space vectors produced by individual two-level VSI. The interactions were analysed and the relationship between the

resulting space vectors and space vectors produced by an individual two-level VSI is then established.

The developed PWM techniques for control of dual-inverter supplied six-phase drive are then discussed. The first is reference sharing algorithm. Two reference sharing algorithm are presented, where the algorithms are adopted from the schemes that were initially introduced for a five-phase drive [Satiawan (2012)]. In the first algorithm, ERS, the reference voltage is split equally between the two modulators. Unequal reference splitting is implemented in the second algorithm, URS, where the reference voltage between the two inverters is apportioned according to the total modulation index value. The modulators are operated in such a way that only one inverter is used for operation up to half of the maximum modulation index. Two-inverter operation is only used for modulation index higher than half of the maximum. For this range of modulation index, the output voltage is obtained by operating one of the inverters with its maximum modulation index value, while the rest is supplied by the other inverter. For both ERS and URS algorithms, each inverter is modulated using PWM method that was previously implemented for a single-sided supply configuration.

The same outcome is obtained from the implementation of ERS and URS algorithms towards the symmetrical and asymmetrical six-phase machines fed by dual-inverter supply. The ERS algorithm produces a number of phase voltage levels and THD that are identical to a single-sided supply of two-level six-phase inverter (which is operated with twice the dc bus voltage value). For the URS algorithm, a multilevel operation is obtained for modulation index higher than half of the maximum modulation index, except for maximum modulation index value where the drive reverts back to two-level operation. The phase voltage THD of URS algorithm is considerably lower than the voltage THD of ERS algorithm for the whole range of modulation index. For the lower half of the range, the voltage THD is lower since the effective dc bus voltage that is applied to the drive is only half of the total dc bus voltage, since only one inverter output is modulated. For the upper half of the modulation index range, a lower voltage THD is obtained since the drive operates in multilevel operation, hence producing a better quality of output voltage waveform. Meanwhile, for the load current THD, the performance of ERS and URS algorithm are almost identical particularly for operation at higher than half of maximum modulation index. For operation at lower modulation value, the performance of URS is a little bit worst than ERS since URS generates dominant switching harmonics that is slightly larger than ERS in the non-producing torque plane ((*x*-*y*) plane).

The other developed PWM control method explained in this thesis is carrier-based PWM. The techniques are adopted from the widely-known carrier-based modulation methods initially developed for the single-sided three-level inverters, where some adjustment on the carrier signals are required so that it can be implemented for the drive with dual-inverter supply structure. The techniques are level-shifted (LS-PWM) and phase-shifted modulation (PS-PWM) where the variation of LS-PWM is PD-PWM, APOD-PWM and POD-PWM. The profile of APOD-PWM and POD-PWM is identical for a three-level inverter, therefore only APOD-PWM is considered for the dual-inverter fed six-phase drives.

For operation at the same average frequency (in this project, 2 kHz), PD-PWM produce a better phase voltage THD than APOD-PWM and PS-PWM where the performance of the last two techniques are almost identical. The results that are obtained from both symmetrical and asymmetrical six-phase drives are consistent with the performance obtained from the three-phase [McGrath and Holmes (2002)] and five-phase [Bodo et al. (2013b)] systems. The load current THD for symmetrical six-phase drives shows that PD-PWM produces the best performance among the three modulation methods. For the asymmetrical six-phase drive, the situation is different. The current THD of PD-PWM is the worst since the THD of load current is highly affected by the dominant switching harmonics that is mapped into the (x-y) plane.

The developed PWM techniques are evaluated using MATLAB/Simulink simulation and verified by experimental works. In general, the results obtained from the simulations and experiments are in good agreement, especially the results that are obtained for the asymmetrical six-phase drive. Some discrepancy between the simulation and experiment result are mainly due to consequence of non-ideal behaviour of the inverter such as dead-time requirement and also semiconductor devices voltage drop. The close agreement between the simulation and experimental results shows that the developed PWM methods are successfully implemented for both symmetrical and asymmetrical configurations of dual-inverter six-phase drives.

8.2 Future works

The research presented in this thesis is confined to development of suitable PWM techniques for control of the dual-inverter fed six-phase open-end winding with equal dc link voltages. Both winding configuration of six-phase machine, symmetrical and asymmetrical, are covered and the developed PWM strategies are mainly based on the

carrier-based PWM approach. The main goal of the developed PWM strategies is minimisation of the harmonic content of the phase voltage and current (especially the low order harmonics) and in the same time trying to maximise the dc bus voltage utilisation for operation in the region of linear modulation. Future expansion from the works presented in this thesis includes:

1) Development of SVPWM techniques, that would enable operation with zero-sequence components equal to zero (on average) for an asymmetrical six-phase machine with a single neutral point supplied by a two-level inverter. As noted in Chapter 3, the zero-sequence components in the (0_+-0_-) axes become of non-zero values for a number of switching state combinations, if the machine is characterised with a single neutral point. This could be done probably by modifying SVPWM techniques that already been developed for an asymmetrical machine configured with two isolated neutral points. The modified SVPWM techniques can be used for SVPWM algorithm for drive with dual-inverter supply configuration such as the ERS and URS algorithms.
2) The SVPWM techniques that are based on complete set of switching states and voltage space vectors (as presented in Chapter 5) could also be investigated for the dual-inverter fed six-phase drives. The aim of the developed SVPWM techniques can be either quality improvement of voltage and current, common mode voltage elimination/minimisation or power sharing capability of the two inverters.
3) Development of SVPWM scheme for the dual-inverter supply with unequal dc link voltage ratio (such as 2:1 or 3:1) could also be investigated. As for three-phase system, the utilisation of unequal dc link voltage ratio leads to better performance due to the increases of phase voltage levels. Similar results for the six-phase system should be expected.
4) Development of possible PWM control that can be applied for a six-phase drive in a single-sided supply mode using a three-level inverter can also be explored. The possible PWM control that can be applied for both symmetrical and asymmetrical six phase machines with both single and two isolated neutral points can be investigated.
5) Besides that, development of post fault operation strategies for the dual-inverter supply topology which enables the drive to continue operation despite the

occurrence of fault should also been explored. Fault detection strategies for the drive topology could also be developed.

6) Finally, development of modulation technique which could extend the operation into over modulation region could also be explored.

Chapter 9

REFERENCES

Abbas, M.A., Christen, R., Jahns, T.M., (1984), Six-phase voltage source inverter driven induction motor, *IEEE Transactions on Industry Applications*, vol. IA-20, no. 5, pp. 1251-1259.

Abolhassani, M.T., (2005), A novel multiphase fault tolerant high torque density permanent magnet motor drive for traction application, *Proc. IEEE International Conference on Electric Machines and Drives IEMDC*, San Antonio, TX, pp. 728-734.

Aneesh, M.A.S., Gopinath, A., Baiju, M.R., (2009), A simple space vector PWM generation scheme for any general *n*-level inverter, *IEEE Transactions on Industrial Electronics*, vol. 56, no. 5, pp. 1649-1656.

Atkinson, G.J., Mecrow, B.C., Jack, A.G., Atkinson, D.J., Sangha, P., Benarous, M., (2005), The design of fault tolerant machines for aerospace applications, *Proc. IEEE International Conference on Electric Machines and Drives IEMDC*, San Antonio, TX, pp. 1863-1869.

Bakhshai, A.R., Joos, G., Jin, H., (1998), Space vector PWM control of a split-phase induction machine using the vector classification technique, *Proc. IEEE Applied Power Electronics Conference and Exposition APEC*, Anaheim, CA, pp. 802-808.

Benamatmane, M., McCoy, T., (1998), Development of a 19 MW PWM converter for U.S. navy surface ships, *Proc. International Conference on Electric Ship ELECSHIP*, Istanbul, Turkey, pp. 109-113.

Blasko, V., (1996), Analysis of a hybrid PWM based on modified space vector and triangle comparison methods, *Proc. IEEE Industry Applications Society Annual Meeting IAS*, San Diego, CA, pp. 947-955.

Bodo, N., Jones, M., Levi, E., (2011a), Multi-level space-vector PWM algorithm for seven-phase open-end winding drives, *Proc. IEEE International Symposium on Industrial Electronics ISIE*, Gdansk, Poland, pp. 1881-1886.

Bodo, N., Levi, E., Jones, M., (2011b), Carrier-based modulation techniques for five-phase open-end winding drive topology, *Proc. IEEE Industrial Electronics Society Annual Meeting IECON* Melbourne, Australia, pp. 3656-3661.

Bodo, N., Dordevic, O., Jones, M., Levi, E., (2012a), A comparison of three-level single-sided and dual-inverter supply for a five-phase drive, *Proc. EPE Power Electronics and Motion Control Conference PEMC*, Novi Sad, Serbia, pp. LS1c.2-1-LS1c.2-6.

Bodo, N., Jones, M., Levi, E., (2012b), PWM techniques for an open-end winding five-phase drive with a single dc source supply, *Proc. IEEE Industrial Electronics Society Annual Meeting IECON*, Montreal, Canada, pp. 3641-3646.

Bodo, N. (2013) PWM stratergies for open-end winding multiphase drives. *PhD thesis.* Liverpool John Moores University, Liverpool, UK.

Bodo, N., Jones, M., Levi, E., (2013a), A PWM method for seven- and nine-phase open-end winding motor drives, *Mathematics and Computers in Simulation*, vol. 90, no. 0, pp. 15-27.

Bodo, N., Levi, E., Jones, M., (2013b), Investigation of carrier-based PWM techniques for a five-phase open-end winding drive topology, *IEEE Transactions on Industrial Electronics*, vol. 60, no. 5, pp. 2054-2065.

Bojoi, R., Tenconi, A., Profumo, F., Griva, G., Martinello, D., (2002), Complete analysis and comparative study of digital modulation techniques for dual three-phase AC motor drives, *Proc. IEEE Annual Power Electronics Specialists Conference PESC*, Queensland, Australia, pp. 851-857.

Bojoi, R., Tenconi, A., Farina, F., Profumo, F., (2005), Dual-source fed multi-phase induction motor drive for fuel cell vehicles: topology and control, *Proc. IEEE Power Electronics Specialists Conference PESC*, Recife, Brazil, pp. 2676-2683.

Casadei, D., Grandi, G., Lega, A., Rossi, C., (2008), Multilevel operation and input power balancing for a dual two-level inverter with insulated dc sources, *IEEE Transactions on Industry Applications*, vol. 44, no. 6, pp. 1815-1824.

Casadei, D., Mengoni, M., Tani, A., Serra, G., Zarri, L., (2010), High torque-density seven-phase induction motor drives for electric vehicle applications, *Proc. IEEE Vehicle Power and Propulsion Conference VPPC*, Lille, France, pp. CD-ROM.

Celanovic, N., Boroyevich, D., (2001), A fast space-vector modulation algorithm for multilevel three-phase converters, *IEEE Transactions on Industry Applications*, vol. 37, no. 2, pp. 637-641.

Che, H.S., Duran, M.J., Levi, E., Jones, M., Hew, W.P., Rahim, N.A., (2013), Post-fault operation of an asymmetrical six-phase induction machine with single and two isolated neutral points, *Proc. IEEE Energy Conversion Congress and exposition ECCE*, Denver, CO, pp. (accepted).

Correa, M.B.R., Jacobina, C.B., da Silva, C.R., Lima, A.M.N., da Silva, E.R.C., (2003a), Six-phase AC drive system with reduced common-mode voltage, *Proc. IEEE International Electric Machines and Drives Conference IEMDC*, Madison, WI, pp. 1852-1858.

Correa, M.B.R., Jacobina, C.B., da Silva, C.R., Lima, A.M.N., da Silva, E.R.C., (2003b), Vector and scalar modulation for six-phase voltage source inverters, *Proc. IEEE Power Electronics Specialist Conference PESC*, Acapulco, Mexico, pp. 562-567.

Corzine, K.A., Sudhoff, S.D., Whitcomb, C.A., (1999), Performance characteristics of a cascaded two-level converter, *IEEE Transactions on Energy Conversion*, vol. 14, no. 3, pp. 433-439.

Corzine, K.A., Baker, J.R., (2002), Multilevel voltage-source duty-cycle modulation: analysis and implementation, *IEEE Transactions on Industrial Electronics*, vol. 49, no. 5, pp. 1009-1016.

Corzine, K.A., Wielebski, M.W., Peng, F., Wang, J., (2003), Control of cascaded multi-level inverters, *Proc. IEEE International Electric Machines and Drives Conference IEMDC*, Madison, WI, pp. 1549-1555.

Dixon, J., Moran, L., Rodriguez, J., Domke, R., (2005), Reactive power compensation technologies: state-of-the-art review, *Proceedings of the IEEE*, vol. 93, no. 12, pp. 2144-2164.

Dong, L., Jia, Q.Y., Jin, H., Hai-bo, J., Min, K., (2008a), Realization of a SPWM inverter for multi-phase induction motor drives, *Proc. International Conference on Electrical Machines and Systems ICEMS*, Wuhan, China, pp. 1287-1290.

Dong, T., Lin, C., Lijun, H., Juntao, P., (2008b), Modeling and simulation of dual-three-phase induction machine with two opened phases, *Proc. IEEE International Conference on Industrial Technology*, Chengdu, China, pp. 1-5.

Dordevic, O. (2013) PWM stratergies for multilevel multiphase ac drives. *PhD thesis.* Liverpool John Moores University, Liverpool, UK.

Dujic, D., Iqbal, A., Levi, E., (2007a), A space vector PWM technique for symmetrical six-phase voltage source inverters, *European Power Electronics Journal*, vol. 17, no. 1, pp. 24-32.

Dujic, D., Jones, M., Levi, E., (2007b), Space vector PWM for nine-phase VSI with sinusoidal output voltage generation: analysis and implementation, *Proc. IEEE Industrial Electronics Society Annual Meeting IECON*, Taipei, Taiwan, pp. 1524-1529.

Dujic, D., Levi, E., Jones, M., (2010), Dc bus utilisation in multiphase VSI supplied drives with a composite stator phase number, *Proc. IEEE International Conference on Industrial Technology ICIT* Viña del Mar, Chile, pp. 1495-1500.

Dujic, D., Jones, M., Levi, E., Prieto, J., Barrero, F., (2011), Switching ripple characteristics of space vector PWM schemes for five-phase two-level voltage source inverters-part 1: flux harmonic distortion factors, *IEEE Transactions on Industrial Electronics*, vol. 58, no. 7, pp. 2789-2798.

Fangbin, C., Huan, Y., Rongxiang, Z., Minglei, Z., (2009), A PWM strategy for six-phase dual stator induction motor fed by two identical voltage source inverters, *Proc. International Conference on Electrical Machines and Systems ICEMS*, Tokyo, Japan, pp. 1-4.

Franquelo, L.G., Prats, M.A.M., Portillo, R.C., Galvan, J.I.L., Perales, M.A., Carrasco, J.M., Diez, E.G., Jimenez, J.L.M., (2006), Three-dimensional space-vector modulation algorithm for four-leg multilevel converters using abc coordinates, *IEEE Transactions on Industrial Electronics*, vol. 53, no. 2, pp. 458-466.

Franquelo, L.G., Rodriguez, J., Leon, J.I., Kouro, S., Portillo, R., Prats, M.A.M., (2008), The age of multilevel converters arrives, *IEEE Industrial Electronics Magazine*, vol. 2, no. 2, pp. 28-39.

Franquelo, L.G., Leon, J.I., Dominguez, E., (2010), Recent advances in high-power industrial applications, *Proc. IEEE International Symposium on Industrial Electronics ISIE*, Bari, Italy, pp. 5-10.

Gao, L., Fletcher, J.E., (2010), A space vector switching strategy for three-level five-phase inverter drives, *IEEE Transactions on Industrial Electronics*, vol. 57, no. 7, pp. 2332-2343.

Gopakumar, K., Sathiakumar, S., Biswas, S.K., Vithayathil, J., (1984), Modified current source inverter fed induction motor drive with reduced torque pulsations, *IEE Proceedings Electric Power Applications*, vol. 131, no. 4, pp. 159-164.

Gopakumar, K., Ranganthan, V.T., Bhat, S.R., (1993), Split-phase induction motor operation from PWM voltage source inverter, *IEEE Transactions on Industry Applications*, vol. 29, no. 5, pp. 927-932.

Grandi, G., Serra, G., Tani, A., (2006), Space vector modulation of a seven-phase voltage source inverter, *Proc. International Symposium on Power Electronics, Electrical Drives, Automation and Motion SPEEDAM*, Taonnina, Italy, pp. 1149-1156.

Grandi, G., Serra, G., Tani, A., (2007a), Space vector modulation of nine-phase voltage source inverters based on three-phase decomposition, *Proc. European Conference on Power Electronics and Applications*, Aalborg, Denmark, pp. CD-ROM.

Grandi, G., Serra, G., Tani, A., (2007b), Space vector modulation of a nine-phase voltage source inverter, *Proc. IEEE International Symposium on Industrial Electronics ISIE*, Vigo, Spain, pp. 431-436.

Grandi, G., Serra, G., Tani, A., (2008), Space vector modulation of a six-phase VSI based on three-phase decomposition, *Proc. International Symposium on Power Electronics, Electrical Drives, Automation and Motion SPEEDAM*, Ischia, Italy, pp. 674-679.

Grandi, G., Sanjeevikumar, P., Ostojic, D., Rossi, C., (2010a), Quad-inverter configuration for multi-phase multi-level AC motor drives, *Proc. IEEE Computational*

Technologies in Electrical and Electronics Engineering SIBIRCON, Irkutsk, Russia, pp. 631-638.

Grandi, G., Tani, A., Sanjeevikumar, P., Ostojic, D., (2010b), Multi-phase multi-level AC motor drive based on four three-phase two-level inverters, *Proc. International Symposium on Power Electronics, Electrical Drives, Automation and Motion SPEEDAM*, Pisa, Italy, pp. 1768-1775.

Grandi, G., Gritli, Y., Filippetti, F., Rossi, C., (2011), Fault-tolerant operating analysis of a quad-inverter multiphase multilevel AC motor drive, *Proc. IEEE Symposium on Diagnostics for Electric Machines, Power Electronics & Drives SDEMPED*, Bologna, Italy, pp. 126-132.

Grandi, G., Sanjeevikumar, P., Gritli, Y., Filippetti, F., (2012a), Fault-tolerant control strategies for quad inverter induction motor drives with one failed inverter, *Proc. International Conference on Electrical Machines ICEM*, Marseille, France, pp. 959-966.

Grandi, G., Sanjeevikumar, P., Gritli, Y., Filippetti, F., (2012b), Experimental investigation of fault-tolerant control strategies for quad-inverter converters, *Proc. Electrical Systems for Aircraft, Railway and Ship Propulsion ESARS*, Bologna, Italy, pp. 1-8.

Gritter, D., Kalsi, S.S., Henderson, N., (2005), Variable speed electric drive options for electric ships, *Proc. IEEE Electric Ship Technologies Symposium*, Philadelphia, PA, pp. 347-354.

Gupta, A.K., Khambadkone, A.M., (2007), A general space vector PWM algorithm for multilevel inverters, including operation in overmodulation range, *IEEE Transactions on Power Electronics*, vol. 22, no. 2, pp. 517-526.

Hadiouche, D., Baghli, L., Rezzoug, A., (2006), Space-vector PWM techniques for dual three-phase AC machine: analysis, performance evaluation, and DSP implementation, *IEEE Transactions on Industry Applications*, vol. 42, no. 4, pp. 1112-1122.

Houldsworth, J.A., Grant, D.A., (1984), The use of harmonic distortion to increase the output voltage of a three-phase PWM inverter, *IEEE Transactions on Industry Applications*, vol. IA-20, no. 5, pp. 1224-1228.

Iqbal, A., Levi, E., Jones, M., Vukosavic, S.N., (2006), Generalised sinusoidal PWM withharmonic injection for multi-phase VSIs, *Proc. IEEE Power Electronics Specialists Conference PESC*, Jeju, Korea, pp. 2871-2877.

Iqbal, A., Moinuddin, S., (2009), Comprehensive relationship between carrier-based PWM and space vector PWM in a five-phase VSI, *IEEE Transactions on Power Electronics*, vol. 24, no. 10, pp. 2379-2390.

Jacobina, C.B., Miranda, R.S., Correa, M.B.D.R., Lima, A.M.N., (2004), Disturbance-free operation of a six-phase ac motor drive system, *Proc. IEEE Power Electronics Specialists Conference PESC*, Aachen, Germany, pp. 925-931 Vol.2.

Jen-Ren, F., Lipo, T.A., (1994), Disturbance-free operation of a multiphase current-regulated motor drive with an opened phase, *IEEE Transactions on Industry Applications*, vol. 30, no. 5, pp. 1267-1274.

Jones, M., Vukosavic, S.N., Dujic, D., Levi, E., (2009), A synchronous current control scheme for multiphase induction motor drives, *IEEE Transactions on Energy Conversion*, vol. 24, no. 4, pp. 860-868.

Jones, M., Satiawan, W., Levi, E., (2010), A five-phase multilevel space-vector PWM algorithm for a dual-inverter supplied drive, *Proc. IEEE Industrial Electronics Society Annual Meeting IECON*, Glendale, AZ, pp. 2461-2466.

Jones, M., Dujic, D., Levi, E., Prieto, J., Barrero, F., (2011a), Switching ripple characteristics of space vector PWM schemes for five-phase two-level voltage source inverters - part 2: current ripple, *IEEE Transactions on Industrial Electronics*, vol. 58, no. 7, pp. 2799-2808.

Jones, M., Satiawan, I.N., Levi, E., (2011b), A three-level five-phase space-vector modulation algorithm based on the decomposition method, *Proc. IEEE International Electric Machines & Drives Conference IEMDC*, Niagara Falls, ON pp. 1219-1224.

Jones, M., Satiawan, I.N.W., Bodo, N., Levi, E., (2012), A dual five-phase space-vector modulation algorithm based on the decomposition method, *IEEE Transactions on Industry Applications*, vol. 48, no. 6, pp. 2110-2120.

Jones, M., Patkar, F., Levi, E., (2013), Carrier-based pulse-width modulation techniques for asymmetrical six-phase open-end winding drives, *IET Electric Power Applications*, vol. 7, no. 6.

Kawabata, T., Kawabata, Y., Nishiyama, K., (1996), New configuration of high-power inverter drives, *Proc. IEEE International Symposium on Industrial Electronics ISIE*, Warsaw, Poland, pp. 850-855.

Kawabata, Y., Nasu, M., Nomoto, T., Ejiogu, E.C., Kawabata, T., (2002), High-efficiency and low acoustic noise drive system using open-winding AC motor and two space-vector-modulated inverters, *IEEE Transactions on Industrial Electronics*, vol. 49, no. 4, pp. 783-789.

Kelly, J.W., Strangas, E.G., Miller, J.M., (2003), Multiphase space vector pulse width modulation, *IEEE Transactions on Energy Conversion*, vol. 18, no. 2, pp. 259-264.

Khan, M.A., Ahmed, S.K.M., Iqbal, A., Rub, H.A., Moinoddin, S.K., (2009), Discontinuous space vector PWM strategies for a seven-phase voltage source inverter, *Proc. IEEE Industrial Electronics Society Annual Meeting IECON*, Porto, Portugal, pp. 397-402.

Kianinezhad, R., Nahid, B., Betin, F., Capolino, G.A., (2005), Multi-vector SVM: a new approach to space vector modulation control for six-phase induction machines, *Proc. IEEE Industrial Electronics Society Annual Meeting IECON*, Raleigh, NC, pp. 1359-1364.

Kianinezhad, R., Nahid-Mobarakeh, B., Baghli, L., Betin, F., Capolino, G.A., (2008), Modeling and control of six-phase symmetrical induction machine under fault conditiondue to open phases, *IEEE Transactions on Industrial Electronics*, vol. 55, no. 5, pp. 1966-1977.

Kim, J.-S., Sul, S.-K., (1995), A novel voltage modulation technique of the space vector PWM, *Proc. International Power Electronics Conference IPEC*, Yokohama, Japan, pp. 742-747.

Klingshirn, E.A., (1983a), High phase order induction motors - part II - experimental results, *IEEE Transactions on Power Apparatus and Systems*, vol. PAS-102, no. 1, pp. 54-59.

Klingshirn, E.A., (1983b), High phase order induction motors - part I - description and theoretical considerations, *IEEE Transactions on Power Apparatus and Systems*, vol. PAS-102, no. 1, pp. 47-53.

Klug, R.D., Klaassen, N., (2005), High power medium voltage drives - innovations, portfolio, trends, *Proc. European Conference on Power Electronics and Applications EPE*, Dresden, Germany, pp. CD-ROM.

Lakshminarayanan, S., Mondal, G., Gopakumar, K., (2007), Multilevel inverter with 18-sided polygonal voltage space vector for an open-end winding induction motor drive, *Proc. The IEEE International Conference on Computer as a Tool EUROCON*, Warsaw, Poland, pp. 1810-1817.

Levi, E., Bojoi, R., Profumo, F., Toliyat, H.A., Williamson, S., (2007), Multiphase induction motor drives - a technology status review, *IET Electric Power Applications*, vol. 1, no. 4, pp. 489-516.

Levi, E., (2008), Multiphase electric machines for variable-speed applications, *IEEE Transactions on Industrial Electronics*, vol. 55, no. 5, pp. 1893-1909.

Levi, E., Jones, M., Satiawan, W., (2010), A multiphase dual-inverter supplied drive structure for electric and hybrid electric vehicles, *Proc. IEEE Vehicle Power and Propulsion Conference VPPC*, Lille, France, pp. CD-ROM paper 95-45630.

Levi, E., Satiawan, I.N.W., Bodo, N., Jones, M., (2012), A space-vector modulation scheme for multilevel open-end winding five-phase drives, *IEEE Transactions on Energy Conversion*, vol. 27, no. 1, pp. 1-10.

Levi, E., Bodo, N., Dordevic, O., Jones, M., (2013), Recent advances in power electronic converter control for multiphase drive systems, *Proc. IEEE Workshop on Electrical Machines Design Control and Diagnosis WEMDCD*, Paris, France, pp. 158-167.

Lopez, O., Alvarez, J., Doval-Gandoy, J., Freijedo, F.D., (2008), Multilevel multiphase space vector PWM algorithm, *IEEE Transactions on Industrial Electronics*, vol. 55, no. 5, pp. 1933-1942.

Lopez, O., Alvarez, J., Doval-Gandoy, J., Freijedo, F.D., (2009), Multilevel multiphase space vector PWM algorithm with switching state redundancy, *IEEE Transactions on Industrial Electronics*, vol. 56, no. 3, pp. 792-804.

Lu, S., Corzine, K., (2005), Multilevel multi-phase propulsion drives, *Proc. IEEE Electric Ship Technologies Symposium*, Philadelphia, PA, pp. 363-370.

Marouani, K., Baghli, L., Hadiouche, D., Kheloui, A., Rezzoug, A., (2008), A new PWM strategy based on a 24-sector vector space decomposition for a six-phase VSI-fed dual stator induction motor, *IEEE Transactions on Industrial Electronics*, vol. 55, no. 5, pp. 1910-1920.

McGrath, B.P., Holmes, D.G., (2002), Multicarrier PWM strategies for multilevel inverters, *IEEE Transactions on Industrial Electronics*, vol. 49, no. 4, pp. 858-867.

McSharry, J.P., Hamer, P.S., Morrison, D., Nessa, J., Rigsby, J.G., (1998), Design, fabrication, back-to-back test of 14200-hp two-pole cylindrical-rotor synchronous motor for ASD application, *IEEE Transactions on Industry Applications*, vol. 34, no. 3, pp. 526-533.

Meynard, T.A., Foch, H., Thomas, P., Courault, J., Jakob, R., Nahrstaedt, M., (2002), Multicell converters: basic concepts and industry applications, *IEEE Transactions on Industrial Electronics*, vol. 49, no. 5, pp. 955-964.

Mohapatra, K.K., Gopakumar, K., Somasekhar, V.T., Umanand, L., (2002), A novel modulation scheme for a six phase induction motor with open-end windings, *Proc. IEEE Industrial Electronics Society Annual Meeting IECON*, Seville, Spain, pp. 810-815.

Mohapatra, K.K., Gopakumar, K., (2006), A novel split phase induction motor drive without harmonic filters and with linear voltage control for the full modulation range, *European Power Electronics Journal*, vol. 16, no. 4, pp. 20-28.

Nabae, A., Takahashi, I., Akagi, H., (1981), A new neutral-point-clamped PWM inverter, *IEEE Transactions on Industry Applications*, vol. IA-17, no. 5, pp. 518-523.

Naik, R.L., Udaya, K.R.Y., (2005), A novel technique for control of cascaded multilevel inverter for photovoltaic power supplies, *Proc. European Conference on Power Electronics and Applications EPE*, Dresden, Germany, pp. CD-ROM.

Nelson, R.H., Krause, P.C., (1974), Induction machine analysis for arbitrary displacement between multiple winding sets, *IEEE Transactions on Power Apparatus and Systems*, vol. PAS-93, no. 3, pp. 841-848.

Neugebauer, T.C., Perreault, D.J., Lang, J.H., Livermore, C., (2004), A six-phase multilevel inverter for MEMS electrostatic induction micromotors, *IEEE Transactions on Circuits and Systems II: Express Briefs*, vol. 51, no. 2, pp. 49-56.

Oleschuk, V., Blaabjerg, F., (2002), Three-level inverters with common-mode voltage cancellation based on synchronous pulsewidth modulation, *Proc. IEEE Annual Power Electronics Specialists Conference PESC*, Queensland, Australia, pp. 863-868.

Oleschuk, V., Griva, G., (2010), Common-mode voltage cancellation in dual three-phase systems with synchronized PWM, *Proc. IEEE International Symposium on Industrial Electronics ISIE*, Bari, Italy, pp. 706-711.

Oriti, G., Julian, L., Lipo, T.A., (1997), An inverter/motor drive with common mode voltage elimination, *Proc. IEEE Industry Applications Conference IAS* New Orleans, LA, pp. 587-592.

Oudjebour, Z., Berkouk, E.M., Sami, N., Belgasmi, S., Arezki, S., Messaif, I., (2004), Indirect space vector control of a double star induction machine fed by two five-levels NPC VSI, *Proc. International Conference on Electrical Machines ICEM*, Krakow, Poland, pp. CD-ROM paper no. 155.

Oudjebour, Z., Berkouk, E.M., (2005), Study of different triangulo – sinusoidal strategies of two five – levels of cells overlapped VSI. Application to double star induction machine drive, *Proc. WSEAS International Conference on Simulation, Modeling and Optimization*, Corfu, Greece, pp. 136-139.

Parsa, L., (2005), On advantages of multi-phase machines, *Proc. IEEE Industrial Electronics Society Annual Meeting IECON*, Raleigh, NC, pp. 1574-1579.

Parsa, L., Goodarzi, A., Toliyat, H.A., (2005), Five-phase interior permanent magnet motor for hybrid electric vehicle application, *Proc. IEEE Conference Vehicle Power and Propulsion VPPC*, Chicago, IL, pp. 631-637.

Parsa, L., Toliyat, H.A., (2005), Five-phase permanent magnet motor drives for ship propulsion applications, *Proc. IEEE Electric Ship Technologies Symposium*, Philadelphia, PA, pp. 371-378.

Patkar, F., Levi, E., Jones, M., (2012), A six-phase multilevel space vector PWM algorithm for a dual-inverter supplied drive, *Proc. IET International Conference on Power Electronics, Machines and Drives PEMD*, Bristol, UK, pp. 1-5.

Patkar, F., Jones, M., (2013), Performance of an asymmetrical six-phase induction machine in single-and two-neutral point configurations, *Proc. Universities' Power Engineering Conference UPEC*, Dublin, Ireland,. (accepted).

Prats, M.M., Carrasco, J.M., Franquelo, L.G., (2002), Effective space-vector modulation algorithm for multilevel converters, *Proc. IEEE Industrial Electronics Society Annual Meeting IECON*, Sevilla, Spain, pp. 3129-3133.

Prats, M.M., Franquelo, L.G., Portillo, R., Leon, J.I., Galvan, E., Carrasco, J.M., (2003), A 3-D space vector modulation generalized algorithm for multilevel converters, *IEEE Power Electronics Letters*, vol. 1, no. 4, pp. 110-114.

Prieto, J., Barrero, F., Jones, M., Levi, E., (2010), A modified continuous PWM technique for asymmetrical six-phase induction machines, *Proc. IEEE International Conference on Industrial Technology ICIT*, Viña del Mar, Chile, pp. 1489-1494.

Prieto, J., Jones, M., Barrero, F., Levi, E., Toral, S., (2011), Comparative analysis of discontinuous and continuous PWM techniques in VSI-fed five-phase induction motor, *IEEE Transactions on Industrial Electronics*, vol. 58, no. 12, pp. 5324-5335.

Rodriguez, J., Franquelo, L.G., Kouro, S., Leon, J.I., Portillo, R.C., Prats, M.A.M., Perez, M.A., (2009), Multilevel converters: an enabling technology for high-power applications, *Proceedings of the IEEE*, vol. 97, no. 11, pp. 1786-1817.

Satiawan, W. (2012) Pulse width modulation control of dual-inverter supply for five-phase variable-speed drives. *PhD Thesis.* Liverpool John Moores University, Liverpool, UK.

Shan, L., Huihui, X., Hongyan, C., (2005), The research of SVPWM control technique of double three-phase induction machine, *Proc. International Conference on Electrical Machines and Systems ICEMS*, Nanjing, China, pp. 109-114.

Shiny, G., Baiju, M.R., (2010), A fractal based space vector PWM scheme for general n-level inverters, *Proc. International Power Electronics Conference IPEC*, Sapporo, Japan, pp. 847-854.

Shivakumar, E.G., Gopakumar, K., Sinha, S.K., Pittet, A., Ranganathan, V.T., (2001a), Space vector PWM control of dual inverter fed open-end winding induction motor drive, *Proc. IEEE Annual Applied Power Electronics Conference and Exposition APEC* Anaheim, CA, pp. 399-405.

Shivakumar, E.G., Somasekhar, V.T., Mohapatra, K.K., Gopakumar, K., Umanand, L., Sinha, S.K., (2001b), A multi level space phasor based PWM strategy for an open-end winding induction motor drive using two inverters with different DC link voltages, *Proc. IEEE International Conference on Power Electronics and Drive Systems PEDS*, Indonesia, pp. 169-175.

Shuai, L., Corzine, K., (2005), Multilevel multi-phase propulsion drives, *Proc. IEEE Electric Ship Technologies Symposium*, Philadephia, PA, pp. 363-370.

Shuai, L., Corzine, K.A., Fikse, T.H., (2005), Distributed control of hybrid motor drives, *Proc. IEEE International Conference on Electric Machines and Drives IEMDC*, San Antonio, TX, pp. 1319-1326.

Shuai, L., Corzine, K.A., (2007), Advanced control and analysis of cascaded multilevel converters based on P-Q compensation, *IEEE Transactions on Power Electronics*, vol. 22, no. 4, pp. 1242-1252.

Singh, G.K., Pant, V., Singh, Y.P., (2003), Voltage source inverter driven multi-phase induction machine, *Computers & Electrical Engineering*, vol. 29, no. 8, pp. 813-834.

Song, Q., Zhang, X., Yu, F., Zhang, C., (2006), Research on PWM techniques of five-phase three-level inverter, *Proc. International Symposium on Power Electronics, Electrical Drives, Automation and Motion SPEEDAM*, Taormina, Italy, pp. 561-565.

Steiner, M., Deplazes, R., Stemmler, H., (2000), A new transformerless topology for AC-fed traction vehicles using multi-star induction motors, *European Power Electronics Journal*, vol. 10, no. 3-4, pp. 45-53.

Stemmler, H., Guggenbach, P., (1993), Configurations of high-power voltage source inverter drives, *Proc. European Conference on Power Electronics and Applications EPE*, Brighton, UK, pp. 7-14.

van der Broeck, H.W., Skudelny, H.C., Stanke, G.V., (1988), Analysis and realization of a pulsewidth modulator based on voltage space vectors, *IEEE Transactions on Industry Applications*, vol. 24, no. 1, pp. 142-150.

von Jauanne, A., Haoran, Z., (1999), A dual-bridge inverter approach to eliminating common-mode voltages and bearing and leakage currents, *IEEE Transactions on Power Electronics*, vol. 14, no. 1, pp. 43-48.

Ward, E.E., Härer, H., (1969), Preliminary investigation of an invertor-fed 5-phase induction motor, *Proceedings of the Institution of Electrical Engineers*, vol. 116, no. 6, pp. 980-984.

Wu, B., (2006), *High-power converters and AC drives,* John Wiley & Sons, Hoboken, New Jersey.

Xiaomin, K., Corzine, K.A., Wielebski, M.W., (2006), Overdistention operation of cascaded multilevel inverters, *IEEE Transactions on Industry Applications*, vol. 42, no. 3, pp. 817-824.

Yanhui, H., Yue, W., Jinlong, W., Yupeng, F., Jinjun, L., (2010), A comparative study of space vector PWM strategy for dual three-phase permanent-magnet synchronous motor drives, *Proc. IEEE Annual Applied Power Electronics Conference and Exposition APEC*, Palm Springs, CA, pp. 915-919.

Yao, W., Lu, Z., Fei, W., Qiao, Z., Gu, Y., Mingfang, Z., (2004), Three-level SVPWM method based on two-level PWM cell in DSP, *Proc. IEEE Annual Applied Power Electronics Conference and Exposition APEC*, Anaheim, CA, pp. 1720-1724.

Yao, W., Hu, H., Lu, Z., Xu, H., (2006), Research on three-level inverter of six-phase synchronous motor, *Proc. IEEE International Power Electronics and Motion Control Conference IPEMC*, Shanghai, China, pp. 1-5.

Yazdani, D., Khajehoddin, S.A., Bakhshai, A., Joos, G., (2007), A generalized space vector classification technique for six-phase inverters, *Proc. IEEE Power Electronics Specialists Conference PESC*, Orlando, FL, pp. 2050-2054.

Youlong, W., Wen, X., Shan, X., (2007), Space vector PWM control of multi-phase induction motor drives based on orthogonal vector spaces concept, *Proc. IEEE Power Electronics Specialists Conference PESC* Orlando, FL, pp. 553-558.

Zdenek, D., (1986), 25 MW high-speed electric drive with thyristor speed control, *Czechoslovak Heavy Industry* vol. 1, no. 4, pp. 5-9.

Zhao, Y., Lipo, T.A., (1995), Space vector PWM control of dual three-phase induction machine using vector space decomposition, *IEEE Transactions on Industry Applications*, vol. 31, no. 5, pp. 1100-1109.

Zhao, Y., Lipo, T.A., (1996a), Modeling and control of a multi-phase induction machine with structural unbalance - Part II. Field-oriented control and experimental verification, *IEEE Transactions on Energy Conversion*, vol. 11, no. 3, pp. 578-584.

Zhao, Y., Lipo, T.A., (1996b), Modeling and control of a multi-phase induction machine with structural unbalance - Part 1. Machine modelling and multi-dimensional current regulation, *IEEE Transactions on Energy Conversion*, vol. 11, no. 3, pp. 570-577.

Zhong, D., Tolbert, L.M., Chiasson, J.N., Ozpineci, B., Hui, L., Huang, A.Q., (2006), Hybrid cascaded H-bridges multilevel motor mrive control for electric vehicles, *Proc. IEEE Power Electronics Specialists Conference PESC*, Jeju, Korea, pp. 1-6.

APPENDIX 1

SIMULATION AND EXPERIMENTAL SET-UP

This appendix explains in more detail about the set-up of the simulations and experiments that have been conducted in order to investigate the performance of the developed PWM techniques for control of dual-inverter supplied six-phase drives

The simulations and experiments were carried out with both symmetrical and asymmetrical six phase induction machines. The parameters of the machine are as presented in Table 3.3 (asymmetrical six-phase machine) and Table 4.3 (symmetrical six-phase machine). These parameters were estimated from the actual machine used in the experiments. In the simulation, the machines are modelled in phase variable form under the assumption that the windings are identical and provide sinusoidal magneto-motive force spatial distribution.

The performance of the developed modulation techniques are analysed and verified by simulations and experiments that are performed over the entire linear modulation range spanning from $M = 0.1$ to $M = M_{max}$ (with 0.1 increments), using V/f = constant control without voltage boost. For $M = 1$, the ratio is 300V/50Hz for the asymmetrical six-phase machine and for the symmetrical six-phase drive, the ratio is 200V/50Hz. The machines were run in no-load operation.

The simulations were conducted using MATLAB/Simulink, where the three-phase diode rectifiers and inverters are modelled using SimPowerSystems toolbox. For the implementation of dual-inverter supply topology, the two inverters are supplied from dc buses that are obtained from two isolated three-phase voltage sources. The isolated voltage sources are to ensure that the flow of zero sequence currents is avoided (even though the common mode voltage is of non-zero value). For the asymmetrical six-phase drive, the two voltage sources provide 106 V rms line-to-line to have approximately 150 V in the dc buses of the two inverters. The symmetrical six-phase drive was supplied by 70.7 V rms line-to-line in order to provide 100 V dc bus. The 150 V and 100V dc buses of each inverter are equivalent to 300V and 200 V dc buses respectively for a three-level single-sided inverter.

In both simulations and experiments, the gating signals are generated only for the upper switches (in particular, IGBTs). The signals for the lower switches are obtained by inverting the signals of the upper switches. A dead time of 6 μs (which corresponds to the dead-time setting in the experimental setup) is included in the inverter model. The forward voltage drops of the IGBTs and reverse diodes are set to 1.2 V and 1.6 V, respectively. Upon investigation, it has been found that the setting of dead-time and voltage drops influence the magnitudes of the low order harmonics.

The experimental set-up of the dual-inverter supplied six-phase drives with two isolated dc sources is shown in Fig. A.1. The machines that have been used in the experiment set-up are presented in Fig. A.2 (asymmetrical six-phase) and Fig. A.3 (symmetrical six-phase). The machines are obtained by rewinding two three-phase induction machines.

The experimental rig utilises two units of custom-built two-level multiphase VSIs to supply the six-phase induction machine. Each inverter has eight legs and utilise Infineon's FS50R12KE3 IGBTs. For this research only six legs are used. The inverters are operated using modulating signals that are developed in MATLAB/Simulink and delivered to the gates of the multiphase inverters via dSPACE module. The modulation algorithms have been implemented using a dSPACE DS1006 processor board. The modulating signals are then delivered to the inverters via the dSPACE DS5101 Digital Waveform Output Board.

The dc bus voltages are obtained from ac supply that is delivered through two isolating transformers and two variacs which are used to adjust the voltage to the required level. The dc bus voltages are obtained by rectifying the ac supply using the diode bridge rectifiers that is internally build in the VSI unit. The inverter dead time is 6μs and the machine is controlled in the same manner as in the simulations (open-loop V/f = constant mode without voltage boost).

The voltage and current waveforms are captured using a four channel Tektronix MSO 2014 Mixed Signal Oscilloscope. The oscilloscope utilises a Tektronix P5205A High Voltage Differential Probe for measuring the voltage while a Tektronix TCP0030 Current Probe is utilised for measuring the current. The captured voltage and current waveforms are measured in 125000 points and then the data is post-processed using MATLAB program for calculation and plotting of the FFT.

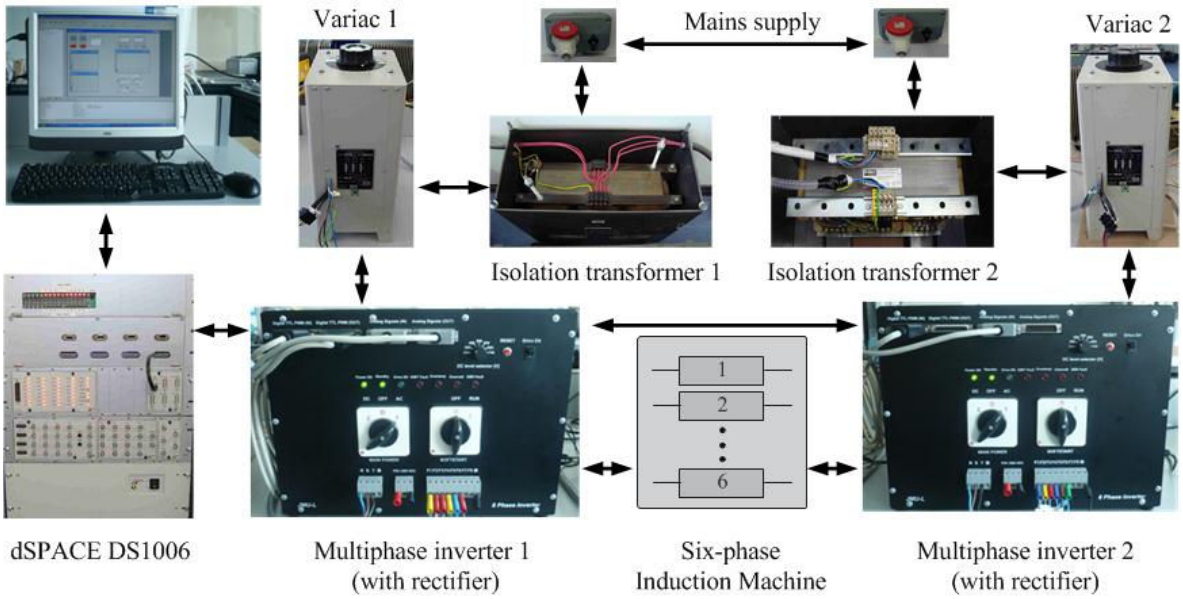

Fig. A.1: Experimental rig of dual-inverter supplied six-phase drives with two isolated dc sources.

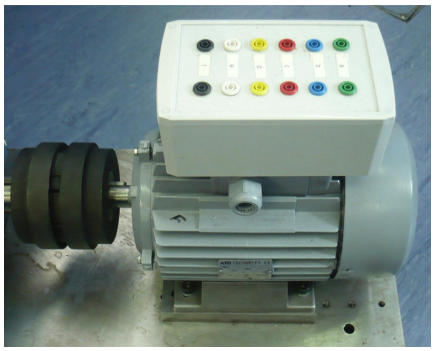

Fig. A.2: Asymmetrical six-phase induction machine.

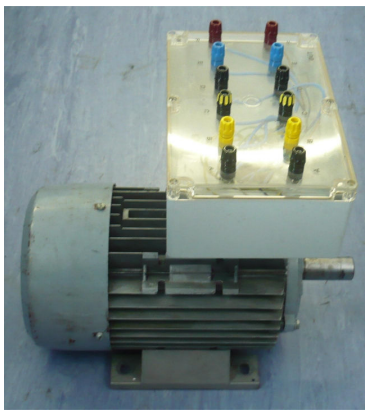

Fig. A.3: Symmetrical six-phase induction machine.

.

APPENDIX 2

PUBLICATIONS FROM THE THESIS

A2.1 JOURNAL PAPER

Jones, M., Patkar, F., Levi, E., (2013), Carrier-based pulse-width modulation techniques for asymmetrical six-phase open-end winding drives, *IET Electric Power Applications*, vol. 7, no. 6.

A2.2 CONFERENCE PAPER

Patkar, F., Levi, E., Jones, M., (2012), A six-phase multilevel space vector PWM algorithm for a dual-inverter supplied drive, *Proc. IET International Conference on Power Electronics, Machines and Drives PEMD*, Bristol, UK, pp. 1-5.

Patkar, F., Jones, M., (2013), Performance of an asymmetrical six-phase induction machine in single-and two-neutral point configurations, *Proc. Universities' Power Engineering Conference UPEC*, Dublin, Ireland.